AD-A042 989 WESTINGHOUSE DEFENSE AND ELECTRONIC SYSTEMS CENTER B--ETC F/G 17/4
EVALUATION OF IR COUNTERMEASURES (MODEL METHODOLOGY).(U)
JUN 72 R F HIGBY, R C BROWN, J B GOODELL DAAJ01-72-C-0447

UNCLASSIFIED NL

1 OF 3
ADA042989

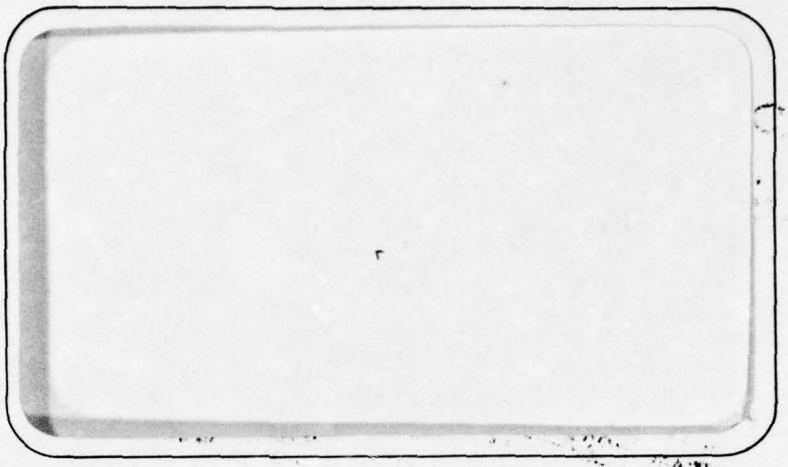

Westinghouse

ELECTRIC CORPORATION

EVALUATION OF IR COUNTERMEASURES

INTERIM TECHNICAL REPORT
(MODEL METHODOLOGY)

June 26, 1972

R. F. Higby
R. C. Brown
J. B. Goodell

Prepared for

U.S. ARMY AVIATION SYSTEM COMMAND
AMCPM-IRCM Project Office
Box 209, 12th & Spruce Streets
St. Louis, Mo. 63166

Under Contract DAAJ01-72-C-0447 Item 2, Data A1

By

WESTINGHOUSE ELECTRIC CORPORATION
Systems Development Division
Strike Systems Avionics, MS 434
Box 746, Baltimore, Md. 21203

ABSTRACT

EVALUATION OF IR COUNTERMEASURES - INTERIM REPORT

The methodology required to synthesize, program and validate the infrared signatures of Army aircraft (notably helicopters) and simulate their interaction with reticled sensors in a computer model to obtain sensor signal to noise ratios and error signals for arbitrary mission and flight profiles is described. The signatures account for exhaust plume emission (including effects of turbine operation and rotor down wash), hot metal parts, directional emittance due to body surface temperature (via thermal balance of internal sources, aero boundary layer conduction, solar heating, nocturnal radiation and plume heating), directionally reflected ambient radiance (including direct and difuse solar, sky and cloud emission, and terrestial surface radiation). Signatures are formulated in their exact spatial distribution of radiant intensity for any spectral band from 1 to 16 microns as viewed from any aspect and LOS geometry.

PREFACE

This interim technical report represents the culmination of the combined efforts and contributions of many people from several organizations toward the realization of a helicopter infrared signature computer model analytic tool for AVSCOM.

The work was performed for the Army Aviation Systems Command AMCPM-IRCM Project Office by Westinghouse SDD-SSA Section under the auspices of Mr. Steve Smith, AVSCOM technical monitor.

Key Westinghouse personnel were Rudy Brown and John Goodell. However, contributions were made in formulating the program philosophy by Ray Mantler (AVSCOM) on the low velocity exhaust phenomena, Doyle Banks (AVSCOM) on kinematic aspects, Dennis Blay (GD) and Leonard Holden (WSMR) on IR source identification, and Bill Lloyd and Jim Hawkins (TI) on interface requirements.

The encouragement and close cooperation by the entire IRCM Project Office, under the command of Col. S. Shirey, and in particular, Steve Smith, are largely responsible for the breath of scope and depth of detail that have been achieved in the signature modeling effort as is reflected in the size of this document.

R. F. Higby 6/26/72

R. F. Higby, Program Manager

TABLE OF CONTENTS

LIST OF FIGURES

LIST OF TABLES

1. INTRODUCTION

This document comprises the interim report on contract DAAJ01-72-C-0447 "Evaluation of Infrared Countermeasures".

The objective of this study was to establish the groundwork required to determine the infrared signatures of Army aircraft under operational conditions, thus facilitating an evaluation of their vulnerability to infrared guided threats.

This ground work consists of identifying relevant physical phenomona and operational conditions which contribute significantly to aircraft infrared signatures and relating them in mathematical form to those characteristics utilized by potential threat sensors.

Characteristics of interest are the spatial distribution of the spectral intensity of the aircraft target as viewed by a remote sensor from any aircraft aspect and contrasted against realistic backgrounds.

Expressing the signature in mathematical form facilitates eventual programming on a digital computer which readily accommodates the many and varied constituents of the infrared signature and permits rapid evaluation of its manifestations.

Relating the computation to operational conditions permits generating inflight and mission profiles of the infrared signature.

Embodying the foregoing atrributes, the infrared signature model to be developed will facilitate its eventual translation into a universal computer model which may best serve the Army's needs for assessing vulnerability and countermeasure effectiveness.

In this context, infrared signature models developed in this program have been structured in such a way as to be amenable to being programmed on AVSCOM computers. Their inputs will be translated into mission and flight parameters and their outputs will be constrained by sensor input requirements.

Thus, in principal, AVSCOM may eventually enter their own computer with arbitrary mission and threat scenarios and obtain the relevant infrared signature data for a given aircraft which may then be utilized to assess its vulnerability.

1.1 Background

Army aircraft are potentially vulnerable to infrared guided weapons. This is primarily because they contain rich sources of infrared emission, such as the exhaust plumes of turbojet engines, and their missions usually require them to fly low and slow in hostile environments which bring them into range of many diverse infrared threats, such as Redeye launched from the ground, or Sidewinder launched from the air.

In order to assess the vulnerability of Army aircraft to infrared threats, it is first necessary to know the infrared signature of the Army aircraft. The infrared signature is a complex manifestation of many interacting phenomena. (e.g., The exhaust plume emission is a function of engine torque and aircraft velocity and altitude. The contribution of tailpipe radiation as well as exhaust plume emission is dependent on the viewing aspect and fuselage obscuration. The irradiance at the plane of the observer is dependent on the transmission of the intervening path which, in turn, is a function of the relative humidity, visibility, altitude, range, wavelength, etc.).

Field measurements accurately obtain a value for the infrared signature of a given aircraft, however, it is only valid and applicable for those conditions under which it was obtained.

This situation is analogous to the proverbial six blind men and the elephant. Each blind man (none of whom had ever seen an elephant) proceeded to touch a different part of the elephant's body as illustrated in Figure 1.1. Each then endeavored to describe to his colleagues what an elephant was. The individual descriptions were predicated on the interpretation of the measured data, namely what the sense of touch conveyed. When all the measurements were compiled, they believed that they had defined the complete signature of the elephant. The signature that they might have devised is illustrated in Figure 1.2.

Analogously, field measurements cannot easily be extrapolated to other operating conditions with any degree of confidence. This results in a high degree of undertainty in any vulnerability assessment.

Of course, if measurements could be obtained under all meteorologic, seasonal, aspect and operating conditions, a good appraisal could be made. However, this is impractical because the expense and time required are prohibitive.

An alternate solution to obtaining a complete description of the infrared signature of a helicopter can be obtained through the marvel of the modern computer. This approach entails formulating analytic models of all of the interacting phenomena involved in synthesizing the signature and programming them on a digital computer. In this form, the signature and consequent vulnerability of a given aircraft may be evaluated for any desired flight and mission profile in a matter of seconds and cents. Confidence in the predictions can be established by comparisons with actual field measurements.

Thus, just as the sensors we use to make field measurements are analogous to the blind men's hands, the validated computer model which facilitates putting these measurements in proper perspective is analogous to our vision which allows us to see the true configuration of an elephant.

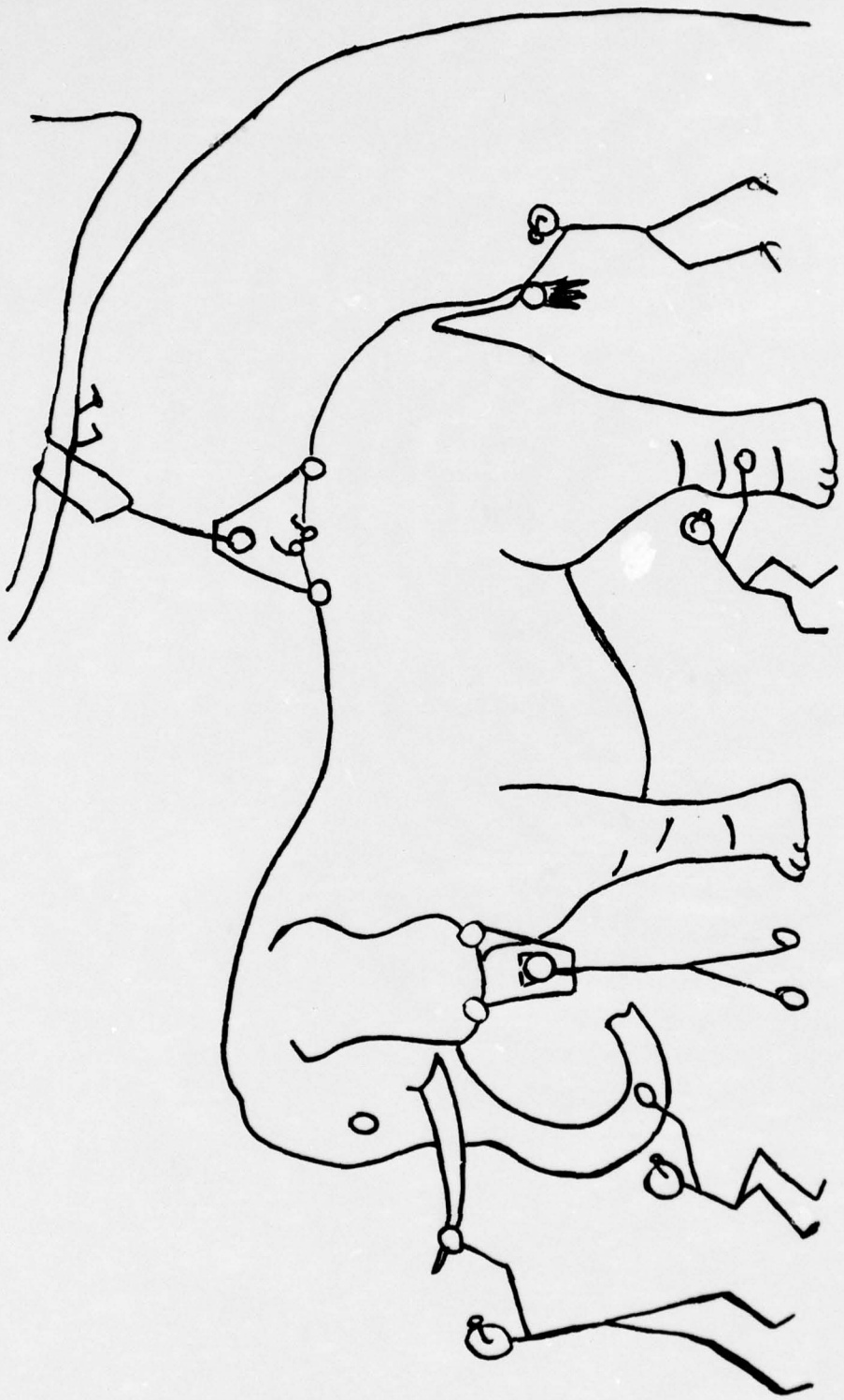

Figure 1.1 Signature Measurements

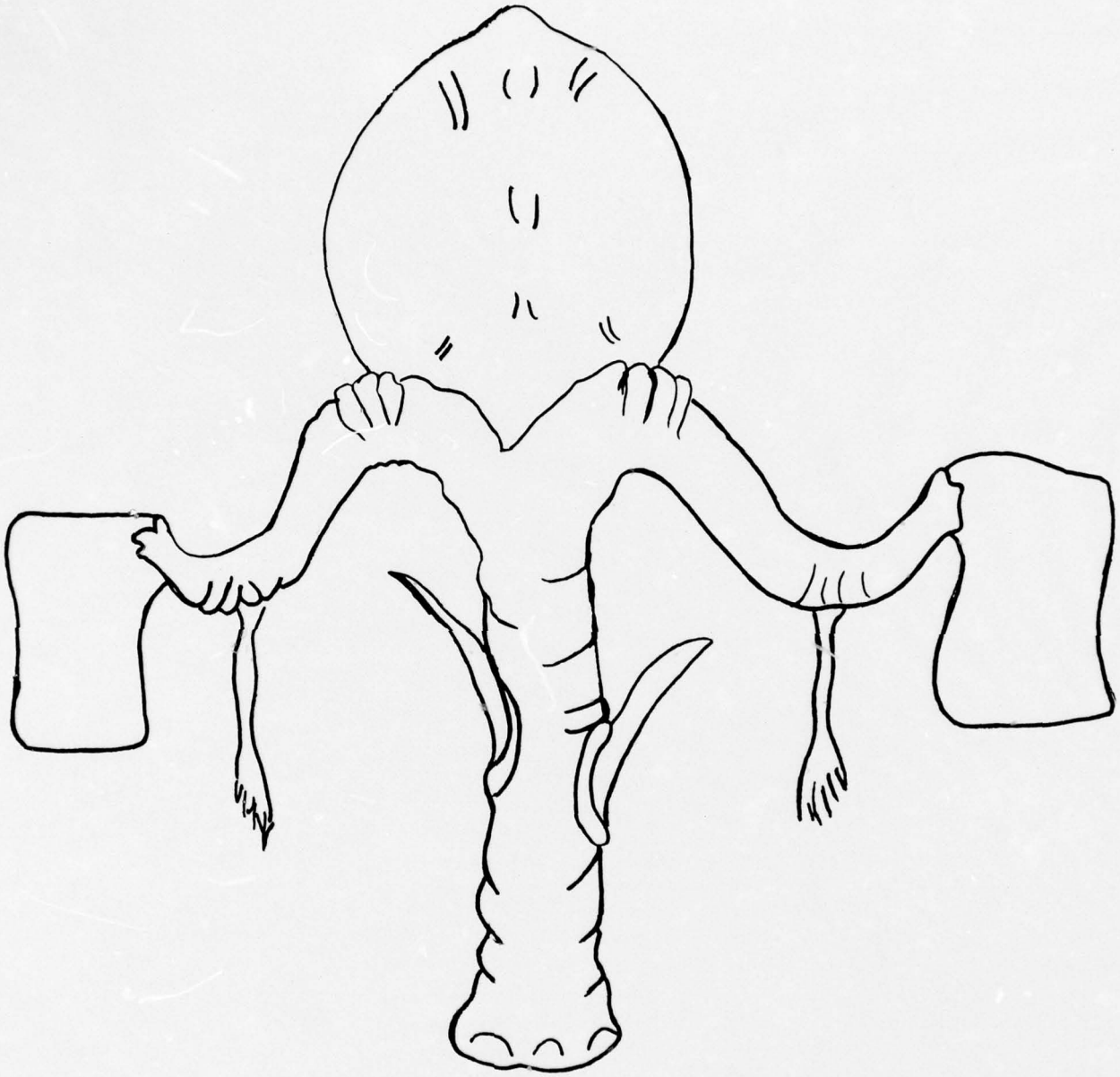

Figure 1.2 Signature Synthesis

1.2 Program Objectives

The objective of the "Evaluation of IR Countermeasures" program was to establish the ground work required for synthesizing infrared signatures of selected Army aircraft (notably helicopters) under operational conditions with and without suppression devices to evaluate detection ranges.

This ground work consits of identifying relevant physical phenomena which contribute significantly to aircraft infrared signatures and defining the methodology to be used in fabricating them in computer models which relate them to characteristics utilized by potential threat sensors.

This document describes the results of the program effort which has been expended under this contract in pursuit of this objective. It includes model identification and description, as well as methodology for analytic and computer synthesis. Also included are a bibliography of contempory modeling efforts, recommendations for constructing the computer model and a critera for validating it.

The major tasks that were carried out in this program are defined below.

1.2.1 Data Survey

A data survey was conducted to establish the current "state-of-the-art" in the applicable model technology areas, identify the experts in the related fields and establish sources of data that may be required during the development stages.

1.2.2 Model Study

The various phenomena relevant to contributing to the infrared signature have been identified. The governing physics were analyzed to yield an interpretation representative of the effect it produces.

The methodology used to obtain analytic models of the given effect have been defined. These resultant models are based on rigouous theoretical considerations and will be modified emperically to obtain the best fit between theory and observation.

The independent variables of all models have been transformed into readily measurable observables to facilitate the most general usage of the final models.

1.2.3 Program Synthesis

The analytic expressions describing the signature contributions have been organized to form a single ensemble with a common input and capable of yielding an output solution compatible with the end use requirements.

This is reflected in a computer flow diagram which has been synthesized to establish the sequence of operations to be performed. Also, the data output formatting has been established.

1.2.4 Validation

Means for determining the sensitivity of the output predictions to variation in the input parameters have been defined.

Methods for comparing computer predictions with measured data to determine the accuracy of the predictions in view of the sensitivity of the tolerance on the input data are described.

1.2.5 Interrim Report

All work carried out in the above tasks has been documented in this interrim report.

In addition, this report contains a recommendation for implementating the computer model from the ground work laid in the program.

1.3 Purpose

This report describes the synthesis of the computer program HIDE (Helicopter Infrared Detection Estimate) which has been synthesized to predict the complete infrared signatures of helicopters.

The purpose of this computer model, in addition to signature prediction, is to facilitate evaluation of vulnerability via detection range estimates and error signal generation, assessing effectiveness of countermeasures and defining meaningful measurements programs.

Vulnerability evaluation is facilitated by providing detection signal to noise ratio output data as well as reticle processed error signals to be used for input into a separate vulnerability model (not described here). The detection and error signal data is obtained by generating signatures for defined mission profiles and transforming them through postulated threat sensors.

In the context of countermeasures, the model is to be used as a tool to provide insight to understanding the causes and/or sources of detectable signature manifestations and assess the effectivenss of potential remedial solutions to minimize them.

HIDE is also to be used to define meaningful measurement programs. This application is illustrated in Figure 1.3. A postulated set of measurement conditions is fed into the model and a mean value signature computed. The measurement conditions values are then deviated proportionately to the tolerance that each condition could be measured in the field. The resultant deviation in the output signature is processed by the survivability model and a spread in vulnerability obtained. If the resultant spread is large, (ranging from high to low vulnerability) then, the measurement set is ambiguous as the results will not be very meaningful due to sensitivity to the measurement

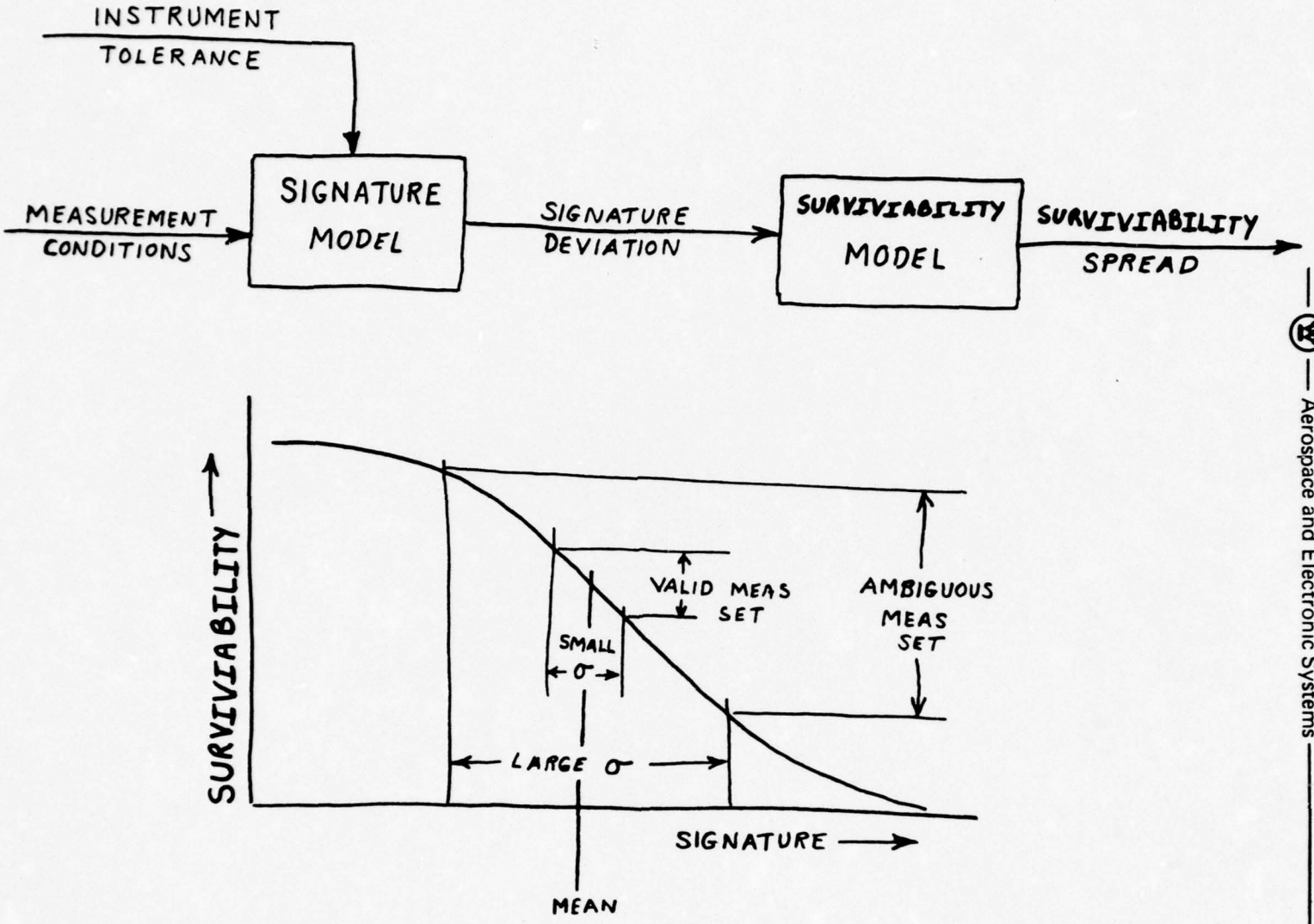

Figure 1.3 Measurement Program Definition

tolerance for the postulated set. (Such might be the case for forward aspect observations where attitude and wind variations or uncertainties could expose more or less plume). Conversely, a postualted measurement set yielding a small deviation in survivability would constitute a meaningful measurement set. In this manner, measurement conditions may be defined and the required instrument accuracy determined before the measurement program commences, thereby providing a high degree of confidence in obtaining valid data.

1.4 Computer Model

The HIDE (Helicopter Infrared Detection Estimate) computer model is designed to predict the infrared signature of a given helicopter for a designated mission profile and processes it with a generic sensor to obtain the output signal to noise ratio and error signal amplitude.

The signature will include exhaust plume emission, tail pipe radiation, surface self-emission and external source reflection, as well as background radiation and atmospheric transmission.

Signatures are to be generated in the form of a profile of the spatial distribution of intensity as would be derived at the image plane of a remote sensor. A signature profile is generated for each aspect angle in both azimuth and elevation relative to the helicopter coordinate system and each range from 0 to sensor signal drop out at arbitrary input step sizes.

Computations may be carried out for any spectral band from 1 to 13 microns with a resolution of better than 3% of the wavelength value. The spatial distribution of the signature may be resolved into as small a grid structure as may be desired. The amplitude resolution and dynamic range will be limited only by the computer which has a range of 10^{100} and quantization of 1 in 10 significant figures.

The physical situation embodied in the computer model is depicted by the sketch in Figure 1.4.

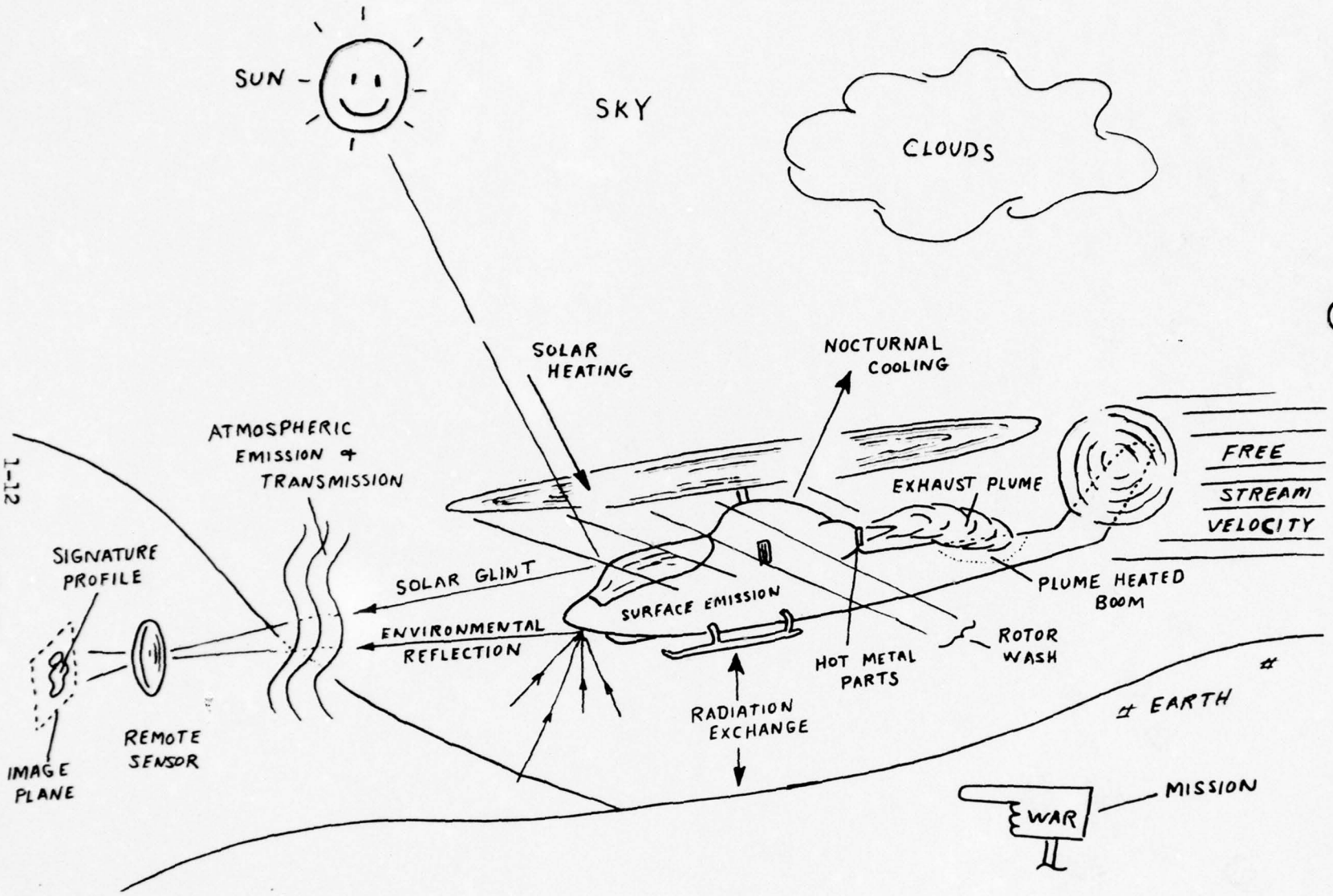

Figure 1.4 Physical Situation

UNCLASSIFIED

The helicopter derives shaft power from a turbine engine to turn the rotors which, in turn, develop lift and thrust for flight. The gas turbine expels its hot exhaust gases into ambient air, where they cool by diffusion. The exhaust plume is a prime source of infrared emission. However, the down wash from the rotor which the turbine drives and the free stream velocity resulting from the rotor generated thrust act as cross-currents distorting and accelerating diffusion of the exhaust plume. As a result, the plume emission is substantially modified. In addition, the distorted plume heats portions of the tail boom which might not otherwise be heated. Thus, the plume emission and body heating are strongly influenced by flight conditions. These dynamic effects are included in the sub-routine PLUME of the HIDE model.

The surface temperatures, other than the exhaust pipe, are dependent on internal sources, solar heating, nocturnal losses, environmental radiation exchange, air temperature and the aerodynamic boundry layer conductivity characteristics as well as mutual coupling between surfaces. This interdependent temperature relationship is solved in the sub-routine TEMPS of the HIDE model.

The effective surface radiation is composed of self-emission due to its temperature and partial pressures of the exhaust products. The total target radiation is attenuated by atmospheric transmission losses and added to by atmospheric emissions in the intervening path between target and sensor. Further, the target radiation is contrasted against a background radiation which could originate from sky, clouds, terrain or some combinations thereof. These backgrounds, of course, are also dependent on solar heating and ambient temperatures. These combinations are computed in the radiative transfer model sub-routine TRANS of the HIDE model.

A profile of the spatial distribution of intensity over the target is projected on to the image plane of a remote sensor. This is facilitated by resolving the target, plume and background into spatial elements, computing the radiance of each element and assigning it to the corresponding spatial position in the image plane. These disection and reconstitution manipulations are carried out in the geometrical sub-routine BODY of the HIDE model.

The signature profile at the image plane is then convolved with the field of view of the sensor to obtain a signal level for comparison with the sensor sensitivity to obtain signal to noise. The high spatial resolution of the signature profile facilitates performing this convolution with the actual spatial pattern of the retecle design. The operation permits error signals to be derived for the specified sensor type. These operations are performed in the sub-routine SENS in the HIDE model.

Most all of the computations indicated above are functions of meterorologic and operating conditions. Thus, they are all driven from common inputs which are obtained as input data for the mission profile to be run.

2. EXHAUST PLUME MODEL

The exhaust plume model computes the spatial distribution of exhaust gas concentrations and temperature. This is facilitated by first determining the exit conditions by employing a turboshaft model representing the specific helicopter engine for the input mission profile operating conditions. The corresponding rotor down-wash, free stream flight, and wind vector velocity distributions are then combined in an exhaust diffusion model to obtain the velocity and subsequent enthalpy functions which lead to the spatial distribution solutions for temperature and partial pressures.

The sequence for establishing the exit conditions is to determine the rotor lift and thrust required for the given mission profile from the air frame specifications. The required shaft horsepower to provide this is also obtained from the air frame specifications. This value is entered into the turbine model with all efficiencies, loss coefficients, compression ratio and temperature limit preset for the particular engine model. The model is then cranked through for the given ambient conditions to determine the fuel and air flow rates required to obtain this shaft horsepower and the consequent exit temperature, pressure, and velocity. These comprise inputs to the diffusion model.

2.1 Turbine Model

The gas turbine engine is a prime source of thermal energy and is therefore a necessary incredient in any infrared signature model.

The magnitude of this source is dependant primarily on three engine attributes: size, configuration and operating conditions. The fraction of thermal energy which is transformed into useable infrared radiation is determined largely by the configuration which dictates the division between conductive transference to raise the temperature of external walls and convective transport to the atmosphere where selective radiation by the exhaust products occur.

In order to establish the magnitude and manefestation of the infrared radiation, it is necessary to synthesize an analytic model which relates engine attributes to infrared radiation transformations. The analytic model then provides a viable translator through which infrared signatures may be interpreted from engine performance specifications.

The models described here are applicable to the gas turbine configurations of the turbo shaft, turbo prop, and turbo jet engines. They are both quantitative and qualitative in that they predict the magnitude and define the heat transfer mechanizms of the derived thermal energy. As such, they provide the inputs required by other analytical models which derive from them the infrared signatures.

2.1.1 Ideal Basic Cycle

To facilitate a better understanding of the turbine model development to be described in the following sections, it is worth while to first analyze the basic turbine cycle of an ideal system where in all processes are considered to be isentropic. This permits fundamental processes to be defined and an exposure to the schematic, graphic and symbolic notation to be used.

Figure 2.1 (a) illustrates in schematic form the basic gas turbine. Air is inducted at station 2 into a compressor C where in it undergoes an adiabatic compression. The compressed air leaves the compressor at station 3 and enters the combustion chamber B. Fuel is added to the compressed air in the combustion chamber. The diffused compressed mixture is then subjected to an isobaric heating process. The hot gasses leaving the combustion chamber enter the turbine T at station 4. The high temperature gas then undergoes an adiabatic expansion where in some of the energy in the high temperature gas is converted into work in turning the turbine. The spent gases are then exhausted from the turbine at station 5. Some of the work done on the turbine is coupled through a shaft to provide the work required by the compressor and the balance is supplied to the load L. The load is shown on a mechanical shaft but this can also represent net jet thrust.

Figure 2.1 (b) illustrates the Pv (pressure-volume) diagram for the ideal cycle. The curve from 2 to 3 depicts the adiabatic compression process. The number represents the thermodynamic state of the system at the corresponding station. Thus, state 2 is described by the pressure P2, temperature T2 and volume 2 at station 2.

For adiabatic processes, the following temperature T, pressure P, and density d relations apply.

$$\frac{Px}{Py} = \left(\frac{dx}{dy}\right)^{K} = \left(\frac{Tx}{Ty}\right)^{K/(K-1)} \qquad (2\text{-}1)$$

where: P = Pressure (lb/ft^2)

d = Density ($Slugs/ft^3$)

T = Temperature (^{o}R)

K = Specific heat ratio

X,Y = Subscripts for state at corresponding station

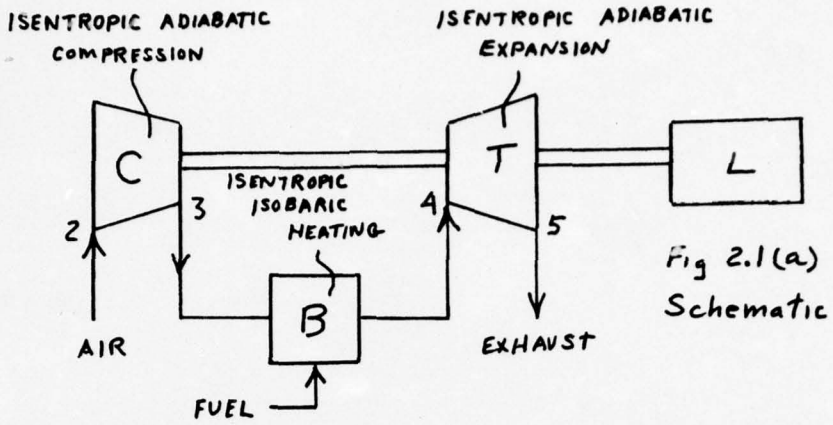

Fig 2.1(a) Schematic

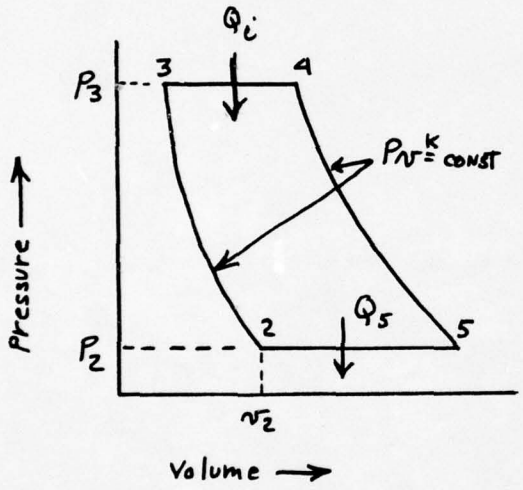

Fig 2.1(b) PV Diagram

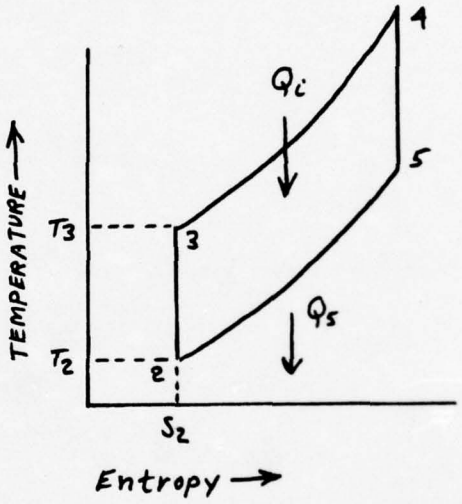

Fig 2.1(c) TS Diagram

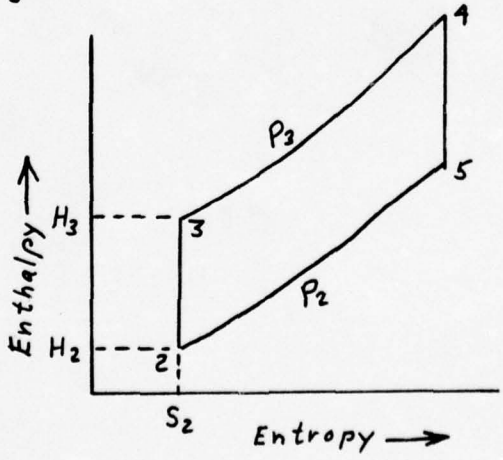

Fig 2.1 (d) HS Diagram

Figure 2.1 Ideal Basic Cycle

Density is a measure of mass per unit volume hence

$$vg = 1/d \qquad ft^3/Slug \qquad (2\text{-}2)$$

where: v = Volume per unit weight (ft^3/lb)

g = Gravitational constant ($31.17\ ft/sec^2$)

From these two relations, it may be derived that

$$Px(vx)^K = Py(vy)^K = \text{Constant} \qquad (2\text{-}3)$$

which defines the Pv curve for adiabatic changes of state.

The curve of figure 2.1 (b) from state 3 to 4 represents an increase in volume without change in pressure due to added heat Qi in an isobaric heating process. For such processes the following relations hold.

$$\frac{vx}{vy} = \frac{dy}{dx} = \frac{Tx}{Ty} \qquad (P = \text{const}) \qquad (2\text{-}4)$$

The curve 4 to 5 in figure 2.1 (b) represents the adiabatic expansion in the turbine. The segment from 5 to 2 represents the equivalent of isobaric cooling, giving up heat Qs to the surrounding air. This equivalence is justified on the basis that the spent gas is exhausted into the atmosphere at atmospheric pressure and the inducted air is taken in at atmospheric temperature and pressure, hence removing the heat from the spent gas makes it the same as the inducted gas thus completing the cycle. In this context, the turbine is viewed as a cyclic process.

Figure 2.1 (c) represents the TS (temperature-entropy) diagram. Entropy may be thought of as a measure of energy derived from an irreversable process which can not be retrieved and, hence is lost to the system so far as contributing to technical work.

The ideal cycle is defined as operating on a perfect gas (i.e. obeying the perfect gas laws), possessing no losses (heat, friction or temperature),

ideal efficiencies (compressor Nc, turbine Nt and combustion Nb efficiencies equal unity), no chemical or physical change in the gas, no differences in mass flow, all heat added instantaneously and completely, and all expansion taking place within the machine.

Figure 2.1 (c) may be interpreted in view of these assumptions. During the compression, the temperature is increased from T2 to T3, but because there are no losses, the process is reversable, hence there is no change in entropy. During the heating process, the temperature is increased from T3 to T4, but because this is not a reversable process, some of this energy will not be recoverable, hence there is a corresponding change in entropy. The expansion process is reversable incuring no change in entropy but does reduce the temperature from T4 to T5. The entropy and temperature difference from T5 to T2 correspond to the system losses in reverting to the beginning of the cycle.

The HS (enthalpy—entropy) diagram of figure 2.1 (d) is the one most commonly used to explain the thermaldynamic behavior of the gas turbine. Enthalpy is defined as the total thermal energy of a system. As such it is proportional to temperature. The comments above about the TS diagram also apply to the HS diagram. It is customary to denote the isobaric portion of the cycle curves with constant pressure values.

The thermal dynamic analysis of the ideal as well as the practical cycles in the suceeding sections is predicated on the work done on and by a unit weight of working fluid, namely one pound of inducted air. All results are then scaled by the quantity of air actually inducted. In this way, the models are completely general and may be tailored to any given application by introducing applicable efficiencies, machine limits and air induction rates.

Let Lc represent the work required to compress one pound of gas and Lt the work delivered as a result of inducting one pound of gas. The specific output work L is then

$$L = Lt - Lc \qquad \text{Btu/LB} \qquad (2\text{-}5)$$

The heat added Qi, is equal to the enthalpy change between states 3 and 4 as read off the HS diagram. This represents thermal energy and may be equated to the product of the temperature difference and specific heat Cp of the gas per unit weight.

$$Qi = H4 - H3 = Cp\ (T4 - T3) \qquad \text{BTU/LB} \qquad (2\text{-}6)$$

The specific output may also be expressed as a difference in enthalpy

$$L = (H4 - H5) - (H3 - H2) = Cp\ (T4 - T5) - Cp\ (T3 - T2) \qquad \text{BTU/LB} \qquad (2\text{-}7)$$

The following equality may be derived from equation (1) for adiabatic processes.

$$\frac{T3}{T2} = \frac{T5}{T4} = \left(\frac{P3}{P2}\right)^{(K-1)/K} \qquad (2\text{-}8)$$

Let $\alpha = T4/T2$ be the temperature cycle ratio and $r = P3/P2$ be the cycle pressure ratio. Using these parameters and the equalities of(8) equation(7)may be reduced to:

$$L = Cp\ T2 \left(\alpha - r^{(K-1)K}\right) \left(\frac{r^{(K-1)/K} - 1}{r^{(K-1)/K}} \right) \qquad \text{BTU/LB} \qquad (2\text{-}9)$$

The maximum value of L is found by differentiating with respect to $r^{(K-1)/K}$.

$L = Lmax$ when $\sqrt{\alpha} = r^{(K-1)/K}$

$$Lmax = Cp\ T2 \left[\alpha - 2\sqrt{\alpha} + 1 \right] \qquad \text{BTU/LB} \qquad (2\text{-}10)$$

By similar manipulations, the heat added becomes

$$Qi = Cp\ T2 \left(\alpha - r^{(K-1)/K} \right) \qquad \text{BTU/LB} \qquad (2\text{-}11)$$

and at Lmax

$$Qi(L=Lmax) = Cp\ T2\ \sqrt{\alpha}\ (\sqrt{\alpha} - 1) \qquad \text{BTU/LB} \qquad (2\text{-}12)$$

The thermal efficiency η_{th} or air cycle efficiency η_a is defined as the ratio of the specific work delivered to the heat added.

$$\eta_{th} = \frac{L}{Qi} = 1 - \left(\frac{1}{r}\right)^{(K-1)/K} \qquad (2\text{-}13)$$

$$\eta_{th}\ (L = Lmax) = 1 - \frac{1}{\sqrt{\alpha}} \qquad (2\text{-}14)$$

The significance of the ideal cycle can be put in perspective by assuming a maximum turbine temperature of 2000°R with an ambient temperature of 500°R and solving equations 10 and 14, using the specific heat of air Cp = .24 BTU/LB - °R.

$$Lmax = .24 \times 500 \times \left[4 - 2\sqrt{4} + 1 \right] = 120 \text{ BTU/LB}$$

$$\eta_{th}\ (L = Lmax) = 1 - \frac{1}{2} = .5$$

Introducing the following conversion factors:

1 BTU = 778 ft - LBS

1 BTU/sec = .000392 horse power = .293 watts

1 LB Fuel = 18,400 BTU (heat of combustion)

these equivalences may be obtained

Lmax = 120 BTU/LB-sec = 93,000 ft - lbs/Lb - sec = .047 hp/LB-Sec = 35 watts/LB-sec

$$\text{Fuel Consumption} = \frac{.24 \times 500\ \sqrt{4}\ (\sqrt{4}-1)}{18{,}400} = .013 \text{ lb fuel/lb air}$$

Thus for the ideal cycle an efficiency of 50% can be obtained and .047 horse power could be derived for each pound of air per second inducted. The fuel to air ratio is less than 2 percent.

These results yield a specific fuel comsumption of

$$SFC = \frac{.013}{.047} = .276 \text{ LB/sec-Hp}$$

for turbo shaft operation, which is considerably better then typical values for practical turbo shafts of .55 lb/sec-hp.

To find the equivalent thrust for the turbojet it is necessary to equate the kinetric energy of the exhaust jet to the specific work.

$$\frac{Wa}{2g} V_5^2 = J \times Lmax \qquad \text{Ft-LBs}$$

where Wa = 1 lB, weight of air

V5 = Exhaust velocity at station 5, ft/sec

J = 778 ft-lb/BTU, conversion factor

$$V5 = \sqrt{2 \times 32.17 \times 778 \times 120} = 2450 \text{ ft/sec}$$

The thrust F may then by obtained from Newton's second law

$$F = \frac{Wa}{9} V5 = \frac{2450}{32.17} = 76.2 \text{ lbs/lb Air-sec}$$

The specific fuel consumption for the turbojet ideal cycle becomes

$$SFC = \frac{.013 \times 3600}{76.2} = .615 \text{ lbs/hr - Fuel/lb Thrust/lb Air-sec}$$

This value again is better then typical values of .96.

The exhaust gas temperature may be obtained from equation(8)for the case of maximum specific work output

$$T4 = T5/\left(\frac{P_3}{P_2}\right)^{(K-1)/K} = T5/\sqrt{\alpha} = \frac{2000}{\sqrt{4}} = 1000^{\circ}R$$

These results are summarized in Table 2-1 along with some typical values for comparison.

TABLE 2-1 PARAMETER VALUES PER POUND OF AIR INDUCTED

Parameter	*Ideal Cycle	Typical
Inlet Temp (T4) ^{o}R	2000	2000
Compress Ratio (r)	11.5	6 - 10
Specific Work (Lmax) BTU	120	
Watts	35	
hp	.047	
Fuel Consump (Wf) lb	.013	.017
Shaft - SFC lb/hp	.276	.55
Exhaust Vel (V5) ft/sec	2450	2000
Exhaust Temp (T5) ^{o}R	1000	1200
Thrust (F) lb	76.2	49
Thrust - SFC lb/hr-lb	.615	.96

* Case for L = Lmax

Equation (13) indicates that the thermal efficiency is solely dependant on the compression ratio.

Given a compression ratio, r, and temperature ratio, α , the specific fuel consumption, SFC, exhaust velocity, V5, and exhaust temperature, T5, are uniquely determined independant of the air induction rate. Conversely, the specific work, L, fuel consumption, Wf, and thrust, F, are proportional to the air induction rate.

2.1.2 Turbojet Engine

The turbojet engine is probably the simplest of practical turbine engines to define. It is based on the ideal cycle with a considerable number of modifications relating to efficiency.

Figure 2.2 (a) illustrates a sketch of a turbojet engine. Figure 2.2 (b) represents its schematic. There are only two differences shown over the basic cycle. One is the addition of the diffuser at the inlet and the other is the nozzel at the outlet. Figure 2.2 (c) shows the HS diagram for the turbojet engine. It will be explained during the analytic development but cursory observation will reveal it is similar to the basic cycle except for alterations which reflect inefficiencies.

During flight, air is ramed into the engine inlet. This ram effect raises the temperature and pressure at the inlet. These changes of state must be taken into account in analyzing the cycle performance.

The first step is to calculate the total temperature, T2, of the ram air leaving the diffuser.

$$T2 = t_o \left(1 + \frac{K2 - 1}{2} Mo^2\right) \quad {}^oR \qquad (2\text{-}15)$$

where t_o = static free stream temperature, ^oR

Mo = Mach number of aircraft velocity

K2 = Average specific heat ratio of air at temperature T2

The mach number may be defined as the aircraft velocity Vo divided by the speed of sound a_o.

$$Mo = \frac{Vo}{a_o} \qquad (2\text{-}16)$$

The specific heat ratio may be defined in terms of the specific heat

$$K = Cp/(Cp - R/MJ) \qquad (2\text{-}17)$$

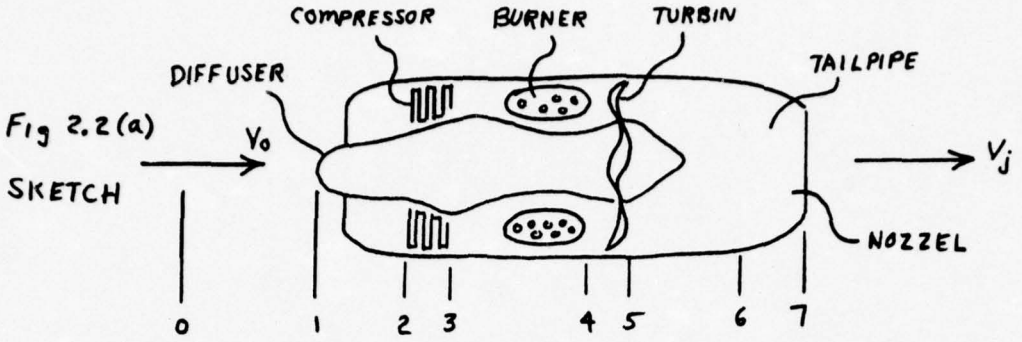

Fig 2.2 (a) SKETCH

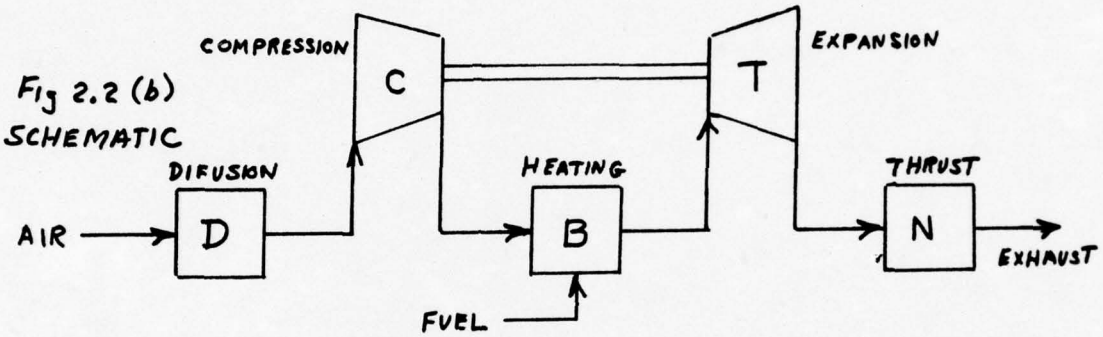

Fig 2.2 (b) SCHEMATIC

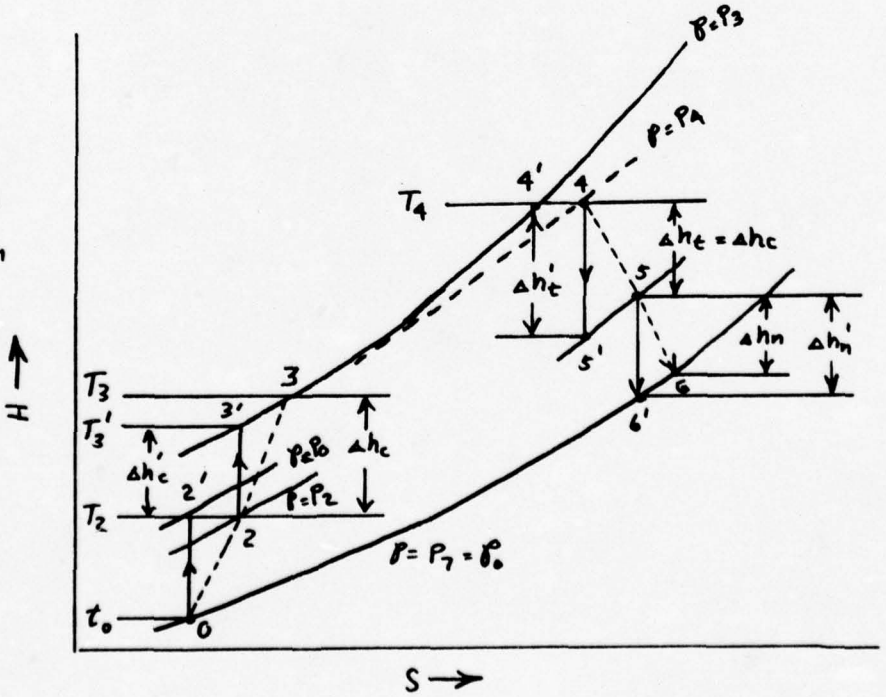

Fig 2.2 (c) HS Diagrom

Figure 2.2 Turbojet Engine

where K = Specific heat ratio

Cp = Specific heat, BTU/LB - ^{o}R

R = 1544 (ft - lb/mole - ^{o}R), Universal gas constant

$\mathcal{M}$ = Molecular weight of fluid, LBS/mole

J = 778 (ft - lbs/BTU), Conversion factor

The specific heat of the working fluid is comprised of the average of the specific heats of the constituent gases in proportion to their concentrations.

$$Cp = \frac{\sum_{J=1}^{N} Cp_J \, PP_J \, M_J}{\sum_{J=1}^{N} PP_J \, M_J} \qquad (BTU/LB - {}^{o}F) \qquad (2\text{-}18)$$

where: PP = Partial pressure (volume fraction)

J = Constituent gas species

With respect to the stations prior to the combustion chamber, the working fluid is ambient air. The composition of dry air is shown in Table 2-2.

TABLE 2-2 DRY AIR COMPOSITION

Constituent	Formula	Per Cent Volume	Mole WT (lB/Mole)
Nitrogen	N2	78.03	28.016
Oxygen	O2	20.99	32
Argon	A	.98	39.994

The molecular weight of dry air may be computed from these values.

$\mathcal{M}$(dry air) = .7803 x 28.016 + .2099 x 32 + .0098 x 39.994 = 28.97 LB/Mole (2-19)

Air is generally not dry but contains some water vapor. This must be taken into account as it affects the density and specific heat of the working fluid.

The quantity of water vapor present is generally specified as a mixing ratio Mx, which is the ratio of one unit by weight of water vapor to 1000 units by weight of dry air. It usually has the units of gms/kilograms but this is also equal to the units used here in lbs/Kilo-lb.

In order to modify the molecular weight of air due to water vapor, the volumetric mixing ratio must be determined. This is facilitated below using the molecular weight of water vapor (H20) of 18.016 lbs/mole.

$$Mx(\text{volume}) = \frac{\mathcal{M}_{(\text{dry air})}}{\mathcal{M}_{(H20)}} M_x \times 10^{-3} = .00161\ Mx$$

ft3 (H20)/ft3(dry air) (2-20)

The molecular weight of wet air may then be derived

$$\mathcal{M}_{(\text{wet air})} = (1-.0016\ Mx)\ \mathcal{M}_{(\text{dry air})} + .0016\ Mx\ \mathcal{M}_{(H20)}$$

$$= 28.97\ (1-.00061\ Mx)\ \text{lb/mole} \quad (2\text{-}21)$$

The composition of the wet air molecule may be obtained by adjusting the dry air molecule concentrations as shown in Table 2-3.

TABLE 2-3 WET AIR COMPOSITION

Constituent	Formula	Per Cent Volume	Mole WT (lb/Mole)
Nitrogen	N2	78.03/(1-.00061 Mx)	28.016
Oxygen	O2	20.99/(1-.00061 Mx)	32
Argon	A	.98/(1-.00061 Mx)	39.994
Water Vapor	H20	.061 Mx	18.016

Mx = Mixing ratio (gm H20/Kgm dry Air)

The specific heats for gases of interest in the turbine engine are extracted from "JANAF Thermalchemical Tables" and are listed in Table 2-4 as a function of temperature. Note that they are given in units of BTU/LB-Mole-^{o}F. This is the same as the product of the specific heats in BTU/LB-^{o}F multiplied by the molecular weight LB/Mole.

The specific heat of the wet air may be obtained using the volumetric fractions from Table 2-3, the specific heat, molecular weight products from Table 2-4, and the molecular weights from Table 2-3 in equation 18 all evaluated at the same temperature.

$$Cp(wet) = \frac{.7803\ [Cp\ M]_{N2} + .2099\ [Cp\ M]_{O2} + .0098\ [Cp\ M]_{A}}{28.97 + .0111\ (1-.00061\ Mx)\ Mx}$$

$$+ \frac{.00061\ Mx(1-.00061\ Mx)\ [Cp\ M]_{H_2O}}{28.97 + .0111(1-.00061 Mx) Mx} \quad BTU/LB-°R \qquad (2\text{-}22)$$

TABLE 2-4 MOLAR SPECIFIC HEATS (BTU/LB-MOLE-^{o}F)

TEMP(^{o}K)	N2	O2	H2O	CO	CO2
100	6.956	6.958	7.961	6.956	6.981
200	6.957	6.991	7.969	6.957	7.734
300	6.961	7.023	8.025	6.965	8.896
400	6.990	7.196	8.186	7.013	9.877
500	7.069	7.431	8.415	7.121	10.666
600	7.196	7.670	8.676	7.276	11.310
700	7.350	7.883	8.954	7.450	11.846
800	7.512	8.063	9.246	7.624	12.293
900	7.670	8.212	9.547	7.786	12.667
1000	7.815	8.336	9.851	7.931	12.980
1100	7.945	8.439	10.152	8.057	13.243
1200	8.061	8.527	10.444	8.168	13.466
1300	8.162	8.604	10.723	8.263	13.656
1400	8.252	8.674	10.987	8.346	13.815
1500	8.330	8.738	11.233	8.417	13.953
1600	8.398	8.800	11.462	8.480	14.074
1700	8.458	8.858	11.674	8.535	14.177
1800	8.512	8.916	11.869	8.583	14.269
1900	8.559	8.973	12.048	8.626	14.352
2000	8.601	9.026	12.214	8.664	14.424

2100	8.638	9.084	12.366	8.698	14.489
2200	8.672	9.139	12.505	8.728	14.547
2300	8.703	9.194	12.634	8.756	14.600
2400	8.731	9.248	12.753	8.781	14.648
2500	8.756	9.301	12.863	8.804	14.692
2600	8.779	9.354	12.905	8.825	14.734
2700	8.800	9.405	13.059	8.844	14.771
2800	8.820	9.455	13.146	8.863	14.807
2900	8.838	9.503	13.228	8.879	14.841
3000	8.855	9.551	13.304	8.895	14.873
3100	8.871	9.596	13.374	8.910	14.902
3200	8.886	9.640	13.441	8.924	14.930
3300	8.900	9.682	13.503	8.937	14.956
3400	8.914	9.723	13.562	8.949	14.982
3500	8.927	9.762	13.617	8.961	15.006
3600	8.939	9.799	13.669	8.973	15.030
3700	8.950	9.835	13.718	8.984	15.053
3800	8.962	9.869	13.764	8.994	15.075
3900	8.972	9.901	13.808	9.004	15.097
4000	8.983	9.932	13.850	9.014	15.119

4100	8.993	9.961	13.890	9.020	15.139
4200	9.002	9.988	13.927	9.033	15.159
4300	9.012	10.015	13.963	9.042	15.179
4400	9.021	10.039	13.997	9.051	15.197
4500	9.030	10.062	14.030	9.059	15.216
4600	9.039	10.084	14.061	9.068	15.234
4700	9.048	10.104	14.091	9.076	15.259
4800	9.057	10.125	14.120	9.084	15.272
4900	9.066	10.140	14.148	9.092	15.290
5000	9.074	10.156	14.174	9.100	15.306
5100	9.083	10.172	14.221	9.107	15.327
5200	9.091	10.187	14.228	9.115	15.349
5300	9.100	10.200	14.254	9.123	15.371
5400	9.109	10.213	14.279	9.130	15.393
5500	9.118	10.235	14.303	9.138	15.415
5600	9.127	10.237	14.328	9.145	15.437
5700	9.136	10.247	14.351	9.153	15.459
5800	9.145	10.258	14.375	9.160	15.481
5900	9.155	10.267	14.398	9.167	15.503
6000	9.165	10.276	14.422	9.175	15.525

The specific heat changes with temperature, therefore, it is necessary to use the average value between the change of state values.

$$\overline{Cp}\ (Tx,\ Ty) = \frac{\int_{Tx}^{Ty} Cp(T)dT}{Ty - Tx} \qquad BTU/LB-°R \qquad (2\text{-}23)$$

In the above relation, the bar denotes the average value between Tx and Ty.

The subscript on the specifc heat ratio denotes the temperature for which the average specific heat was evaluated. When a double subscript is used, it denotes that the specifc heat was evaluated between the temperatures of the state denoted by each digit of the double subscript.

We may now enter the HS diagram with ambient temperature to and pressure po, and where they intersect, project vertically upward to state 2' an amount corresponding to an enthalpy increase due to total ram temperature T2. The vertical projection assumes an adiabatic compression for which we can calculate the total pressure P_2 using equation (1) and transforming with equation (15).

$$Po = p_o \left(\frac{T_2}{To}\right)^{K_2/(K2-1)} = p_o \left(1 + \frac{K_2 - 1}{2}\ MO^2\right)^{K_2/(K2-1)} \qquad LB/ft^2 \qquad (2\text{-}24)$$

The inefficiencies in the diffuser for the ram air process result in a pressure loss with no change in temperature. This is denoted in the HS diagram by translating horizontally from the adiabatic state 2' to the actual state 2. This indicates an increase in entropy with no change in enthalpy. The dotted line between states 0 and 2 indicate the real system path on the HS curve. This ram inefficiency is refered to as the ram recovery factor, Err, and is equated functionally to the final total pressure, P2, leaving the diffuser.

$$Err = \frac{P2 - \rho o}{Po - \rho o} \qquad (2\text{-}25)$$

The corrected total pressure, P2, then becomes

$$P2 = Err\ (Po - \rho o) + \rho o = \rho 0 \left[1 + \left\{ \left(1 + \frac{K2-1}{2} M_o^2\right)^{K2/(K2-1)} - 1 \right\} Err \right] LB/ft^2 \qquad (2\text{-}26)$$

A typical value for the ram recovery ratio is 0.8.

The constant pressure curve P2 is shown in the HS diagram. It may be noted that the ram efficiency causes a reduction in total pressure entering the compressor resulting in a gain in entropy without changing the enthalpy.

To analyze the compression cycle, it is necessary to first assume adiabatic compression and then modify the results to accomodate losses.

Let the compression ratio be r_c, then using equation (1) the following identities are obtained.

$$r_c = \frac{P3}{P2} = \left(\frac{T3'}{T2}\right)^{K23'/(K23'-1)} \qquad (2\text{-}27)$$

T3' represents the adiabatic tmperature from which we may obtain the adiabatic enthalpy change $\Delta h'_c$ illustrated in figure 2.2 (c).

$$\Delta h'c = \overline{C}p23'\ (T'3 - T2) = \overline{C}p\ 23' T_2 \left(r_c^{(K23'-1)/K23'} - 1 \right) \ BTU/LB \qquad (2\text{-}28)$$

Losses due to compression inefficiencies increase enthalpy. Let η_c represent the compression efficiency. Then, the actual enthalpy change due to compression losses becomes:

$$\Delta hc = \frac{\Delta h'c}{\eta_c} = \frac{\overline{C}P23'\ T2}{\eta_c} \left(r_c^{(K23'-1)/K23'} - 1 \right) \ BTU/LB \qquad (2\text{-}29)$$

From this energy the actual compression temperature may be obtained.

$$T3 = \frac{\Delta hc}{CP23'} + T2 = T2 \left[\frac{\left(r_c^{(K23'-1)/K23'} - 1 \right)}{\eta_c} + 1 \right] \ {}^{o}R \qquad (2\text{-}30)$$

To correctly evaluate equations (29) and (30), the average specific heat $\bar{C}p23'$ for the temperature interval T2 to T3' and its resultant specific heat ratio K23' as obtained from equation (17), (18) and (23) should be used to obtain an estimate of T3. The specific heat $\bar{C}P23'$ and specific heat ratio K23' in equations (29) and (30) should than be changed to $\bar{C}P23$ and K23, respectively, that is re-evaluated for the temperature interval T2 to T3 using equations (17), (18) and (23). This process should continue until the change in successive T3 values becomes insignificant (less than $1^{o}R$ which is better than the accuracy that the physical temperature can be measured).

The compression pressure is obtained directly from equation (27).

$$P3 = P2r_c \qquad \text{LB/ft2} \qquad (2\text{-}31)$$

A typical value of isentropic compression efficiency is .85.

In addition to the isentropic efficiency, there are mechanical losses due to friction in the bearings which results in energy being lost to the system. This does not show up as a change in enthalpy. If η_{mc} represents the mechanical efficiency, then the work required by the compresser to compress one pound of air may be expressed as:

$$Lc = \frac{\Delta hc}{\eta_{Mc}} = \frac{\bar{C}p23\ T2}{\eta c\ \eta_{mc}} \left(r_c^{(K23-1)/K23} - 1 \right) \quad \text{BTU/LB} \qquad (2\text{-}32)$$

A typical value for mechanical efficiency is 0.98.

The air entering the combustion chamber is mixed with fuel which raises its enthalpy through an isobaric heating process from the heat liberated in the combustion process. This is illustrated in figure 2.2 (c) along the isentropric pressure curve from state 3 to isentropic state 4'.

Let Wa be the weight of a unit of air entering the combustion chamber and Wf be the weight of fuel added to the unit of air. Let f be the ratio of the fuel and air weights. Then the weight of the mixture Wg leaving the combustion chamber becomes:

$$Wg = Wa + Wf = Wa\ (1 + f) \qquad \text{LBS} \qquad (2\text{-}33)$$

The enthalpy balance equation for the gas leaving the combustion chamber for isentropic conditions is derived by using the ideal fuel to air ratio f' and correcting for the actual ratio f latter. The ideal fuel to air ratio assumes complete combustion of the fuel while the actual accounts for incomplete combustion.

$$HA3 + f'h_f + f'\ \Delta Hc = (1 + f')\ Hg4 \qquad (2\text{-}34)$$

where: HA3 = Enthalpy of a pound of air entering the combustion chamber BTU/LB

f' = Ideal fuel to air ratio by weight

h_f = Heat of vaporization of fuel BTU/LB

ΔHc = Heat of combustion of fuel vapor BTU/LB

Hg4 = Enthalpy of a pound of gas leaving combustion chamber BTU/LB

The heat of vaporization may be expressed as a function of liquid fuel temperature t_L. For liquid hydrocarbon fuels, the following relation is used.

$$h_f = 0.5\ t_L - 287 \qquad \text{BTU/LB} \qquad (2\text{-}35)$$

The heat of combustion ΔHc is obtained by taking the difference between the heats of formation of the reactants ΔHf (fuel) and the heat of formation of the products of the reaction ΔHf (products) per pound of fuel.

$$\Delta Hc = \sum \Delta Hf\ (\text{products}) - \sum \Delta Hf\ (\text{fuel}) \qquad \text{BTU/LB} \qquad (2\text{-}36)$$

To solve this equation, it is necessary to know the weights of the reaction products. This is determined by obtaining the chemical balance for the fuel formula and air.

For purposes of generalizing the equations, the fuel formula will be expressed in terms of its hydrocarbon ratio x and the number n of carbon atoms in one molecule of fuel.

$$\text{fuel molecule} = (CHx)\ n \qquad (2\text{-}37)$$

Since the number of molecules in a given volume of gas at constant pressure and temperature is a constant independent of the molecular weight or mixture of gasses contained within the volume, the number of molecules of each constituent gas is proportional to the fraction of the volume it occupies.

The composition of air was given in Table 2-3. If all constituents are divided by the coefficient of oxygen, an equivalent molecular unit for air may be represented by the following composition.

$$(AIR) = \left[(O2) + 3.717\ (N2) + .047(A) + .0029\ Mx\ (1-.00061\ Mx)\ (H20)\right] \quad (2\text{-}38)$$

The chemical balance equation may now be written using these formulas.

$$(CHx)n + n\left(1 + \frac{x}{4}\right)(Air) \rightarrow n(CO2) + \frac{nx}{2}(H20) + n\left(1 + \frac{x}{4}\right)\left[3.717\ (N2) + .047(A) + .0029\ Mx\ (1-.00061\ Mx)(H20)\right]$$

This is the stoichiometric equation for combustion, i.e. the exact quantity of air required for complete combustion of the fuel and from it is obtained the number of molecules of the products of reaction for each molecule of reactant. Equation (36) may now be rewritten as

$$\Delta Hc = \frac{n\,\Delta H_f(CO2)\,\mathcal{M}(CO2) + \frac{nx}{2}\,\Delta H_f(H20)\,\mathcal{M}(H20) - \Delta H_f(CnHxn)}{\mathcal{M}(CnHxn)} \quad BTU/LB \qquad (2\text{-}40)$$

In this expression $\mathcal{M}$ represents the molecular weight of the species with in the parempathesis in units of pounds per mole.

Table 2-5 lists the molecular weights and heats of formation for a number of reaction products.

Table 2-6 lists the molecular weights of a number of fuel molecules and their attendant heats of combustion as obtained from equation (40).

TABLE 2-5 REACTION PRODUCTS

Constituent	Formula	Molar Weight (LBS/Mole)	Heat of Formation (BTU/LB-Mole)
Air		28.970	0
Argon	A	39.994	0
Carbon	C	12.010	0
Carbon Dioxide	CO2	44.010	169,143
Hydrogen	H2	2.016	0
Nitrogen	N2	28.016	0
Oxygen	O2	32.000	0
Water Vapor	H2O	18.016	102,788

TABLE 2-6 LIQUID HYDROCARBON FUEL CHARACTERISTICS

Hydrocarbon Fuel	Composition	Hydro-Carbon Ratio, H/C	Molecular Weight, $\bar{m}$	$+\Delta H_c^o$, B/lB	Stoichiometric Fuel-Air Ratio, fo
Paraffin Series					
Methane	CH_4	4.000	16.042	21,565	0.05812
Ethane	C_2H_6	3.000	30.068	20,517	0.06224
Propane	C_3H_8	2.667	44.094	20,037	0.06390
n-Butant	C_4H_{10}	2.500	58.120	19,761	0.06479
n-Pentane	C_5H_{12}	2.400	72.146	19,590	0.06534
n-Hexane	C_6H_{14}	2.333	86.172	19,479	0.06572
n-Heptane	C_7H_{16}	2.285	100.198	19,400	0.06600
n-Octane	C_8H_{18}	2.250	114.224	19,399	0.06621
n-Nonane	C_9H_{20}	2.222	128.250	19,294	0.06637
n-Decane	$C_{10}H_{22}$	2.200	142.276	19,257	0.06650
Olefin Series					
Ethene	C_2H_4	2.000	28.052	20,319	0.06775
Propene	C_3H_6	2.000	42.078	19,757	0.06775
1-Butene	C_4H_8	2.000	56.104	19,555	0.06775
1-Pentene	C_5H_{10}	2.000	70.130	19,413	0.06775
1-Hexene	C_6H_{12}	2.000	84.156	19,330	0.06775
1-Heptene	C_7H_{14}	2.000	98.182	19,271	0.06775
1-Octene	C_8H_{16}	2.000	112.208	19,226	0.06775
1-Nonene	C_9H_{18}	2.000	126.234	19,191	0.06775
1-Decene	$C_{10}H_{20}$	2.000	140.260	19,165	0.06775
Alkylbenzene Series					
Benzene	C_6H_6	1.000	78.108	17,494	0.07546
n-Methylbenzene	C_7H_8	1.143	92.134	17,655	0.07417
n-Ethylbenzene	C_8H_{10}	1.250	106.160	17,823	0.07325
n-Propylbenzene	C_9H_{12}	1.333	120.186	17,944	0.07257
n-Butylbenzene	$C_{10}H_{14}$	1.400	134.212	18,042	0.07208
n-Amylbenzene	$C_{11}H_{16}$	1.455	148.238	18,125	0.07160

The following relations have been found to give a good approximation of the heat of combustion for liquid hydrocarbon fuels.

$$\Delta Hc = 15,936 + 15,800 \frac{WH}{WC} \quad \text{BTU/LB} \qquad (2\text{-}41)$$

$$\Delta Hc = 19,960 + 6360\ S - 3780\ S^2 \quad \text{BTU/LB} \qquad (2\text{-}42)$$

where WH/WC is the hydrogen to carbon weight ratio and S the specific gravity at 60 degrees F of the fuel.

Equation (41) may be rewritten in terms of the hydrogen to carbon atom ratio of the fuel molecule.

$$\Delta Hc = 15,936 + 1,312\ x \quad \text{BTU/LB} \qquad (2\text{-}43)$$

Equation (34) may now be rewritten in terms of the ideal fuel ratio.

$$f' = \frac{Hg4 - HA3}{h_f + \Delta Hc - Hg4} \qquad (2\text{-}44)$$

This equation may be solved using T4 as the maximum permissable turbine inlet temperature which is constrained due to metallurgic limitations on the temperature of the turbine blades.

$$f' = \frac{\bar{C}_{p43}\ (T4 - T3)}{.5\ t_L \quad 15,648 + 1,312\ x - \bar{C}_{p4} T4} \qquad (2\text{-}45)$$

The actual fuel to air ratio f takes into account the combustion efficiency η_B.

$$f = f'/\eta_B \qquad (2\text{-}46)$$

The partial pressures of the constituient gasses of the products of combustion are required in order to compute the specific heat of the working fluid in and beyond the combustion chamber.

They may be derived by modifying equation (39) to reflect the actual fuel to air ratio. The actual fuel to air ratio is by definition the ratio of the weight of fuel to the weight of air which may be expressed in terms of their molecular weights.

$$f = \frac{W(Fuel)\ lbs}{W(Air)\ lbs} = \frac{\mathcal{M}_{(fuel)}\ Lbs/mole}{N\ \mathcal{M}(Air)\ Lbs/mole} \qquad (2\text{-}47)$$

In this expression N is the number of moles of air required to equal the specified weight of air.

The left hand side of equation (39) which represents the reactants may now be rewritten to include all of the air entering the combustion chamber.

$$\text{Reactants} = (CHx)_n + \eta_\beta\, n\left(1+\frac{x}{4}\right)(Air) + \left[N - \eta_\beta n\left(1+\frac{x}{4}\right)\right](Air) \qquad (2\text{-}48)$$

η_β is introduced to take note of the fact that complete combustion will not be achieved.

The factor N may be defined using equations (38), (39) and (47).

$$N = \frac{\mathcal{M}_{(C_n H_{xn})}}{f\left[\mathcal{M}(O2) + 3.717\ \mathcal{M}(N2) + .047\ \mathcal{M}(A) + .0029Mx(1-.00061Mx)\mathcal{M}(H2O)\right]}$$

$$N = \frac{n(12.01 + 1.008x)}{f\ \left[\ 138 + .052\ (1-.00061Mx)\ Mx\ \right]} \qquad (2\text{-}49)$$

The products of the reaction may now be defined by modifying the right hand side of equation (30) to reflect the added air.

$$\text{Products} = \eta_\beta n(CO2) + \frac{\eta_\beta n x}{2}(H2O) + \eta_\beta n\left(1+\frac{x}{4}\right)\left[3.717(N2) + .047(A) + .0029Mx\ (1-.00061Mx)(H2O)\right] + (1-\eta_\beta)(C_nH_{xn}) + \left[N - \eta_\beta n\left(1+\frac{x}{4}\right)\right]\left[(O2) + 3.717(N2) + .047(A) + .0029Mx\ (1-.00061\ Mx)(H2O)\right] \qquad (2\text{-}50)$$

The partial pressures of each exhaust product species may now be determined by summing up the number of moles of each specifies present.

$$PP(Species) = \frac{N(Species)}{\Sigma N(Species)} \qquad (2\text{-}51)$$

This is facilitated with the aid of Table 2-7.

TABLE 2-7 PARTIAL PRESSURE COMPOSITION

Species	N(Species)
CO2	$\eta_B n$
H2O	$\eta_B nx/2 + .0029\ N(1-.00061Mx)\ Mx$
N2	$3.717\ N$
A	$.047\ N$
O2	$N-\eta_B n\ (1 + \frac{x}{4})$
$(CHx)_n$	$1-\eta_B$
$\sum N(\text{Species}) = 1 + \eta_B\ (\frac{\eta x}{4} - 1) + N\left[4.764 + .0029\ (1-.00061\ Mx)\ Mx\right]$	

The exact solution to equation (45) for the ideal fuel to air ratio is obtained by initially assuming a value for $\bar{C}p43$ and then carrying out the operations indicated in equations (49) and (51). With the number of molecules of each species determined, a better estimate of the specific heat $\bar{C}p43$ can be obtained from Table 2-3 using equations (18) and (23). This iteration should be continued until the change in specific heat is less than 1/T4.

The heating process is not truely isentropic as some pressure losses are incurred in the combustion process. This is indicated by the dashed line in the HS diagram of figure 2.2 (c). Thus P4 is the actual pressure of the gasses leaving the combustion chamber. These losses are on the order of 3 percent of the pressure P3 entering the combustion chamber.

The enthalpy change in the turbine due to adiabatic expansion is indicated in figure 2.2 (c) by the vertical line segment $\Delta h't$. But, because the turbine is not perfect, the actual enthalpy drop Δht is reduced by the turbine efficiency ηt.

$$\Delta ht = \eta t\ (H4-H5') = \eta t\ \bar{C}p45'\ (T4-T5') \qquad \text{BTU/LB} \qquad (2\text{-}52)$$

The work derived from the turbine per pound of gas passed through it is further reduced by mechanical losses such as friction in the bearings. Let Lt be the work produced by the turbine per pound of gas and η_{mt} be the mechanical efficiency.

$$L_t = \eta_{mt} \Delta h_t = \eta_{mt} \eta_t \bar{C}_{p45'} (T_4 - T_{5'}) \qquad \text{BTU/LB} \qquad (2\text{-}53)$$

Typical values for turbine isentropic and mechanical efficiencies are 0.9 and 0.98 respectively.

In the turbojet, the work accomplished by the turbine must be sufficient to equal the work required by the compressor and overcome parasititic losses, L_λ.

$$L_t = \frac{L_c + L_\lambda}{(1-\bar{X})(1+f)} \qquad \text{BTU/LB} \qquad (2\text{-}54)$$

Two factors are introduced in equation (54) to account for changes in the mass flow rate of the system. The first factor (1-X) accounts for the fraction X of the induced air which is bled out of the system and used for cooling, deicing etc. Work of compression is done on this bled air but it is not available to develop turbine work, hence the turbine must develop more work per pound of induced air then ideally required.

The second factor is the fuel to air ratio which admitts to an increase in gas leaving the combustion chamber over that which entered it.

The parasitic load is attributeable to pressure losses and auxillary equipment. Pressure losses consume approximately 0.8 to 1.0 BTU/LB while auxillary equipment takes 0.18 to 0.24 BTU/LB. Bled air fraction X is on the order of .05.

Solving equation (54) permits determination of the adiabatic temperature T5' leaving the turbine by rewritting equation (53).

$$T_{5'} = T_4 - \frac{L_t}{\eta_{mt} \eta_t C_{p45'}} \qquad {}^{o}R \qquad (2\text{-}55)$$

The isentropic temperature facilitates obtaining the adiabatic pressure P5 through the relation of equation (1).

$$P5 = P4\left(\frac{T5'}{T4}\right)^{K45'/(K45'-1)} \qquad \text{LB/ft2} \qquad (2\text{-}56)$$

The actual temperature at state 5 leaving the turbine may be derived from the actual enthalpy change.

$$\Delta ht = \bar{C}p45\ (T4-T5) \qquad \text{BTU/LB} \qquad (2\text{-}57)$$

$$T5 = T4 - \frac{\Delta ht}{\bar{C}p45} = T4 - \frac{Lt}{\eta_{mt}\bar{C}p45} \qquad {}^{o}R \qquad (2\text{-}58)$$

The isentropic enthalpy drop across a perfectly expanded nozzel due to adiabatic expansion to ambient pressure is (H6'-H5) as denoted by the vertical line from state point 5 to 6' in the HS diagram. However, due to nozzel efficiency, some enthalpy is lost to the system as indicated by the dashed line from state point 5 to 6. Let the nozzel efficiency be ηn, then the enthalpy drop across the nozzel becomes

$$\Delta hn = H5-H6 = \eta n\ (H5-H6') = \eta n\ \bar{C}p56'\ (T5-T6') \qquad \text{BTU/LB} \qquad (2\text{-}59)$$

a typical value for the nozzel efficiency is 0.93.

With the use of equation (1) and the assumption that the nozzel is fully expanded, i.e. $P6 = P_o$

$$T6' = T5\left(\frac{P6}{P5}\right)^{(K56'-1)/K56'} = T5\left(\frac{P_o}{P5}\right)^{(K56'-1)/K56'} \qquad {}^{o}R \qquad (2\text{-}60)$$

The specific output or work developed by the nozzel, L, per pound of indicated air becomes

$$L = \Delta hn\ (1-x)(1+f) = \eta n\ \bar{C}p56'\ T5\left[1-\left(\frac{P_o}{P5}\right)^{(K56'-1)/K56'}\right](1-x)(1+f) \qquad (2\text{-}61)$$

The temperature of the exhaust gas leaving the nozzel is

$$T6 = T5 - \frac{\Delta hn}{\bar{C}p56} = T5\left\{1-\eta n\frac{Cp56'}{Cp56}\left[1-\left(\frac{P_o}{P5}\right)^{(K56'-1)/K56'}\right]\right\} \qquad {}^{o}R \qquad (2\text{-}62)$$

The jet velocity is obtained by equating the enthalpy drop to the kenetic energy of the jet stream.

$$\dot{W}g \ \Delta hn = \tfrac{1}{2} \frac{\dot{W}g}{g} Vj^2 \qquad \text{BTU/LB} \qquad (2\text{-}63)$$

where $\dot{w}g$ = Weight flow rate of gas, lbs/sec

Vj = Exit velocity, ft/sec

$$Vj = \sqrt{2g \ \Delta hn} = \sqrt{2g \ \bar{C}56 \ (T5-T6)J} \qquad \text{ft/sec} \qquad (2\text{-}64)$$

The thrust may now be obtained using the momentum equation

$$Fj = \frac{\dot{W}g}{g} Vj - \frac{\dot{W}a}{g} Vo \qquad \text{lbs} \qquad (2\text{-}65)$$

The thrust developed per unit weight of air inducted becomes

$$\frac{Fj}{\dot{W}a} = \left[(1-X)(1+f) \ Vj - Vo\right]/g \qquad \text{lbs/lb} \qquad (2\text{-}66)$$

The specific fuel consumption is

$$\text{Thrust SFC} = \frac{(1-X)\dot{W}af}{Fj} 3600 = \frac{3600 \ g \ f}{(1+f)Vj - Vo/(1-X)} \qquad \text{lbs/hr - lb} \qquad (2\text{-}67)$$

The thermal efficiency as defined by equation (13) is

$$\eta th = \frac{L}{Qi} = \frac{\Delta hn \ (1+f)}{f \ \Delta Hc} = \frac{\bar{C}56 \ (T5-T6)(1+f)}{f(15,936 + 1312x)} \qquad (2\text{-}68)$$

The propulsive efficiency ηp is defined as the ratio of the work accomplished to the work delivered.

$$\eta p = \frac{FjVo}{\dot{W}aL} = \frac{Vo\left[(1-X)(1+f)Vj - Vo\right]}{g \ \bar{C}56 \ (T6-T5)(1-X)(1+f)} \qquad (2\text{-}69)$$

The overall efficiency ηo is simply the product of the thermal and propulsive efficiency.

$$\eta o = \eta th \, \eta p = \frac{Vo \left[(1-X)(1+f)Vj - Vo\right]}{g \ f \ (15936 + 1312x) \ (1-X)} \qquad (2\text{-}70)$$

Equation (66) gives the thrust per unit weight of the inducted into the turbine. Thus, the air flow $\dot{W}a$ may be scaled to yield a given thrust or conversely a given thrust scaled to yield the air flow. This scaling should be done only at static sea level conditions for maximum continuous thrust.

The air inducted may be defined in terms of static ambient density do and and equivalent inlet area Ai and velocity Vi. It must also be equal to the weight flow exiting in the engine after adjustments for bleeds and added fuel.

$$\frac{\dot{W}a}{g} = do\ Ai\ Vi = \frac{dj\ Aj\ Vj}{(1-\mathbf{X})(1+f)} \qquad \text{lb/sec} \qquad (2\text{-}71)$$

With the use of equation (4), the density of the exhaust gasses dj may be obtained with a correction for molecular weights.

$$dj = do\ \frac{to}{Tj}\ \frac{\mathcal{M}(mix)}{\mathcal{M}(air)} \qquad \text{slugs/ft3} \qquad (2\text{-}72)$$

Equation (71) may now be solved for the exit area Aj

$$Aj = \frac{\dot{v}i\ (i-\mathbf{X})(1+f)}{Vj\ \frac{\mathcal{M}(mix)}{\mathcal{M}(air)}\left(\frac{to}{Tj}\right)} \qquad \text{ft2} \qquad (2\text{-}73)$$

where $\dot{v}i$ is proportional to the volumetric flow rate equal to the equivalent inlet area and velocity. It is obtained using the static sea level air weight flow rate at maximum continuous thrust.

$$\dot{v}i = Ai\ Vi = \frac{\dot{W}a\ (SLS)}{g\ \ do\ (SLS)} = 13.1\ \dot{W}a\ (SLS) \qquad \text{ft3/sec} \qquad (2\text{-}74)$$

The ambient free stream parameter a_o, to, P_o, and do vary with the weather and altitude. They are the cause of the variation in performance which will be encountered with environmental changes.

Values for these parameters should be obtained from actual measurements or from tables for standard atmospheres.

A summary of equations which define the turbojet turbine model are given in Figure 2.3 in the form of a branch diagram. This form illustrates the interelation between various parameters from input to output. The ballooned terms are defined by the equations to which their arrows point.

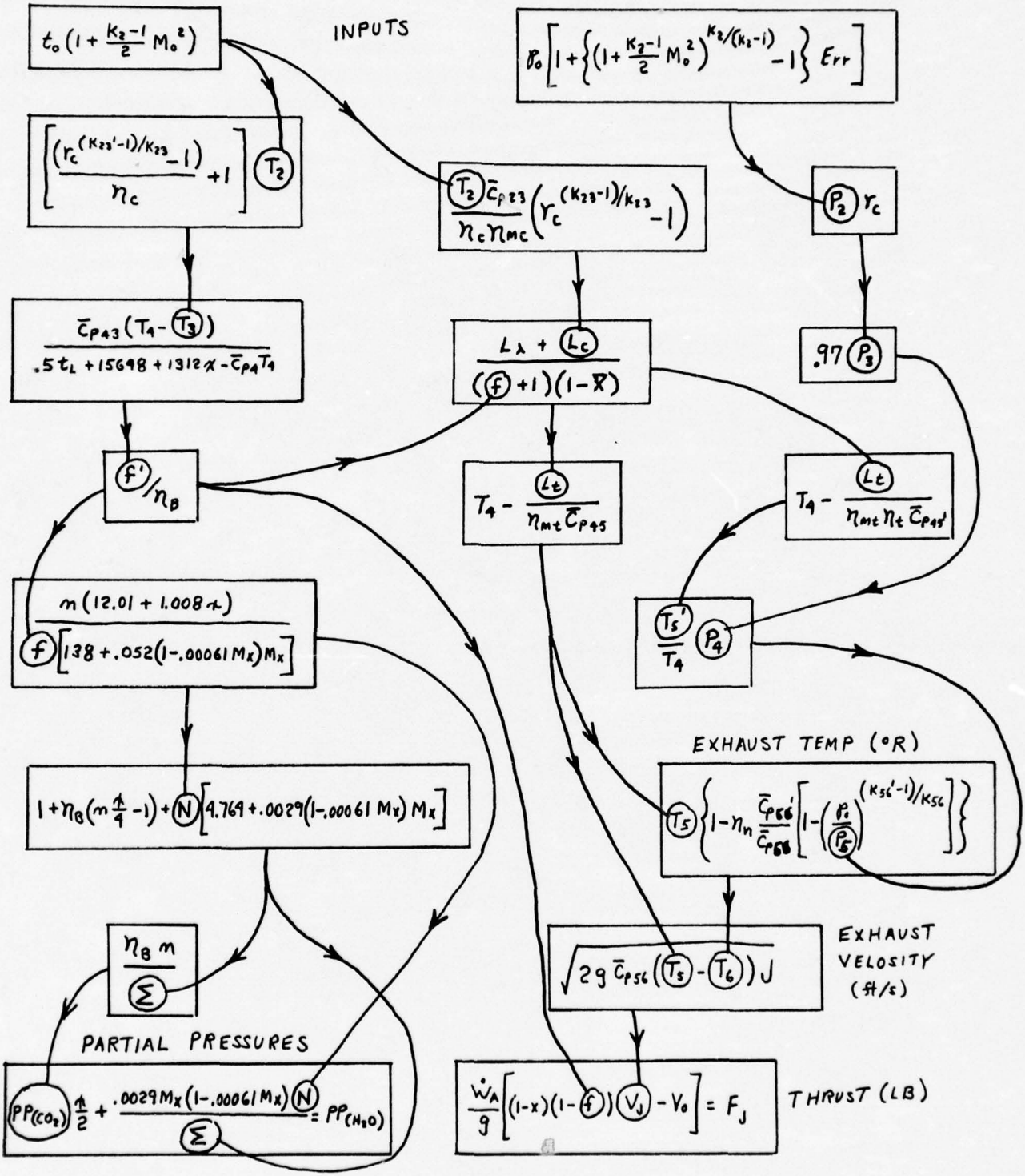

Figure 2.3 Turbojet Model

2.1.3 Turbo Shaft Engine

The turbo shaft engine is similar to the turbojet engine up to the station corresponding to the turbine outlet. At this point, instead of expanding the gas through a nozzel to generate thrust, the gas is expanded through the blades of a power turbine which is mechanically coupled via an output shaft to a propeller in a turbo prop verision or rotor in the helicoper version to generate thrust.

The turbo shaft engine is depicted pictorially in figure 2.4. It may be observed that the difference between the turboshaft and the turbojet in Figure 2.4 is the inclusion of a second turbine and shaft in figure 2.4A, a power turbine PT and load L in Figure 2.4B and one additional thermal dynamic state in Figure 2.4C accounting for the enthalpy drop accross the power turbine.

The enthalpy-entropy diagram of Figure 2.4C illustrates the operational factors included for determining the resultant exit conditions.

The ambient temperature and pressure are entered as state 0. The enthalpy increase due to ram air is shown at state 2', and the ram efficiency shown as a translation to state 2. The compression due to the compressor compression ratio results in an ideal enthalpy increase to state 3', but the compressor efficiency and mechanical efficiency alter this point to state 3. The heating process, being irreversible, moves the operating point along the constant pressure curve to state 4'. The temperature here is determining by the fuel to air ratio and combustion efficiency, but is not allowed to exceed the turbine inlet temperature limit. Pressure losses in the combustion chamber result in a translation to state 4. An enthalpy drop to state 5' is required to provide work for the compressor including any bleed air drained off from the compressor. Due to turbine efficiency and mechanical losses, the operating

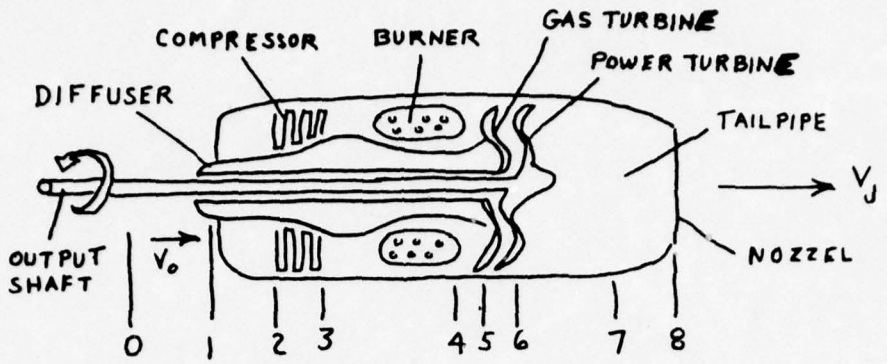

Fig 2.4(a) SKETCH

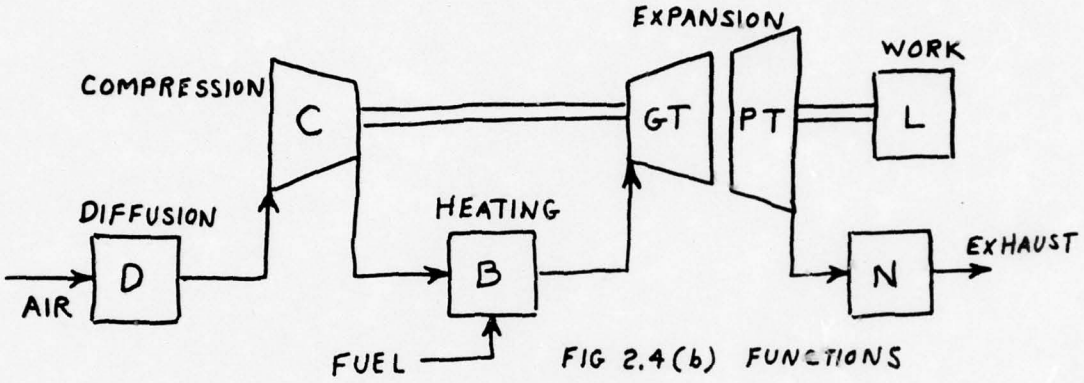

FIG 2.4(b) FUNCTIONS

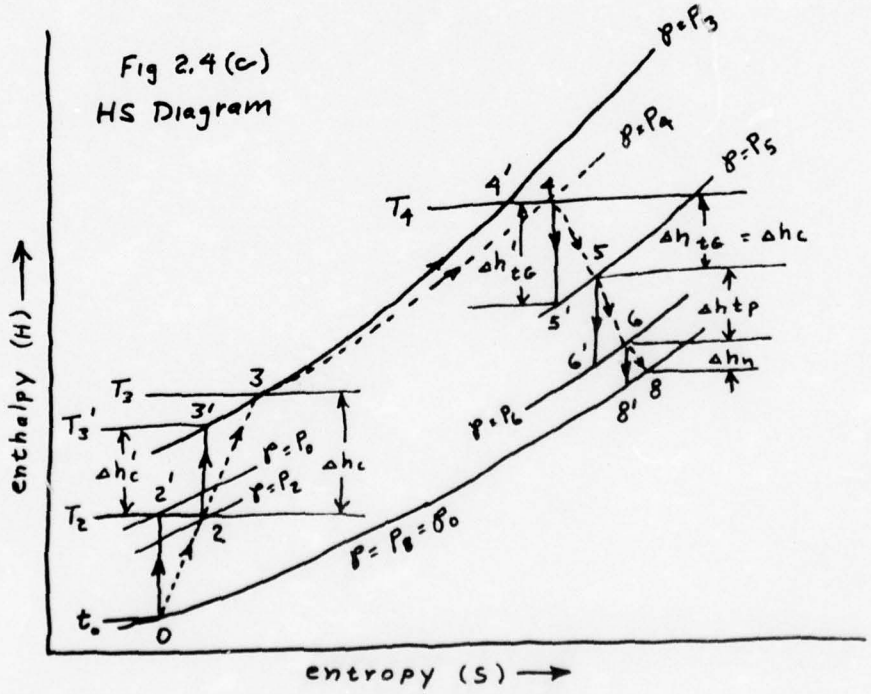

Figure 2.4 Turboshaft Engine

point becomes state 5. An enthalpy drop is then encountered doing work on the power turbine. Turbine efficiency and mechanical losses restrict the shaft horsepower that may be derived from the resultant enthalpy change to state 6. A small state change is then encountered in exhausting the gas through a nozzel with a given efficiency and pressure drop to state 8 or ambient conditions.

All of the turbine input/output parameters which are addressed have been underlined in the above description.

The previous analysis of the turbojet up to and including station 5, the gas turbine outlet, apply to the turboshaft. Thus, the state proporties T5 and P5 are as defined by equations (56) and (58).

The enthalpy drop across the power turbine due to adiabatic expansion is defined as $\Delta h_{s'}$, shown as the vertical line segment 5-6' in figure 2.3. But becuase of isentropic efficiency, it is translated along the dashed line 5-6 and indicated as Δh_s in the figure.

$$\Delta hs = \eta s\ (H5-H6') = \eta s\ \bar{C}p56'\ (T5-T6') \qquad \text{BTU/LB} \qquad (2\text{-}75)$$

The work derived after allowances for mechanical losses, ηms, per pound of gas is

$$Ls = \eta ms\ \Delta hs = \eta ms\ \eta s\ \bar{C}p56'\ (T5-T6') \qquad \text{BTU/LB} \qquad (2\text{-}76)$$

This equation contains two unknown Ls and T6', therefore can not be solved directly, T6' must first be determined. To do this, a constraint on the turbo shaft design must be introduced.

The turbo shaft engine is not intended to generate an significant thrust but must facilitate sufficient pressure drop at the nozzel to exhaust the spent gasses. Let P6 be the pressure required to accomplish this purpose. Then from equation (1)

$$\frac{T6'}{T5} = \left(\frac{P6}{P5}\right)^{(K56'-1)/K56'} \qquad \text{BTU/LB} \qquad (2\text{-}77)$$

Rearranging equation (75) yields

$$\Delta hs = \eta s\ \bar{C}p56'\ T5\left(1 - \frac{T6'}{T5}\right) = \eta s \bar{C}_p 56'\ T5\left[1 - \left(\frac{P6}{P4}\right)^{(K56'-1)/K56'}\right] \text{BTU/LB} \quad (2\text{-}78)$$

which facilitates a solution to equation (76).

Thus the shaft horsepower developed becomes

$$Ws = \frac{\Delta hs}{\eta ms} \quad \frac{788}{550} \times 3600 \qquad hp/hr/Lb\ Gas \qquad (2\text{-}79)$$

where: ηms = Mechanical efficiency of power turbine

788 = Ft - LBS/BTU

550 = FT - LBS/horse power

3600 = SEC/hour

The state temperature T6 may be obtained by equating the actual power turbine enthalpy drop to the actual temperature difference.

$$\Delta hs = \bar{C}p56\ (T5-T6)$$

$$\text{hence}\quad T6 = T5\left\{1 - \eta s \frac{C56'}{C56}\left[1 - \left(\frac{P6}{P5}\right)^{(K56'-1)/K56'}\right]\right\} \qquad (2\text{-}80)$$

The enthalpy drop across the nozzel then becomes

$$\Delta hn = \eta n\ \bar{C}p68'\ (T6 - T8') \qquad \text{BTU/LB} \qquad (2\text{-}81)$$

and from equation (1)

$$\frac{T8'}{T6} = \left(\frac{P8}{P6}\right)^{(K68'-1)/K68'}$$

yielding

$$\Delta hn = \eta n\ \bar{C}p68'\ T6\left[1 - \left(\frac{P8}{P6}\right)^{(K68'-1)/K68'}\right] \quad \text{BTU/LB} \qquad (2\text{-}82)$$

The exhaust temperature T8 becomes

$$\Delta hn = \bar{C}p68\ (T6 - T8)$$

$$T8 = T6\left\{1 - \eta n \frac{\bar{C}P68'}{\bar{C}P68}\left[1 - \left(\frac{P8}{P6}\right)^{(K68'-1)/K68'}\right]\right\} \qquad (2\text{-}83)$$

These values may then be used in equations (64) and (73) to define the exhaust velocity and exit area. The exhaust partial pressures are the same as were defined for the turbojet.

A summary of the turboshaft equations is given in figure 2.5 and a glossary depicting inputs required and outputs generated in presented in Table 2-8 .

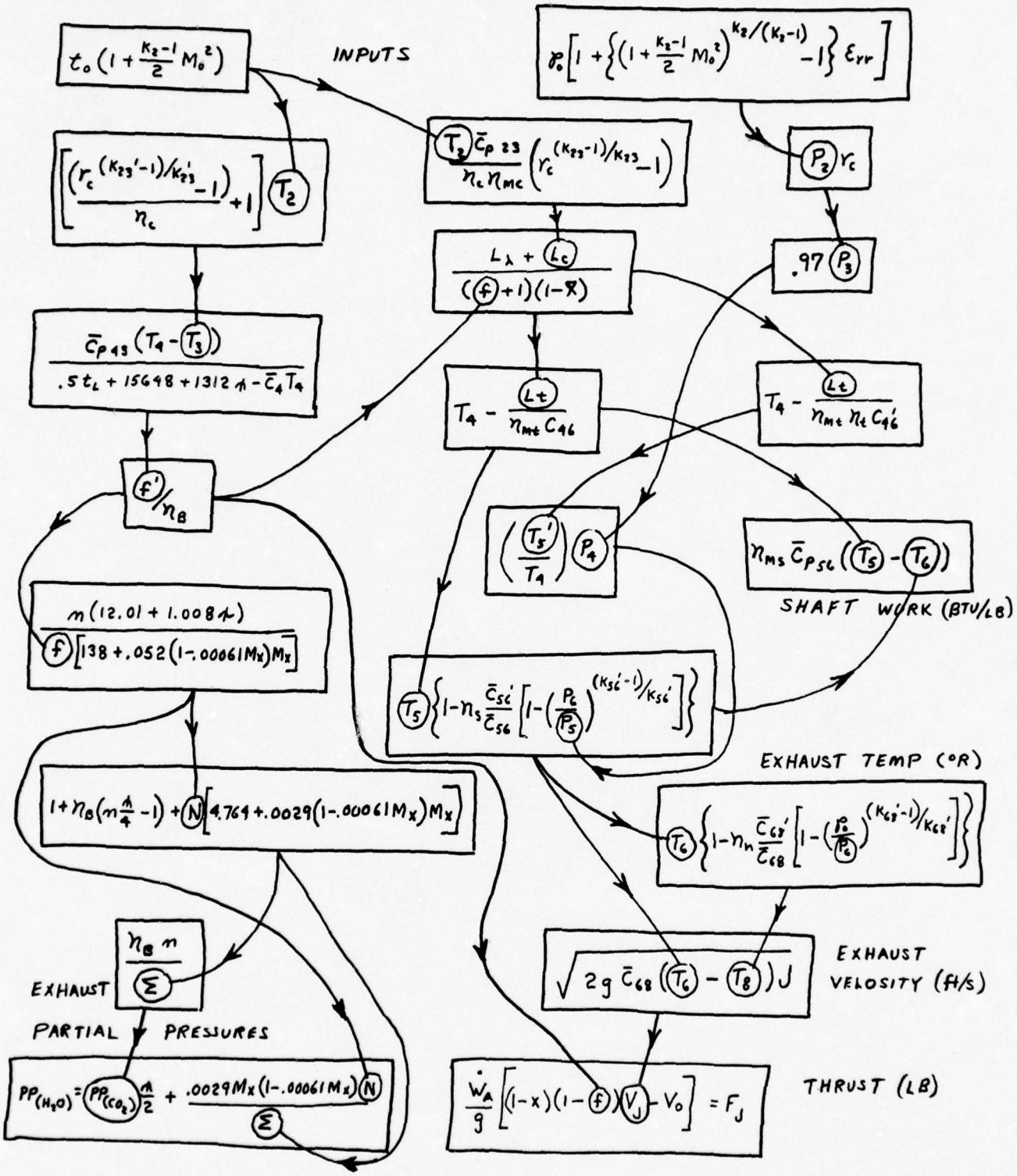

Figure 2.5 Turboshaft Model

Table 2.8 Turbine Glossary

INPUTS

L_s = Shaft work (BTU/LB)

Vo = Free stream velocity (ft/sec)

Mo = Free stream mach number

to = Ambient air temperature (^{o}R)

ρ_o = Ambient air pressure (lbs/ft2)

P6 = Exhaust pressure drop (lbs/ft2)

X = Fraction air bleed off compressor

α = Hydrogen to carbon ratio

t_L = Liquid fuel temperature (^{o}R)

Mx = Water Vapor mixing ratio (gm/Kgm)

ENGINE DATA

W_a = Air flow rate (lbs/sec)

r_c = Compression ratio

E_{rr} = Ram air efficiency

η_t = Gas Turbine efficiency

η_c = Compression efficiency

η_B = Combustion efficiency

η_n = Nozzel efficiency

η_s = Power Turbine efficiency

η_{mt} = Mechanical efficiency of Gas turbine

η_{mc} = Mechanical efficiency of compressor

η_{ms} = Mechanical efficiency of power turbine

L_λ = Parrrasitic losses (BTU/LB)

CONSTANTS

g = Gravitational constant

J = Mechanical equivalent of heat

OUTPUTS

T_j = Exhaust gas temperature (^{o}R)

F_j = Thrust (lbs)

V_j = Exhaust gas velocity (ft/sec)

PP(H2O) = Partial pressure water vapor

PP(CO2) = Partial pressure carbon dioxide

P_j = Exit pressure lb/sgft)

COMPUTED DATA

f = Actual fuel to air ratio

f' = Ideal fuel to air ratio

T = Stagnation temp. (^{o}R)

P = Stagnation pressure (lbs/ft2)

$\overline{C}_p$ = Specific heat (BTU/lb-^{o}R)

K = Specific heat ratio

Lt = Work developed by turbine (BTU/LB)

Lc = Work done on compressor (BTU/LB)

Ls = Shaft work delivered (BTU/LB)

SUBSCRIPTS - State (station) Numbers

PRIMES = Insentropic Values

2.2 PLUME DIFFUSION MODEL

The spreading of the exhaust jet into the main stream air is a turbulent mixing process. It is particularly complicated in the case of the helicopter due to the inclusion of the rotor down-wash and the fact that the free stream may be directed in any angle relative to the exhaust stream. Rigorous diffusion models due not exist which address this complex mix. Therefore, empirically derived relations for the diffusion model have been extracted from Kücheman and Weber "Aerodynamics of Propulsion", McGraw Hill, 1953 - Chapter 10.

The diffusion model is keyed to a velocity distribution of a jet exhaust which has been empirically fitted to measured data and found to agree well with measurements of various observers. This model is described pictorially in Figure 2.6 and was used in this analysis.

The dynamic effect of the moving vehicle on stretching the spatial distribution is also taken into account by the operator lambda, λ , which is the ratio of the free stream to exit velocity.

$$\lambda = \frac{V_o}{V_e} \qquad (2\text{-}84)$$

where

λ = free stream velocity compensation factor

V_o = free stream or vehicle velocity, ft/sec

V_e = exit velocity ft/sec

The model, depicted in Figure 2.6 is seen to contain a core of constant velocity. This core is bounded by a triangular area with a base equal to the exit nozzle diameter and a height equal to six plus exit nozzle diameters depending on the vehicle velocity. The velocity along the axis beyond the core is seen to be proportional to distance from the tip of the core. Thus, the axial or X axis velocity distribution may be described by two conditional equations.

$$V_x = V_e \quad X \leq 6\, D_e / (1 - \lambda) \qquad (2\text{-}85)$$

$$V_x - \frac{6\, D_e}{X}\, V_e + V_o \quad X > 6\, D_e / (1 - \lambda) \qquad (2\text{-}86)$$

where

V_x = velocity on axis, ft/sec

X = distance along axis, ft.

D_e = exit nozzle diameter, ft.

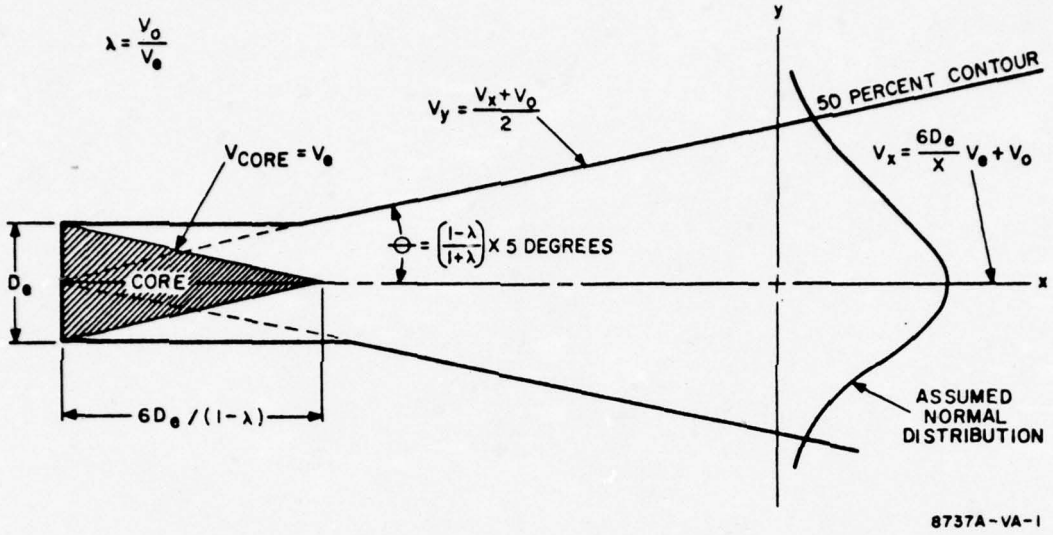

Figure 2.6a Jet Exhaust

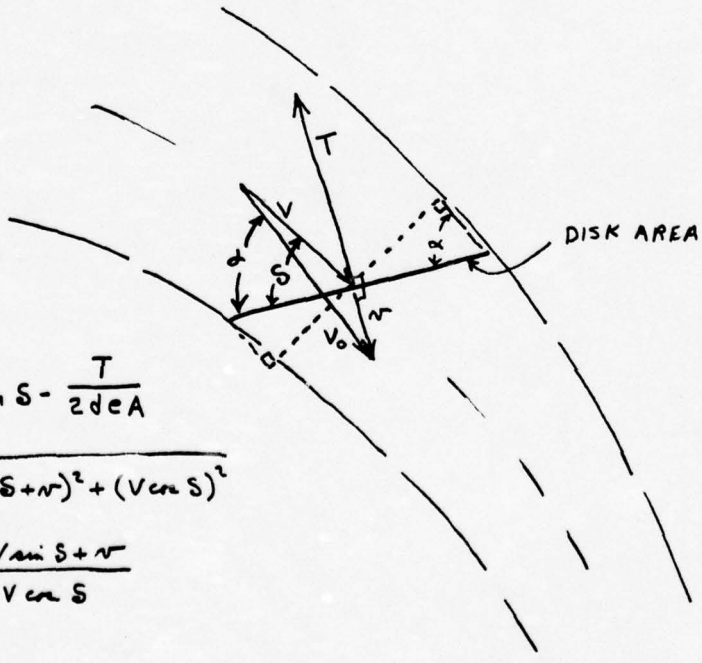

$$v^2 + vV\sin S - \frac{T}{2\rho eA}$$

$$V_e = \sqrt{(V\sin S + v)^2 + (V\cos S)^2}$$

$$\tan\alpha = \frac{V\sin S + v}{V\cos S}$$

Figure 2.6b Main Stream

Figure 2.6 Velosity Models

There is also shown in Figure 2.6 a 50 percent axial velocity contour. For a distance equal to approximately six plus exit diameters, it has a radius equal to the exit nozzle radius. From this point on it is defined by a cone with a vertex located on axis at the exit nozzle and subtending a half angle of five minus degrees depending on vehicle velocity. The radial position of this 50 percent of axial velocity contour or Y axis displacement is defined by the following conditional equations:

$$V_y = \frac{V_x + V_e}{2} \quad Y = Y' \tag{2-87}$$

$$Y' = \frac{D_e}{2} \quad X \leqslant 6\, D_e / (1 - \lambda) \tag{2-88}$$

$$Y' = X \tan \left[5 \left(\frac{1 - \lambda}{1 + \lambda} \right) \right] \quad X \geqslant 6\, D_e / (1 - \lambda) \tag{2-89}$$

The velocity distribution off axis is assumed to be normally distributed for axial distances greater than six plus exit diameters.

$$V_y = V_e + (V_x - V_e) \exp \left(\frac{-1}{2} \frac{Y^2}{\sigma^2} \right) \tag{2-90}$$

The variance, σ^2, for this expression may be obtained by inserting the conditions for the 50 percent contour and solving for sigma (i.e. set $V_y = \frac{V_x + V_e}{2}$ and $Y = Y'$). This yields a standard deviation of

$$\sigma = \frac{Y'}{\sqrt{2 \ln 2}} \tag{2-91}$$

Substituting equation (2-89) into (2-91) and the result into (2-90) and reducing the form yields the off-axis velocity distribution beyond the core vertex.

$$V_y = V_e + \frac{6\, D_e\, V_e}{X} \exp \left[- \ln(2) \frac{Y^2}{X^2 \tan^2 \left(5 \left(\frac{1-\lambda}{1+\lambda} \right) \right)} \right] \tag{2-92}$$

$$X > 6\, D_e / (1 - \lambda)$$

If the main stream is at an angle α to the jet axis, as is the case in the helicopter, it tends to bend the jet gradually into its own direction. The velocity maximum is no longer on the jet axis, but displaced through a normal distance h which depends on the angle of incidence α, distance from the exit x, and the relative stream velocities λ.

To a first order approximation, this displacement may be expressed as

$$h = \alpha \frac{\lambda}{1 + \lambda} X \tag{2-93}$$

The velocity maximum V_M is also reduced as a result of more turbulent mixing. This effect may be expressed as

$$V_M = V_x + .35 \alpha \frac{X}{D_e} \lambda (V_e - V_x) \qquad (2\text{-}94)$$

While these relationships are empirical, they have been derived from the results of many observations and thus do reflect a best fit with measured data. However, the characteristics of the flow field around the helicopter jet may prove to be beyond the bounds of applicability in some operating conditions. This will be borne out in the validation exercises.

2.3 MAIN STREAM VELOCITY

The main stream velocity is the resultant vector sum of the rotor down-wash, flight velocity and wind velocity. It is derived with the aid of Figure 2.6b.

The mass flow of air in unit time may be defined as

$$\dot{m} = de\ Z\ (V \sin S + v) A \qquad \text{lb/sec} \qquad (2\text{-}95)$$

where

$\dot{m}$ = Mass air flow rate, lbs/sec
d = Density, lbs/ft^3
A = Area of rotor disk, ft^2
V = Vector sum of wind and flight velocities, ft/sec
S = Angle between free stream velocity and rotor blade
v = Induced velocity, ft/sec
e = Entrainment factor

The entrainment factor accounts for the air outside the disk being entrained by the rotor action. It is approximated as

$$e = \sqrt{1 + \frac{V^2 \cos 2S}{(V \sin S + v)^2}} \qquad (2\text{-}96)$$

From Newton's second law, which states that force T is equal to the rate of change of momentum,

$$T = \frac{\dot{m}}{g} v_1 = \frac{deA}{g} (V \sin S + v)\ v_1 \qquad \text{lbs} \qquad (2\text{-}97)$$

where v_1 is velocity far down stream.

Also the kinetic energy imparted to the air is

$$KE = \frac{\dot{m} v_1^2}{g\ 2} = deA\ (V \sin S + v)\ V_1^2/2\ g \qquad (2\text{-}98)$$

The rotor induced power is equal to the kinetic energy

$$Tv = KE = deA\ (V\sin S + v)\ v_1^{\ 2}/2\ g \qquad (2\text{-}99)$$

Solving this equation for thrust and equating it to equation (2-97) yields

$$V_1 = 2v \qquad (2\text{-}100)$$

Making this substitution into equation (2-97) gives the induced flow velocity v as

$$v^2 + v\ V \sin S - T/2\ deA = 0 \qquad (2\text{-}101)$$

From Figure 2.6b, the main stream velocity Vo may be computed as

$$Vo = \sqrt{(V \sin S + v)2 + (V \cos S)2} \qquad (2\text{-}102)$$

and the incidence angle as

$$\tan \alpha = \sqrt{\frac{V \sin S + v}{V \cos S}} \qquad (2\text{-}103)$$

These results may be substituted into equations (2-93) and (2-94) to derive the displaced exhaust jet velocity profile.

This assumes that the jet axis is parallel to the plane of the rotor disk. If not, α must be altered accordingly.

The thrust value to be used here is the equivalent shaft load, Ls, used in the turbine model and which is obtained from the air frame specifications as required for the given flight conditions.

2.4 TEMPERATURE DISTRIBUTION

The concentration of each exhaust gas species is defined in terms of the local velocity u = V-Vo and exit velocity u_e = Ve-Vo

$$PP(gas) = PP(gas\text{-}exit)\left[1 - u/ue\right] \qquad (2\text{-}104)$$

The local temperature is also expressed as a velocity function

$$CpT = C_{p\infty}to + (C_{pc}\ Tc - C_{p\infty}to)u/u_e + (u_e - u)u/2 \qquad (2\text{-}105)$$

Where the specific heat may be related to velocity by

$$Cp = (Cpe + Cp\infty)\ (u/u_e) + Cp\infty \qquad (2\text{-}106)$$

These relations in conjunction with the velocity distributions defined in Figure 2.6 are used to compute the spatial distribution of exhaust gas partial pressures and temperatures which will be used in the radiative transfer sub-routine TRANS to calculate the plume emission and transmission. This distribution is also used to determine the fuselage intercepts to obtain the plume heated boom temperature as described in the BODY sub-routine.

3. BODY SUBROUTINE

3.1 Introduction and Approach

This section presents the methodology employed in implementing the BODY subroutine. The BODY subroutine performs four major functions: 1) minor-surface self-determination, 2) line-of-sight ray intercept determination, 3) determination of the obscuration of the plume or body by the various surface elements, and 4) geometrical reconstitution of the various surfaces used to model the helicopter.

BODY performs a minor surface self-determination by subdividing the tail boom into separate surfaces in accordance with the intersecting temperature contours of the plume which are first derived from PLUME.

Once surface temperatures have been established, HIDE calls BODY again to perform the surface reconstitution, determination of obscuration, and the line-of-sight ray intercept tasks.

In performing the line-of-sight ray intercept test, BODY identifies the major and minor surfaces in the line-of-sight, computes the angles of incidence, reflection and the surface normal and the range from the observer to the surface.

The helicopter to be modeled is first disected into major surfaces by selecting and sizing simple geometric planar and conic shapes, which best represent the actual fuselage contour, and assebmling them together in the manner of a 3 dimensional jigsaw puzzle. Figure 3.1 illustrates pictorially an example of such a disection and reconstitution of the AHIG helicopter.

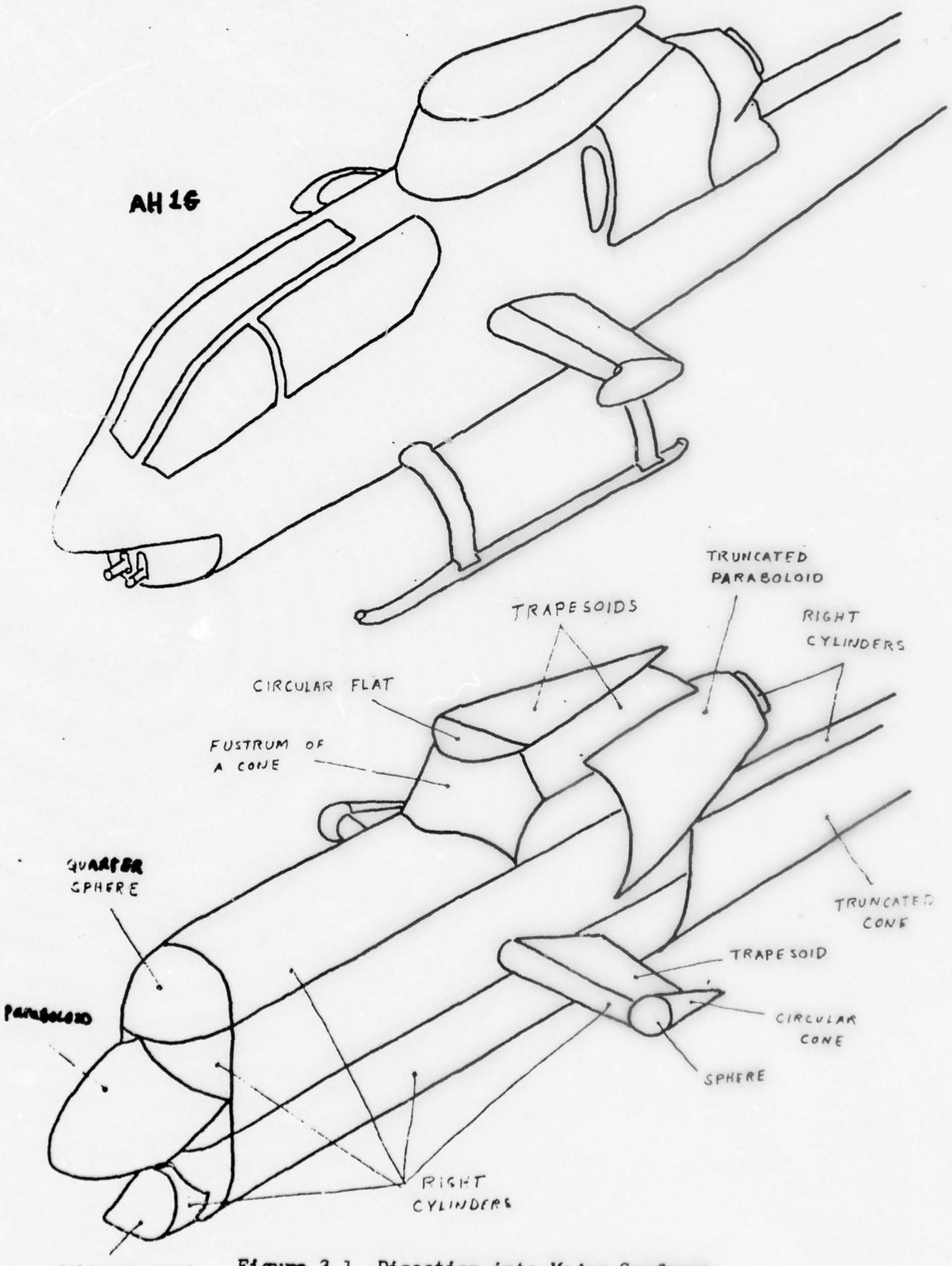

Figure 3.1 Disection into Major Surfaces

This method is patterned after "RAVFAC", which is a computer program developed for NASA by Levin and Lubkowitz of Lockheed for determining the radiation view factors in configuration studies. The program uses symmetric surfaces for which universal intercept geometry may be obtained. This facilitates rapid computer determination of obscuration and shadowing.

The basic shapes currently available are:

Planar Surfaces

- Rectangle
- Disc
- Trapesoid

Conic Surfaces

- Cylinder
- Cone
- Sphere
- Circular paraboloid

Each surface type is defined in terms of its own coordinate system and size factors.

An example of this method used to reconstruct the horizontal stabilizers on the AHIG is shown in Figure 3.2. The construction indicated consists of using rectangular flats for the horizontal surfaces and a right cylinder for the leading edge. The end is terminated with an ice cream cone consisting of a sphere and a cone.

Each basic shape is defined by five size parameters γ, B_{max}, γ_{max}, B_{min}, and γ_{min}. These are illustrated in the surface geometrics shown in the lower portion of the figure. It may be noted that they may represent different dimensions in different shapes. These size factors allow the shapes to be truncated and segmented giving rise to a wide variety of specific geometries.

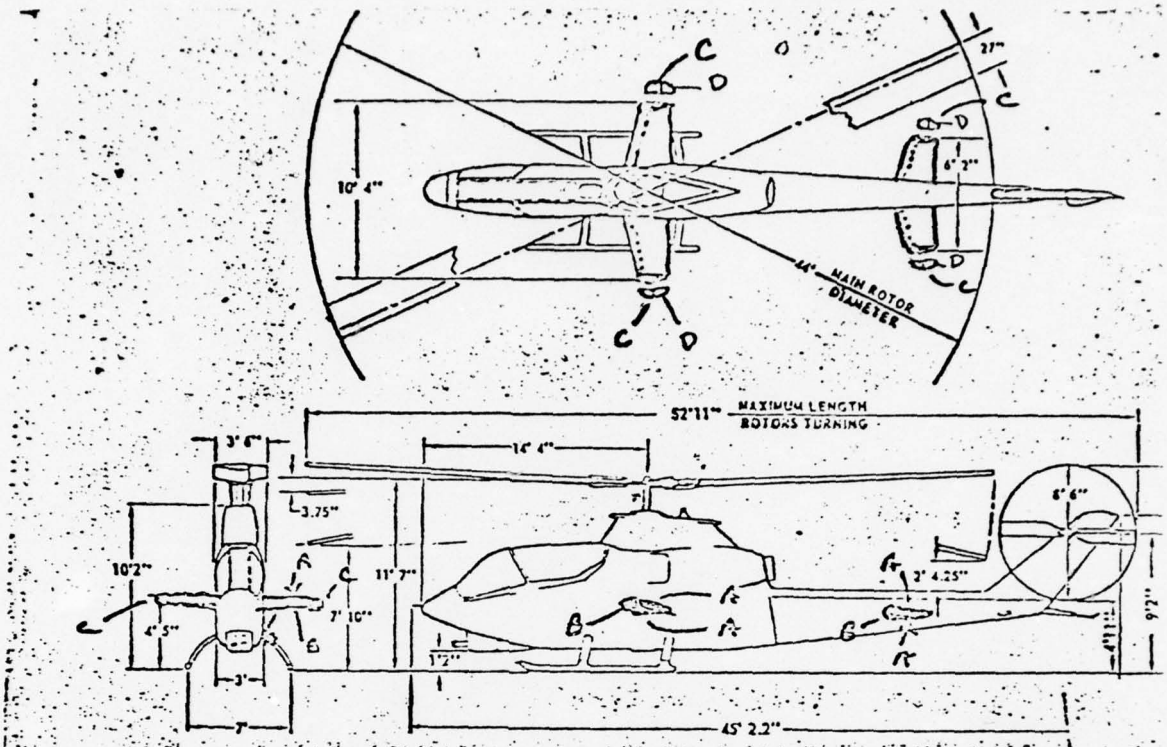

Horizontal stabilizers (4) sets of combinations of right circular cylinders and rectangular flats and hemispherical caps.

20 MAJOR SURFACES

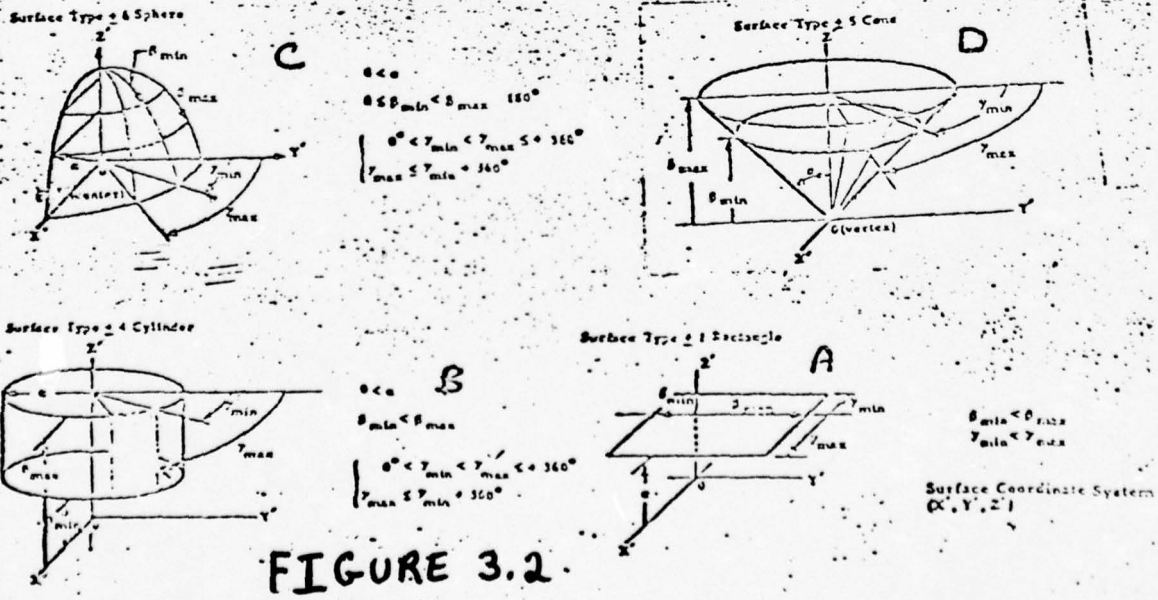

FIGURE 3.2.

Each basic shape is also associated with its own coordinate system and 3 orientation angles. These angles (not shown) allow the surface to be rotated in yaw, pitch, and roll with respect to its local coordinate system so as to become properly alignedin the composite target coordinate system.

In addition, each shape is associated with three location parameters (not shown) which allow the shape to be translated to its proper spatial position in the target coordinate system.

An example of the size, location and orientation data is shown in Figure 3.3, where the surface assemblage for an air-to-air missile is shown. (This example was chosen because of its relative simplicity).

Each major surface is comprised of one or more minor surfaces. Major surfaces are identified by dissimularity of shapes. Minor surfaces are identified by dissimularities in thermal or radiometric characteristics within a given major surface. For example, if a major surface encompasses a heated and unheated compartment, then the major is subdivided at the compartment interface. This facilitates representation of the surface temperature gradient that would occur in the real world. The same criteria is used to define minor surfaces where material differences are encountered, such as wa ll thickness, insulation, windows, emissivity, etc.

Minor surfaces need only be specified by size parameters, since the location and orientation are already contained in the major surface data. Minor surfaces are further assigned the thermal and radiometric parameters:

- Conductivity
- Specific heat
- Thickness (wall)
- Emissivity (Total for radiative transfer)

MISSILE STRUCTURE

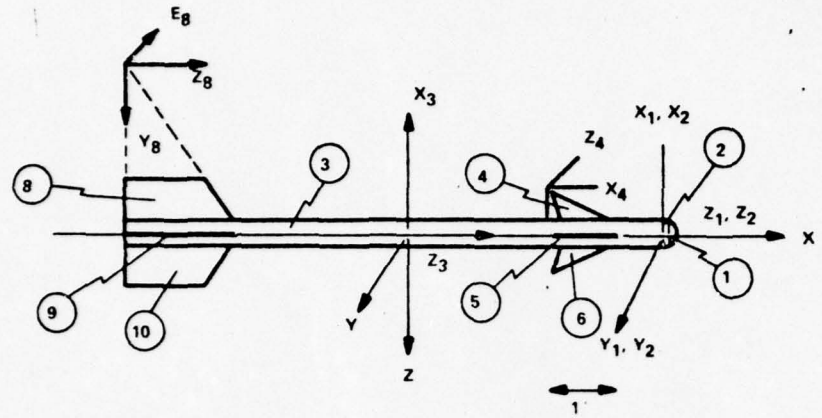

SURFACE NUMBER	SURFACE TYPE	SURFACE GEOMETRY – GEOMETRIC LIMITS (FT, DEG) ALPHA	BMIN	BMAX	GMIN	GMAX	REFLECTIVITY TYPE	SURFACE LOCATION (FEET) RX	RY	RZ	SURFACE ORIENTATION (DEG) PSI	THETA	PHI	SURFACE PARAMETERS	
1	SPHERE	.21	.00	56.40	.00	360.00	0	4.36	.00	.00	.00	90.00	.00	.050	.000
2	SPHERE	.21	56.40	90.00	.00	360.00	1	4.36	.00	.00	.00	90.00	.00	.000	1.000
3	CYLNDR	.21	-4.73	4.36	.00	360.00	1	.00	.00	.00	.00	90.00	.00	.000	1.000
4	TRAPSD	.00	.00	.44	18.00	67.00	1	2.45	.00	-.65	.00	.00	90.00	.000	1.000
5	TRAPSD	.00	.00	.44	18.00	67.00	1	2.45	.65	.00	.00	.00	180.00	.000	1.000
6	TRAPSD	.00	.00	.44	18.00	67.00	1	2.45	.00	.65	.00	.00	270.00	.000	1.000
7	TRAPSD	.00	.00	.44	18.00	67.00	1	2.45	-.65	.00	.00	.00	.00	.000	1.000
8	TRAPSD	.00	1.90	2.59	.00	35.00	1	-4.73	.00	-2.80	.00	.00	90.00	.000	1.000
9	TRAPSD	.00	1.90	2.59	.00	35.00	1	-4.73	2.80	.00	.00	.00	180.00	.000	1.000
10	TRAPSD	.00	1.90	2.59	.00	35.00	1	-4.73	.00	2.80	.00	.00	270.00	.000	1.000
11	TRAPSD	.00	1.90	2.59	.00	35.00	1	-4.73	-2.80	.00	.00	.00	.00	.000	1.000

S71-1434-VA-8

FIGURE 3.3 TYPICAL DATA SET

- o Absorbtivity (Total for solar heating)
- o Reflectivity type (Directional function for spectral emission and reflection)

Minor surfaces are also defined automatically by the computer. The exhaust plume will heat different portions of the tail boom, depending on flight conditions. Therefore, the spatial distribution of the plume gas temperature is predeterminedin the subroutine PLUME. The intersection of constant temperature plume contours with the boom are used to define minor surfaces of the boom. These surfaces are then assigned the value of the plume gas temperature they are in contact with. This procedure is called "self determining surface definition."

The coordinate system for the line of sight geometry is illustrated in Figure 3.4.

The target is positioned in a body centered coordinate system as indicated by the X, Y, Z axes. The target center of gravity is located at the origin. All angles and ranges are taken relative to this coordinate system.

A hypothetical image mosaic is then postulated consisting of J by K elements. This mosaic is positioned such that a perpendicular taken from the mosaic center of coordinates, J and K axes, would intercept the target center of coordinates, namely, its center of gravity. This perpendicular is referred to as the mosaic line of sight centerline. Target attitude is defined by the direction angles of this centerline relative to the target coordinate system.

The image mosaic elements are located on centers separated in both the J and K directions by the spatial dimension S. This represents the projection of the resolution element in microradians at the plane of the target. A ray is

FIG. 3.4 LOS RAY INTERCEPT GEOMETRY

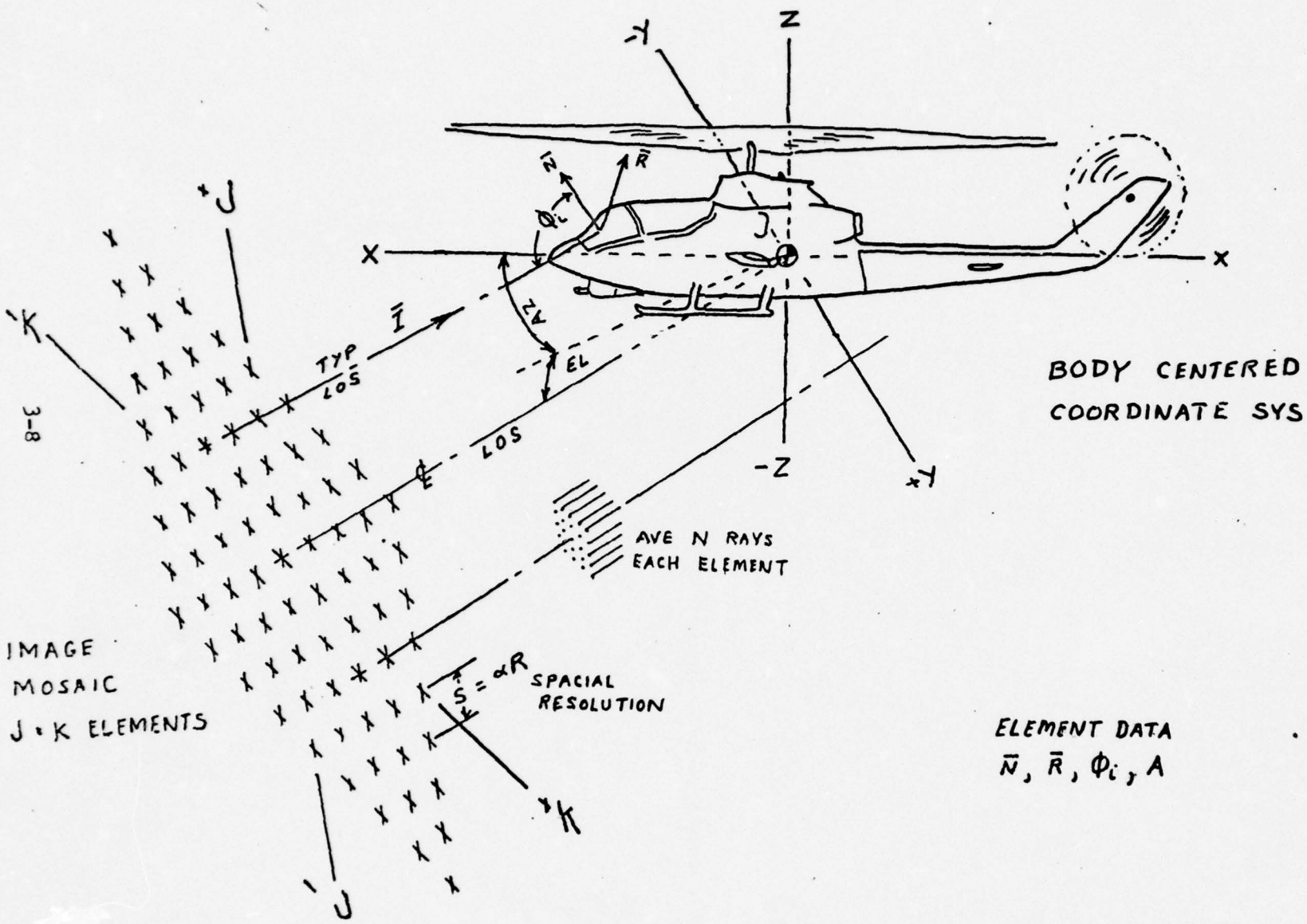

projected from each mosaic element center parallel to the centerline into the plane of the target. If it intercepts the target, the geometry is solved to obtain the angle of incidence; the surface type intercepted; and the unit vectors for the surface normal, reflected and incident rays. This data is required to compute the reflected and emitted radiation from each surface element. If the ray does not intercept the target, this is taken note of and assigned a background value at a later stage.

Each mosaic element is further subdivided into N rays. The computations described above are carried out for each sub-element ray and the results averaged and assigned as a single value to the parent mosaic element. In this manner, two aspects of resolution are accounted for, one being the resolution of the image mosaic which must be carried in storage and is relative only to the sensor resolution and the other is the sub-element resolution which is relative to the finesse of the target detail lying within the projection of the mosaic resolution element which assures obtaining a reasonable representation of target signal.

Only the major surfaces are searched for intercepts initially. If two or more surfaces are intercepted, then only the closest surface to the receiver is used. This accounts for obscuration and also permits surfaces to be nested one within the other, since only the outer-most surface will be used. After the major surface has been determined, the minor surfaces within the major are searched for the intercepted one. This two step search, major then minor, minimizes machine time.

The unit vectors are obtained at the point of interception for the angle of incidence, angle of reflection, and surface normal. These angles are entered into a temporary buffer, along with the minor surface identification, and

its attendent characteristic data. These data are then used by other subroutines to eventually determine the apparent effective radiance of the surface element. This value is then brought back and assigned to the corresponding spatial mosaic element.

3.2 Preparation of Input Data for BODY

The discussion here will describe the details of the procedure for preparing or generating helicopter structural modeling data to be used as input to BODY. Structural modeling is defined as simply the technique of combining various conic and planar surfaces through the use of solid analytic geometry and Ealer angle transformations to represent a helicopter structurally.

A set of "drawn-to-scale" three view drawings of the helicopter of interest is required (such as illustrated by Figure 3.5). One then outlines particular sections that are to be approximated by various geometrical surfaces which will provide the best fit. In general, one tries to approximate the major (most pronounced) sections of the helicopter. Every effort is made to use as few properly oriented surfaces as possible. This is because the computer processing time is roughly proportional to the number of surfaces employed.

Further, one should try to approximate the section of interest with the simplest surface. For example, given a choice between approximating the helicopter's rotor with a flat circular disc or an ellipsoid properly defined, one might want to give greater weight to the circular disc, because of its simple representation. On the other hand, one wants to maintain the proper significiance or surface pronounciation. That is, using the above cited example, one would want to make sure he does not select the simpler surface at the expense of not incorporating the proper surface pronounciation afforded by the rotor.

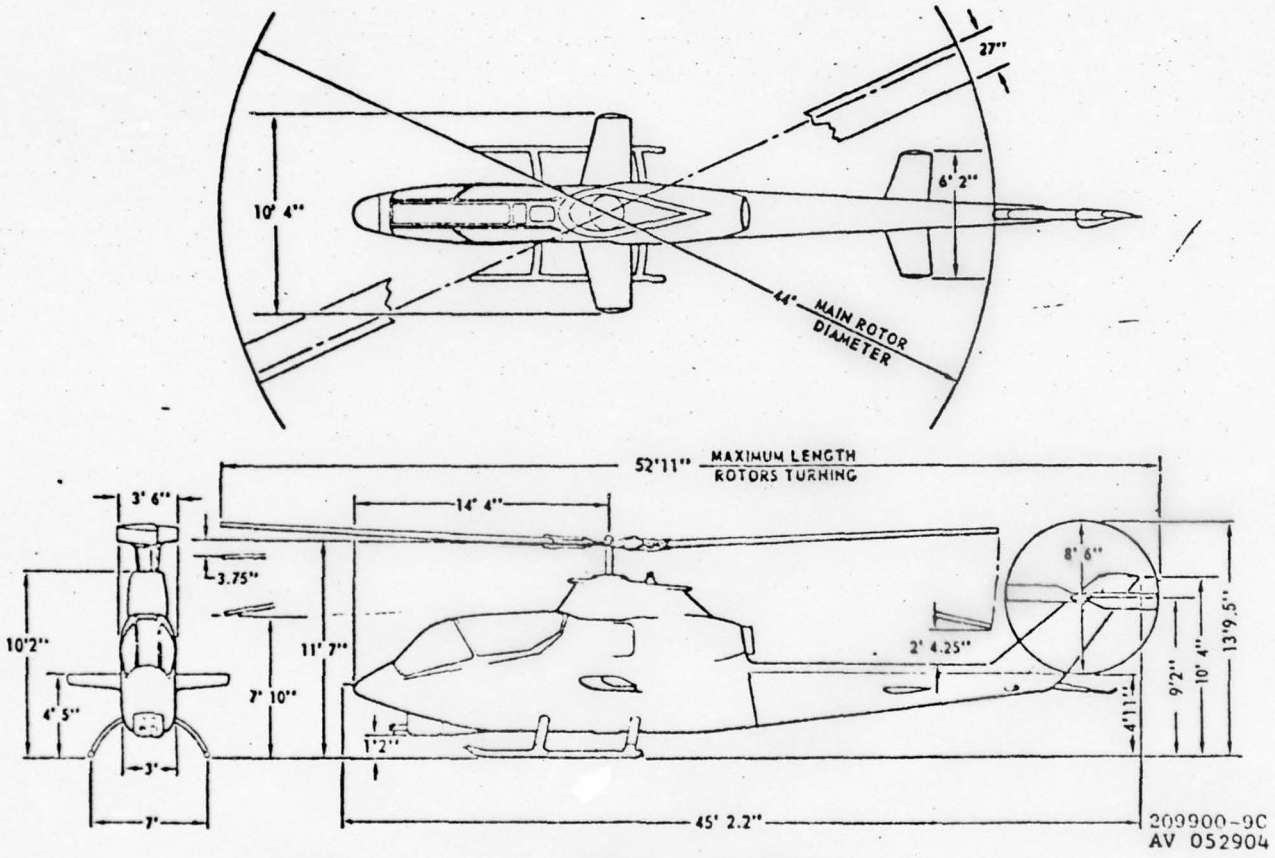

FIGURE 3.5 AH-1G PLAN VIEW

The surface geometries used are those illustrated in Figure 3.6 which were developed for configuration studies. These surfaces lend themselves to universal intercept solutions required later in the model which reduces computer search time. Other geometries can be generated but the impact of their intercept solutions on computation time should be considered.

The best procedure is to make transparent templates of a series of sizes of each basic geometric shape. The template should include grid lines. Figure 3.7 is an example of a cone surface template. By superimposing the template over the plan view the best shape fit is easily obtained and the size factors read directly off the template. The actual size parameters may then be obtained by multiplying by the scale factor ratio between the template grids and the plan view drawing.

Utilization of these simple symetric geometries also facilitates fabrication of cardboard models which may be used to gain visualization of the computer representation.

3.2.1 Major Surfaces

An example of the above procedure is illustrated in figures 3.8 through 3.19 where an AH-1G has been directed into 52 major surface elements. For clarity the plan view of figure 1 has been reproduced in each case and the surface being fitted identified with heavy outlines. The specific surface is identified at the top of the drawing and the geometric shape representing it is shown below.

The surfaces shown represent the least separatable geometric shapes into which the helicopter can be resolved. They therefore are called major surfaces.

Each geometric surface type is associated with its own coordinate system (SCS), and truncation indicies. This is patterned after the "RAVFAC" Computer Program.

Surface Type ± 1 Rectangle

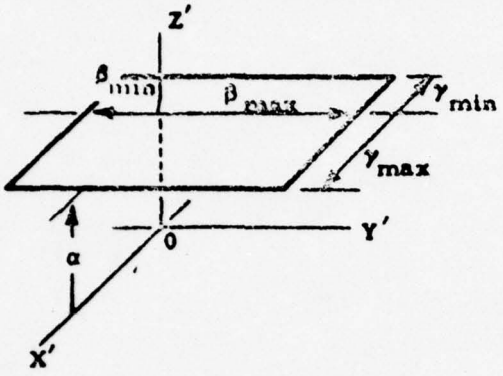

$\beta_{min} < \beta_{max}$
$\gamma_{min} < \gamma_{max}$

Surface Coordinate System
(X', Y', Z')

Surface Type ± 2 Disc

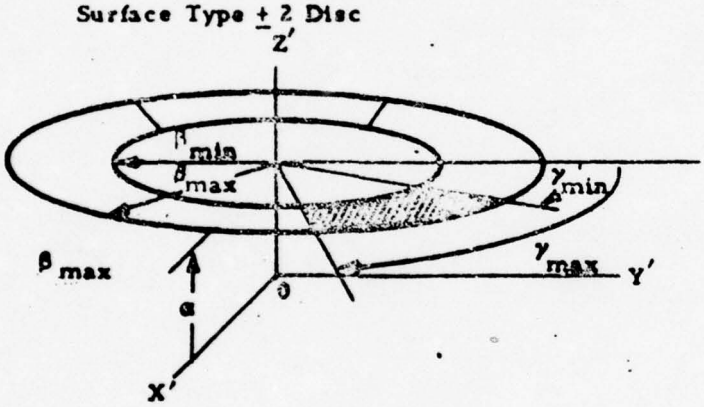

$0 \leq \beta_{min} < \beta_{max}$

$0^\circ < \gamma_{min} < \gamma_{max} \leq +360^\circ$
$\gamma_{max} \leq \gamma_{min} + 360^\circ$

Surface Type ± 3 Trapesoid

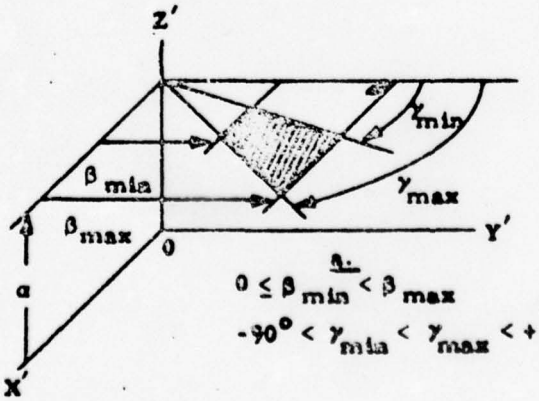

a.

$0 \leq \beta_{min} < \beta_{max}$
$-90^\circ < \gamma_{min} < \gamma_{max} < +90^\circ$

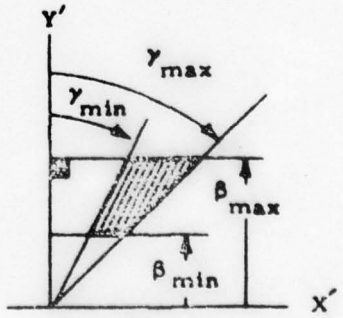

b.

$\beta_{min} < \beta_{max} \leq 0$
$+90^\circ < \gamma_{min} < \gamma_{max} < +270^\circ$

Fig. 3.6 Input Surface Types (Sheet 1)

Surface Type ± 4 Cylinder

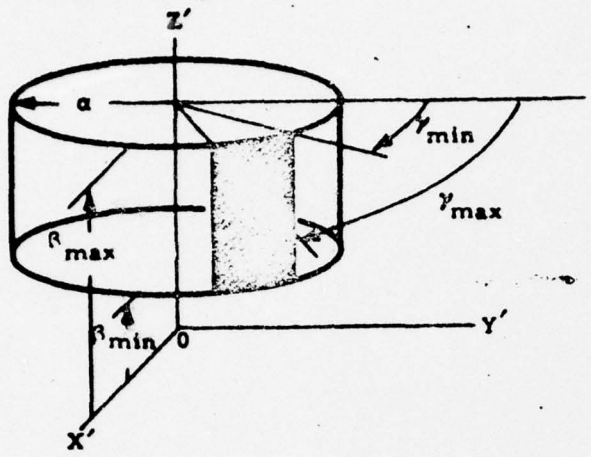

$0 < \alpha$

$\beta_{min} < \beta_{max}$

$$\begin{cases} 0^\circ < \gamma_{min} < \gamma_{max} \leq +360^\circ \\ \gamma_{max} \leq \gamma_{min} + 360^\circ \end{cases}$$

Surface Type ± 5 Cone

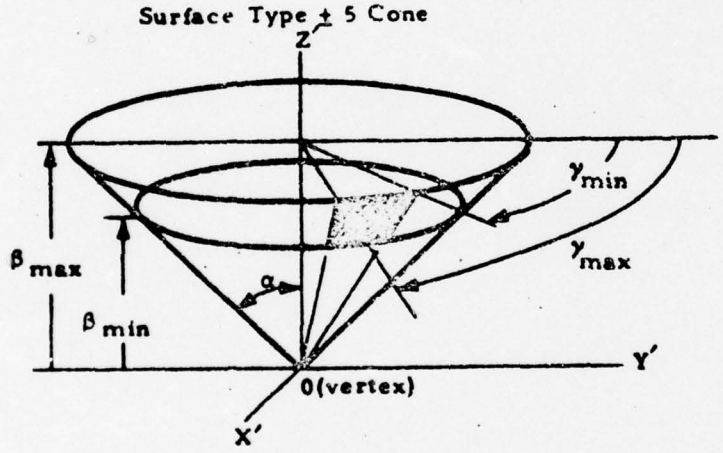

$0 < \alpha$

$0 \leq \beta_{min} < \beta_{max}$

$$\begin{cases} 0^\circ < \gamma_{min} < \gamma_{max} \leq +360^\circ \\ \gamma_{max} \leq \gamma_{min} + 360^\circ \end{cases}$$

Surface Type ± 6 Sphere

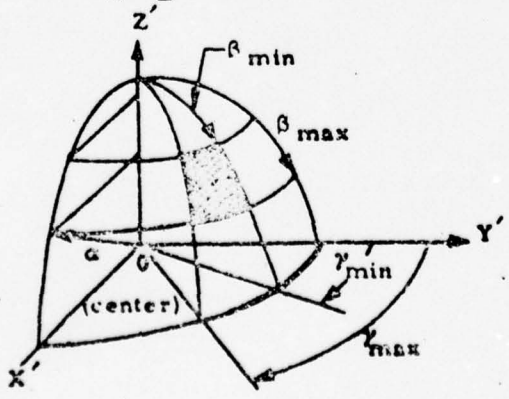

$0 < \alpha$

$0 \leq \beta_{min} < \beta_{max} \quad 180^\circ$

$$\begin{cases} 0^\circ < \gamma_{min} < \gamma_{max} \leq +360^\circ \\ \gamma_{max} \leq \gamma_{min} + 360^\circ \end{cases}$$

Fig. 3.6 Input Surface Types (Sheet 2)

Surface Type ± 7 Circular Paraboloid

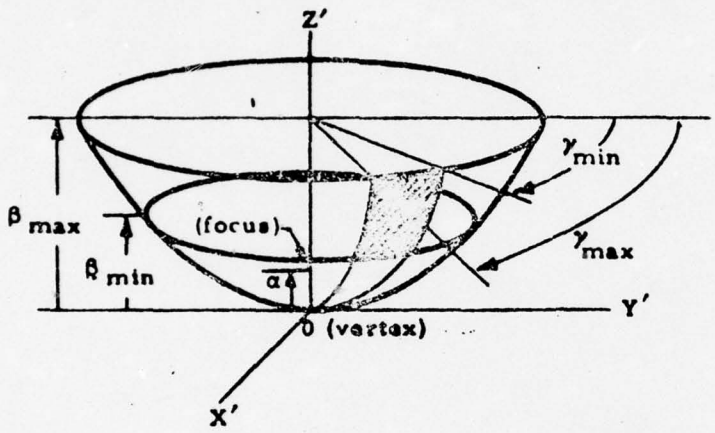

$$0 < \alpha$$

$$0 \leq \beta_{min} < \beta_{max}$$

$$\begin{cases} 0^\circ < \gamma_{min} < \gamma_{max} \leq +360^\circ \\ \gamma_{max} \leq \gamma_{min} + 360^\circ \end{cases}$$

Fig. 3.6 Input Surface Types (Sheet 3)

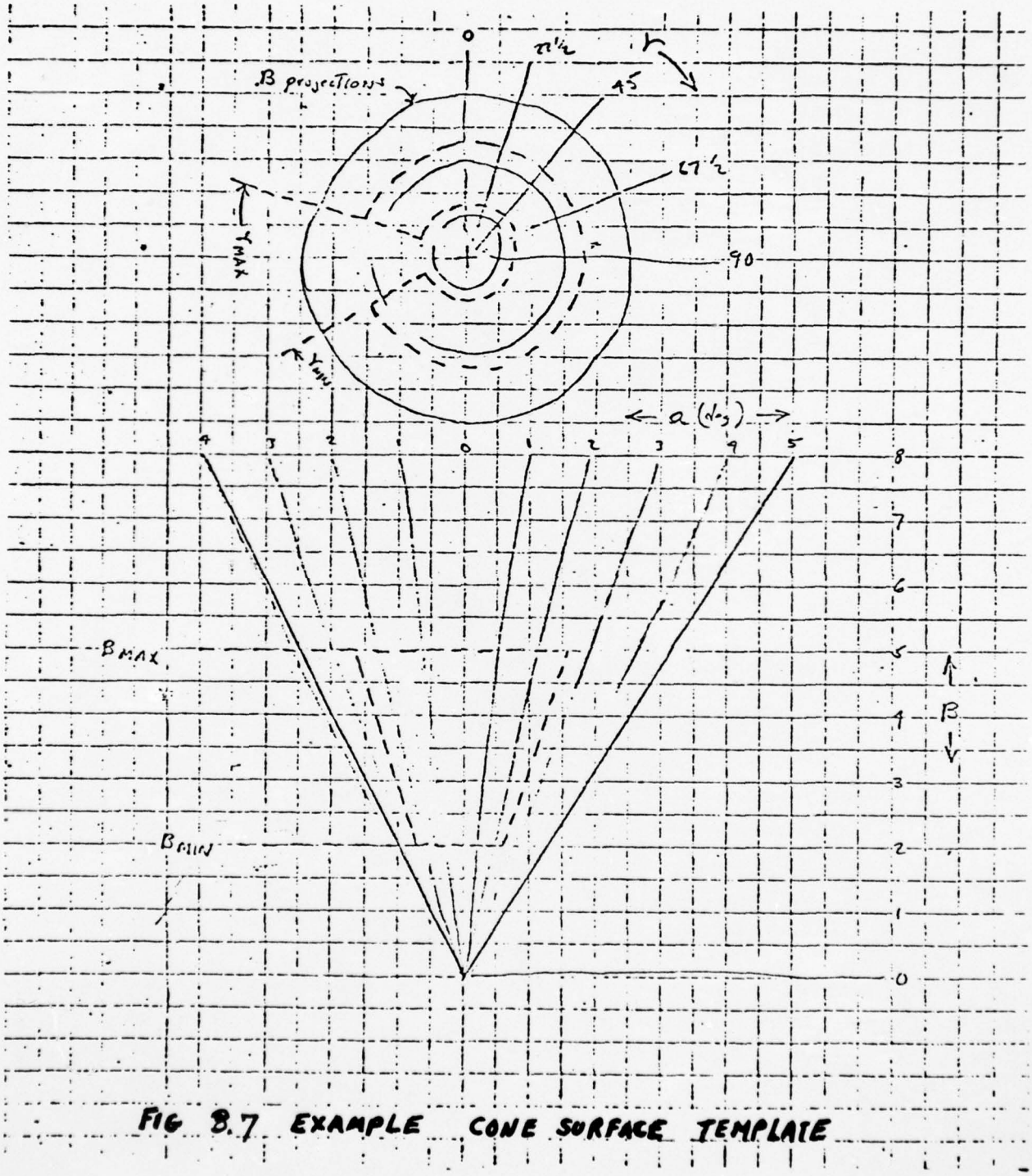

FIG 8.7 EXAMPLE CONE SURFACE TEMPLATE

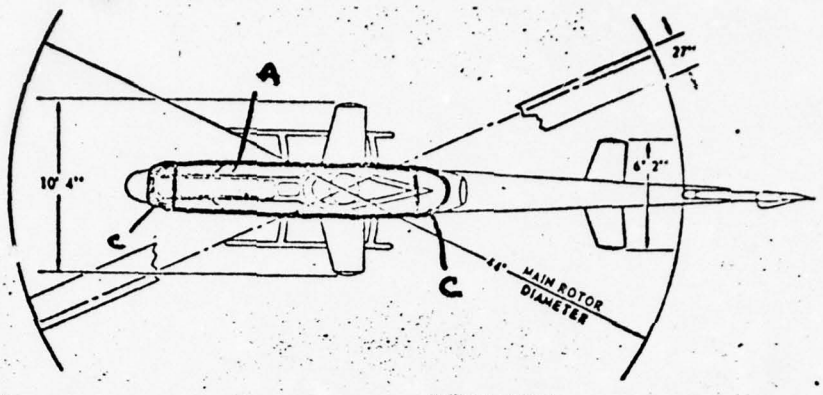

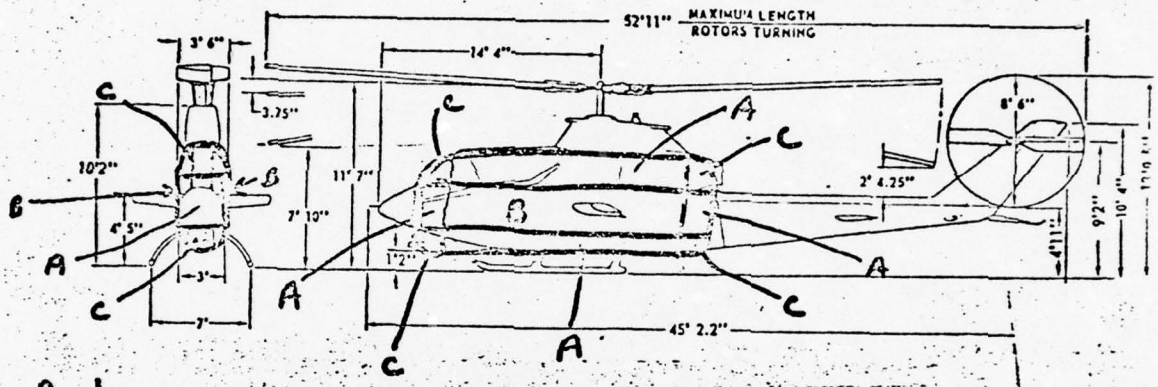

Body

10 MAJOR SURFACES

A (4) right cylinders

B (2) rectangular flats

C (4) quarter spheres

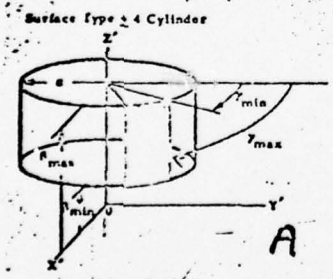

$0 < a$

$\beta_{min} < \beta_{max}$

$0° < \gamma_{min} < \gamma_{max} \leq + 360°$

$\gamma_{max} \leq \gamma_{min} + 360°$

F1

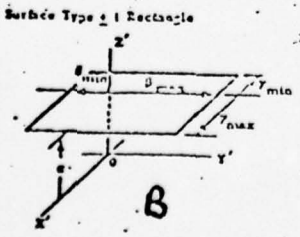

$\beta_{min} < \beta_{max}$

$\gamma_{min} < \gamma_{max}$

Surface Coordinate System (X', Y', Z')

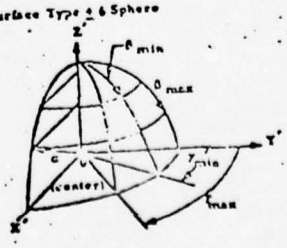

$0 < a$

$0 \leq \beta_{min} < \beta_{max} \leq 180°$

$0° < \gamma_{min} < \gamma_{max} \leq + 360°$

$\gamma_{max} \leq \gamma_{min} + 360°$

Fig 3.8 - BODY SECTION

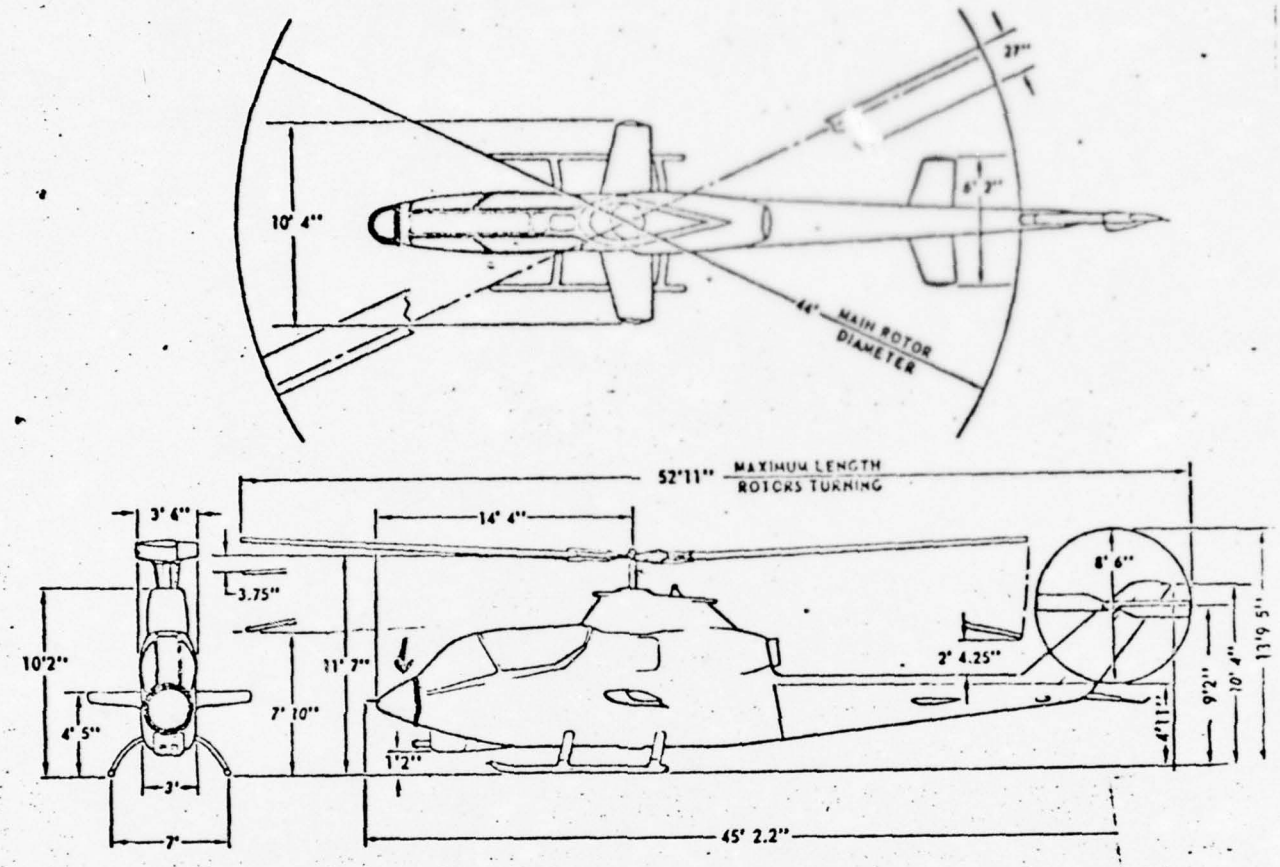

NOSE SECTION paraboloid

1 MAJOR SURFACE

Surface Type ± 7 Circular Paraboloid

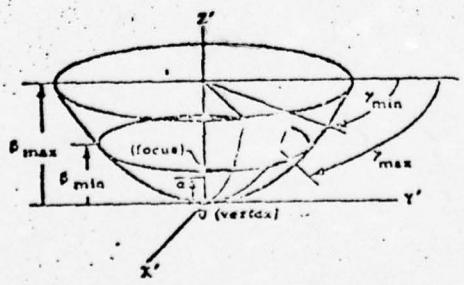

$0 < a$

$0 \leq \beta_{min} < \beta_{max}$

$\begin{cases} 0^\circ < \gamma_{min} < \gamma_{max} \leq +36 \\ \gamma_{max} \leq \gamma_{min} + 360^\circ \end{cases}$

FIGURE 3.9 NOSE SECTION

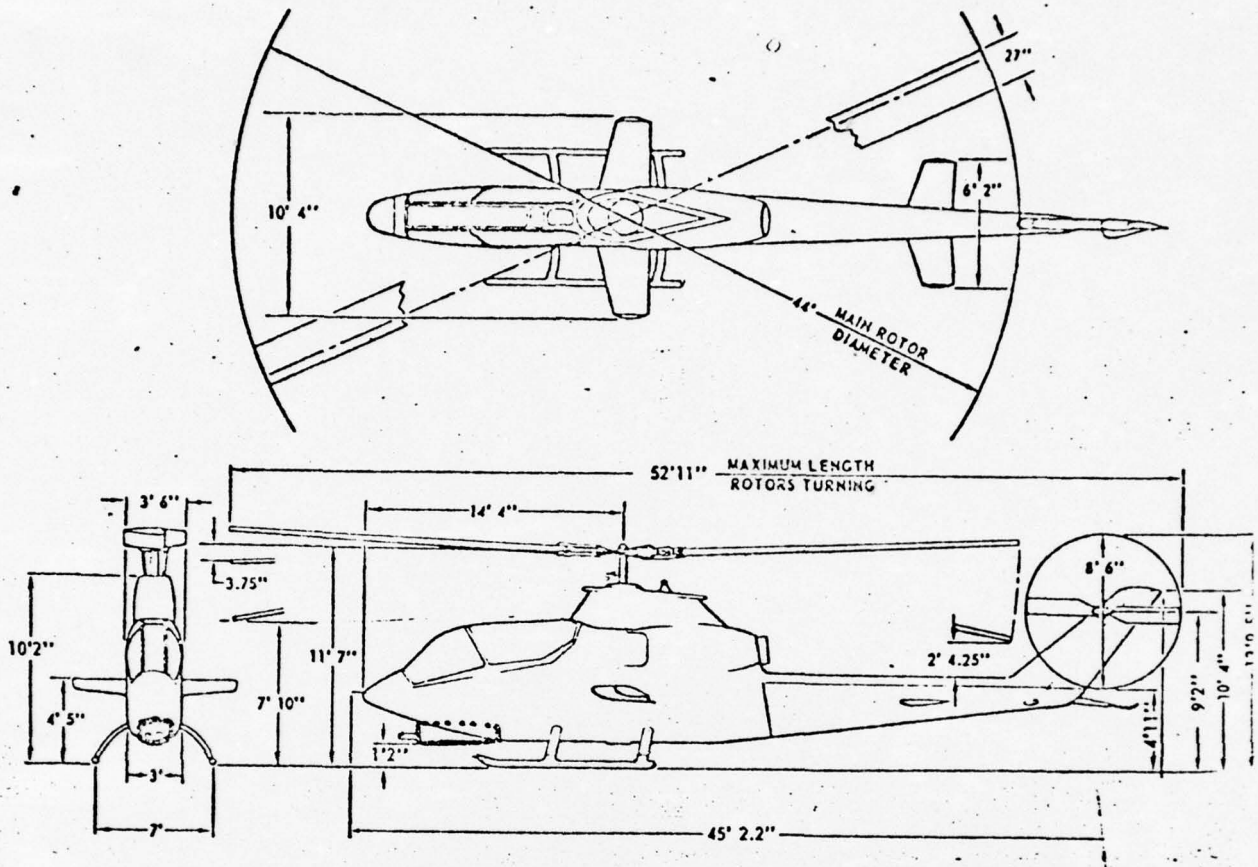

GUN BAY right cylinder

1 MAJOR SURFACE

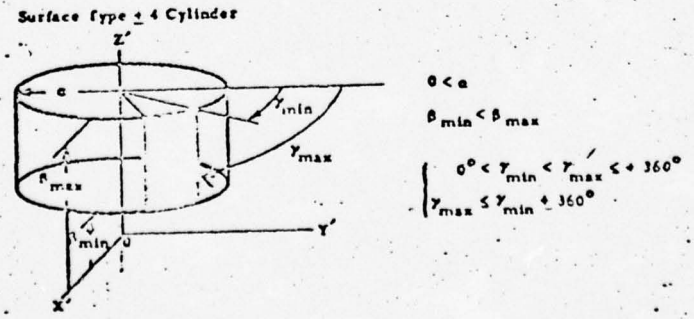

FIGURE 3.10. GUN BAY

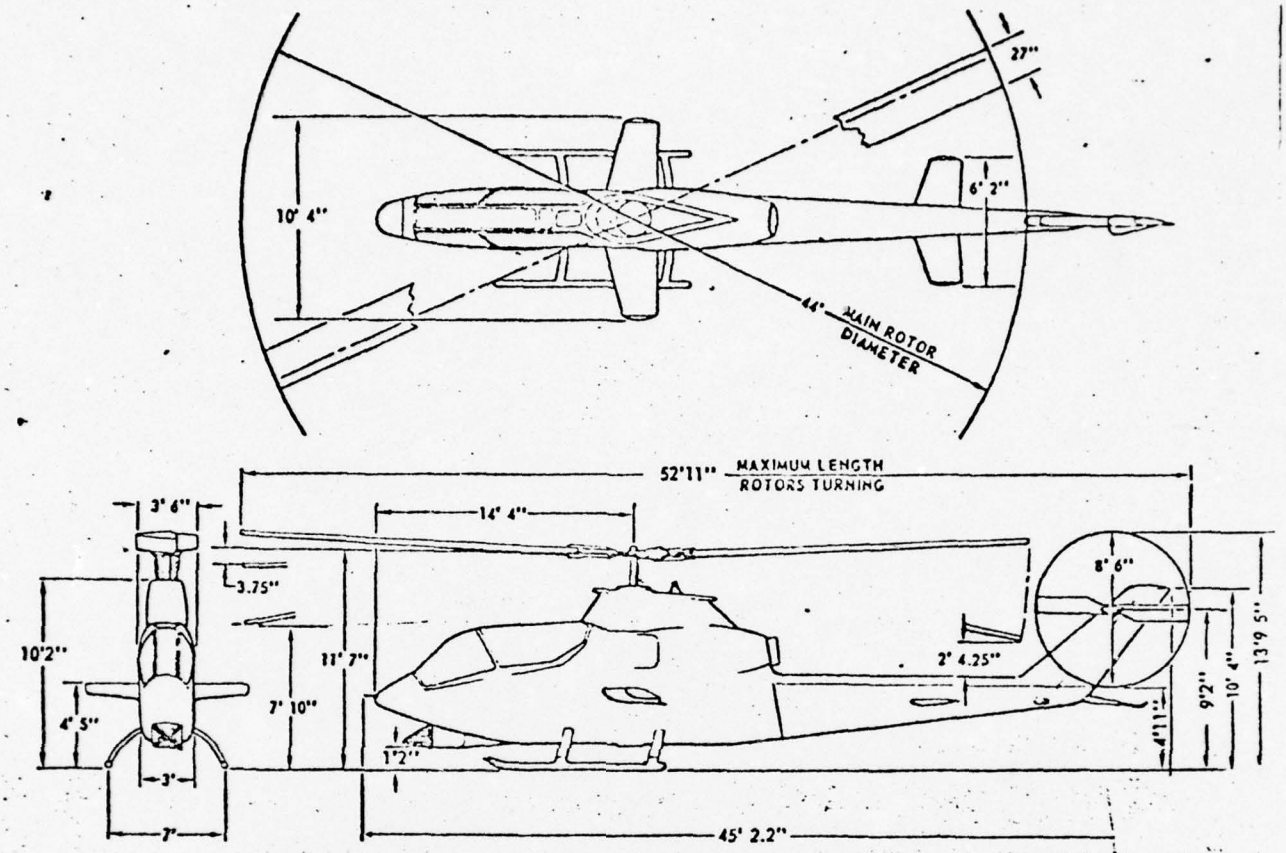

GUN circular cone

1 MAJOR SURFACE

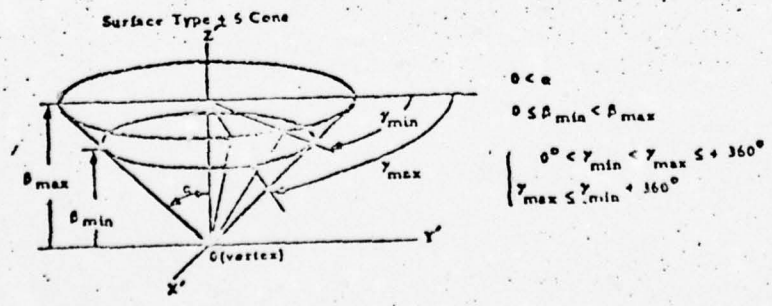

FIGURE 3.11 GUN

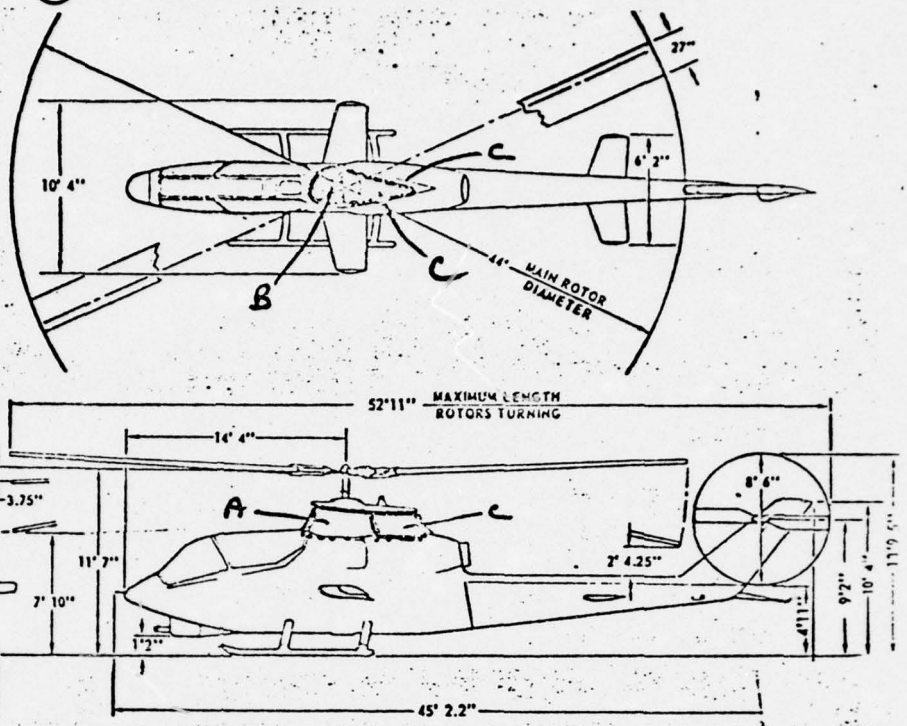

ROTOR HUB

5 MAJOR SURFACES

A Frostrom of a cone

B hemispherical flat

C Triangular flat

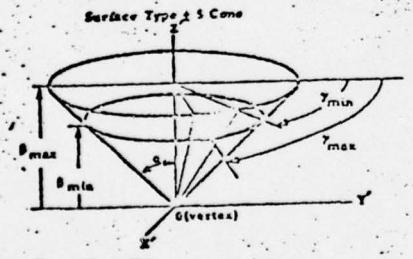

A

$0 \leq \beta_{min} < \beta_{max}$

$0° < \gamma_{min} < \gamma_{max} \leq + 360°$

$\gamma_{max} \leq \gamma_{min} + 360°$

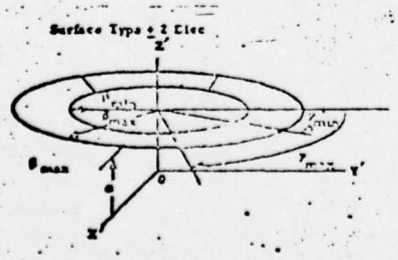

B

$0 \leq \beta_{min} < \beta_{max}$

$0° < \gamma_{min} < \gamma_{max} \leq °$

$\gamma_{max} \leq \gamma_{min} + 360°$

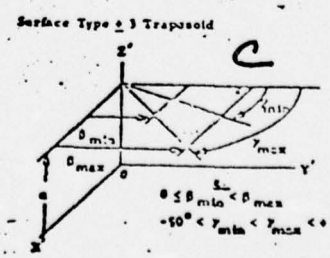

$0 \leq \beta_{min} < \beta_{max}$

$-50° < \gamma_{min} < \gamma_{max} < + 90°$

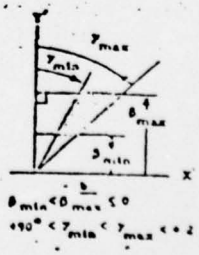

$\beta_{min} < \beta_{max} \leq 0$

$+90° < \gamma_{min} < \gamma_{max} < + 2$

FIG 3.12 ROTOR HUB

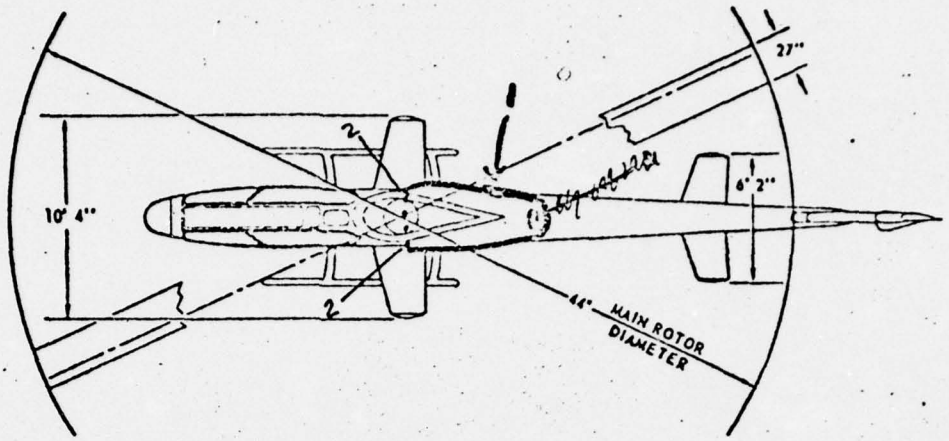

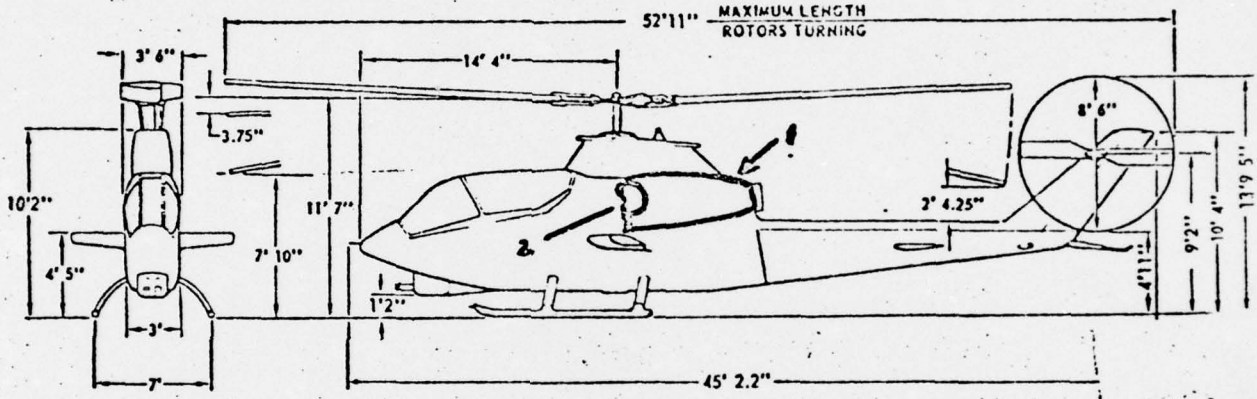

ENGINE COMPARTMENT & AIR INTAKE DUCT

1 Truncated paraboloid 2 paraboloid

3 MAJOR SURFACES

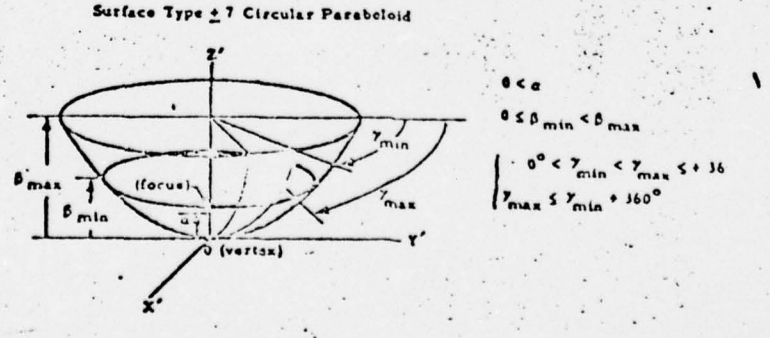

FIGURE 3.13 ENGINE COMPARTMENT

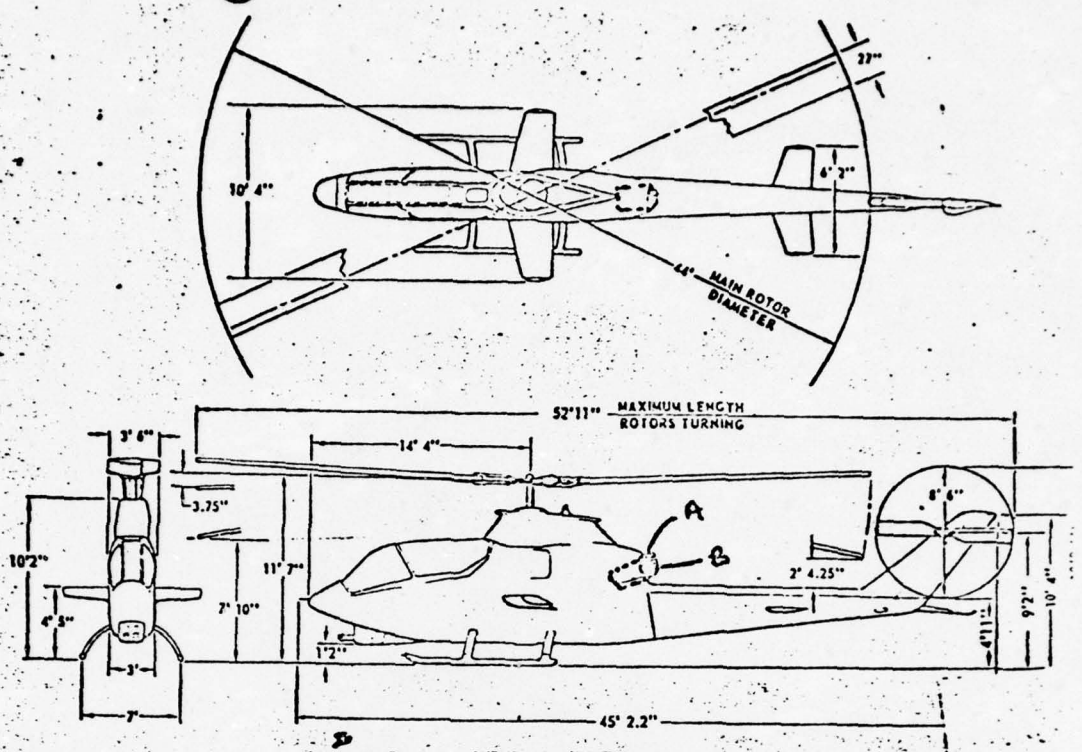

TAIL PIPE

2 MAJOR SURFACES

B right circular disk

A right circular cylinder

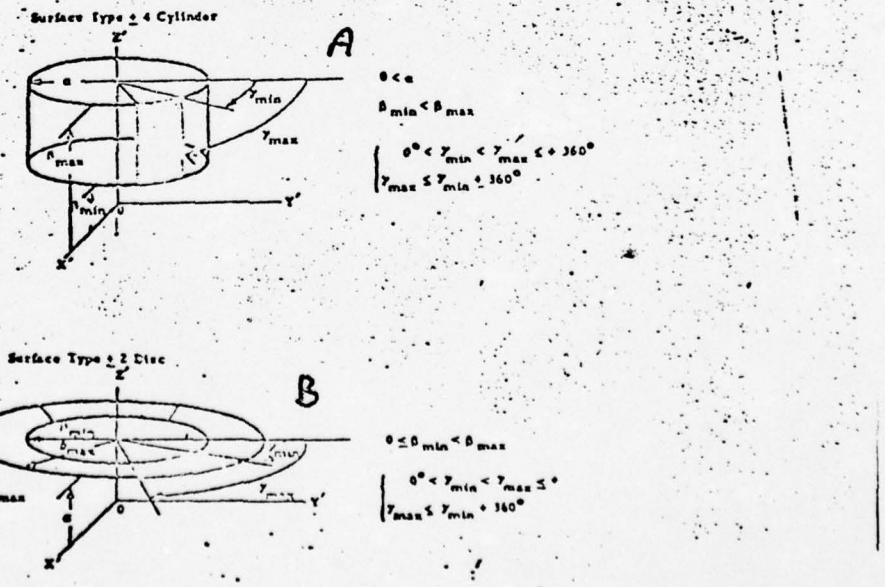

FIG 3.14 TAIL PIPE

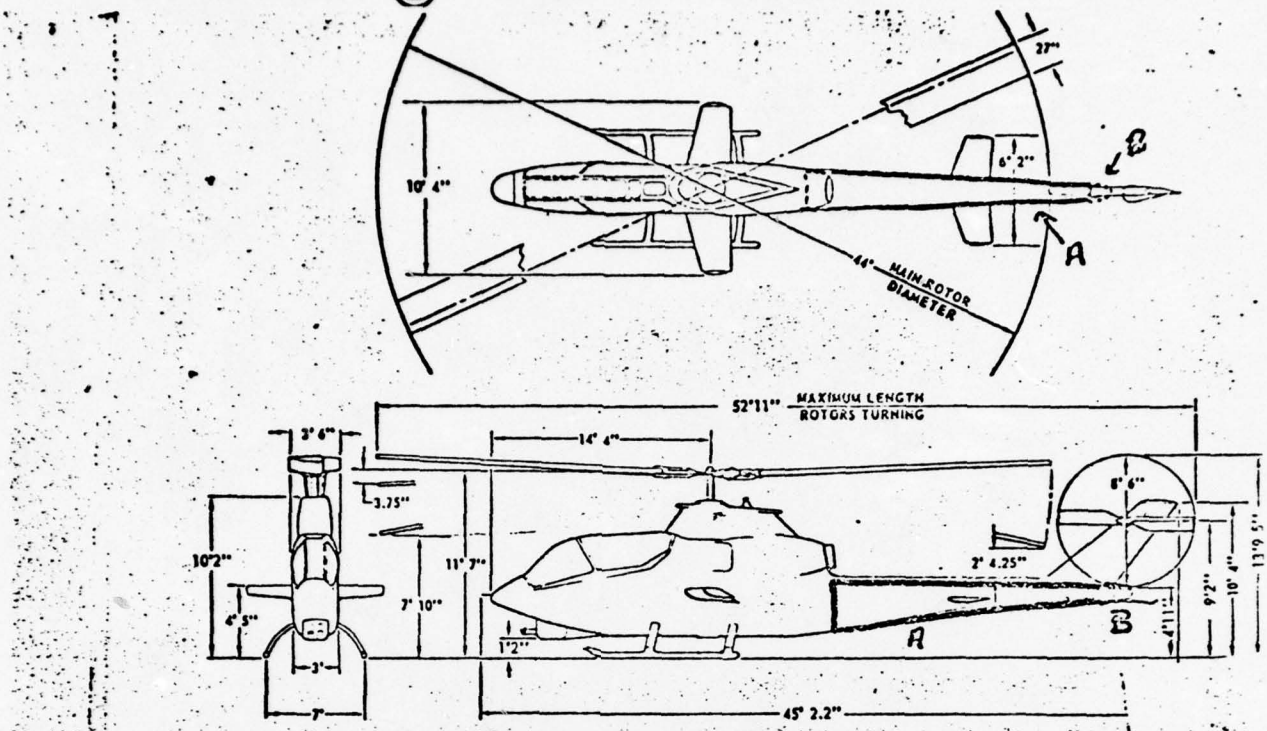

TAIL BOOM

2 MAJOR SURFACES

A Circular cone

B circular paraboloid

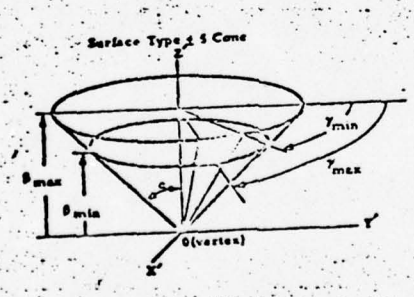

$0 < a$

$0 \leq \beta_{min} < \beta_{max}$

$\begin{cases} 0° < \gamma_{min} < \gamma_{max} \leq +360° \\ \gamma_{max} \leq \gamma_{min} + 360° \end{cases}$

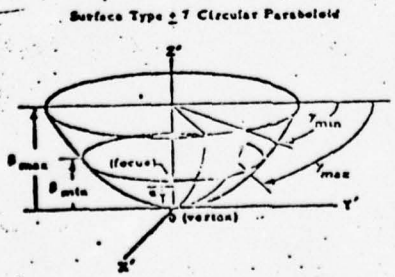

$0 < a$

$0 \leq \beta_{min} < \beta_{max}$

$\begin{cases} 0° < \gamma_{min} < \gamma_{max} \leq +36 \\ \gamma_{max} \leq \gamma_{min} + 360° \end{cases}$

FIG 3.25 TAIL BOOM

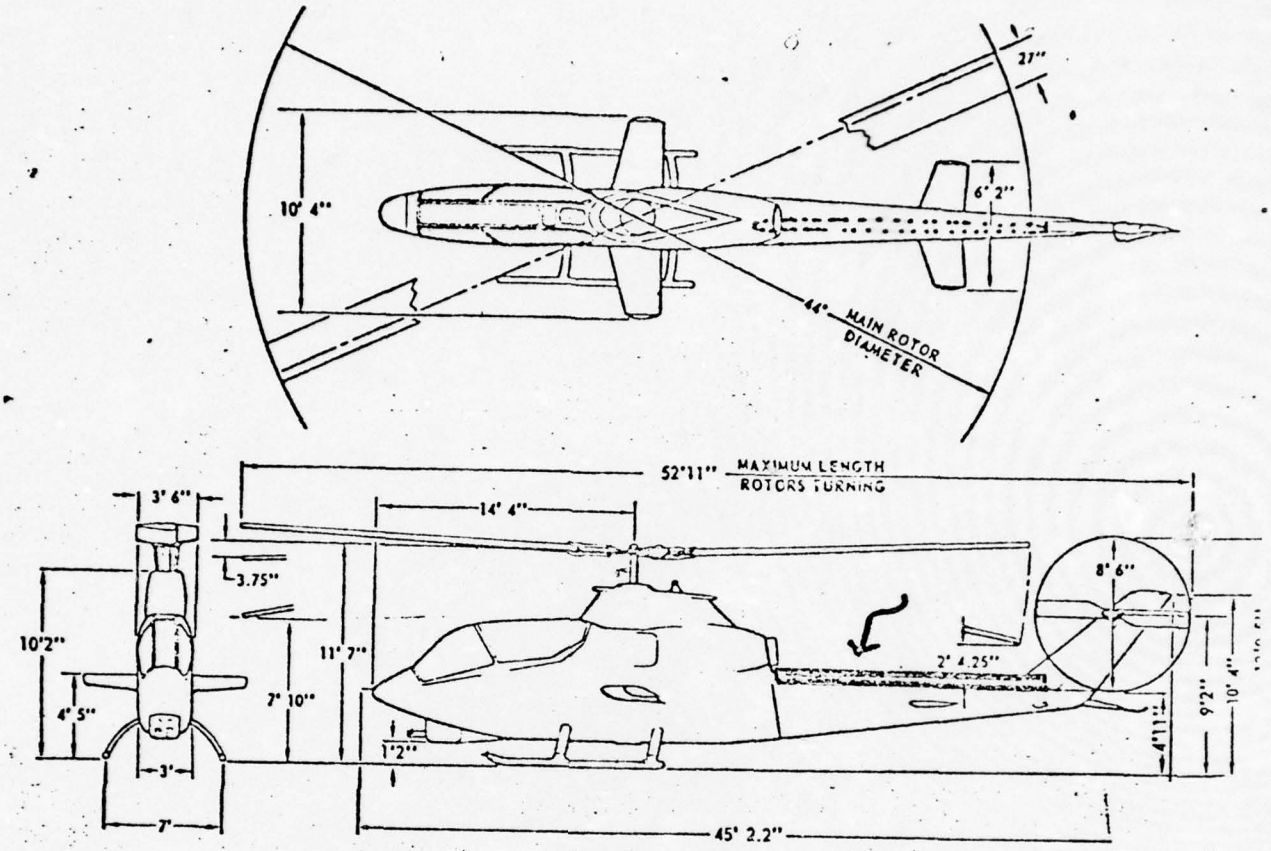

TAIL ROTOR DRIVE · right cylinder

1 MAJOR SURFACE

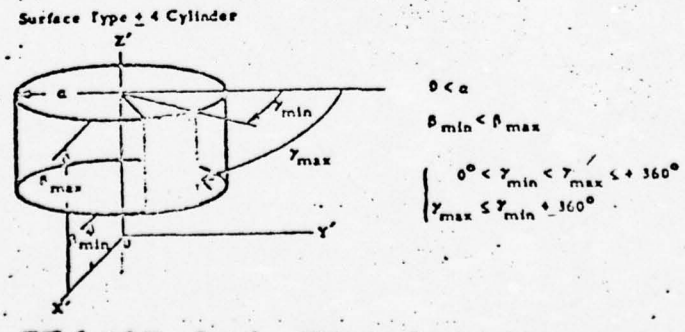

FIGURE 3.16 TAIL ROTOR DRIVE

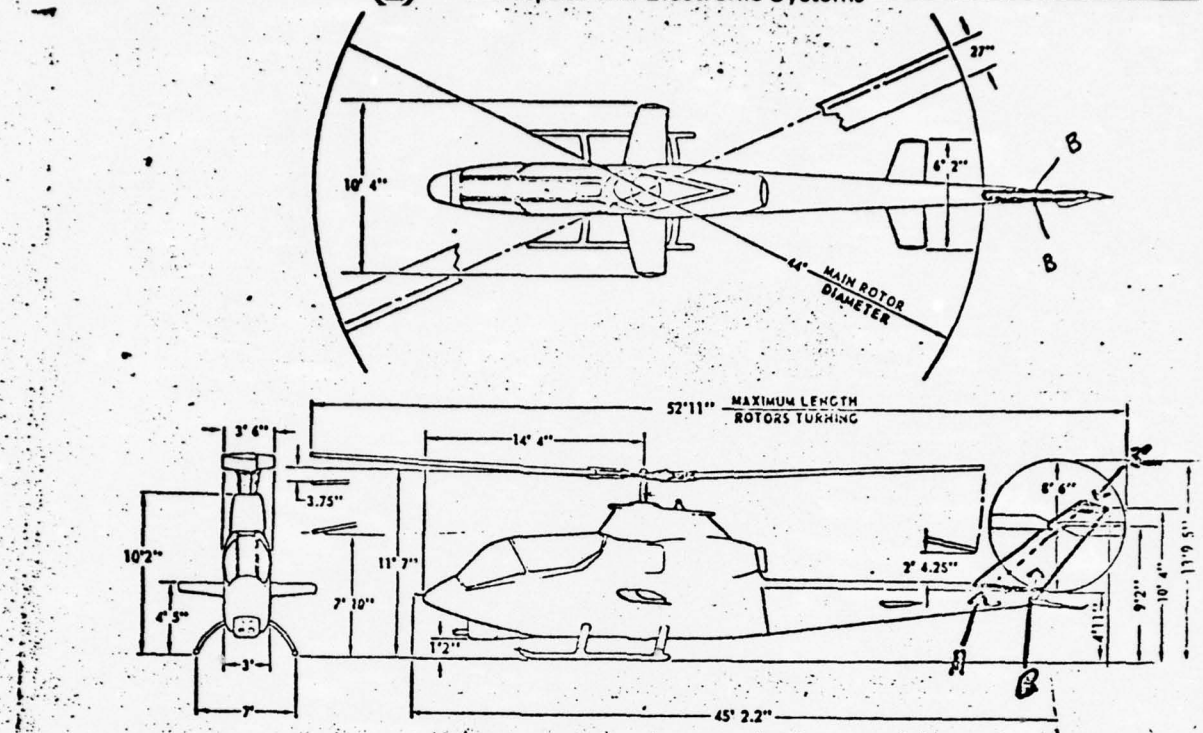

TAIL FIN A cylinder B (2) rectangular flats C triangular flat

4 MAJOR SURFACES

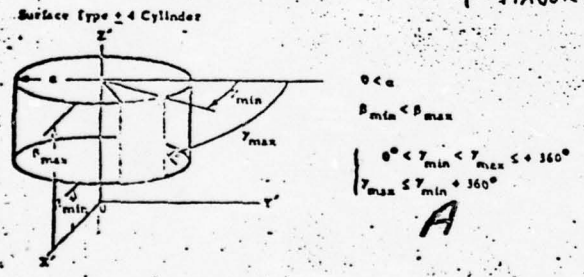

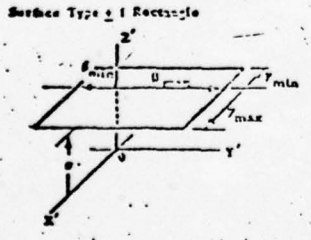

βmin < βmax
γmin < γmax B

Surface Coordinate System (X', Y', Z')

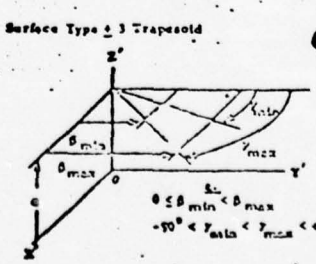

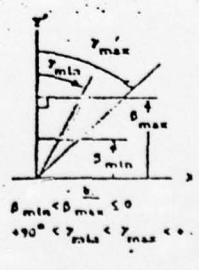

FIG. 3.17 TAIL FIN

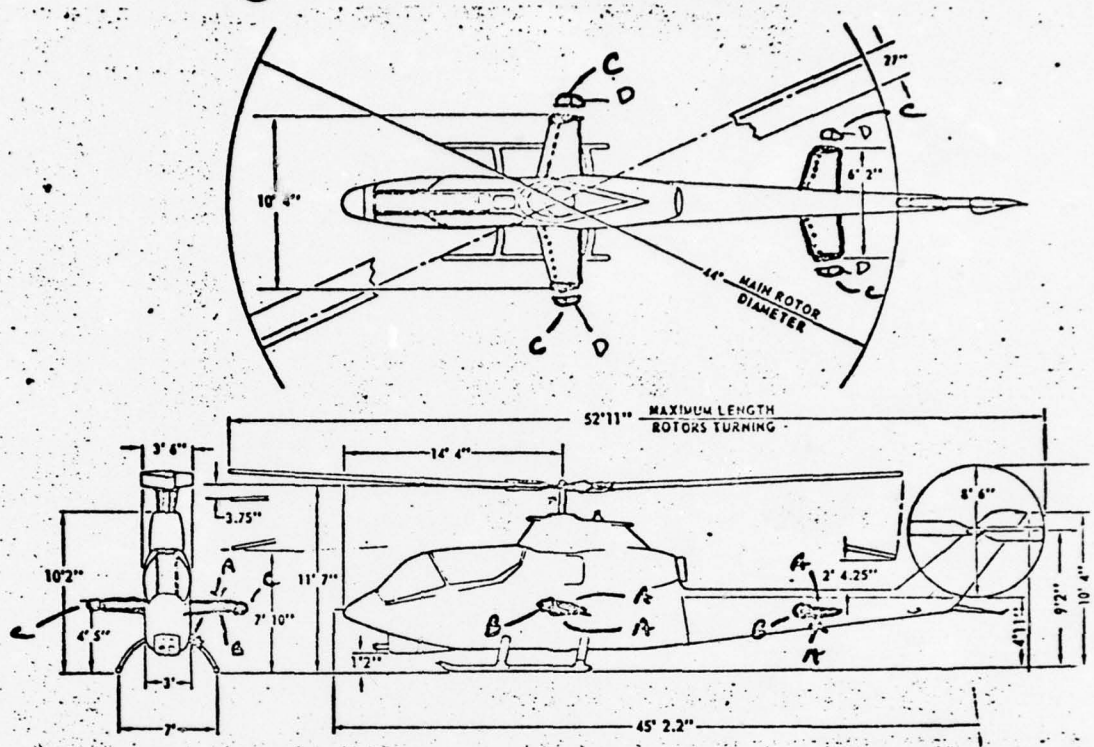

Horizontal stabilizers

20 MAJOR SURFACES

(4) sets of combinations of right circular cylinders and rectangular flats and hemispherical caps.

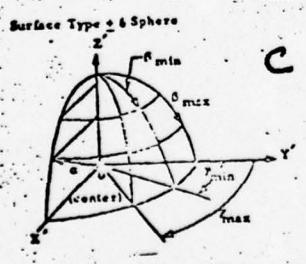

$0 < a$

$0 \leq \beta_{min} < \beta_{max} \leq 180°$

$0° < \gamma_{min} < \gamma_{max} \leq \gamma_{min} + 360°$

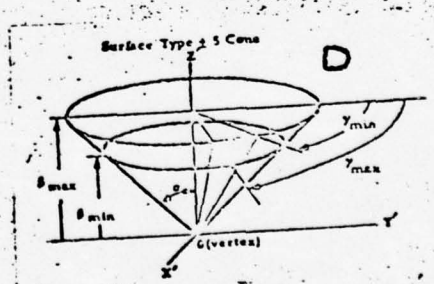

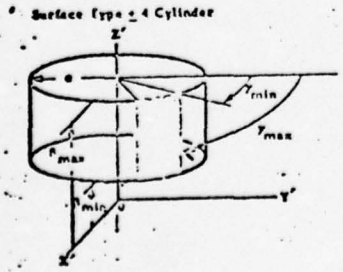

$0 < a$

B

$\beta_{min} < \beta_{max}$

$0° < \gamma_{min} < \gamma_{max} < \gamma_{min} + 360°$

$\gamma_{max} \leq \gamma_{min} + 360°$

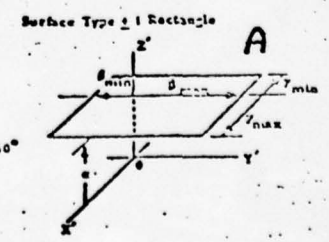

$\beta_{min} < \beta_{max}$

$\gamma_{min} < \gamma_{max}$

Surface Coordinate System (X', Y', Z')

FIG 3.18 HORIZONTAL STABALIZER

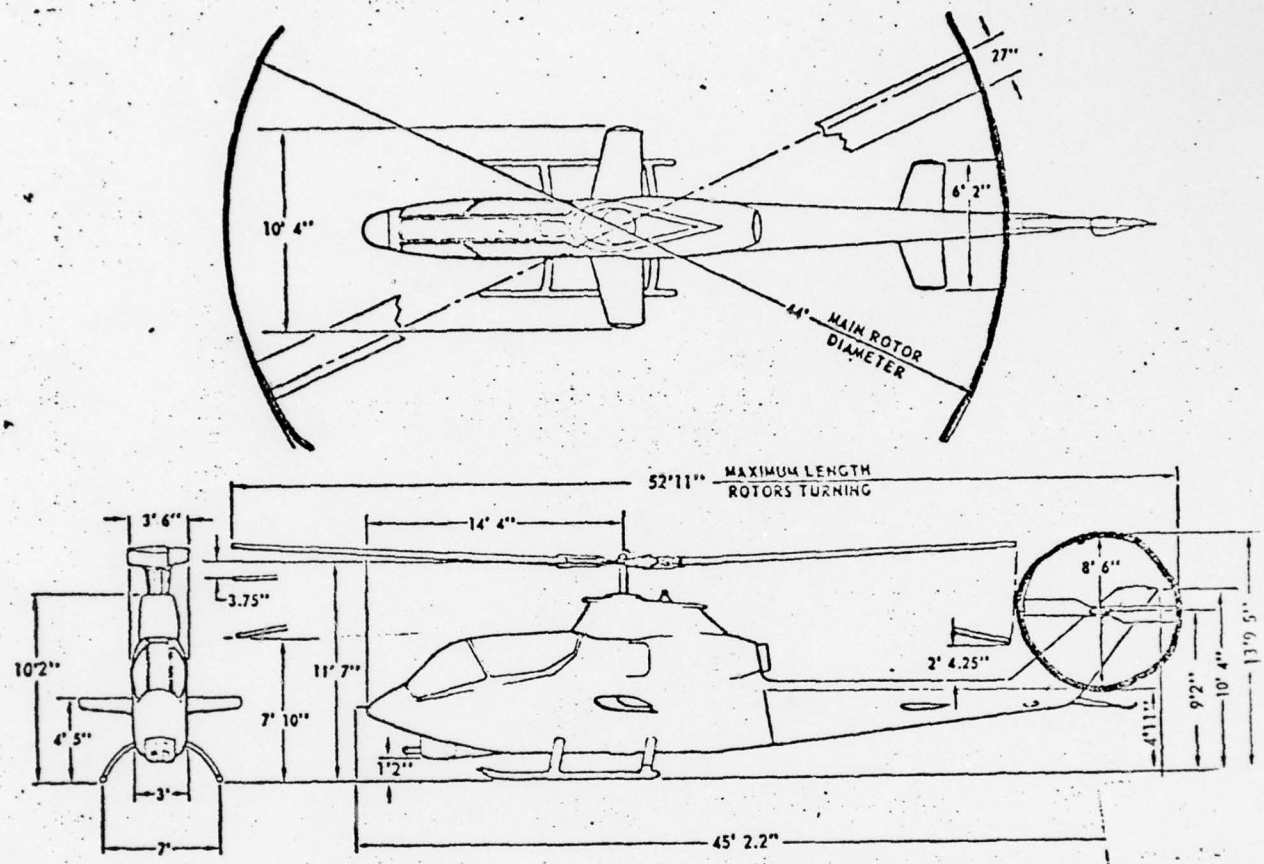

MAIN & TAIL ROTOR

CIRCULAR DISKS

2 MAJOR SURFACES

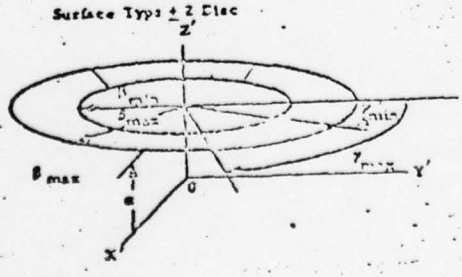

$0 \le \beta_{min} < \beta_{max}$

$0° < \gamma_{min} < \gamma_{max} \le +$

$\gamma_{max} \le \gamma_{min} + 360°$

FIGURE 3.19 Rotor Disks

AD-A042 989 WESTINGHOUSE DEFENSE AND ELECTRONIC SYSTEMS CENTER B--ETC F/G 17/4
EVALUATION OF IR COUNTERMEASURES (MODEL METHODOLOGY).(U)
JUN 72 R F HIGBY, R C BROWN, J B GOODELL DAAJ01-72-C-0447

UNCLASSIFIED NL

2 OF 3
ADA042989

The truncation indicies β_{min}, β_{max}, δ_{min} and γ_{max} are used to taylor the geometry such to obtain a segment giving the best fit. Alpha (α) is a size parameter which scales the geometry to the appropriate size. Values for these parameters may be obtained directly from the superposition on the plan drawing.

Each surface will be described analytically with respect to the helicopter's body axes defined as the control coordinate system (CCS). The longitudinal axis (Y) is positive proceeding along the body from the origin to the nose, the width axis (X) is positive proceeding from the origin to the tip of the right most part, and the height axis (Z) is positive proceeding from the origin to the highest part of the helicopter. The origin is defined to be the center of gravity of the aircraft. Negative directions are defined accordingly.

Using the layout drawings, one positions and properly orients surface/sections in a manner strongly analogous to putting together a three-dimensional geometric puzzle. This is accomplished by assigning appropriate values of roll, pitch, and yaw to the SCS to bring them into the proper orientation in CCS and displacement values of X, Y and Z to translate the SCS to the proper position in the CCS.

One should be aware of the simplicity in representation offered by sometimes imbedding one surface within another. For example, some helicopter cockpits can be modeled as an ellipsoid partially imbedded in an elliptical cylinder.

3.2.2 Minor Surfaces

Minor surfaces are subelements of major surfaces. They are distinguished by radiometric or thermal discontinuities occuring in the major surfaces.

For example, if there is an emissivity difference existing on a major surface such as a window, then the area outlined by the different emissivity is broken out as a separate minor surface, such as the window.

All surfaces will exchange radiation with the environment such as solar heat from the sun. But all of the major surface may not be in view of the sun at any given time. In the real world this would set up a thermal gradient. To account for this gradient or permit a temperature difference to occur in the computer it is necessary to restrict surfaces to a maximum exposure angle.

Each side of a 4 sided retangular box has a 180 degree exposure angle and its solar exposure is uniquely defined by a cosine relation. It is felt that conic surfaces can also be represented by equivalent rectangles so far as their average solar heat load is concerned. For this reason, all conic surfaces should be subdivided into at least four radial sections equivalent to the 180 degree exposure angles of an equivalent rectangle. The normal vectors to each of these surfaces is tabulated as an additional input to BODY.

While the above rationale used the sun as an example, the same thing applies to the earth and sky as extended external sources. For this reason, the preference for conic subdivision is a top section, bottom section and two side sections. However, this is not a necessity as the geometry facilitates computing appropriate contributions from each external source, but it does facilitate a consistent methodology which can preclude ambiguous interpretation of program predictions.

Minor surface subdivisions are also dictated by internal compartment temperature differences. For example, if a surface element covers both a heated compartment such as the cockpit and an unheated compartment such as the tail boom, then the surface element must be subdivided at the interface.

The disection of major surfaces into minor surfaces are illustrated by the dashed lines in figures 3.9 through 3.19. Each minor surface is associated with its individual truncation indicies for the major surface geometry.

When the surfaces have been defined and the ray intercept subroutine programmed, a test should be made to confirm the geometric representation of surfaces. This is accomplished by assigning each surface a number and generating a computer printout of each surface number intercepted by a mosaic of rays encompassing the entire structure at various orientation angles.

An example of such a check print is illustrated in the lower portion of figure 3.20. In this example, a target structure represented by 3 surfaces and is viewed at a shallow aspect angle of 3 degrees. The surfaces intercepted are printed out numerically. (The upper portion of the figure is related to a check on the intercept geometry itself such as the angle of incidence and reflection).

The mechanics of the ray intercept geometry are discussed in section 3.3.

3.3 Analytics

This section presents the equations that must be exercised in order to determine whether a ray, from a particular sensor element, intersects the target.

3.3.1 Coordinate Systems

Here we define the relationships between the n-th surface, the composite helicopter, the earth-referenced coordinate system and the sensor-coordinate system. Reference figure 3.21

Let (x_n, y_n, z_n) be the surface coordinate system of surface n, R_n the location

```
 71/09/20. 15.21.46.
PROGRAM   GEOREF

TGT DIAM =  10.6    CM OR  4.17323 INCHES
TGT LGTH =  275.3   CM OR  9.03215 FEET
ASPECT ANGLE =  3    DEGREES
RANGE =  1    KM
ANGULAR RESOLUTION =  20   MIC-RAD
 TARGET RESOLUTION =  2    CM

  10*COS ANG INC >=     3.14*AZ REFL RAD >=     1.57*ZEN REFL RAD >=
 +IIII+IIII*IIII+IIII+  +IIII+IIII*IIII+IIII+  +IIII+IIII*IIII+IIII+
+                                                                    +
-                                                                    -
-                                                                    -
-     26630000000          87789999999          27830000000        -
-     789710000000         411499999999         344300000000       -
*    1799840000000        8311379999999                           *
-     789710000000         411499999999         344300000000       -
-     26630000000          87789999999          27830000000        -
-                                                                    -
-                                                                    -
+                                                                    +
 +IIII+IIII*IIII+IIII+  +IIII+IIII*IIII+IIII+  +IIII+IIII*IIII+IIII+
```

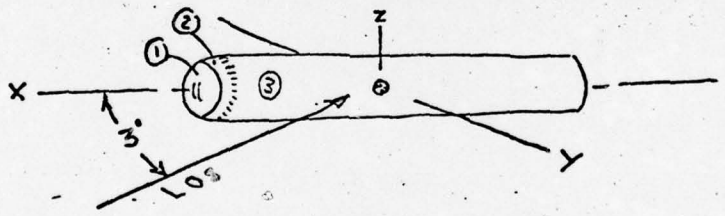


```
 +IIII+IIII*IIII+IIII+  +IIII+IIII*IIII+IIII+  +IIII+IIII*IIII+IIII+
+                                                                    +
-                                                                    -
-                                                                    -
-     11113333333          11113333333          11113333333        -
-     111123333333         111123333333         111123333333       -
*    1111113333333        1111113333333                           *
-     111123333333         111123333333         111123333333       -
-     11113333333          11113333333          11113333333        -
-                                                                    -
-                                                                    -
+                                                                    +
 +IIII+IIII*IIII+IIII+  +IIII+IIII*IIII+IIII+  +IIII+IIII*IIII+IIII+
```

FIGURE 3.20 SAMPLE of SURFACE CHECK

of that surface coordinate system relative to the helicopter-centered coordinate system (X_H, Y_H, Z_H); R_H the location of the helicopter axes relative to the Earth-referenced coordinate system (X_e, Y_e, Z_e), R_S the location of the sensor (i, j, k) axes relative to (X_e, Y_e, Z_e). Let U_{jk} be a unit vector parallel to the i axis originating in the sensor mosaic element i, j, k axes U_{jk} is given by

$$\underline{U}_{jk}^{[ijk]} = \begin{bmatrix} 1 \\ 0 \\ 0 \end{bmatrix} \qquad (3.3.1)$$

Let R_{jk} be the origin of U_{jk} relative to (ijk) axes;

$$R_{jk}^{[ijk]} = \begin{bmatrix} 0 \\ j\delta_j \\ k\delta_k \end{bmatrix} \qquad (3.3.2)$$

Through various vector manipulations, the following equation may be formed (assuming δU_{jk} intercepts surface n)

$$R'_{jk} = -R_n - R_T + R_S + R_{jk} + \delta U_{jk} \qquad (3.3.3)$$

where R'_{jk} is the position intercept vector relative to (X_n, Y_n, Z_n). In (X_n, Y_n, Z_n) axes this takes the form:

$$\begin{bmatrix} R'_{jk_1} \\ R'_{jk_2} \\ R'_{jk_3} \end{bmatrix} = \begin{bmatrix} R_1 + \delta C_1 \\ R_2 + \delta C_2 \\ R_3 + \delta C_3 \end{bmatrix} \qquad (3.3.4)$$

where

$$\begin{bmatrix} R'_{jk_1} \\ R'_{jk_2} \\ R'_{jk_3} \end{bmatrix} \equiv R'^{[x_n, y_n, z_n]}_{jk} \qquad (3.3.5)$$

$$R \equiv R_n - R_T + R_s + R_{jk} \qquad (3.3.6)$$

$$\begin{bmatrix} R_1 \\ R_2 \\ R_3 \end{bmatrix} \equiv R^{[x_n, y_n, z_n]} \qquad (3.3.7)$$

$$\begin{bmatrix} C_1 \\ C_2 \\ C_3 \end{bmatrix} \equiv U_{jk}^{[x_n, y_n, z_n]} \qquad (3.3.8)$$

Let T_H be the transformation matrix into helicopter-body centered axes;

i.e., $$R_H^{[x,y,z]} = T_H R_H^{[x_e, y_e, z_e]} \qquad (3.3.9)$$

Let T_{Hn} be the transformation from helicopter bay centered axes into nth surface axes, and T_S the transformation into sensor axes; then :

$$\begin{bmatrix} R_1 \\ R_2 \\ R_3 \end{bmatrix} = T_{Hn}\left(-R_n^{[x,y,z]} + T_H\left(-R_H^{[x,y,z]} + R_S^{[x,y,z]} + T_S^T R_{jk}^{[i,j,K]}\right)\right) \qquad (3.3.10)$$

$$\begin{bmatrix} C_1 \\ C_2 \\ C_3 \end{bmatrix} = T_{Hn} T_H T_S^T U_{jk}^{[i,j,k]} \qquad (3.3.11)$$

The intersection point may be obtained by solving for δ as in NASA report no. CR-61321, p. 3-6.

A preliminary test may be obtained as follows. The position of the nth surface origin relative to i, j, k axes is

$$R_{sn} = -R_s + R_H + R_n \tag{3.3.12}$$

$$R_{sn}^{[i,j,k]} = T_s \left(R_H^{[x,y,z]} + T_H^T R_n^{[x,y,z]} - R_s^{[x,y,z]} \right) \tag{3.3.13}$$

Letting

$$\begin{bmatrix} R_{sn_1} \\ R_{sn_2} \\ R_{sn_3} \end{bmatrix} = R_{sn}^{[i,j,k]} \tag{3.3.14}$$

Then intersection is possible if

$$\left(\left(j\delta_j - R_{sn_2} \right)^2 + \left(k\delta_k - R_{sn_3} \right)^2 \right)^{1/2} > r_{max_n} \tag{3.3.15}$$

where r_{max_n} is the maximum radius of the nth surface.

A simpler test is given by

$$\left| j\delta_j - R_{sn_2} \right| > r_{max_n} \quad \text{or} \tag{3.3.16}$$

$$\left| k\delta_k - R_{sn_3} \right| > r_{max_n} \tag{3.3.17}$$

3.3.2 Solution of δ for the Intercept Test

The solution of the above cited ray intercept vector equations for is $\delta = (\alpha - R_3)/C_3$ for intersection with a flat surface (where α is defined by figure 3.6) and for a conic surface.

$$\delta = -(2R_1C_1 + 2R_2C_2 - 2cR_3C_3 - bC_3)$$
$$\pm \{(2R_1C_1 + 2R_2C_2 - 2cR_3C_3 - bC_3)^2$$
$$- 4(C_1^2 + C_2^2 - cC_3^2)[R_1^2 + R_2^2 - a - (b + cR_3)R_3]\}^{1/2}$$

where for:	~~cylinder~~	cone or cone frustrum	sphere	circular parabaloid
$a =$	α^2	0	α^2	0
$b =$	0	0	0	4α
$c =$	0	$\tan^2\alpha$	-1	0

4. THERMAL MODELING OF ARMY AIRCRAFT

4.1 Introduction and Approach

This section describes the thermal modeling in the Army aircraft infrared signature study. Thermal modeling or the simulation of heat transfer and heat distribution both within and external to the structure of the various helicopters is required in order to account for the external surface temperature effects on the infrared signature.

The effects of internal heat transfer due to conduction and convection (free and forced) and external heat transfer due to environmental radiation and forced convection (aerodynamic heating) are modeled. See Figure 4.1 for a depiction of the heat flow-transfer mechanisms model.

Heat distribution within the cabin is due primarily to the conduction of heat between various internal heat sources and internal heat convection. Conduction of heat occurs because heat dissipating devices in the cabin transfer heat to the walls through wall-adjoining structures. Such devices are power supplies, oil heaters, electronic control panels, etc.

Free convective heat within the cabin occurs because each heat dissipating unit causes the air around it to heat up. Forced convective heating is the result of blowers or fans moving air in the cabin.

Metal conduction of heat occurs between various external surfaces because of the temperature differences of the various surfaces. Heat flows from areas of higher temperatures to areas of lower temperatures. The net heat transfer is dependent upon the internal heat contribution to the various surfaces interacting with the environment.

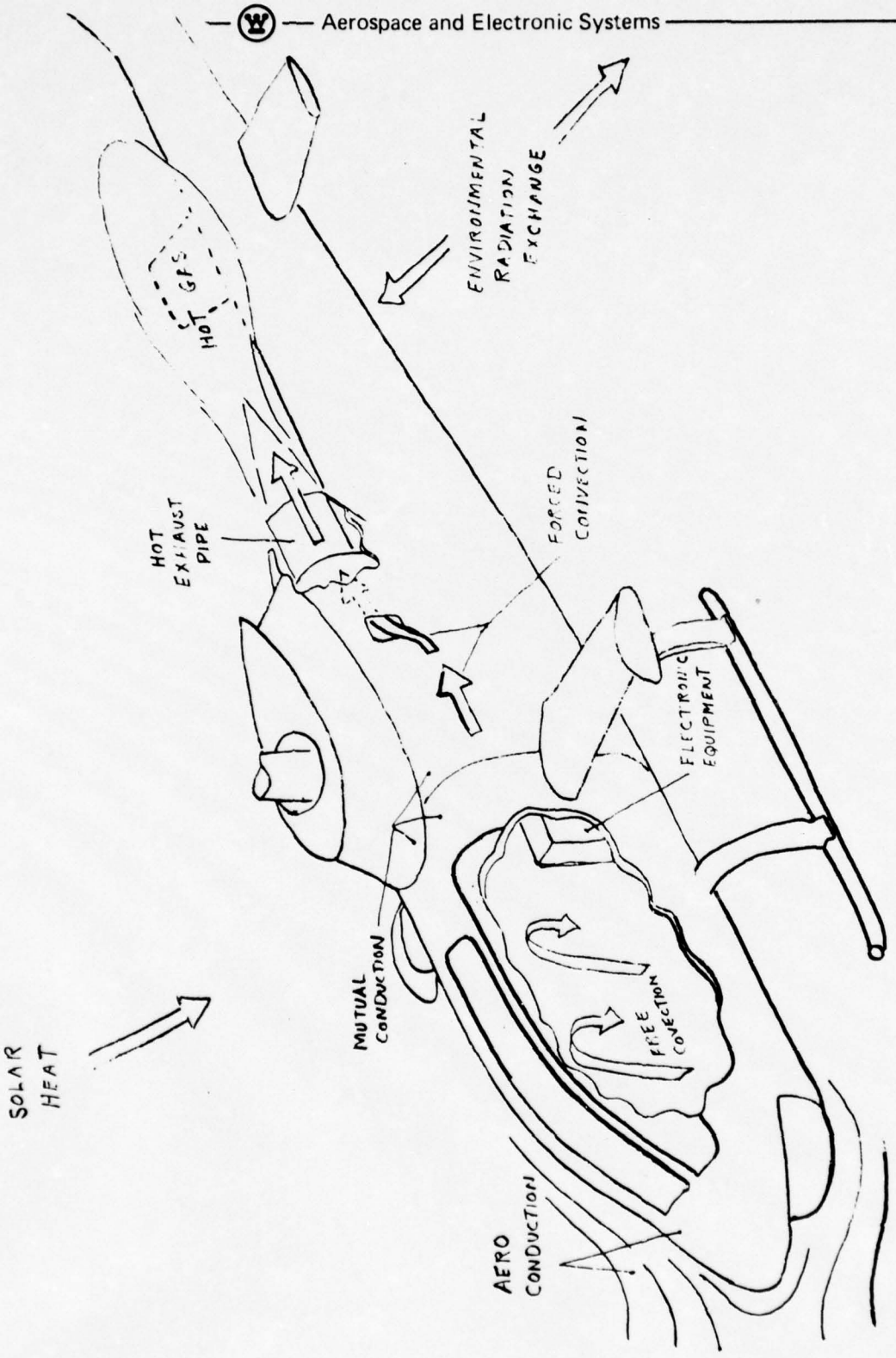

Figure 4.1 Heat Transfer Mechanisms

Aero-conduction or aerodynamic heating on the external surfaces results from the fast flowing air moving across the surface of the aircraft. Aerodynamic heating generally does not become significant until an aircraft is traveling at speeds greater than Mach 2; thus ly aerodynamic heating is not expected to contribute significantly to the signature of Army aircraft.

The temperature of the hot metal parts that comprise and that are connected to the exhaust tail pipe are not derived by analytical solution. These temperatures are assigned by the program.

The radiative exchange with environment (the terrain, the sun) also influences the external temperature of a surface.

Schematically, the various heat sources and sinks and transfer mechanisms as they influence a specific surface may be represented as depicted in figure 4.2.

The external temperature of the surface of interest represented here is T_{SX}. It is shown located on the outer periphery of the illustrated cabin enclosure. Exterior transfer mediums consist of Q_A (aero heating), Q_E (environmental radiation), Q_I (insolation), and Q_P (plume convection). Internal sources are Q_C (compartment air convection), Q_B (power dissipating sources) and Q_M (mutal conduction from adjacent surfaces).

4.2 Internal Heat Transfer and Distribution

For each helicopter, one obtains a copy of the following documents:

1) Operator's manual for the particular helicopter

2) Organizational Maintenance Manual for the particular helicopter (dash twenty and dash thirty-four series of Army aircraft maintenance technical manual).

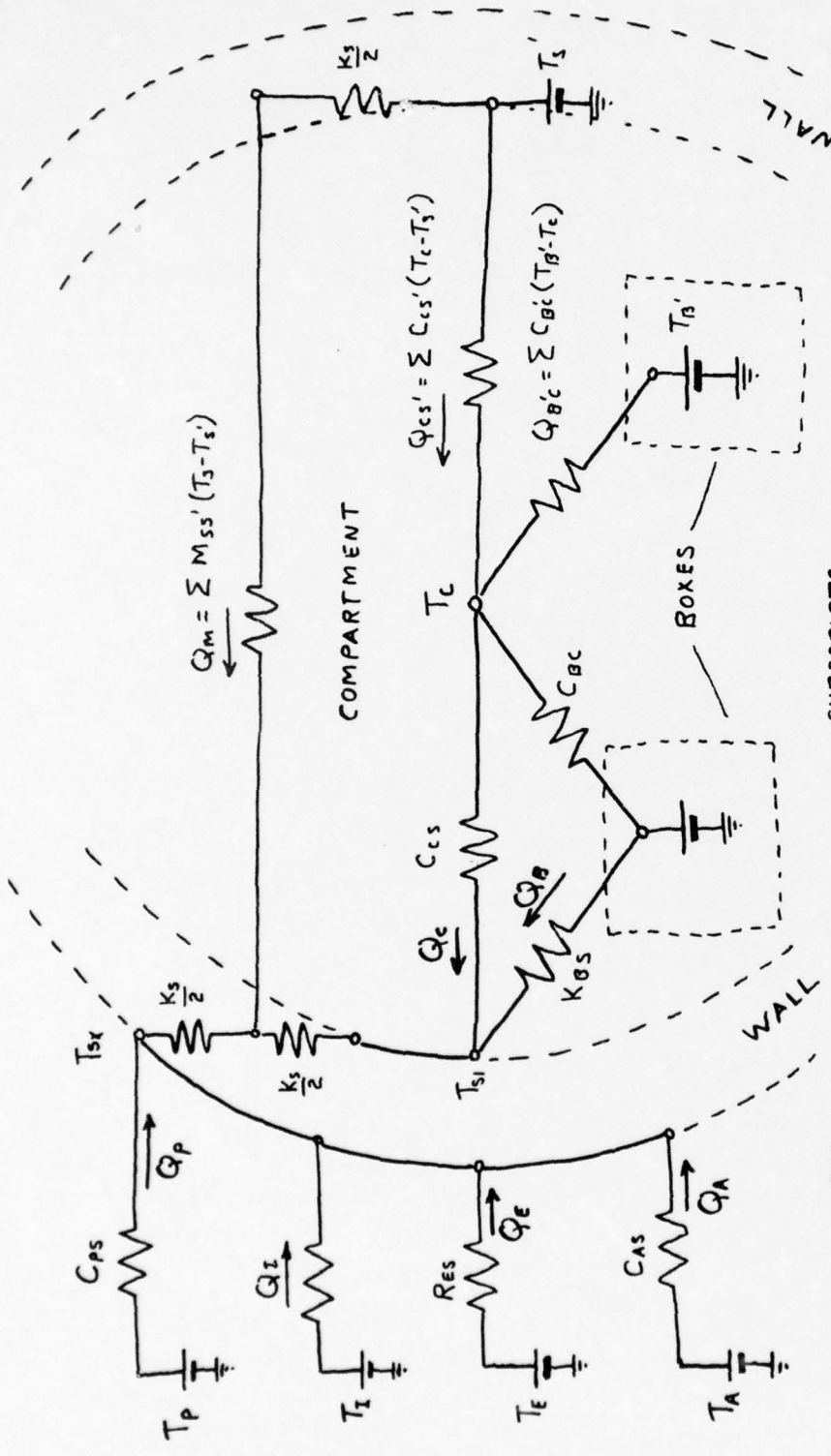

Figure 4.2 Thermal Model Schematic

3) Army aircraft specification for paints and coatings used on the particular aircraft.

4) A layout drawing for the particular helicopter. This drawing has to be detailed and accurate enough to allow extraction of the dimensions, location, and configuration of the various power dissipating sources on the helicopter.

All of the above documents can be obtained through the technical publications group at U.S. Army Publication Center in St. Louis, Missouri.

The above documents are required to identify all the pertinent electrical equipment, propulsion plants, armaments, and the mounting fixtures and arrangements of the same. All these units produce heat in varying amounts. By noting the input power requirements, the current, power efficiencies, specified thermal outputs, shapes, type of materials, thicknesses, lengths, and widths, and perhaps a few other related items, one can tabulate the necessary data for approximating the heat exchange of a particular surface.

A list of the data that should be tabulated for each heat-generating source on a helicopter appears in Table 4.1.

TABLE 4.1

DATA TO BE TABULATED FOR EACH HEAT-GENERATING SOURCE

SOURCE	UNITS
Heat Dissipation of Source	BTU/hr
Geometrical Approximation of Source	
Material of Source	
Specific heat of material (40-80°F)	BTU/lb °F
Density of Material	Slugs/ft^3
Thermal conductivity of material	BTU/hr/ft^2/°F/ft
Length of source	Feet
Width of source	Feet
Thickness of source	Feet
Location on aircraft (with respect to c.g. of aircraft)	
Wall joining structure (yes or no)*	

*If answer is "no" then we assume no conductive heating due to this box.

Each cabin-internal heat generating source contributes heat to the cabin air through two mechanisms, convection and conduction. Convection can either be free or forced. Free convection is heating due to the various sources heating the surrounding air. Forced convection is a result of fans or blowers moving heated or cooled air. Air ducts that are opened or closed to allow ambient air to flow through are also examples of forced convection for cooling purposes.

4.3 Conductive Heating

The contribution of heat Q_{Bi} to the i-th external surface due to conductive heat from N sources is:

$$Q_{Bi} = \sum_{j=1}^{N} R_{Bij}(T_i - T_{Bj})/A_i \quad \text{BTU/HR Sq. Ft.} \qquad (4.1)$$

Q_{Bi} = quantity of heat per unit time due to conduction (BTU/hr sq.ft.)

T_{Bj} = temperature of the j-th box feeding the i-th surface (^{o}F)

T_i = wall temperature of the i-th surface (^{o}F)

where

$$R_{Bij} = \frac{L_{ij}}{K_{ij} A_{ij}} \quad \text{BTU/HR/}^{o}\text{F}$$

L = Length of the portion mounted to the inner wall (ft)

K = thermal conductivity coefficient for wall joining structure (BTU/HR/Sq.Ft./^{o}F)

A_{ij} = Cross sectional area of portion in contact with wall (sq. ft.)

A_i = Cross section area of surface i (sq. ft.)

4.4 Convective Heating

The contribution of heat Q_{cv} to the cabin air due to free convective heating from the N sources is:

$$Q_{cv} = \sum_{j=1}^{N} R_{cvj} (T_c - T_{Bj}) \quad \text{BTU/HR/Sq.Ft.} \qquad (4.2)$$

where

Q_{cv} = quantity of heat per unit time due to free convection (BTU/hr/sq.ft.)

T_{Bj} = temperature of the j-th box feeding convective heating to the cabin (^{o}F)

T_c = temperature of the cabin air (^{o}F)

R_{cvj} = thermal resistance coefficient for free convective heating

$$= 0.548\,(K/L)(FL^3\,(T_c - T_{Bj}))^{0.25} \text{ (BTU/HR/Sq.Ft./}^{o}\text{F)} \qquad (4.3)$$

where

K = thermal conductivity coefficient for the material of the source (BTU/HR/Sq.Ft.)/^{o}F)

L = characteristic length of source (feet)

F = convective parameter of air

$$= (P^2\, Cp/T^3 \mu K) \qquad (4.4)$$

where

P = absolute pressure of air evaluated at the film temperature (U-/Sq.Ft.)

C_p = specific heat of air at film temperature (BTU/lb/^{o}F)

T = film temperature = $(T_c + T_{Bj})/2$ (^{o}F) (4.5)

μ = absolute viscosity of air at the film temperature (lb/ft/hr)

K = thermal conductivity of air (BTU/HR/Ft./^{o}F)

Values of the characteristic length L have been established from laboratory studies of freely suspended vertical plates, horizontal cylinders, vertical cylinders, and planes with the heated surface facing upward or downward. The characteristic length L should be evaluated as follows:

(1) Horizontal planes

L = (length)(width)/ (length + width)

(2) Vertical planes (rectangular)

L = height of plane in vertical direction, but limited to two feet even if height is greater.

(3) Vertical planes (non-rectangular)

L = surface area of plane divided by horizontal width of plane. For circular sections, L = 0.785 x diameter

(4) Cylindrical surfaces, horizontal

L = diameter of cylinder

(5) Cylindrical surfaces, vertical

L = height of cylinder, but limited to two feet even if height is greater

(6) Spheres, L = one half diameter of sphere

The following thermal properties of air are necessary to make the above computations.

a) Specific heat of air: $C_p = 0.02\,T - 0.88$ $(32^\circ F \leq T \leq 200^\circ F)$ BTU/ft/°F)

b) thermal conductivity of air: $K = 0.00002T + 0.0140$ $(32^\circ F \leq T \leq 200^\circ F)$ (BTU/HR/Ft/°F)

c) absolute viscosity of air: $u = .28T + 162$ $(32^\circ F \leq T \leq 200^\circ F)$ (lb/ft/HR)

d) pressure of air: P = 14.7 (sea level pressure) LB/IN^2

Cabin air heating or cooling due to forced convection from the air-moving sources can be determined by the following relation:

$$Q_{FCV} = \sum_{j=1}^{N} 820.0\ W\ (T_C - T_j)\ W/HR \qquad (4.6)$$

where

Q_{FCV} = heat absorbed or convected in the heat exchange passage expressed in watts

N = number of air-moving sources

W = air flow rate pound per hour

T_j = inlet temperature ^oF in the case of external ducks

T_j = exit temperature ^oF in the case of internal boxes

The temperature of the cabin air is the sum of the free and forced convective components of heat due to the various internal sources.

The heat contribution on the i-th external surface due to cabin air temperature is:

$$Q_{t_i} = K_M\ (T_i - T_c)\quad (BTU/ft^2/^oF) \qquad (4.7)$$

where

K_M = thermal conductivity of the surface-air interface

T_i = external wall temperature of the surface

T_c = cabin air temperature

4.5 External Heat Sources

Referring to Figure 4.2, we see that the radiative heat due to the aircraft's exhaust plume, the sun, the earth's surface and the ambient air all contribute heat to an aircraft's surface.

The temperature of those parts that are directly heated by the aircraft's hot exhaust gases will not be derived by the heat balance equations solution techniques. Those parts will be assigned a temperature corresponding to the constant temperature plume contours that they intersect.

The plume heat load is always zero. If the surface is in contact with the plume, the thermal conductivity is set to infinity which automatically sets the surface temperature equal to the plume temperature at the point of contact. If the plume does not contact the given surface, the thermal conductivity is set equal to zero. In either case, the plume heat load is set equal to zero, i.e.:

$$Q_{P_i} = (T_i - T_P)/C_P = 0 \quad (BTU/ft^2/^\circ F) \qquad (4.8)$$

where

Q_P = heat due to plume conductive heating

T_i = the temperature of the surface in contact with the plume ($^\circ$F)

T_P = temperature of the intercept contour of the plume ($^\circ$F)

C_P = thermal resistance coefficient

4.6 Insolation, Ambient Air and Environmental Heating

The effects of insolation, ambient air, and other environmental heating factors will be modeled after the derivations of Zimmerman and Robinson in "Thermal Evaluation of Air-Cooled Electronic Equipment" (Wright Air Development Center Technical Report no. 6579, 1952).

The solar heat load is expressed as:

$$Q_{s_i} = \alpha_i G_{SL} \cos \phi_i \qquad W/sq.ft. \qquad (4.9)$$

where

α_i = solar absorptivity

G_{SL} = solar irradiation (W/sq.ft.)

ϕ_i = angle of incidence made by the i-th surface normal and the rays of the sun (degrees)

The aerodynamic heat is defined for turbulent flow as

$$Q_{A_i} = 4530\left(T_o/100\right)^{1.4}\left[\left(M_o P_o\right)^{0.8}/\left(X_{m_i}\right)^{0.2}\right]\left[\left(T_i/T_o\right) - 0.178\,M_o^2 - 1\right]/\sqrt{T_i} \quad \text{(W/sq.ft.)} \qquad (4.10$$

or for laminar flow when $1.78 \times {}_2MoPo \leq (To/100)^{1.27}$ as

$$Q_{A_i} = 175\left(T_o/100\right)^{1.25}\left[\sqrt{M_o P_o}/\left(\sqrt{X_{1_i}} + \sqrt{X_{2_i}}\right)\right]\left[\left(T_i/T_o\right) - 0.178\,M_o^2 - 1\right] \quad \text{(W/sq.ft.)} \qquad (4.11$$

To = Atmospheric temperature (°K)

Po = Atmospheric pressure (inches of mercury)

Mo = Free stream Mach number

Xm_i = Mean distance of surface from stagnation point (ft.)

T_i = Surface temperature (°K)

X_{1_i} = Distance from leading edge of surface to stagnation point (ft)

X_{2_i} = Distance from trailing edge of surface to stagnation point (ft)

The environmental heat load is expressed as

$$Q_{E_i} = 0.532\,\varepsilon_i\left(T_i/100\right)^4 - \left(\varepsilon_i/2\right)\left[\left(H_G + H_S\right) + \cos B_i\left(H_G - H_S\right)\right] \quad \text{(W/sq.ft.)} \qquad (4.12)$$

where

ε_i = Total emissivity of the surface

H_G = Upwelling irradiance from the ground (W/sq. ft.)

H_S = Down welling irradiance from the sky (W/sq. ft.)

B_i = Angle surface normal makes with the horizontal

The cosine of B is negative if the normal is above the horizontal. Values for H_G and H_S are defined as functions of altitude, cloud cover, surface temperature, and type.

Values for H_G and H_S can be read from Figure 4.3 which was extracted from Robinson and Zimmerman report entitled "Thermal Evaluation of Air-Cooled Electronic Equipment" dated September 1952, WADC technical report No. 6579.

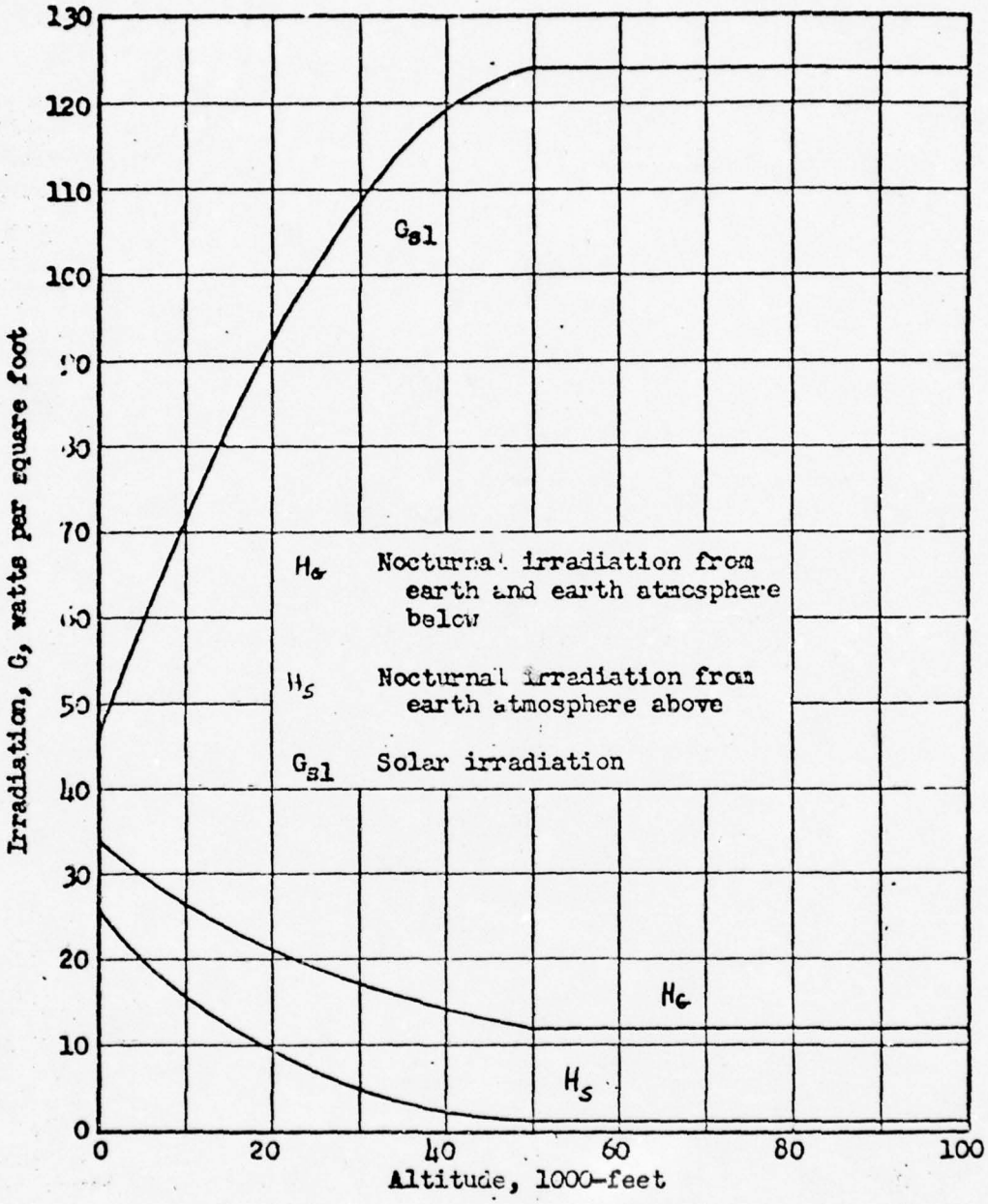

Figure 4.3 Solar and Atmospheric Irradiation
(Ref. 1, p. IV-19)

4.7 Mutal Coupling of Heat of External Surfaces

The result of the exchange of thermal energy of one surface element with another through mutual conduction is called the external heat load. The net transferred is dependent on the temperatures of the various elements and the associated mutual conduction coefficients. The net loss or gain is established by summing up the net transfers with each connecting element. The sign convention is that losses are negative and gains positive.

$$Q_{M_i} = \sum_{S=j}^{K} K_{is}(T_i - T_s) \quad W/m^2 \tag{4.13}$$

where:

Q_{M_i} = External heat transfer via conduction, W/m^2

K_{is} = Mutual conduction coefficient between the i surface and the S surface $W/M^2/^oK$

T_i = Temperature of the i surface, deg K

T_s = Temperature of the S surface, deg K

$$K_{ij} = 5.678 \frac{K_i K_j}{K_i + K_j} \frac{L_{ij}}{A_i} \quad W/m^2/^oK \tag{4.14}$$

where

K_{ij} = Mutual conduction from surface i to surface j $W/M^2/^oK$

K_i = Conduction of surface i $W/^oK/ft$ $BTU/HR/FT/^oK$

K_j = Conduction of surface j $W/^oK/ft$ $BTU/HR/FT/^oK$

L_{ij} = Length of common interface between surface elements i and j, feet

A_i = Area of surface element i, ft^2

5.678 = Conversion factor for metric system

The conduction of a given surface, i, is based on an empirical relation used by heating and air conditioning engineers and takes into account both convective and conductive processes.

$$K_i = \sqrt{h_i \, k_i \, t_i} \quad \text{BTU/M/ft/}^\circ\text{F} \tag{4.15}$$

where

K_i = Conduction coefficient of surface element i BTU/M/ft/$^\circ$F

h_i = Convection film coefficient of surface element i, BTU/hr -ft^2 -$^\circ$F

t_i = Equivalent thickness of surface element i, ft

This equation applies to the internal heat transfer within the wall of the surface element structure. Hence, the convection film coefficient applies to the transfer of heat from point to point along the inner wall by free convection which is acting in parallel to the transfer by conduction from point to point. The equivalent thickness is the thickness of the cross section of solid structure within the wall of the surface element i.

4.8 Thermal Inertia of a Surface

The heat capacity, C, per unit area is simply taken as the product of the weight of the structure per unit area, W, and the specific heat of the structure material, C_p.

$$C = C_p \, W \, 5.78 \quad \text{W/M}^2/^\circ\text{K} \tag{4.16}$$

where

C = heat capacity per unit area, W/M^2/$^\circ$K

C_p = specific heat, BTU/lb/$^\circ$F

5.78 = Conversion factor for metric system

4.9 Heat Balance Equation Solutions

Using the equations presented, a system of simultaneous differential equations may be written relating these heats for each surface on the helicopter.

$$C_i \frac{dT_i}{dt} = Q_{Ai} + Q_{Ei} + Q_{Ii} + Q_{Pi} + Q_{Ci} + Q_{Bi} + Q_{Mi} \qquad (4.17)$$

$$C_j \frac{dT_j}{dt} = Q_{Aj} + Q_{Ej} + Q_{Ij} + Q_{Pj} + Q_{Cj} + Q_{Bj} + Q_{Mj}$$

$$C_K \frac{dT_K}{dt} = Q_{A_K} + Q_{E_K} + Q_{I_K} + Q_{P_K} + Q_{C_K} + Q_{B_K} + Q_{M_K} \text{ BTU/Ft}^2\text{/M}$$

where:

C = Specific heat

Q = Heat loads

T = Temperature

t = Time

i, j and k = Various surface elements

These equations are solved on a digital computer using predictor corrector methods. The computer program subroutine that will solve these equations has been dubbed the name "TEMPS".

Figure 4.4 depicts the sequence of tasks necessary to prepare the thermal properties of each helicopter for "TEMPS".

In an earlier part of this section, it was indicated that the primary task in the development of the thermal model is the identification of all the pertinent sources of heat.

Once the location and heat dissipation of each source has been established, the "assignment" of each heat source to minor surfaces can be made. This assignment, stated simply, consists of determining the conductive heating relationship between the various heat sources and surfaces. Different wall surfaces receive different amounts of conductive and convective heat simply because the different wall-adjoining structures carry different heat loads.

Layout drawings that show how heat sources are mounted on the aircraft are used in assigning the various heat sources to various minor surfaces. A wall joining structure is treated as a "power" line. The "power" being carried across the line is conductive heat. The thermal resistance across a line is computed in TEMPS using the equations presented in earlier sections. The user just supplies TEMPS with the geometrical approximation of the wall-adjoining structure and corresponding thermal conductance and dimensional data. Once derived, the thermal resistance of each wall-joining structure and the heat dissipation of each source can be stored on cards or other input media for future usage of TEMPS.

Using the geometrical approximation and dimensional data tabulated for each heat source, thermal resistances for convective heating within the cabin are also computed.

Heating due to environmental factors is supplied as input to TEMPS from other programs.

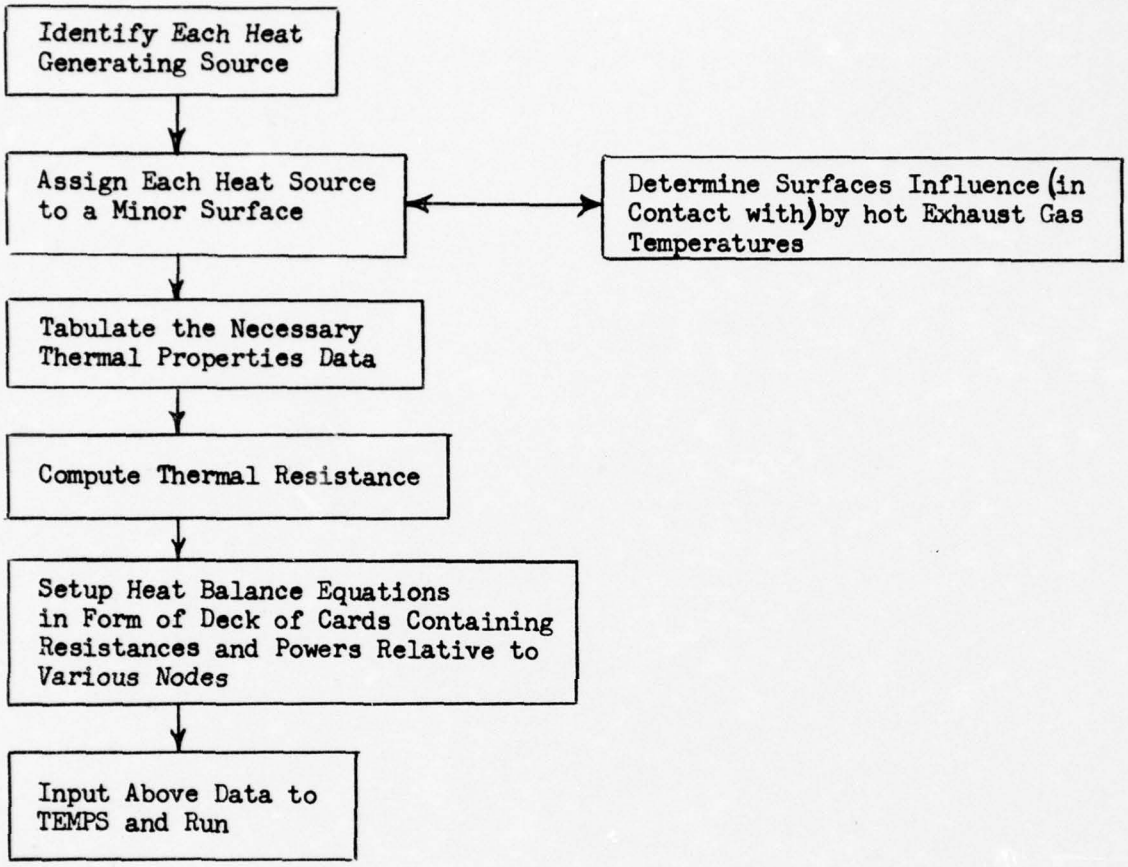

Figure 4.4 Preparation of Helicopter Thermal Properties Data for TEMPS

5. RADIATIVE TRANSFER MODEL

This section describes the methodology to be used to derive the various radiative transfer processes encountered in synthesizing the infrared signature of Army aircraft.

The first part describes the overall model while the latter sections describe the philosophy of the approach and the detailed techniques and analytics to be used.

The radiative transfer model will be programmed as a subroutine in HIDE called TRANS.

5.1 Model Description

The subroutine TRANS computes the radiative transfer between target, background, and sensor. It includes atmospheric transmission; atmospheric, terrestial, solar, exhaust, and target surface emission; and solar and environmental reflection. The radiative transfer computations are carried out for any specified spectral band within the 1 to 16 micron region suitably weighted by the spectral response of the sensor.

Figure 5.1 illustrates the composition of the effective apparent background radiance as computed in the program. For line of sights above the horizon, the background radiance consists of a mix of clear and cloudy sky emission depending on cloud cover and zenith angle and diffuse solar scattering. For line of sights below the horizon, the background radiance consists of terrestial emission, plus reflected sky emission, as defined above, and solar albeto all attenuated along the path to the receiver and atmospheric emission and diffuse solar in the path added in. The background radiance is computed for

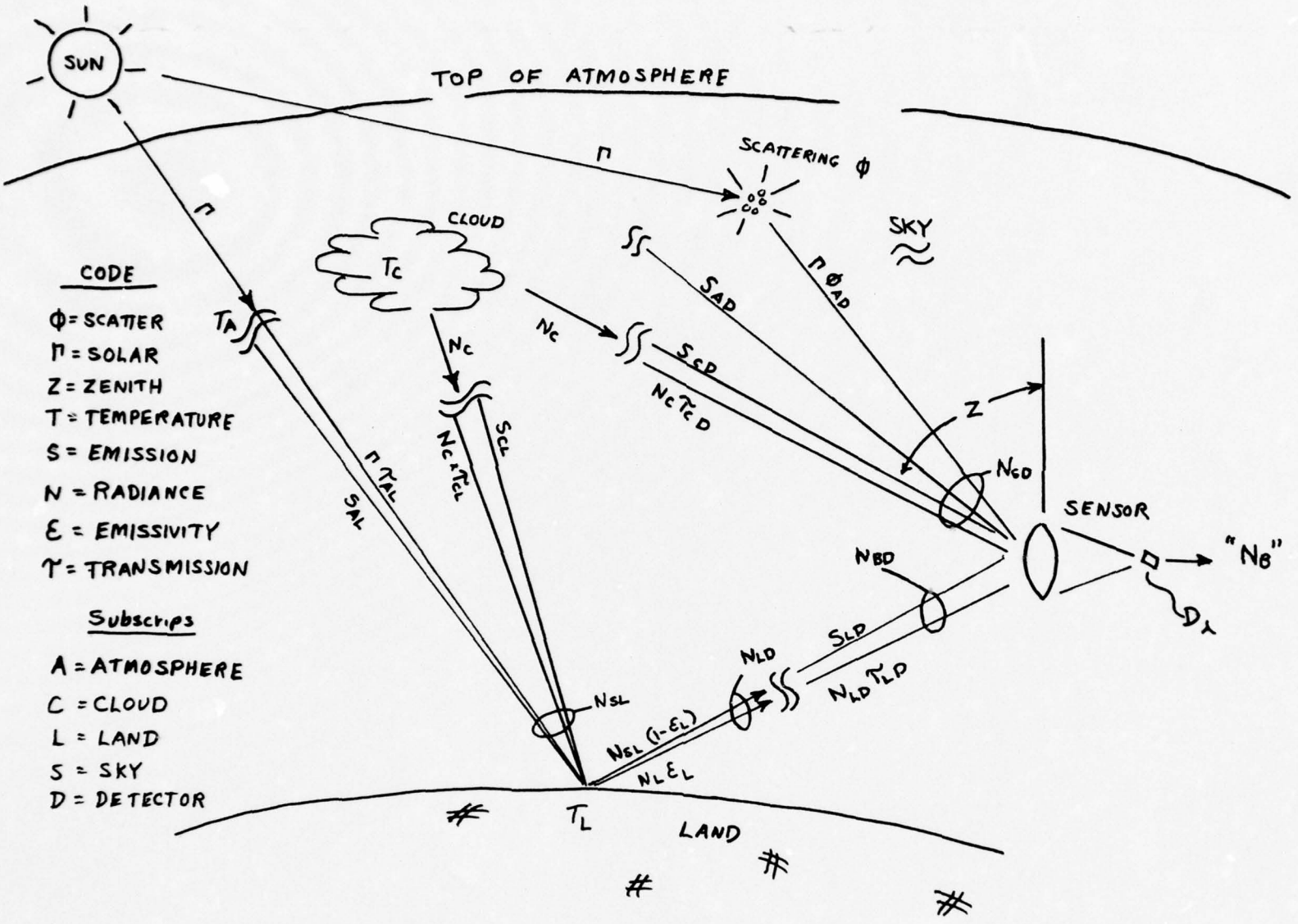

Fig. 5.1 BACKGROUND RADIANCE

wavelength by wavelength at the sensor and weighted by its spectral response, and then integrated over all wavelengths to obtain the effective apparent background radiance.

These quantities are expressed by the following relations.

$$"N_B" = \int_\omega \int_\lambda D\left\{c(z)\left[\Gamma\phi_{CD} + S_{CD} + N_c\tau_{CD}\right] + \left[1 - c(z)\right]\left(S_{AD} + \Gamma\phi_{AD}\right)\right\} d\lambda\, d\omega \qquad z < \text{horizon} \tag{5-1}$$

$$"N_B" = \int_\omega \int_\lambda D\left\{\tau_{LD}\left[N_{SL}(1-\varepsilon_L) + N_L\varepsilon_L\right] + S_{LD} + \Gamma\phi_{LD}\right\} d\lambda\, d\omega \qquad z > \text{horizon} \tag{5-2}$$

Where

$$N_{SL} = \int_{2\pi} \left[c(z)\left[\Gamma\phi_{CL} + S_{CL} + N_c\tau_{CL}\right] + \left[1 - c(z)\right]\left(S_{AL} + \Gamma\phi_{AL}\right)\right] d\Omega \tag{5-3}$$

In these expressions, the wavelength subscript has been suppressed for clarity. The symbols and subscripts are as defined in Figure 5-1, symbols denoting radiative transfer processes and subscripts denoting path lengths (i.e., S_{CL} is the emission in the path from the cloud to the land). The solid angle ω represents the mosaic element field of view and the angle Ω represents all angles over a hemisphere normal to a land element. The emissivity functions are directionally dependent as will be described later.

The composition of the effective apparent target radiance is illustrated in Figure 5.2. The target radiance is seen to consist of an emitted component due to its temperature and a reflected background component comprised in the manner described above. These components are directionally dependent and suitably depleted and abedded by the path transfer characteristics and sensor spectral weighting as was described above. They are described by the following relation.

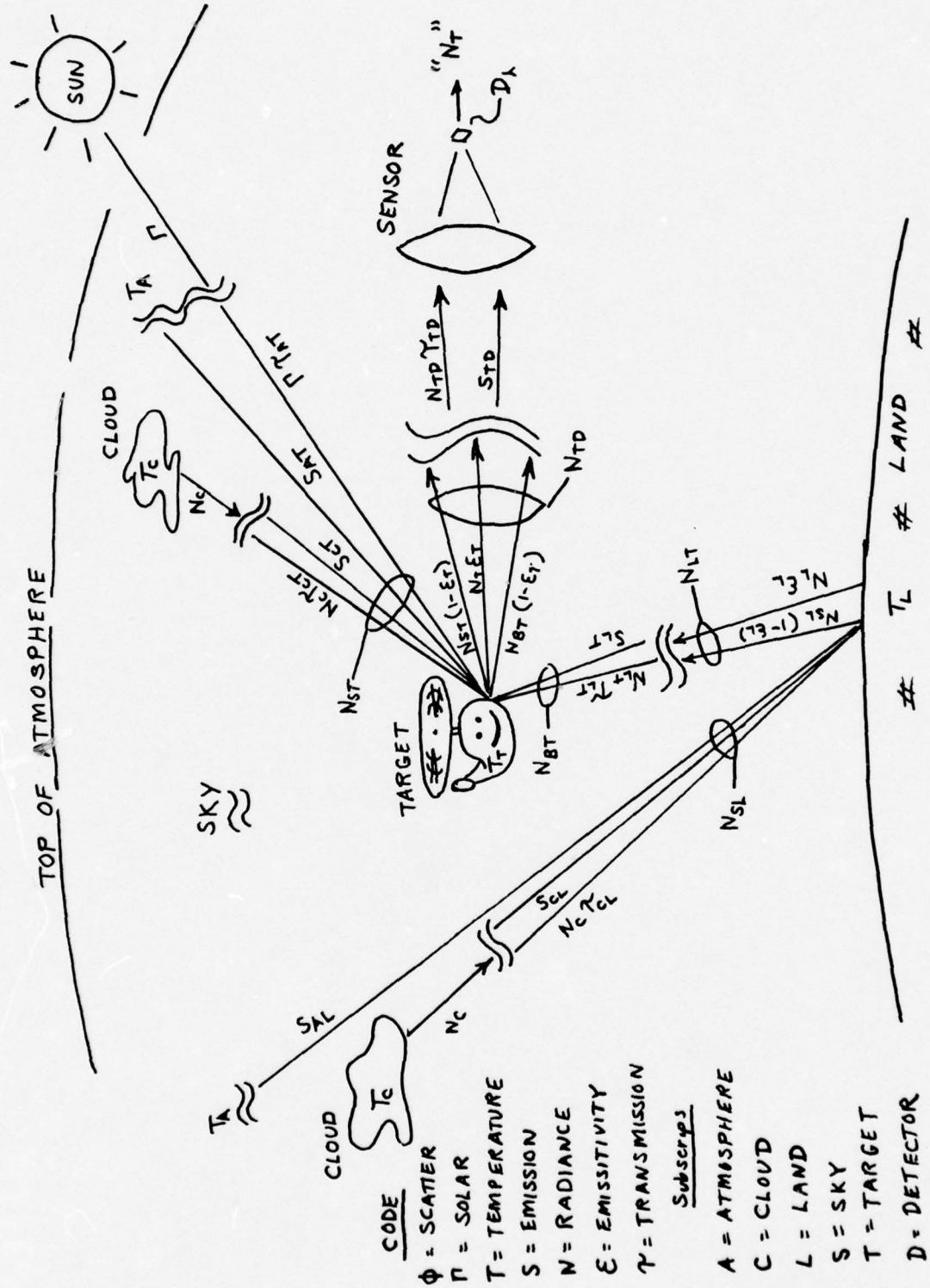

Fig. 5.2 TARGET RADIANCE

$$"N_T" = \int_\omega \int_\lambda D \left\{ \tau_{TD} \left[N_T \varepsilon_T + \int_{2\pi} (1-\varepsilon_T)(N_{BT} + N_{ST})\, d\Omega \right] + S_{TD} + \Gamma \phi_{TD} \right\} d\lambda\, d\omega \qquad (5\text{-}4)$$

The reflected background values N_{BT} and N_{ST} are obtained in the same manner as the background radiance is, except without the sensor spectral weighting and using the appropriate angles and path lengths. These values must be integrated over a hemisphere normal to the target surface element.

The directional emittance and reflectivities are obtained using a bi-directional reflectance model developed by Maxwell at the University of Michigan and monostatic measurements on surface samples from the target Signature Data Compilation file at the University of Michigan.

The reflectance model is defined as

$$\rho(\theta_i, \phi_i; \theta_r, \phi_r) = \frac{R(B)}{R(0)} \frac{\rho'(\theta_N, \phi_N; \theta_N, \phi_N) \cos^2 \theta_N}{\cos \theta_i \cos \theta_r} \qquad (5\text{-}5)$$

where: P^1 = Bidirectional reflectance, $ster^{-1}$

θ = Zenith angle measured to surface unit normal vector

ϕ = Azimuth angle measured to a reference plane

i = Incident ray

r = Reflected ray

N = Surface unit normal

R(S) = Fresnel reflectance for specular surface at a specular angle S

B = One half the angle formed by incident and reflected rays

The Fresnel indexes n and k are obtained from a measurement of the Brewster angle and the normal reflections.

$$R(0) = \frac{(n-1)^2 + k^2}{(n+1)^2 + k^2} \qquad (5\text{-}6)$$

This model has been shown to agree well with actual measurements and facilitates weighting the reflectance from all angles of incidence on a target surface. It is used for all target surfaces, except specular such as glass, and man-made backgrounds such as roads. Other backgrounds are treated as labertian or diffuse reflecting surfaces. Specular reflection off optical surfaces are treated as ideal specular reflection of the background the reflected elemental field of view encompasses.

The directional emissivity is obtained from the bidirectional reflectance function using the following relation.

$$\varepsilon(\theta_r, \phi_r) = 1 - \int_{2\pi} \rho'(\theta_i, \phi_i; \theta_r, \phi_r)\, d\theta_i\, d\phi_i \qquad (5\text{-}7)$$

Thus, only one set of monostatic reflectance data and one set of Fresnel indexes are required for each different surface type encountered to completely describe the directional emittance and reflectance of target and background surfaces.

The atmospheric transmission and emission model utilized was developed and validated for the Naval Research Laboratories. It is applicable for any spectral band in the 1 to 16 micron region with a resolution of better than 3% of the wavelength value.

A thumbnail sketch of this model is illustrated in Figure 5.3 where the observer is shown located at height H viewing a target with a line of sight (LOS) zenith angle Z.

The atmospheric model contains four constituent absorbing gases, water vapor (H_2O), carbon dioxide (CO_2), nitrous oxide (N_2O), and ozone (O_3). Their density distributions with altitude are depicted in the profile curves at the right hand side of the figure.

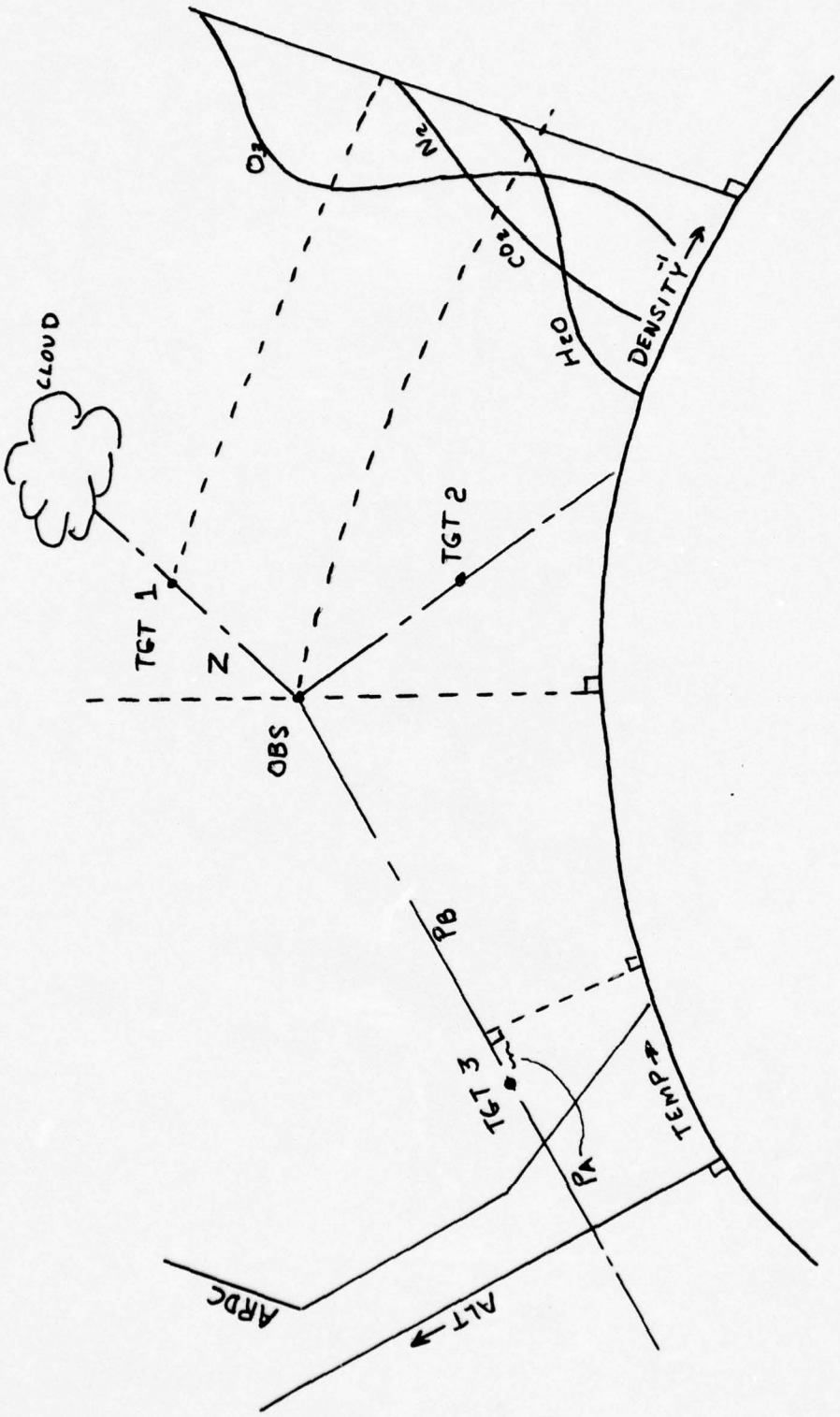

Fig. 5.3 ATMOSPHERIC LOS PATH

The amount of each absorbing gas in a vertical path between the target and observer heights is obtained by integrating the density distributions between these limits. This quantity is then multiplied by the ratio of the height difference to the slant range, R, to obtain the quantity in the LOS path.

The transmission, T_λ , at each wavelength is then computed by using an equation of the following form:

$$\tau_\lambda = e^{-A_1(H_2O)^{\beta_1}} \times e^{-A_2(CO_2)^{\beta_2}} \times e^{-A_3(N_2O)^{\beta_3}} \times e^{-A_4(O_3)^{\beta_4}} \qquad (5\text{-}8)$$

The A's and B's refer to the absorption coefficient and exponent respectively at each wavelength. The numberical subscripts refer to the absorbing species, and the quantity in the brackets refer to the quantity of absorber in the path of each identified species.

The target radiance reaching the observer is then the product of the target radiance and the transmission.

The apparent target radiance as seen by the observer also includes the atmospheric emissions of the intervening path. This component is defined as the integral over the path of the emissivity, ϵ , of a unit volume of air times the black body radiance, $N(T_A)$, at air temperature, T_A, times the transmission, T_S, of the portion of the path, S, between the observer and the unit volume of air. The unit volume of air is endowed with a density of absorbers or conversely emitters and a temperature as dictated by its altitude.

$$S_{TD} = \int_{R_{TD}} \epsilon\, N(T_A)\, \tau_s\, ds \qquad (5\text{-}9)$$

Clear sky emission is obtained by the same procedure described for determining the LOS path emission except that the path length is set equal to infinity, or a terminal height of 100 KM for practical purposes.

$$S_{AD} = \int_{\infty} \varepsilon \, N(T_A) \, \tau_s \, ds \tag{5-10}$$

A cloudy sky emission takes on the same form as the apparent target radiance, except that the range, R_C, is that to the cloud and the cloud temperature, T_C, is assumed to be the same as the air temperature at the cloud height. The cloud emissivity is assumed to be unity.

$$N_{CD} = \int_{R_{CD}} \varepsilon \, N(T_A) \tau_s \, ds + N(T_C) \, \tau_{R_{CD}} \tag{5-11}$$

The earth background is treated similarly to the cloud background for a cloud at sea level. Thus, the above equation is used and the range is that to the earth's surface and the cloud temperature is set equal to the terrestial temperature except that the appropriate emissivity must be used with the given background type.

There are three types of paths over which the target may be viewed. These are denoted as 1, 2 and 3 in Figure 5-3. The first type has the target above the observer, in which case, the background cloud be clear or cloudy. The second type has the target in line with the earth, in which case, the background could be cloudy or earth. In both of these cases, the above equations apply directly.

The third case, has a LOS which passes tangent to the earth at some heights above it. This case can only have a clear or cloudy background. However, except for the instance where a cloud is between the observer and the tangent point, this is a two path case. That is, the LOS passes from the observer height to a lower height at the tangent point and then rises to a higher terminal height.

For this case, the first path is treated as though the observer was located at the tangent point and the background radiance computed for this point using the above procedures. The second path is from the observer to the tangent point and the cloudy sky equation is used except that the background radiance obtained from the first path is entered in the equation in place of the black body radiance term.

The same procedure applies to the target if it lies beyond the tangent point.

Thus, in the various ways described, infrared apparent radiance is obtained for a target or background viewed from any heights along any zenith angle at any range with or without clouds present.

The exhaust plume radiance is also computed in the TRANS subroutine whenever a LOS ray intersects the plume.

The spatial distribution of temperature and partial pressures of the exhaust gas species are computed in the subroutine PLUME. Those functions are used here to define the temperature and gas concentration along the intercepting LOS ray.

Only two exhaust gas species are included in the model, water vapor and carbon dioxide. The transmittance over a unit length dL of the LOS path L through the plume is

$$d\tau_\lambda = EXP\left\{-\left[A_\lambda(T, PP_{H_2O}) + B_\lambda(T, PP_{CO_2})\right] dL\right\} \tag{5-12}$$

where τ = Transmission

A_λ = Absorption coefficient of water vapor

B_λ = Absorption coefficient of carbon dioxide

T = Temperature

PP_{H2O} = Partial pressure of water vapor

PP_{CO2} = Partial pressure of carbon dioxide

λ = Wavelength

The absorption coefficients are functions of both temperature and wavelength.

The transmittance through a path length L of plume is

$$\tau(L) = EXP\left\{-\int_0^L \left[A(L) + B(L)\right] dL\right\} \tag{5-13}$$

where the wavelength subscript has been suppressed for clarity and the absorption coefficients expressed as functions of path length L which imply that the temperature and partial pressure is a function of position along the path.

By setting the incremental emission equal to the incremental transmission,

$$\frac{d\epsilon_\lambda}{dL} = \frac{d\tau_\lambda}{dL} \tag{5-14}$$

the plume radiance may be expressed as

$$N(L) = \int_0^S N(T)\,\tau(L)\,\frac{d\epsilon}{dL}\,dL \tag{5-15}$$

where N(T) represents the black body radiance at the temperature T, S represents the entire path through the plume and L the path length up to the point being evaluated within the integral.

These operations are carried out by numerical integration in the computer program.

The total plume signal N(P) consists of the plume emission N(L) and the background radiance N(B) transmitted through the plume.

$$N(P) = N(L) + \tau(L)N(B) \qquad (5\text{-}16)$$

This radiance is then treated like the target radiance in that it is attenuated by atmospheric transmission and increased by scattering and emission in the path.

The BODY subroutine determines whether the LOS ray intersects the target surface, plume, both or neither. The appropriate radiative transfer computation from one or more of those described above is then selected by computer logic.

5.2 ATMOSPHERIC ABSORBTION AND EMISSION

To understand the relation between gas transmission and emission, consider the following simple example of the gas emission at one end of a one dimensional slab. The radiation arriving at the observation end results from summing the contributions from each grey body element along the slab multiplied by the transmittance of the gas intervening between the element and the observation end.

That is:

$$E = \int_0^L E(X)\ B(X)\ \tau(X)dX, \qquad (5\text{-}17)$$

where E(X) is the emissivity of the element. B(X) is the black-body radiation. τ(X) is the intervening gas transmittance, and L is the slab length.

The difficulty with (17) involves specifying E(X) because measurement of this quantity in a gas is difficult. τ(X), on the other hand, yields easily to experiments.

Through Kirchoff's law, $E(X)T(X)dX$ can be replaced by $-\frac{dT(X)}{dX}dX = -dT(X)$ and (17) therefore becomes $E = \int_0^L B(X)dT(X)$ (2) (5-18)

(18) has an especially simple form. Moreover, it contains easily specified quantities, namely the black body formula and the gas transmittance.

5.2.1 B(X) dT(X) CURVES

Closer inspection of (18) reveals an interesting geometrical interpretation. (18) has the form of the integral of y times dx, where y = B(X), and dx = dT(X). In cartesian coordinates B(X) defines the absissae and T(X) defines the ordinates. Thus the integral, (18), is simply the area under the curve when B(X) is plotted as a function of T(X).

In many cases, E computations follow straight forwardly; for example, atmospheric black body radiance. Radiances from materials having uniform temperatures are evident almost from inspection, since in many cases transmittance is either known or easily determined. B(X) follows from Planck's radiation formula.

The central problem therefore becomes the specification of transmittance. Often this is known from previously measured data. Less frequently, atomic oscillator strength calculations must be performed to determine transmission.

Oscillator line strength calculations are extremely tedious and complicated. The enormous number of molecular vibration-rotation energy levels, each one contributing to transmittance, often requires most of an electronic computers' capacity. As a consequence, the overall radiance computations all too often become stalled at the line strength stage, which becomes an end in itself.

To avoid this, one often interpolates or extrapolates existing data to fit problem conditions. This can be very effective, especially if the interpolation-extrapolation formulas are well chosen. In one example, described in detail below, transmittance equations, fitted to within 2% of laboratory transmittance data over a range of several orders of magnitude predicted atmospheric transmittance and emitance with surprising accuracy.

5.2.2 Engineering Models

Curve fitted formulas, provided they are derived with an understanding of the basic problem physics, and provided they produce required accuracies throughout the problem ranges, can often supply more insight than brute force computations for isolated transmittance values. In many cases, derived from

data, these are at least as accurate as results based on lengthy oscillator strength calculations which, in fact, often assume approximate line shape factors, hence, are actually curve fits on a basic level.

D. Burch, an extensive author on gas transmission, affirmed many times the difficulty of approximating line strength models to actual conditions. Resonance transfer during collisions, self-broadening, foreign-broadening, molecular polarizabilities, etc., complicate matters. For example, self-broadening in atmospheric CO_2 perturbs line structure less than nitrogen induced CO_2 broadening, whereas self broadening in water vapor predominates all other water vapor line perturbations. In view of the many inherent difficulties, a strong case can be made for a good engineering model.

Sometimes, insufficient data prohibits formulation of a good engineering model, hence, oscillator strength computations may be necessary. This possibility must be prepared for with the necessary computer facilities and knowledgeable personnel. The program schedule moreover must provide time to make the necessary oscillator strength computations for these unusual situations. A conceivable, well-planned and effective program intended to produce the most useful results, will provide for both alternatives. Where feasible, an appropriate candidate model function will be fitted to various data sets according to some goodness of fit criteria. Subsequent study will test the results against specific problem parameters, and where possible, experimental results.

5.2.3 Curve Fit Example

To illustrate the method of approximating by an engineering model, the following example of atmospheric transmission will amply suffice. The

spectral region under consideration here is the eight to thirteen micrometer spectral region where little data is available on the water vapor absorption lines.

Water vapor absorption in the eight to thirteen micron spectrum eludes experimentalists and theorists. Here, absorption is very weak, hence the experimentalist requires much water vapor, either by way of a very long absorbing path or a high water vapor density within a small path. Both are difficult to obtain. The path length required is of the order of several kilometers, much too great for even multiple pass systems. High vapor pressures at normal temperatures force condensation. Furthermore, Burch has shown that even if short path, high pressure water vapor absorbers were available, they could probably not be representative. An equivalent path of ten micrometers water vapor distributed over one kilometer does not have the same characteristics as the same amount distributed over a tenth kilometer, and having ten times the H_2O vapor pressure.

On the other hand, the importance of the eight to thirteen micrometer window, demands some estimate of water vapor absorption. Hence, a curve fit was made using data from actual atmospheric transmission measurements. This together with supporting data from other spectral regions verified the reasonableness of the engineering model.

The mathematical model has the form, e^{-ax^b}. The rationale for this ensued from a consideration of the rigorous expressions for abosrption derived from the oscillator strength calculations, namely $T = e^{-\left[\int \sum_i S_i(V_i)\, dV\right] dx}$ where the exponential term symbolizes line strength associated with a frequency centered around V_i.

To this mathematical form, Yates and Taylor's atmospheric transmission measurements over the Chesapeake Bay supplied the raw input data. From their data, absorption due to gasses other than water vapor were removed; principally CO_2, O_3, NO_2. Included also was scattering. These had well specifiable transmission characteristics. Water vapor accounted for the residual absorption.

In addition to the Yates and Taylor atmospheric transmission measurements, the basic model was fitted to laboratory data in other spectral regions, in order to test the validity of the model. Furthermore, the model was tested against detailed absorption computations based on the quasi-random model. These were made by Wyatt, Plass and Stull, and showed generally good agreement with laboratory data in spectral regions from one to about nine micrometers. Incidentally, Stull in a private communication indicated that mathematical difficulties prevented computations extending further into the eight to thirteen micrometer window.

The simple expression, e^{-ax^b} showed remarkable agreement when the coefficients a and b were fitted in the least square sense to laboratory data and also to Wyatt, Plass and Stull's calculated data. This remarkable agreement where good data was available had the significance that it showed the basic mathematical form to be quite reasonable. Extrapolations are always dangerous, of course, but good agreement with laboratory data (to less than 2%) over the spectral region from one to ten microns both for water vapor and CO_2 gave confidence that extrapolations into the eight to thirteen micrometer region were not entirely unreasonable.

Agreement with Yates and Yalor was, on the average, between ten and 20 percent, which about equalled the consistency of their data. This certainly

suffices for estimation purposes. More significantly, transmission computations based on this model and applied to a later set of measurements made by Streete in Florida over a very long path lengths (twenty six kilometers, compared to a maximum of sixteen kilometers in the case of Yates and Taylor) indicated better agreement than any other existing models. Moreover, the engineering model showed a surprising effect, also supported by the very long path measurements, that is, that the eight to thirteen micrometer window apparently ceases to be a window at very long path lengths, and almost abruptly, at some critical path length about 25 precipitable centimeters of water vapor) becomes almost opaque to radiation. Streete observed this phenomenon when he attempted to compensate his instrument by accounting for thermal emission along the path. Burch later offered a possible explanation for the abrupt transmittance fall-off based on strong self-broadening of water vapor.

The engineering model suggested the "critical path length" by the following. The a and b coefficients showed highly correlated trends related to weak and strong absorption bands. For strong bands, the a coefficients, expectedly, had higher values, while the b coefficients approached the value, one half (this concurs with the Goody statistical model). For weak bands, the coefficients became very small (of the order of 5×10^{-4}), while the b coefficients varied from one and a half to two.

This is consistent with Burch's explanation of Streete's results. Burch observed, that in a real abosrption region where essentially only wings of strong lines centered several microns away absorb, line strength increases linearly with pressure (precipitable cm of H_2O); on the other hand the self broadening predominance in H_2O vapor causes a further line strength increase,

also proportional (since it is a pressure effect). Thus, in weak absorbing bands, line strength should vary quadratically with precipitable water vapor.

Evidently, for short paths, the smallness of the a coefficient dominates the exponent and produces almost unity transmittance over long path lengths. For very long path lengths, however, the water vapor path raised almost to the second power begins to reduce transmittance sharply. It is interesting that extrapolations from the Yates and Taylor data to Street's measurements showed a consistent trend. Street's results, have, in fact, sharpended the controversy over which is the best infrared spectral region for optical radar, communications, and passive sensing systems.

Subsequent study revealed an almost log-linear relationship between the a and b tables corresponding to given spectral regions.

The above example illustrates the effectiveness of a good engineering model, both in predicting and providing insight into trends, not always evident from more rigorous and complex models. A very important bonus follows from the simple expression (in this case), since it can be differentiated, integrated, or otherwise manipulated to provide data for emission computations. (The present engineering model also provided excellent agreement with measured values when applied to atmospheric emission calculations).

5.2.4 Care Needed When Extrapolating

Care should be used, however, in any such model in order not to go beyond its regions of validity. For example, as stated earlier, the same number of precipitable centimeters of water vapor over a one kilometer path and a ten kilometer path do not produce the same transmittance. This results primarily from collision line broadening. In the case of atmospheric transmission, line broadening effects due to pressure variations in the atmospheric gasses

do not appear to cause wide transmission variations. This probably results in part from the fact that the partial pressure of atmospheric water vapor rarely exceeds .04 atmospheres, and usually has about half this value. At high temperatures and/or pressures, gas emissivities and transmissivities would be expected to show large departures from the model described above.

5.3 Direct Solar Radiation

Direct solar radiation, impinging on an arbitrarily oriented surface produces an amount of power equal to

$$I = I_o \, T \cos A \qquad (5\text{-}19)$$

where I_o is the solar constant,

T is the transmittance of the atmosphere and,

A is the angle between the surface normal and the solar rays.

cos A can be written in terms of local zenith and azimuth by the equation:

$$\cos A = \cos Z \cos \Theta + \sin Z \sin \Theta \cos (\alpha - \phi), \text{ where} \qquad (5\text{-}20)$$

Z is the solar zenith,

α is the solar azimuth,

θ is the surface normal zenith, and

ϕ is the surface normal azimuth.

The solar zenith will, of course, affect the transmittance through the air mass dependence.

5.4 SCATTERING

5.4.1 Mie Theory

Particle scattering has been discussed in great detail by numerous workers. The most famous of these are undoubtedly Lord Rayleight and G. Mie, after whom two scattering phenomena are named. Rayleight scattering deals with particles of small sizes compared with the wavelengths of the scattered light, while Mie scattering concerns large particle scattering. The division, however, is artificial since Rayleigh scattering is really a special case of Mie's scattering theory (Ann. d. Physik (4), 25, (1908), 377) in which Mie obtained, using electromagnetic vector fields, a rigorous solution for the diffraction of a plane monochromatic wave by a homogeneous sphere of any diameter and composition situated in a homogeneous medium. Mie's solutions are given in the form of series expansions which are characterized by the parameter $\alpha = \frac{2\pi r}{\lambda}$, where r is the radius of the scattering particle and λ is the wavelength. For $\alpha < 1.0$ the effective scattering cross section is proportional to λ^{-4} according to Rayleigh 's approximation. With $\alpha >$ 6, the scattering coefficient becomes a periodic function and approaches a final value of 2. Rayleigh scattering is equally intense in forward and backward directions, while Mie scattering is predominantly a forward scattering phenomenon.

5.4.2 Scalar Apprxomation

Mie's theory is elegant and amply verified by much experimental data. On the other hand, its complexity makes it tedious, lengthy and cumbersome. Therefore, simpler approximate formulas have substituted for the rigorous Mie theory in many cases of practical interest. Chief among these is the scalar diffraction theory.

Scalar diffraction theory replaces the vector optical field with a harmonic scalar function. The well known Helmholtz-Kirchoff diffraction formula illustrates the scalar approximation to the vector field. By substituting a scalar function for the rigorous, but complicated vector formulation, one acquires in many cases, a relatively simple, closed form expression which generally predicts diffracted fields reasonably accurately. Loss of accuracy occurs in limiting cases such as when dimensions are of the order of a wavelength, or for special boundary conditions. The scalar theory provides no knowledge of polarization.

Applied to particle scattering, scalar theory is especially simple. One often approximates a sphere by a disc, then applies Babinet's principle which implies that the far field intensity pattern is the same as that which a hole with the same radius as the disc in an otherwise opaque screen would produce. Thus the far field pattern according to this approximation is the simple Airy distribution.

5.4.3 Atmospheric Complications

The atmosphere greatly complicates things because it contains an enormous variety of particle types and sizes. Moreover these distributions can change very quickly, spoiling estimates made on the basis of previous distributions.

Studies have been made of particle size distributions at specific locations on the earth. Some postulated particle size distributions fit experimental data quite well. D. Deirmendjian (Appl. Opt. 3, No. 2, Feb. 1964, p. 187) found that a particle size distribution given by $n(4) = 5.33 \times 10^{4} \times r_e^{-8.944\, r}$ agreed well with published counts made by Gilbert (J. B. Harvard, PhD Thesis, University of Washington, 1960). Previously, Deirmendjian had used successfully a distribution of the form $n(4) = ar^{-4}$ where a is a constant.

The first form compared with data taken in Los Angeles to represent typical coastal conditions.

H. Dessens (La Meterol., 1947, p. 321) used spider webs to trap aerosol particles. Measuring these particles, Dessens found their sizes to be most frequently (78%), 0.40 micrometers. This agreed with observations of H. Kohler (MZ 38: 359-365, 1921). Other expressions which fit aerosol size distributions fairly well are:

$$n(r) = C \exp\left((a-a_m)^2/6\right)$$ (J. Bricard, Annales de Phys. 14, 148, 1940)

$$n(r) = C \exp\left(-A \log^2 (a/a_m)\right)$$ (L. Foitzik, Zeits, fur Meterorol. 4, 321, 1950)

This brief discussion suggests the complexity of the atmospheric scattering problem. It should be apparent at this juncture that atmospheric scattering is very difficult to describe with any flexibility to account for changing conditions. In spite of this difficulty, various authors have attempted to define mathematically atmospheric scattering.

Numerical calculations were carried out by Bullrich, et al. (Geofis. Pura Appl. 23, 69, 1952), Moller, et al. (Geofis. Pura Appl. 23, 141, 1953) and Feigelson, et al. (Calculations of the Brightness of Light, Trudy, Inst. Atm. Phys., #1, 1958 (Consultants Bureau, New York, 1960). A recent, very comprehensive study on atmospheric scattering was authored by G. N. Plass. Using a large computer, Plass calculated multiple scattering of light along various atmospheric slant paths on the basis of Mie's scattering theory and applying Monte-Carlo techniques. His studies include scattering at all visible wavelengths and over very many atmospheric conditions. His results are given in a set of extensive tables.

5.4.4 Phenomenological Approach

Various authors have attempted to simplify the atmospheric scattering problem by using a phenomenological approach. Since aerosols are size distributed in the air, it is expected that neither pure Rayleigh scattering (λ^{-4} dependence, symmetrical forward and backward scattering, with minima at right angles to the incident light) or pure large-particle scattering (wavelength independent, predominantly forward scattering) would predominate. Hence a tendency toward forward scattering, increasing with haze or fog, wavelength dependent, but not as strongly as λ^{-4} would be expected in the actual atmosphere. Such a dependence has in fact been noted. Moller (Appl. Opts. 3, 2, Feb. 1964, p. 157) obtained an average extinction coefficient at sea level ($k = 1.1 \times 10^{-3}$ to 8×10^{-2} km^{-1}). Moller also found the average wavelength extinction coefficient for one air mass to be $8.8 \times 10^{-3} \lambda^{-4} + 0.1 \times 10^{-1} \lambda^{-1}$.* This agrees well with the Geophysical Handbook data which assumes an exponential decrease of both particles corresponding to λ^{-4} attenuation, and particles corresponding to λ^{-1} attenuation. The Geophysical Handbook data ascribes a scale height of 8 km to the first type and a scale height of about 1.5 km to the second. Moller's average data is not completely useful, however, for the reason that it is average.

5.4.5 Visual Range

A practical approach to the problem of describing atmospheric scattering relies on the concept of visual range. Visual range is, by definition, that range where the contrast between an object and the surrounding sky background

*Wavelength in microns

is less than 2 percent, the contrast being defined by the expression $\frac{O-B}{B}$, where O is the brightness of the object and B is the brightness of the sky background. The connection with extinction by scattering ensues from the fact that the brightness of the sky background results from light scattered into the field of view of the observer. Thus, light from an observed object is attenuated by scattering at the same time that skylight is scattered into the field of view. An excellent exposition of the entire problem of atmospheric scattering in the visible spectral region is given by W. E. K. Middleton in his book, "Vision Through the Atmosphere." The book concerns itself almost entirely with atmospheric extinction of visible light by scattering processes and their effects on visibility. Middleton shows that the visual range and the scattering extinction coefficients extinction coefficients are related through the equation $k = V/3.912$, where k is the atmospheric extinction coefficient and V is the visual range.

Further, Middleton shows that molecular scattering processes and atmospheric absorption play a negligible role in visual range problems compared with aerosol scattering. Thus, visual range measurements, in effect, perform the necessary integration over the large scattering particles. The difficult problem of determining aerosol size distribution and the resulting Mie scattering calculations is sidestepped.

5.4.6 Visual Range Measurements

Visual range is such a useful concept that several visual range measuring instruments have been devised. The Waldrop Visual Range attachment for telescopes developed for the British Navy during World War II is a good example of the simplicity with which visual range can be measured. This instrument consists of a prism with very weak refracting power which can be

adjusted over the objective lens of a telescope so as to vary the aperture, and a scale to indicate aperture.

The prism refracts clear sky into the field, while the clear portion of the objective passes the object. By adjusting the prism until the brightness of the sky matches that of the scene and reading the scale, visual range is directly indicated.

5.4.7 Slant Range

A paragraph above cited a Geophysical Handbook value of about 1.5 km for the scale height of large scattering particles. Scale height implies an exponential dependence, since, by definition, the scale height is that height at which the density falls to 1/e of its ground level value. The scale height also defines the height of a uniform particle distribution which contains the same quantity of particles in a vertical column as the corresponding exponential distribution.

When an exponential function validly defines the scattering coefficient, transmittance along a slant path becomes

$$T = \exp\ k^{\circ} H_{\circ} \sec z \left(e^{-h/H_{\circ}} - 1\right) ,$$

where $k^{\circ} = \frac{3.912 \times .55}{V.R. \times \lambda}$ is the scattering coefficient at ground level,

h is the altitude,

$H_{\circ}$ is the scale height, and

z is the zenith distance.

When z = 0 (vertical path) and h becomes very large;

$$T = \exp\left(-k^{\circ} H_{\circ}\right) .$$

For nearly horizontal surface paths,

$$T = e^{-R\, k^{\circ}} ,$$

where R is the range.

Scale height is thus seen to be a very useful concept for estimating slant path transmittance.

5.4.8 Modification to $k \sim 1/\lambda$

Moller's inverse first power dependence of the scattering coefficient on wavelength allows extrapolation to other wave lengths once the visual range is specified for a particular visible wavelength. For example, Yates and Taylor specified visual range at .55 micrometers. Using their method, the following extrapolates scattering losses to other wavelengths.

Transmission due to scattering is $T = \exp(-kR)$, where k is the scattering coefficient and R is the range. Put in terms of the visual range, the formula becomes,

$$T = \exp(-3.912\ R/V.R.) \quad .$$

Visual range is cited at .55 micrometers, hence assuming the validity of Moller's and Yates and Taylor's inverse relation, the scattering coefficient at another wavelength becomes $3.912/V.R.\ (\lambda/.55)$, and the corresponding transmission is $T = \exp(-3.912\ R/V.R.\ (\lambda/.55))$.

Particle scattering may not vary inversely with the wavelength, however, at least not exactly. Westinghouse made a study of other inverse power relations between wavelength and scattering coefficient, based on the Yates and Taylor data. Briefly, inverse power ratios up to inverse fourth were studied, using as criteria, the best data fit. Inverse powers producing best fits range from below unity to about 2.2. The dependence was not critical, however, and all inverse powers with this range produced acceptable results. These findings generally supported Moller's formula, but also indicated that agreement under some conditions may be improved by varying the inverse power law.

5.4.9 Factors Affecting Particle Distribution

The preceeding discussion presupposed an exponential relation between particle density and altitude, with a scale height of approximately 1.5 km. This, of course, can only be approximate since many local factors influence particle sizes and types. For example, soot, and dirt particles over smoke stacks, trees over sandy areas, particle size distribution over turbulent water, snow, rain, hail, etc. create special distributions. These distributions may peak above ground level as in the case of measurements made over Hawaii. Each situation requires special consideration.

5.4.10 Monte Carlo Methods

Visual range provides a practical tool for estimating atmospheric attenuation by scattering. It is entirely phenomenological, however, and often the problem is not to determine on the spot estimates, but to examine in detail how particle size and type distributions affect scattering losses.

The Monte Carlo method is the most powerful technique for attacking the scattering problem. In this method, scattered energy is calculated for each individual particle. Using Mie's rigorous theory, (thus accounting for polarization) a new direction for scattered flux is determined on a statistical basis, as are path lengths between scatterers. The process continues throughout the scattering medium until the light escapes or is absorbed. Particle sizes and types are included in the computations. The Monte Carlo method requires many ray traces. It is analogous to transmission calculations starting from molecular vibration-rotation levels. Evidently, Monte Carlo techniques require large computers.

5.5 ATMOSPHERIC ATTENUATION COEFFICIENTS

The following paragraphs outline in detail the steps required to construct a transmission model, and to apply the model to transmittance and emittance computations along slant ranges. Included are curve fits to meteorlogical data including water vapor lapse rates, atmospheric temperature and pressure, ozone, carbon dioxide, and nitrous oxide distributions. The procedure also describes a method for estimating scattering effects through the concept of visual range.

5.5.1 Model Preparation

The atmospheric transmission model has five transmission components. These are: H_2O, CO_2, N_2O, O_3, and scattering.

The following formulas express transmittance of these components:

$$\tau_{H_2O} = \exp\left(-a\, P_1^{\,b}\right) \tag{5-21}$$

$$\tau_{CO_2} = \exp\left(-a\, P_2^{\,b}\right) \tag{5-22}$$

$$\tau_{N_2O} = \exp\left(-a\, \sqrt{P_3}\right) \tag{5-23}$$

$$\tau_{O_3} = \exp\left(-a\, \sqrt{P_4}\right) \tag{5-24}$$

$$\tau_{scat} = \exp\left(-k\, R\right) \tag{5-25}$$

a and b are constantsdependent on spectral regions and gases, P_i's are gas paths reduced to standard conditions (300°K, 1 atm.), k is the scattering extinction coefficient, and R is the range.

5.5 1.1 H_2O Transmittance

The formula expressing H_2O transmittance is exp $(-a\ P_1^{\ b})$. The a's and b's must be fitted by a least mean squares method using transmittance data for standard conditions over several path lengths.

See paragraph 5.5.1.2 for a description of the least mean squares method.

For the 1 to 10 micrometer region, refer to calculated results of Wyatt Plass & Stull (Applied Optics 3, 2, Feb. 1964, pp 229-241).

For the 10 to 20 micrometer region, refer to Yates & Taylor (Infrared Transmission of the Atmosphere, NRL Report 5453, U.S. Naval Res. Lab., Wash., D.C., 1960), or Handbook of Military Infrared Technology).

The transmittances of the other components must be extracted from the Yates & Taylor data before H_2O can be evaluated. Therefore, complete the other transmittance steps before attempting to calculate H_2O from the Yates & Taylor data

$$\tau_{H_2O} = \tau^{\circ}/\tau_{CO_2}/\tau_{N_2O}/\tau_{O_3}/\tau_{scat} \qquad (5\text{-}26)$$

where τ° is the measured infrared transmittance.

The Yates and Taylor data require a correction factor to reduce their precipitable centimeters of H_2O to standard conditions.

Multiply their stated precipitable centimeters of H_2O by

$$H_2O\,(\text{CORRECTED}) = \left(\frac{T}{T_0}\right)^{1/2}\left(\frac{P_0}{P}\right) H_2O\,(\text{STATED}) \qquad (5\text{-}27)$$

where

$T_0 = 300^{\circ}K$ and

$P_0 = 1$ atm.

The Yates & Taylor data include T and P.

5 5 1.2 Normal Equations for Least Mean Squares Fit

5 5.1.2.1 Determining the Constants

Assume that N data for equivalent gas paths and corresponding transmittances are given, and find the best fits for H_2O and CO_2 using a formula of the form

$$\tau = \exp(-a\, w^b). \tag{5-28}$$

This leads to:

$$-\ln \tau = a\, w^b, \tag{5-29}$$

or taking another ln;

$$\ln(-\ln \tau) = \ln a + b \ln w, \tag{5-30}$$

where a and b are the constants to be determined, and

w is the total gas path. (5-31)

To find a and b, solve the following set of two linear equations in two unknowns:

$$N \ln a + b \sum \ln w_i = \sum \ln(-\ln \tau_i) \tag{5-32}$$

$$\ln a \sum \ln w_i + b \sum (\ln w_i)^2 = \sum \ln w_i \ln(-\ln \tau_i). \tag{5-33}$$

The sums include the N data for equivalent paths (w_i) and corresponding transmittances (τ_i).

5 5.1.2.2 Goodness of Fit

When the a's and b's are known, they can be inserted into the proper equations to compute transmittance. Thus, computed transmittance can be compared point by point with the experimental data as follows. Let $T_e(w_i)$ be the actual data and $T_c(w_i)$ be the computed data for the i-th path length. A good figure of merit for testing goodness of fit is

$$F.M. = \sum_i^N (T_e(w_i) - T_c(w_i))^2. \tag{5-34}$$

The smaller this quantity, the better the fit.

5.5 1.3 CO_2 Transmittance

The transmittance of CO_2 is defined by the formula,

$$CO_2 = \exp\ (-a\ P_2^{\ b}) \qquad (5\text{-}35)$$

where P is the equivalent CO_2 path at standard conditions.

The a's and b's will be fitted to calculated data of Wyatt Plass & Stull (Applied Optics 3, 2, Feb. 1964, pp 243-254). The data includes the spectral region from one to eighteen micrometers at 2.5 cm^{-1} intervals.

Use the least mean squares method described in paragraph 5.5.1.2.

5 5 1.4 N_2O Transmittance

The transmittance of N_2O is described by the formula,

$$\tau\ N_2O = \exp\ (-a\ \sqrt{P_3}). \qquad (5\text{-}36)$$

Data to determine a in the best least mean squares sense can be obtained from the Handbook of Military Infrared Technology; T.L. Altshuler, "Infrared Transmission and Background Radiation by Clear Atmosphere," General Electric Document, 61SD199 (1961).

Fit the transmittance formula to the data over several path lengths for various a values to produce the best least mean squares fit. This determines the constant, a.

5.5.1.5 O_3 Transmittance

The formula

$$\tau\ O_3 = \exp\ (-a\ \sqrt{P}), \qquad (5\text{-}37)$$

where P is the equivalent millimeters of O_3 at standard conditions, and

a is a constant

models O_3 transmittance.

Data for O_3 transmittance can be obtained from the Handbook of Geophysics. The constant, a, will be fitted to the data in the same manner as the N_2O model of paragraph 5.5.1.4.

5 5 1.6 Extinction by Scattering

The formula

$$\tau_S = \exp(-kR), \qquad (5\text{-}38)$$

models scattering transmittance,

where k is the extinction coefficient, and

R is the range.

The constant k is defined in terms of the visual range and wavelength according to the formula

$$k = \frac{2.152}{(VR)\lambda}, \qquad (5\text{-}39)$$

where VR is the visual range and

λ is the wavelength in microns.

VR will be obtained from on the spot measurements and its units (kilometers, miles, etc.) will be the same as those of R.

5 6 Distributions

5 6.1 Temperature

The temperature profile follows the ARDC (1959) model and has the following four lapse rates.

0 to 11 Kilometers

$$T = Tg - \frac{72}{11} h, \qquad (5\text{-}40)$$

Tg is the ground temperature (^{o}K) and

h is the altitude in kilometers.

11 to 25 Kilometers

$$T = Tg - 72$$

25 to 48 Kilometers

$$T = Tg - 72 + \frac{72}{23} (h - 25)$$

48 Kilometers and Above

$$T = Tg$$

6.2 Pressure

Pressure varies exponentially with a scale height of 8 kilometers. Thus,

$$P = Pg\ e^{-h/8}, \qquad (5\text{-}41)$$

where Pg is the ground level pressure and

h is the altitude in kilometers.

6.3 H_2O Mixing Ratio

H_2O mixing ratio varies exponentially with altitude according to the formula

$$M = Mo \exp(-.497\ h) \qquad (5\text{-}42)$$

where Mo is the ground level mixing ratio, and

h is the altitude in kilometers.

5 6.4 Ozone

The ozone distribution is the "standard" distribution reported by Green (Applied Optics 3, 2, Feb 1964, pp 203-208), and the Handbook of Geophysics.

The integrated amount of O_3 above an altitude y, is

$$w_1 = w_p \left\{1 + \exp \quad (y_1 - y_p)/h\right\}^{-1}. \qquad (5\text{-}43)$$

The integrated quantity between two altitudes is $w_2 - w_1$, where $w_1 \neq w_2$ are the integrated quantities above altitudes y_1 and y_2.

5 6.5 Scattering Particles

The large scattering particles which affect visual range have an exponential lapse rate with a scale height of 1.5 kilometers. The formula is

$$\rho_{scat.} = \rho_o \exp\left(-\frac{h}{1.5}\right), \qquad (5\text{-}44)$$

where ρ_o is the ground level density, and

h is the altitude in kilometers.

5.7 Transmission Computation

Transmittance calculations require equivalent path data. This data depends on slant path meteorological conditions. First, however, the computation procedure is described for horizontal paths where meteorological densities remain constant.

5.7.1 Horizontal Gas Paths

H_2O

The precipitable centimeters of H_2O per kilometer of air are

$$w = 6.11 \times 10^2 \; m \times \frac{P^2}{T^{3/2}} \quad \text{pre cm/km} \qquad (5\text{-}45)$$

where m is the mixing ratio,

P is the pressure and

T is the temperature.

CO_2

The equivalent path of CO_2 is

$$p = 32\ (P)\ \left(\frac{300}{T}\right)^{3/2} \text{ atmospheric cm/km path.} \qquad (5\text{-}46)$$

N_2O

The equivalent path of N_2O is

$$p = .028\ (P)\left(\frac{300}{T}\right)^{3/2} \qquad (5\text{-}47)$$

with the same symbols as above.

Ozone

The ozone distribution function expresses equivalent millimeters of ozone per kilometer air path. The formula is

$$p = \frac{2.18}{1 + \exp\left[(y - 23.35)/4.63\right]} \text{ mm/km air path,} \qquad (5\text{-}48)$$

where y is the altitude.

Scattering

The extinction coefficient for scattering transmittance was defined in Paragraph 5.5.1.6.

$$k = \frac{2.152}{(VR)\lambda}\ , \qquad (5\text{-}49)$$

where VR is the visual range, and

λ is the wavelength.

Multiplication by Range

The quantities defined in Paragraphs above must be multiplied by range. The resultant product is the quantity to be inserted in the transmission equations. Thus, for example

$$\tau\ H_2O = \exp\left(-a(wr)^b\right), \qquad (5\text{-}50)$$

where a and b are water vapor parameters for the desired spectral band,

w is the equivalent path per kilometer dry.

R is the range in kilometers.

Composite Transmittance

The composite transmittance is the product of the five component transmittance factors. Thus,

$$\tau = H_2O \times \tau CO_2 \times \tau N_2O \times \tau \text{ scat.} \times \tau O_3 \qquad (5\text{-}51)$$

5.7.2 Slant Paths, Gas Path Computations

Slant paths require a different procedure to obtain equivalent amounts of gas. First, the following geometric factor must be evaluated.

Geometrical Factor

Let h_1 be the initial altitude and h_2 be the final altitude. The path length between these two altitudes, for a given zenith distance, Z, is

$$R = -(R_e + h_1)\cos Z + \sqrt{(R_e + h_1)^2 \cos^2 Z + (R_e + h_2)^2 - (R_e + h_1)^2}\ ,$$

$$= -(R_e + h_1)\cos Z + \sqrt{(R_e + h_2)^2 - (R_e + h_1)^2 \sin^2 Z}, \qquad (5\text{-}52)$$

where R_e is the radius of the earth.

To obtain the geometrical factor, divide R by the absolute value of $h_2 - h_1$; thus,

$$\text{Scale Factor} = \frac{R}{h_2 - h_1}\ . \qquad (5\text{-}53)$$

The scale factor is sometimes called the "air mass", although the term usually refers to all the air in the earth's atmosphere in a vertical column starting from ground level. For example, three air masses normally denotes the amount of air contained in three vertical columns of the earth's atmosphere. The function, sec Z, approximates air mass up to about 80 degrees zenith distance. Three air masses correspond to about Z = 70 degrees.

The procedure here for calculating equivalent amounts of gas over a slant range between the two altitudes, h_1 and h_2, requires the following two steps.

1. Calculate the equivalent amounts of each gas in a vertical column between altitudes h_1 and h_2.

2. Multiply this by the scale factor derived in equation (5-53).

The following paragraphs explain how to calculate equivalent amounts of each gas in a vertical column between h_1 and h_2.

Water Vapor

The precipitable centimeters of water vapor in a vertical column reduced to standard conditions (300°K, 1 atm) are

$$w = 611\, m_o \int \frac{P^2}{T^{3/2}} e^{-.497h}\, dh. \qquad (5\text{-}54)$$

where m_o is the ground level mixing ratio, and

P and T are pressure and temperature.

The integral breaks into four separate regions because of temperature discontinuities. The following equations express the precipitable centimeters of water in a vertical column corrected to standard conditions whose base lies at the bottom of the corresponding temperature zone.

0-11 Kilometers

$$w = \frac{817.9\, m_o\, P_o^2}{T_o^{3/2}} \left[1 - e^{-.747h} + \frac{13.143}{T_o} \left(1 - e^{-.747h}\right) - \frac{9.818}{T_o} h\, e^{-.737h} \right], \quad (0 \leq h \leq 11 \text{ km}) \qquad (5\text{-}55)$$

P_o, T_o and m_o are ground level pressure, temperature and mixing ratio.

11-25 Kilometers

$$w = \frac{817.9\, m_o\, P_o^2}{T_{11}^{3/2}} \left[.00027 - e^{-.747h} \right], \quad 11 \text{ km} \leq h \leq 25 \text{ km}. \qquad (5\text{-}56)$$

T_{11} is the temperature at 11 kilometers. This equals $T_o - 72^\circ$.

25-48 Kilometers

$$w = \frac{817.9\, m_o\, P_o^2}{T^{1\,3/2}} \left[7.75 \times 10^{-9} + \frac{9.59 \times 10^{-7}}{T^1} - 1.339\, e^{-.747h} \right.$$

$$\left. - \frac{4.696}{T^1} e^{-.747h} (1.339 + h) \right] \quad (25 \leq h \leq 48 \text{ km}). \qquad (5\text{-}57)$$

where $T^1 = T_o - 150.26^\circ$.

48- ∞ Kilometers

$$w = \frac{817.9\, m_o\, P_o^2}{T_o^{3/2}} \left[1.122 \times 10^{-14} - e^{-.747h} \right] \quad h > 48 \text{ km} \qquad (5\text{-}58)$$

Quantity Between Two Altitudes

The four equations above express integrated quantities from the bottoms of each respective temperature region. They can also yield total gas quantities between arbitrary altitudes. For example, the precipitable centimeters of water corrected to standard conditions in a vertical column between altitudes h_1 and h_2 (11 km $> h_2 > h_1$) are $W_2 - W_1$, where W_1 and W_2 are quantities of water between ground level and h_1 and h_2 respectively.

When the vertical column includes more than one temperature region, add the total quantities in each region. For example, if h_1 = 2 km and h_2 = 20 km, determine the gas quantity from 2 to 11 km ($W_{11} - W_2$) according to equation (5-55) and add this to the amount from 11 to 20 km ($W_{20} - W_{11}$) as determined from equation (5-56).

Simpler Approximate Form

The quantity of water from ground level to eleven kilometers greatly predominates the quantity of water above eleven kilometers. Moreover, the magnitude of the third and fourth terms of the equation for water vapor contribute less than five percent, and can be neglected without great accuracy loss. The precepitable centimeters of water can be expressed to a good approximation for all temperature regions by the formula

$$w = \frac{818\, m_o\, P_o^2}{T_o^{3/2}} \left\{ 1 - e^{-.747h} \right\} \quad 0 \leq h. \tag{5-59}$$

Carbon Dioxide, Nitrous Oxide

The equivalent centimeters of CO_2 and N_2O must also be calculated separately in four regions. Each has a constant mixing ratio so the two gas quantities differ only by a constant. First evaluate four basic integrals over the same four regions as for H_2O.

0-11 Kilometers

$$\rho = (P)^2 \left(\frac{300}{T}\right)^{3/2} \left[4(1-e^{-h/4}) + \frac{9.818}{T} \left[-4h\, e^{-h/4} + 16\left[1 - e^{-h/4}\right]\right]\right] \tag{5-60}$$

P in atmospheres,

T in degrees Kelvin.

11-25 Kilometers

$$\rho = (P)^2 \left(\frac{300}{T_{11}}\right)^{3/2} 4 \left\{ e^{-2.75} - e^{-.25h} \right\} \qquad (5\text{-}61)$$

25-48 Kilometers

$$\rho = (P)^2 \left(\frac{300}{T}\right)^{3/2} \left[4 \left(e^{-50/8} - e^{-h/4}\right) + \frac{3}{2} \frac{a'}{T'} \left[4 \left(25\, e^{-50/8} - he^{-h/4}\right) \right.\right.$$

$$\left.\left. + 16 \left(e^{-50/8} - e^{-h/4}\right) \right] \right] \qquad (5\text{-}62)$$

$a' = -72/23$

$T' = T_{11} - 78.26.$

48 Kilometers

$$q = (P)^2 \left(\frac{300}{T_{45}}\right)^{3/2} 4 \left\{ 3^{-90/8} - e^{-h/4} \right\} \qquad (5\text{-}63)$$

Approximation

The above equations for carbon dioxide and nitros oxide can be replaced, to a good approximation, by the simpler equation:

$$q = (P_q)^2 \left(\frac{300}{T_q}\right)^{3/2} \left[4.4 - \left\{ 7.6\, e^{-314h} - 3.2\, e^{-417\, h^{1.057}} \right\} \right] . \qquad (5\text{-}64)$$

P_q and T_q are ground level pressure and temperature.

This approximation holds for all altitudes.

CO_2 Mixing Ratio

Multiply the equations above by 32 to obtain the equivalent centimeters of CO_2 above a height, h.

Nitrous Oxide, Equivalent Centimeters

Multiply the above equations by .28 to obtain the equivalent centimeters of N_2O above a height, h.

Ozone

Equations (5-54) defined the ozone distribution above a height, y_1. To be consistent with the above treatment..... this paragraph defines the amount of ozone up to a height, y_1. This is simply the amount above a height, $y = 0$, minus the amount above a height, y_1. The amount between two heights, y_1 and y_2 is therefore

$$(w_1 - w_2) - (w_0 - w_1) \approx w_1 - w_2, \tag{5-65}$$

or, the amount above a height, y_1 minus the amount above a height, y_2:

$$W_{1,2} = w_p \left\{1 + \exp \quad (y_1-y_p)/h\right\}^{-1} - w_p \left\{1 + \exp \quad (y_2-y_1)/h\right\}^{-1} \text{mm } O_3. \tag{5-66}$$

$w_p = .218$

$y_p = 23.25$

$h = 4.63$

Scattering

The transmittance due to large scattering particles over slant paths between two heights, y_1 and y_2 is:

$$\tau_s = \exp \{ - (S.F.)\, k_o/a\, (e^{-a\, y_1} - e^{-a\, y_2}). \qquad (5\text{-}67)$$

S.F. is the scale factor described by equation 5-53.

$k_o = 2.152/(VR)\lambda$, where VR is the visual range, and

λ is the wavelength, and

a is the inverse of the scale height. For $h_s = 1.5$, $a = .667$.

Recapitulation

Paragraph 5.7.2 described the procedure for computing precipitable centimeters of water, and equivalent paths of CO_2, N_2O and O_3. These quantities must be inserted into the transmission equations, $\tau = \exp(-a\, P^b)$ where P is now the total amount of gas including range (reduced to standard conditions) between initial and final heights, multiplied by the scale factor described in equation (5-53).... a and b are constants appropriate to each gas and spectral band.

Composite Transmittance

The composite slant path transmittance is

$$\tau = \tau_{2O} \times \tau_{CO_2} \times \tau_{N_2O} \times \tau_{O_3} \times \tau_{sc.} \qquad (5\text{-}68)$$

5.8 Sky Radiance

~~5.8.1~~ Mathematical Formula

Clear sky emission is described by the formula

$$W = \int_o^{R_o} \beta \, \frac{d\tau}{dR} \, dR \text{ watts/cm}^2\text{/str.} \qquad (5\text{-}69)$$

β is Planck's blackbody radiance formula,

τ is the composite transmittance, excluding scattering,

R is the slant path,

R_o is the slant path range.

β depends implicitly on slant range R_1 through its temperature dependence. Transmittance depends on slant range through its dependence on temperature, pressure, mixing ratios and path length.

The differentiation and integration are carried out with respect to slant paths.

5.8.2 Cloud Presence

The formula for sky emission in the presence of clouds contains two terms. One term expresses sky emission along a slant path up to the cloud; the second term expresses the radiance contributed by the cloud:

$$W_c = \int_0^{R_o} \beta \frac{d\tau}{dR} dR + \beta(T_c)\tau, \qquad (5\text{-}70)$$

where:

R_o is the range to the cloud,

T_o is the effective temperature of the cloud, and

$\beta(T_c)$ is the blackbody radiance of the cloud.

5.8.3 Interpolating by Continued Fractions

This method assumes that the unknown functions (given by pairs of points) can be requested by a rational polynomial

$$y = \frac{a + bx + cx^2 + \ldots}{a' + b'x + c'x^2 + \ldots} \qquad (5\text{-}71)$$

As a result, y can be written as a continued fraction:

$$Y = Y_1 + \cfrac{X - X_1}{\rho_1(X_1X_2) + \cfrac{X - X_2}{\rho_2(X_1X_2X_3) - Y_1 + \cfrac{X - X_3}{\rho_3(X_1X_2X_3X_4) - \rho_1(X_1X_2) + \cfrac{X - X_4}{\rho_4(X_1X_2X_3X_4X_5) - \rho_2(X_1X_2X_3)}}}} \qquad (5\text{-}72)$$

The p's are "Reciprocal Differences" defined as follows.

$$\rho_1(XX_1) = \frac{X - X_1}{Y - Y_1} \qquad (5\text{-}73)$$

$$\rho_2(XX_1X_2) = \frac{X - X_2}{\rho_1(XX_1) - \rho_1(X_2X_1)} + Y_1$$

$$\rho_3(XX_1X_2X_3) = \frac{X - X_3}{\rho_2(XX_1X_2) - \rho_2(X_1X_2X_3)} + \rho_1(X_1X_2)$$

$$\rho_4(XX_1X_2X_3X_4) = \frac{X - X_4}{\rho_3(XX_1X_2X_3) - \rho_3(X_1X_2X_3X_4)} + \rho_2(X_1X_2X_3)$$

To construct a continued function, first prepare a table which contains the original data points and then reciprocal differences as shown below:

X_1	Y_1				(5-74)
		$\rho_1(X_1X_2)$			
X_2	Y_2		$\rho_2(X_1X_2X_3)$		
		$\rho_1(X_2X_3)$		$\rho_3(X_1X_2X_3X_4)$	
X_3	Y_3		$\rho_2(X_2X_3X_4)$		$\rho_4(X_1X_2X_3X_4X_5)$
		$\rho_1(X_3X_4)$		$\rho_3(X_2X_3X_4X_5)$	
X_4	Y_4		$\rho_2(X_3X_4X_5)$		
X_5	Y_5	$\rho_1(X_4X_5)$			

Each reciprocal difference is calculated from previous results.

Example: A Sine Table

Angle (o)	Sine	P_1	P_2	P_3	P_4
10	.17365				
		59.3923			
20	.34202		5.46117		
		63.2992		48.2356	
30	.5		3.76962		-1.87190
		70.0341		40.75410	
40	.64279		2.44503		
		81.1314			
50	.76604				

Therefore

$$y = .17365 + \cfrac{x-10}{59.3923 + \cfrac{x-20}{5.2875 + \cfrac{x-30}{-11.1567 + \cfrac{x-40}{-7.33807}}}}$$

$\therefore$ SIN $15^\circ \sim .25\,88\,288$

actual value: .2588190

% error = 3×10^{-3} %

The error = 3×10^{-3}% (This is probably due to round-off to 5 figures). The continued fractions can be truncated for faster interpolations (with less accuracy), or augmented for greater accuracy.

For example, the linear interpolation using only first recriprocal differences produces

$$y = .17365 + \frac{(15) - 10}{59.3923} = .25784$$

% error = .379.

Or writing $y = .17365 + \cfrac{(15) - 10}{59.3923 + \cfrac{(15) - 10}{5.2875 + .259198}}$

% error = .146%

Interpolation between two points on a smooth curve may require only the first recriprocal difference between the two points; i.e.

$$y = y_1 + \frac{X - X_1}{\frac{X_1 - X_2}{Y_1 - Y_2}} \qquad (5\text{-}75)$$

This is a linear interpolation although it's form is not the usual one.

More accuracy requires more data points and higher reciprocal difference computations.

Problems at hand should determine the order of approximation. The next order above linear often produces the most important accuracy improvement.

5.8.4 Gaussian Integration

Gaussian integration selects a number of ordinates spaced at unequal intervals, and adds the corresponding weighted abscissae. For example, a three point Gaussian integration proceeds as follows.

First, the integral, $\int_a^b f(x)\,dx$ becomes the integral $(b-a)\int_{-1/2}^{1/2} f(v)\,dv$ by the transformation

$$X = (b-a)v + \frac{b+a}{2} \qquad (5\text{-}76)$$

Tables give the three u values with their weighting factors:

$u_1 = -.3872983346$ $\quad R_1 = 5/18$

$u_2 = 0$ $\quad R_2 = 4/9$

$u_3 = .3872983346$ $\quad R_3 = 5/18$

These produce corresponding values of f(x). With the weights, R_1, R_2 & R_3, the integral is approximated by a sum of these terms:

$$\int_a^b f(x) \cong (b-a) \left[5/18\, f'(-.3872983346) + 4/9\, f'(0) + 5/18\, f'(.3872983346) \right]. \quad (5\text{-}77)$$

f(x) of course has been replaced by

$$f\left((b-a)\,U + \frac{b+a}{2}\right) \quad (5\text{-}78)$$

5.8.5 Clear Sky Radiance, Step-by-Step Computation

This computation uses both the continued fraction interpolation method and Gaussian integration.

1. Select first a slant range and divide the range into several increments. The increments need not necessarily be equal although equal increments may be more convenient.

2. Compute Transmittance from the origin (observer) to the end of each increment. The final increment is the transmittance of the entire slant path. Compute also, $\beta(T)$, the blackbody radiance at the end of each increment, including the origin. This requires temperature specification at these points.

This procedure will produce a set of point pairs for β and τ :

$\tau(R = 0)$	$\beta(R = 0)$
$\tau(R_1)$	$\beta(R_1)$
$\tau(R_2)$	$\beta(R_2)$
⋮	⋮

3. From these construct a continued fractions table. For example, let $\tau_0 = \tau(R = 0)$, $\beta_0 = \beta(R = 0)$; $\tau_1 = \tau(R_1)$, $\beta_1 = \beta(R_1)$ etc. Then the tables become

τ_0	β_0				
		$\rho_1(\tau_0\tau_1)$			
τ_1	β_1		$\rho_2(\tau_0\tau_1\tau_2)$		
		$\rho_1(\tau_1\tau_2)$		$\rho_3(\tau_0\tau_1\tau_2\tau_3)$	
τ_2	β_2		$\rho_2(\tau_1\tau_2\tau_3)$		$\rho_4(\tau_0\tau_1\tau_2\tau_3\tau_4)$
		$\rho_1(\tau_2\tau_3)$		$\rho_3(\tau_1\tau_2\tau_3\tau_4)$	
τ_3	β_3		$\rho_3(\tau_2\tau_3\tau_4)$		
		$\rho_1(\tau_3\tau_4)$			
τ_4	β_4				

4. Set up the continued fractions:

$$\beta(\tau) = \beta_0 + \cfrac{\tau - \tau_0}{\rho_1(\tau_0\tau_1) + \cfrac{\tau - \tau_1}{\rho_2(\tau_0\tau_1\tau_2) - \beta_0 + \cfrac{\tau - \tau_2}{\text{etc.}}}}$$

This enables $\beta(\tau)$ to be computed for any corresponding τ value using reciprocal differences.

5. Use the initial transmittance ($\tau = 1$), and final transmittance (τ_f), for the transformation required in the Gaussian routine:

$$\tau = (\tau_f - 1)v + \frac{\tau_f + 1}{2}$$

A three point Gaussian integration uses u values described above. For example

$$\tau(u_1) = -(\tau_f - 1).3872983346 + \frac{\tau_f + 1}{2}$$

etc.

Find the three β values by interpolation corresponding to the three τ values.

6. Integrate by forming the weighted sums:

$$\int \beta d\tau = (\tau_f - 1)\left\{\frac{5}{18}\beta(\tau(u_1)) + \frac{4}{9}\beta(\tau(u_2)) + \frac{5}{18}\beta(\tau(u_3)).\right.$$

The absolute value of this quantity is the sky radiance along the slant path.

.9 Diffuse Sky Radiance

The basic formula expressing sky radiance in the visible spectral region is:

$$B(\mu, Z, z) = \frac{(f I_o \cos Z)/\pi}{\left\{1 + \frac{2n}{3} - a\sin Z\left(\frac{1}{3} + \frac{n}{4}\right)\right\}}\left\{(1 + n\sin z)\left(1 - a\sin^2\frac{\mu}{2}\sin z \sin Z\right)\right\} \quad (1)$$

(5-79)

When the solar constant, I_o is 135 mw - cm^{-2} -hr, has units of mw-cm^{-2}-hr-str^{-1}.

Z is the solar zenith,

z is the observer zenith,

μ is the observer azimuth relative to the sun,

f is the fraction of solar radiation reaching the earth,

n is the ratio minus one of the horizon radiancy to zenith radiancy. On a clear day, this varies around .5.

a equals $\frac{r-1}{r}$, where r is the forward to backward scattering ratio. Since r varies from about 10 to 20 on a clear day, a varies from about .9 to .95.

Scattered Radiation Reaching the Earth

The factor, f, is defined by the formula:

$$f = 1 - \tau_s - \rho \quad \text{where} \tag{5-80}$$

$$\tau_s = \exp\left[(A \exp(-.193m) - 1) \right] \; ; \; A = 0.481 + 0.1623W, \text{ and}$$

$$\rho = \exp\left[-2.50/(wm)^{.0975} \right]$$

W is the ratio vapor content in precipitable centrimeters, and m is the air mass.

Formula (1) applies to the visible spectral regions as τ_s and ρ account for scattering and absorption in twenty-seven wavelengths throughout this region. Zenith and azimuth radiance distributions are controlled by the parameters μ and a, also characterize the visible spectral region.

Other spectral regions require different values for and, of course, I_o, the solar constant.

Scattering loss can be estimated through the formula

$$\tau = \exp\left\{ -(S.F.)\, k_o/a \left(e^{-a\mu_1} - e^{-a\mu_2} \right) \right\} \tag{5-81}$$

as described in equation (5-67).

5.9.1 Reflection From an Arbitrarily Oriented Surface

This paragraph describes a procedure for computing radiation in a specified direction due to reflection of clear sky radiations by a surface which has bi-directional reflectance characteristics. The input data are the desired look angle in terms of local zenith and azimuth (or local elevation and azimuth), the sky radiance distribution in terms of these coordinates, the surface orientation, and the bi-directional surface

reflectance in terms of the surface coordinate system. The output will be in terms of local zenith and azimuth.

The computation procedure requires at least two coordinate systems, the local system, and the system containing the surface normal. This requires coordinate transformations and thus complicates the computation but allows sky radiance to be in terms of local zenith and azimuth. Besides, local zenith and azimuth more meaningfully express the output.

5.10.1 Flow Diagram

The computational procedure, constructed around the University of Michigan's reflectance model, follows the accompanying flow diagram. Each step of the diagram is discussed in detail below.

5.10.2 Input Surface Orientation, Zenith & Azimuth Reflection Direction

The reflecting surface coordinates will generally coincide with local zenith and azimuth coordinates so a transformation between these two coordinates must be made. The matrix

$$\begin{pmatrix} \cos Z \cos A & -\sin A & \sin Z \cos A \\ \cos Z \sin A & \cos A & \sin Z \sin A \\ -\sin Z & 0 & \cos Z \end{pmatrix} \qquad (5\text{-}82)$$

where Z is the zenith of the surface normal and A is its azimuth, express local zenith and azimuth coordinates in terms of surface coordinates. For $Z = A = 0$, both coordinate systems coincide.

For example, a unit vector in the local system with zenith, θ, and azimuth, ϕ,

$\vec{E} = \sin\theta \cos\phi + \sin\theta \sin\phi\, j + \cos k$ in the local system (i, j, and k are unit vectors along the local x, y, and z axis). In the coordinate system of the surface this becomes

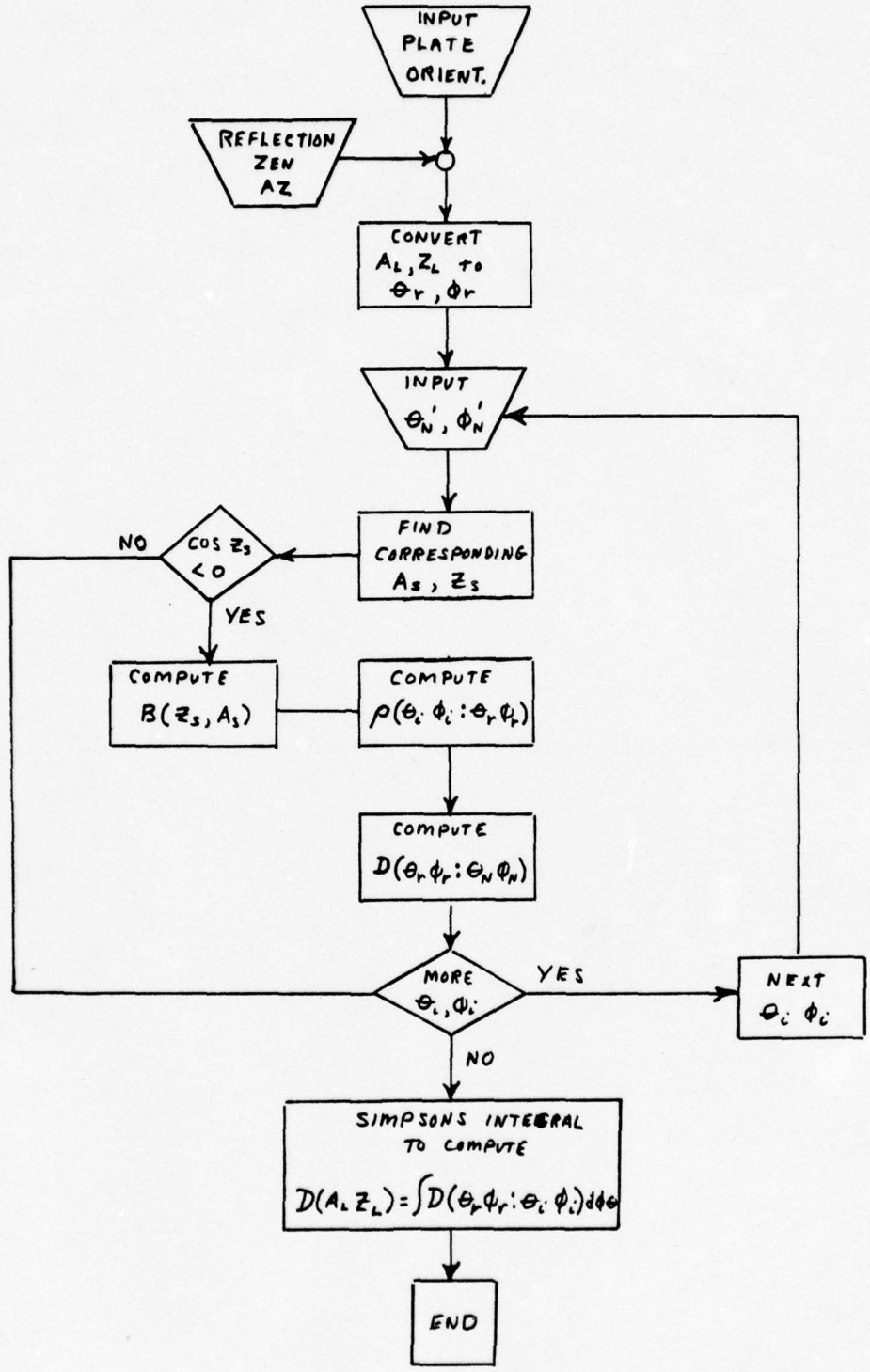

Fig. 5.4 DIRECTIONAL REFLECTANCE FLOW DIAGRAM

$$\vec{E} = \sin\theta\cos\phi\{\cos Z\cos A\,\hat{i}' - \sin A\,\hat{j}' + \sin Z\cos A\,\hat{k}'\}$$
$$+ \sin\theta\sin\phi\{\cos Z\sin A\,\hat{i}' + \cos A\,\hat{j}' + \sin Z\cos A\,\hat{k}'\} \quad (5\text{-}83)$$
$$+ \cos\phi\{-\sin Z\,\hat{i}' + \cos Z\,\hat{k}'\}$$

$\hat{i}', \hat{j}'$ & $\hat{k}'$ are unit vectors in surface coordinate system

$$\vec{E} = \{\sin\theta\cos\phi\cos Z\cos A + \sin\theta\sin\phi\cos Z\sin A - \cos\phi\sin Z\}\hat{i}'$$
$$+ \{-\sin\theta\cos\phi\sin A + \sin\theta\sin\phi\cos A\}\hat{j}' \quad (5\text{-}84)$$
$$+ \{\sin\theta\cos\phi\sin Z\cos A + \sin\theta\sin\phi\sin Z\cos A + \cos\phi\cos Z\}\hat{k}'$$

From these components, θ_r and ϕ_r follow easily since E must have the form:

$$E = \sin\theta_r\cos\phi_r\,\hat{i}' + \sin\theta_r\sin\phi_r\,\hat{j}' + \cos\theta_r\,\hat{k}' \quad (5\text{-}85)$$

Thus,

$$\tan\phi_r = \frac{-\sin\theta\cos\phi\sin A + \sin\theta\sin\phi\cos A}{\sin\theta\cos\phi\cos Z\cos A + \sin\theta\sin\phi\cos Z\sin A - \cos\phi\sin Z}, \quad (5\text{-}86)$$

and $\cos\theta_r = \sin\theta\cos\phi\sin Z\cos A + \sin\theta\sin\phi\sin Z\cos A + \cos\phi\cos Z.$ (5-87)

Thus, local zenith and azimuth inputs and the coordinates of the surface normal specify the angle θ_r and ϕ_r. These angles are constants throughout one integration cycle.

5.10.3 Input θ_i, ϕ_i and Convert to Local Zenith and Azimuth

Assume sky radiance to depend only on local zenith. Use the inverse matrix to express θ_i and ϕ_i coordinates in terms of sky zenith and azimuth. Thus the matrix

$$\begin{pmatrix} \cos Z\cos A & \cos Z\sin A & -\sin Z \\ -\sin A & \cos A & 0 \\ \sin Z\cos A & \sin Z\sin A & \cos Z \end{pmatrix}$$ expresses i, j and k (5-89)

in terms of i, j and k.

$$\vec{B} = \sin\theta_i \cos\phi_i \hat{i} + \sin\theta_i \sin\phi_i \hat{j} + \cos\theta_i \hat{k} \text{ in the surface system,} \quad (5\text{-}90)$$

and

$$\vec{B} = \sin\theta_i \cos\phi_i (\cos Z\cos A\hat{i} + \cos Z \sin A\hat{j} - \sin Z\hat{k}) + \sin\theta_i \sin\phi_i (-\sin A i - \cos A j) + \cos\theta_i (\sin Z\cos A i + \sin Z\sin A j + \cos Z k) \quad (5\text{-}91)$$

Since this also equals

$$\vec{B} = \sin Z_s \cos A_s \hat{i} + \sin Z_s \sin A_s \hat{j} + \cos Z_s \hat{k}; \quad (5\text{-}92)$$

$$\cos Z_s = -\sin\theta_i \cos\phi_i \sin Z + \cos\theta_i \cos Z, \text{ and} \quad (5\text{-}93)$$

$$\tan A_s = \frac{\sin\theta_i \cos\phi_i \cos Z \sin A + \sin\theta_i \sin\phi_i \cos A + \cos\theta_i \sin Z \sin A}{\sin\theta_i \cos\phi_i \cos Z \cos A - \sin\theta_i \sin\phi_i \sin A + \cos\theta_i \sin Z \cos A} \quad (5\text{-}94)$$

5.10.4 Selection of θ_i, ϕ_i

θ_i and ϕ_i will be chosen in steps of equal increments. $0 \leq \theta_i \leq 90^\circ$, while $0 \leq \phi_i \leq 360^\circ$. The number of equal steps will be determined primarily by available computer time. For example, θ_i could have nine steps of 10 degrees each, while ϕ_i could have 36 steps of 10 degrees, giving a total of 360 steps.

5.10.5 Sky Radiance

Infrared sky radiance only exists for zenith distances from zero to ninety degrees. For angles greater than ninety degrees, when $\cos Z_s < 0$, it is assumed to equal zero.

For $0 \leq Z_s \leq 90^\circ$, sky radiance values will be interpolated from sky radiance values spaced 18 degrees apart. The interpolation routine is described in another section.

5.10.6 Bi-Directional Reflectance

This will be defined for $\theta_r, \phi_r, \theta_i, \phi_i$ in the University of Michigan data. The product of this and the sky radiance in the direction, θ_i, ϕ_i is the radiance contribution in the direction θ_r, ϕ_r . This is the function $D(\theta_i, \phi_i : \theta_r, \phi_r)$.

5.10.7 Simpson's Rule for Two Dimensional Integration

The $D(\theta_i, \phi_i : \theta_r, \phi_r)$ will form a set of 2mx2n data. Let these be $D_{00}, D_{01}, D_{02} \cdots D_{0n}, D_{11}, D_{12}, D_{13} \cdots D_{12n} \ldots\ldots, D_{2m0}, D_{2m1} \ldots\ldots$ where m's can represent the θ_r steps and n's represent the ϕ_r steps. Let the step intervals be $\Delta\theta_r$ and $\Delta\phi_r$ respectively. Simpson's rule applied in this case produces the integral approximation:

$$\vec{D} = \frac{\Delta\theta_i}{3}\left\{\frac{\Delta\phi_i}{3}(D_{00} + 4D_{01} + 2D_{02} + 4D_{03} + \cdots\cdots + D_{02m})\right.$$

$$+ \frac{4\Delta\phi_i}{3}(D_{10} + 4D_{11} + 2D_{12} + 4D_{13} + \cdots\cdots + D_{12m})$$

$$+ \frac{2\Delta\phi_i}{3}(D_{20} + 4D_{21} + 2D_{22} + 4D_{23} + \cdots\cdots + D_{22m})$$

$$+ \frac{4\Delta\phi_i}{3}(D_{30} + 4D_{31} + 2D_{32} + 4D_{33} + \cdots\cdots + D_{32m}) \qquad (5\text{-}95)$$

$$+ \cdots\cdots\cdots\cdots\cdots\cdots\cdots\cdots,$$

$$+ \cdots\cdots\cdots\cdots\cdots\cdots\cdots\cdots$$

$$\left. + \frac{\Delta\phi_i}{3}(D_{2n0} + 4D_{2n1} + 2D_{2n2} + 4D_{2n3} + \cdots\cdots D_{2n2m})\right\}.$$

5.11 EXHAUST GAS EMISSIVITY

The emissivity coefficients of the high temperature exhaust gases that flow out of a helicopter's exit nozzle are derived through the use of a semi-empirical procedure. The method consists of first collecting and judiciously compiling tables of measured data for the gases, temperatures, and wavelengths of interest. Then classical high temperature gas emissivity theory is used in conjunction with the gas emissivity/absorptivity data to determine the probable form, and accuracy of the equations to be used in attempting to curve fit the tabulated data.

5.11.1 Raw Data

The equation forms, accuracies, and curve fit techniques to be tried depend largely upon the particular gas species of interest. In the Army Aircraft IR signature study, we are primarily interested in high temperature water vapor (H_2O) and carbon dioxide (CO_2). Westinghouse is compiling the latest available measurements covering a temperature range of 300 to 3000°K at wavelengths varying from one to twenty microns.

The raw data is extracted from reports on various measurement programs such as the many high temperature H_2O measurements made by Dr. C.B. Ludwig of General Dynamics and the CO_2 measurements made by Dr. W. Malkmus also of General Dynamics. Further, Westinghouse periodically consults such authorities directly to discuss the nature of the measurement set up conditions so as to be aware of peculiarities of the data that may not have appeared in the open literature. Some of these other authorities are persons such as Dr. Dave Anding and Dr. Robert Turner of University of Michigan and Dr. Fred Simmons of Aerospace Corporation. By consulting these authorities as well as our own in-house experts we are able to make a fairly judicious and selective tabulation of relevant data.

After the data has been properly tabulated and reasonable equation forms decided upon, Westinghouse then proceeds to curvefit the data to these forms, generally in the least squares sense.

The data storage and compilation can be symbolically depicted by figure 5.5.

5.11.2 Derivation of Equation Forms

From classical gas emissivity theory, the emissivity at any given temperature (using the concept of effective bandwidths) is of the form:

FIGURE 5.5 FORM OF DATA

			E(L, I)			
		I	1	2	3	N
L	W(L)	T(I)	300	600	1000	3000
1	1.61		.E-7	.167E-3	.1E-2	.129E-1
2	1.67		.5E-9	.56E-4		
3						
.						
.						
M						

L = Wavelength index

W(L) = Wavelength

I - Temperature index

T(I) - Temperature

E(L,I) - Emissivity of wavelength W(L) and temperature T(I)

$$\epsilon_\lambda = \left[1 - \exp\left(-E_\lambda R\right) \right] \int_{\Delta\lambda} N_\lambda \, d\lambda \qquad (5\text{-}96)$$

where E_λ is the average absorption coefficient for the spectral region of width $\Delta\lambda$, the optical depth is R, N_λ denotes the blackbody spectral radiancy at the temperature of the gas. In general, the spectroscopic constants required as inputs to this equation are not available for polyatomic gases like H_2O and CO_2. Thus, as suggested by Dr. S.S. Penner in "Quantitative Molecular Spectroscopy and Gas Emissivities", the absence of such data and gas mixtures, a semi-empirical curvefit to measured data is the most fruitful approach to the determination of high temperature gas emissivity.

A detailed account is given elsewhere on the rationale of the semi-empirical approach generally taken here.

Included here for illustrative purposes is a sample of the kinds of computer processing necessary to arrive at a useful curve fit. The nature of the data suggested an equation of the form:

$$Log\,(E_\lambda) = A_\lambda + B_\lambda \times Log(T) + C_\lambda \times Log\,(T^2) \qquad (5\text{-}97)$$

where E_λ = emissivity at wavelength, λ,

A_λ, B_λ, C_λ = empirical constants at wavelength, λ,

T = temperature

A sample of the output for this particular case is presented in Figures 5.6 and 5.7 "TEMPS" refers to the seven temperatures for which data was tabulated. Looking further on in figure 5.6 "LAMBA" refers to the wavelengths. As indicated by the header information, the emission coefficient data was fitted to the parabolic form in the least squares sense.

For each wavelength, the measured data is presented first followed by a second line (that always starts with "0.00") of calculated data. The calculated data is generated by using the empirical coefficients generated at each wavelength.

Figure 5.7 presents the coefficients used for each wavelength and also a brief error analysis. For this particular case, the parabolic least squares fit yields reasonably good results. As can be seen, the absolute error is on the order of 5-10% for wavelengths greater than 3 microns and 15-25% for wavelengths of 3.03 to 3.70 microns.

The computer flow diagram for carrying out the operations is shown in Figure 5.8. Program memonics are listed in figure 5.9.

EHAUST GAS EMISSIØN CØEFICIENT CURVE FIT
PARABØLIC FØRM E= 10**(A+B*LGT(T)+C*LGT(T)**) (1/CM)
E=EMISSIØN CØEFICIENT T=TEMP (DEG K)
EMISSIVITY=1-EXP(-E*R) R=PATHLENGTH (CM)

FIG. 5.7

WATER VAPØR - H20

EMISSIØN CØEFICIENT AS A FUNCTIØN ØF TEMPERATURE"
1ST LINE MEAS DATA, 2ND LINE CAL VAL AT EACH LAMBA

TEMPS / LAMBA	300	600	1000	1500	2000	2500	3000
3.03	.22E-002	.16E-001	.54E-001	.16E+000	.23E+000	.25E+000	.26E+000
0.00	.21E-002	.18E-001	.62E-001	.13E+000	.20E+000	.25E+000	.30E+000
3.08	.41E-002	.10E-001	.32E-001	.12E+000	.19E+000	.22E+000	.22E+000
0.00	.35E-002	.14E-001	.39E-001	.83E-001	.14E+000	.21E+000	.30E+000
3.12	.33E-002	.70E-002	.20E-001	.87E-001	.15E+000	.18E+000	.19E+000
0.00	.28E-002	.97E-002	.26E-001	.59E-001	.11E+000	.17E+000	.26E+000
3.18	.64E-003	.55E-002	.14E-001	.61E-001	.11E+000	.14E+000	.15E+000
0.00	.62E-003	.52E-002	.20E-001	.50E-001	.90E-001	.14E+000	.19E+000
3.22	.90E-002	.48E-002	.10E-001	.42E-001	.88E-001	.12E+000	.13E+000
0.00	.72E-002	.74E-002	.13E-001	.28E-001	.57E-001	.11E+000	.20E+000
3.28	.34E-002	.40E-002	.76E-002	.29E-001	.67E-001	.95E-001	.11E+000
0.00	.30E-002	.48E-002	.10E-001	.23E-001	.46E-001	.86E-001	.15E+000
3.33	.30E-002	.33E-002	.59E-002	.21E-001	.51E-001	.77E-001	.88E+000
0.00	.33E-002	.27E-002	.57E-002	.19E-001	.59E-001	.17E+000	.45E+000
3.39	.26E-002	.27E-002	.48E-002	.16E-001	.40E-001	.62E-001	.73E-001
0.00	.24E-002	.31E-002	.60E-002	.14E-001	.29E-001	.55E-001	.10E+000
3.45	.21E-002	.23E-002	.40E-002	.12E-001	.31E-001	.50E-001	.60E-001
0.00	.20E-002	.25E-002	.49E-002	.11E-001	.23E-001	.44E-001	.80E-001
3.51	.17E-002	.20E-002	.35E-002	.10E-001	.24E-001	.41E-001	.50E-001
0.00	.16E-002	.22E-002	.42E-002	.93E-002	.19E-001	.36E-001	.64E-001
3.57	.15E-002	.18E-002	.31E-002	.86E-002	.19E-001	.34E-001	.42E-001
0.00	.14E-002	.19E-002	.36E-002	.80E-002	.16E-001	.30E-001	.52E-001
3.64	.12E-002	.16E-002	.29E-002	.76E-002	.15E-001	.28E-001	.34E-001
0.00	.12E-002	.17E-002	.33E-002	.70E-002	.14E-001	.24E-001	.41E-001
3.70	.11E-002	.14E-002	.27E-002	.71E-002	.13E-001	.25E-001	.30E-001
0.00	.10E-002	.15E-002	.30E-002	.63E-002	.12E-001	.21E-001	.35E-001
3.78	.91E-003	.13E-002	.25E-002	.67E-002	.11E-001	.21E-001	.27E-001
0.00	.87E-003	.14E-002	.28E-002	.58E-002	.11E-001	.19E-001	.31E-001
3.85	.80E-003	.13E-002	.24E-002	.65E-002	.11E-001	.20E-001	.26E-001
0.00	.77E-003	.13E-002	.27E-002	.57E-002	.10E-001	.18E-001	.29E-001
3.92	.68E-003	.12E-002	.23E-002	.64E-002	.10E-001	.18E-001	.25E-001
0.00	.66E-003	.12E-002	.26E-002	.54E-002	.10E-001	.17E-001	.27E-001
4.00	.59E-003	.12E-002	.23E-002	.64E-002	.10E-001	.17E-001	.25E-001
0.00	.58E-003	.12E-002	.26E-002	.55E-002	.10E-001	.17E-001	.26E-001
4.08	.52E-003	.13E-002	.24E-002	.65E-002	.11E-001	.16E-001	.25E-001
0.00	.52E-003	.12E-002	.28E-002	.58E-002	.10E-001	.17E-001	.25E-001
4.16	.45E-003	.13E-002	.26E-002	.67E-002	.12E-001	.17E-001	.25E-001
0.00	.45E-003	.12E-002	.29E-002	.62E-002	.11E-001	.17E-001	.26E-001
4.25	.42E-003	.14E-002	.30E-002	.72E-002	.13E-001	.19E-001	.27E-001
0.00	.42E-003	.13E-002	.33E-002	.71E-002	.12E-001	.19E-001	.28E-001
4.35	.39E-003	.16E-002	.38E-002	.81E-002	.16E-001	.23E-001	.29E-001
0.00	.39E-003	.15E-002	.40E-002	.86E-002	.15E-001	.22E-001	.31E-001
4.44	.39E-003	.20E-002	.52E-002	.10E-001	.22E-001	.29E-001	.35E-001
0.00	.39E-003	.19E-002	.54E-002	.12E-001	.19E-001	.28E-001	.37E-001
4.55	.48E-003	.29E-002	.81E-002	.16E-001	.33E-001	.39E-001	.45E-001
0.00	.48E-003	.28E-002	.84E-002	.18E-001	.28E-001	.39E-001	.49E-001
4.65	.88E-003	.68E-002	.15E-001	.27E-001	.48E-001	.53E-001	.63E-001
0.00	.93E-003	.58E-002	.16E-001	.31E-001	.44E-001	.54E-001	.61E-001
4.75	.18E-002	.12E-001	.29E-001	.47E-001	.70E-001	.73E-001	.84E-001
0.00	.19E-002	.11E-001	.30E-001	.51E-001	.66E-001	.76E-001	.81E-001
4.88	.38E-002	.25E-001	.52E-001	.79E-001	.99E-001	.10E+000	.11E+000
0.00	.40E-002	.23E-001	.54E-001	.83E-001	.99E-001	.11E+000	.11E+000
5.00	.78E-002	.49E-001	.87E-001	.12E+000	.14E+000	.14E+000	.15E+000
0.00	.82E-002	.42E-001	.91E-001	.13E+000	.14E+000	.14E+000	.14E+000

LAMBA	CURVE FIT COEFICIENTS A	B	C	STD ERROR	IN PER CENT
3.03	-.2017E+002	+.1055E+002	-.1408E+001	+.2090E-001	+.1272E+002
3.08	-.8499E+001	+.2803E+001	-.1471E+000	+.3568E-001	+.2602E+002
3.12	-.5292E+001	+.4894E+000	+.2485E+000	+.3310E-001	+.2871E+002
3.18	-.1639E+002	+.7347E+001	-.8176E+000	+.1577E-001	+.2084E+002
3.22	+.1166E+002	-.1057E+002	+.2017E+001	+.3015E-001	+.3718E+002
3.28	+.5811E+001	-.6970E+001	+.1456E+001	+.1871E-001	+.2612E+002
3.33	+.2244E+002	-.1875E+002	+.3507E+001	+.1686E+000	+.5053E+002
3.39	+.8709E+001	-.8995E+001	+.1784E+001	+.1135E-001	+.2188E+002
3.45	+.8686E+001	-.9019E+001	+.1785E+001	+.8283E-002	+.1918E+002
3.51	+.7996E+001	-.8588E+001	+.1710E+001	+.5880E-002	+.1631E+002
3.57	+.7079E+001	-.7990E+001	+.1606E+001	+.4220E-002	+.1407E+002
3.64	+.5763E+001	-.7114E+001	+.1455E+001	+.3083E-002	+.1171E+002
3.70	+.4823E+001	-.6507E+001	+.1353E+001	+.2633E-002	+.1174E+002
3.78	+.3767E+001	-.5830E+001	+.1241E+001	+.1834E-002	+.1035E+002
3.85	+.2575E+001	-.5050E+001	+.1112E+001	+.1334E-002	+.8896E+001
3.92	+.1501E+001	-.4335E+001	+.1008E+001	+.9151E-003	+.8318E+001
4.00	+.1104E-001	-.3416E+001	+.8504E+000	+.5590E-003	+.7607E+001
4.08	-.2147E+001	-.1990E+001	+.6177E+000	+.3592E-003	+.7413E+001
4.16	-.4056E+001	-.7553E+000	+.4213E+000	+.4937E-003	+.6631E+001
4.25	-.6032E+001	+.5710E+000	+.2098E+000	+.5005E-003	+.5261E+001
4.35	-.8819E+001	+.2397E+001	-.8516E-001	+.8588E-003	+.5497E+001
4.44	-.1192E+002	+.4474E+001	-.4190E+000	+.1478E-002	+.7598E+001
4.55	-.1500E+002	+.6643E+001	-.7797E+000	+.2202E-002	+.7245E+001
4.65	-.1779E+002	+.8902E+001	-.1189E+001	+.2392E-002	+.9224E+001
4.75	-.1875E+002	+.9902E+001	-.1387E+001	+.2530E-002	+.5340E+001
4.88	-.1931E+002	+.1067E+002	-.1553E+001	+.3242E-002	+.5496E+001
5.00	-.1905E+002	+.1036E+002	-.1619E+001	+.6048E-002	+.7130E+001

Fig. 5.7 CURVE FIT COEFICIENTS

FLOW DIAGRAM FOR PROGRAM THAT COMPUTES COMPUTES COEFFICIENTS A, B, & C FOR LEAST SQUARES FIT OF WATER VAPOR (H_2O) Data to FORM

E = 10**(A+B*LGT(T)+C*LGT(T)**2)

TO DERIVE EMISSIVITY APPROXIMATION

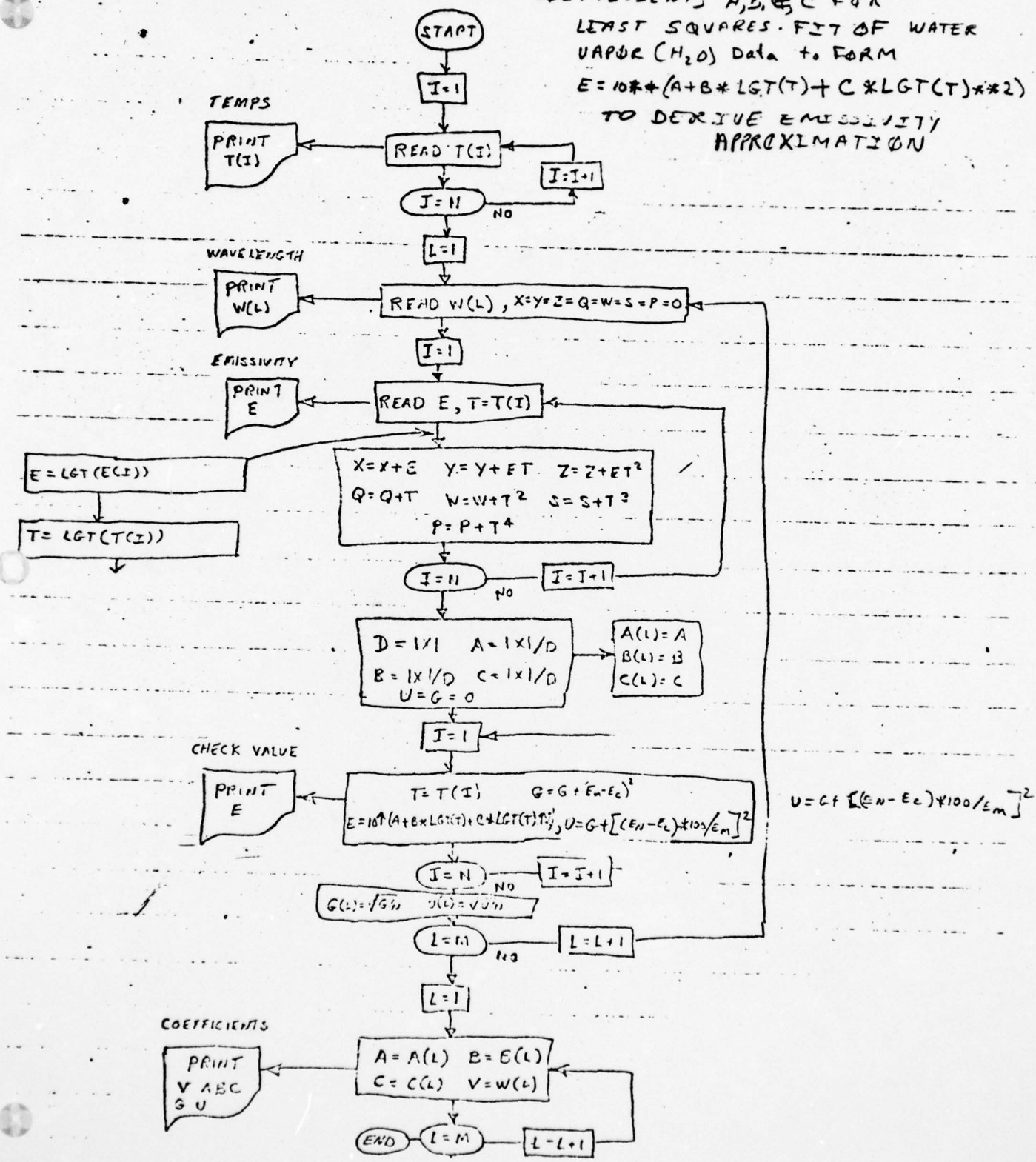

Fig. 5.8 FLOW DIAGRAM FOR COEF. FIT

Fig. 5.9(HTFIT)

EXPLANATION OF PROGRAM MNEMONICS

MNEMONICS	EXPLANATION (UNITS)
A(1), 1=1, 50(MAX)	Auxiliary storage vectors for storing the coefficients A,B,C
B(I), I=1, 50(MAX)	as a function of wavelength (Dimensionless)
C(I), I=1, 50(MAX)	
N	The number of different temperatures used in the particular set of measurements (Dimensionless)
M	The number of different wavelengths used (Dimensionless)
T(I), I=1, 50(MAX)	Vector containing the temperatures used in acquiring the raw absorption data (degrees Kelvin K^{O})
W(I), I=1, 50(MAX)	The wavelengths utilized in the measurements (microns)
G(I), I=1, 50(MAX)	Auxiliary storage vector containing the statistical standard error of the fit as a function of wavelength

$$G(I) = \sqrt{\sum_{I=0}^{N} (E(I) - E(I + N))^2/N}$$

Figure 5.9 (HTFIT) (CON'T)

EXPLANATION OF PROGRAM MNEMONICS (Continued)

MNEMONICS	EXPLANATION (UNITS)
U(I) I = 1, 50(MAX)	Auxiliary storage vector containing the statistical percentage error.
E(I), I=1, 50(MAX)	Vector containing the emissivity (I/CM) the first M values of E(I) are experimentally derived values; the next M values are computed values computed using the coefficients A, B, C.

Standard Error G(L):

$$G(L) = \sqrt{\frac{\sum_{I=0}^{N} (E(I) - E(I+N))^2}{N}}$$

in percent:

$$U(L) = \sqrt{\frac{\sum_{I=0}^{N} (E(I) - E(I+N)) \times 100/E(I)^2}{N}}$$

When E(I) = meas. value

E(I+N) = calculated value

UNCLASSIFIED

5.12 Plume Radiant Intensity

The geometrical model of the plume spatial distribution is based on the premise that equipotential thermal contours exist within the plume. Consequently, the plume composition can be represented by homogeneous temperature and partial pressure zones bounded by zonal surfaces.

The zones are numbered from the innermost out, reflecting step reductions in temperature. The first zone is the volume contained within the smallest zonal boundary. The second zone is the volume contained within the region between the surfaces of the smallest and the next larger zonal boundaries. The third zone is the volume bounded by the last-mentioned zonal boundary and the next larger one, etc.

Each of these zones is characterized by an average temperature and partial pressure of the constituent exhaust gasses within the volumes defined by the zonal boundaries.

Given the zonal characteristics, the radiance of a ray through the plume may be readily calculated.

Consider a line-of-sight ray which intersects all zones. Since the line of sight ray originates at the sensor, the radiance of interest is that directed toward the sensor or in the opposite direction along the line of sight ray. Consequently, starting with the side of the plume opposite the sensor, the emission of each zone attenuated by the intervening zones is computed in turn progressing along the ray toward the sensor and the resulting contributions of each are summed up. For example, this may be expressed mathematically for a four zone case as follows.

$$
\begin{aligned}
N_{\lambda} = \; & N_{T4} \epsilon_{R4} \tau_{R3} \tau_{R2} \tau_{L1} \tau_{S2} \tau_{S3} \tau_{S4} \\
+ \; & N_{T3} \epsilon_{R3} \tau_{R2} \tau_{L1} \tau_{S2} \tau_{S3} \tau_{S4} \\
+ \; & N_{T2} \epsilon_{R2} \tau_{L1} \tau_{S2} \tau_{S3} \tau_{S4} \\
+ \; & N_{T1} \epsilon_{L1} \tau_{S2} \tau_{S3} \tau_{S4} \qquad (5\text{-}98) \\
+ \; & N_{T2} \epsilon_{S2} \tau_{S3} \tau_{S4} \\
+ \; & N_{T3} \epsilon_{S3} \tau_{S4} \\
+ \; & N_{T4} \epsilon_{S4}
\end{aligned}
$$

In this expression the numeric portion of the alphanumeric subscripts refer to the zone numbers. The alphabetic portion of the alphanumeric subscripts refer to the following:

T = Zone temperature

S = Portion of zone lying above the X axis

R = Portion of zone lying below the X axis

The symbols refer to the following:

N = Black body radiance for subscripted temperature

ϵ = Emissivity of subscripted region

τ = Transmission of subscripted region

All of these parameters apply to monochromatic wavelength values. The lambda subscript, λ, has been omitted for clarity.

The transmission through any zonal region is equal to the product of transmissions of the significant absorbers contained within the region. In this instance only water vapor and carbon dioxide are considered as the significant absorbers among the varied exhaust gas species.

$$\tau_{Z_\lambda} = \tau_{Z_\lambda}(H_2O) \times \tau_{Z_\lambda}(CO_2) \qquad (5\text{-}99)$$

The transmission of each constituent gasses is calculated using Beer's law applicable over the relatively short path length of the plume zones and spectral resolution used herein.

$$\tau_{Z_\lambda}(GAS) = \exp\left[-K_{T_\lambda}(GAS) \times L_Z \times PP_Z(GAS)\right] \qquad (5\text{-}100)$$

where:

K = Absorption coefficient of particular absorbing exhaust gas, cm^{-1}

L = Path length of zonal region, cm

PP = Partial pressure of particular absorbing exhaust gas

The emissivity of each zonal segment is obtained from the transmission value.

$$\epsilon_{Z_\lambda} = 1 - \tau_{Z_\lambda} \qquad (5\text{-}101)$$

The effective radiance of the plume as seen by a remote sensor maybe calculated from the following equation

$$N_{eff} = \int_{\lambda_1}^{\lambda_2} S_\lambda N_\lambda \tau_\lambda(R)\, d\lambda \qquad W/STER/cm^2 \qquad (5\text{-}102)$$

where

N_{eff} = Effective radiance, $W/STER/cm^2$

S_λ = Relative spectral response of sensor

N_λ = Spectral radiance of plume, watts/ster/micron/cm^2

$\tau_\lambda(R)$ = Atmospheric transmission

R = Range between sensor and plume.

AD-A042 989 WESTINGHOUSE DEFENSE AND ELECTRONIC SYSTEMS CENTER B--ETC F/G 17/4
EVALUATION OF IR COUNTERMEASURES (MODEL METHODOLOGY).(U)
JUN 72 R F HIGBY, R C BROWN, J B GOODELL DAAJ01-72-C-0447

UNCLASSIFIED NL

3 OF 3
ADA042989

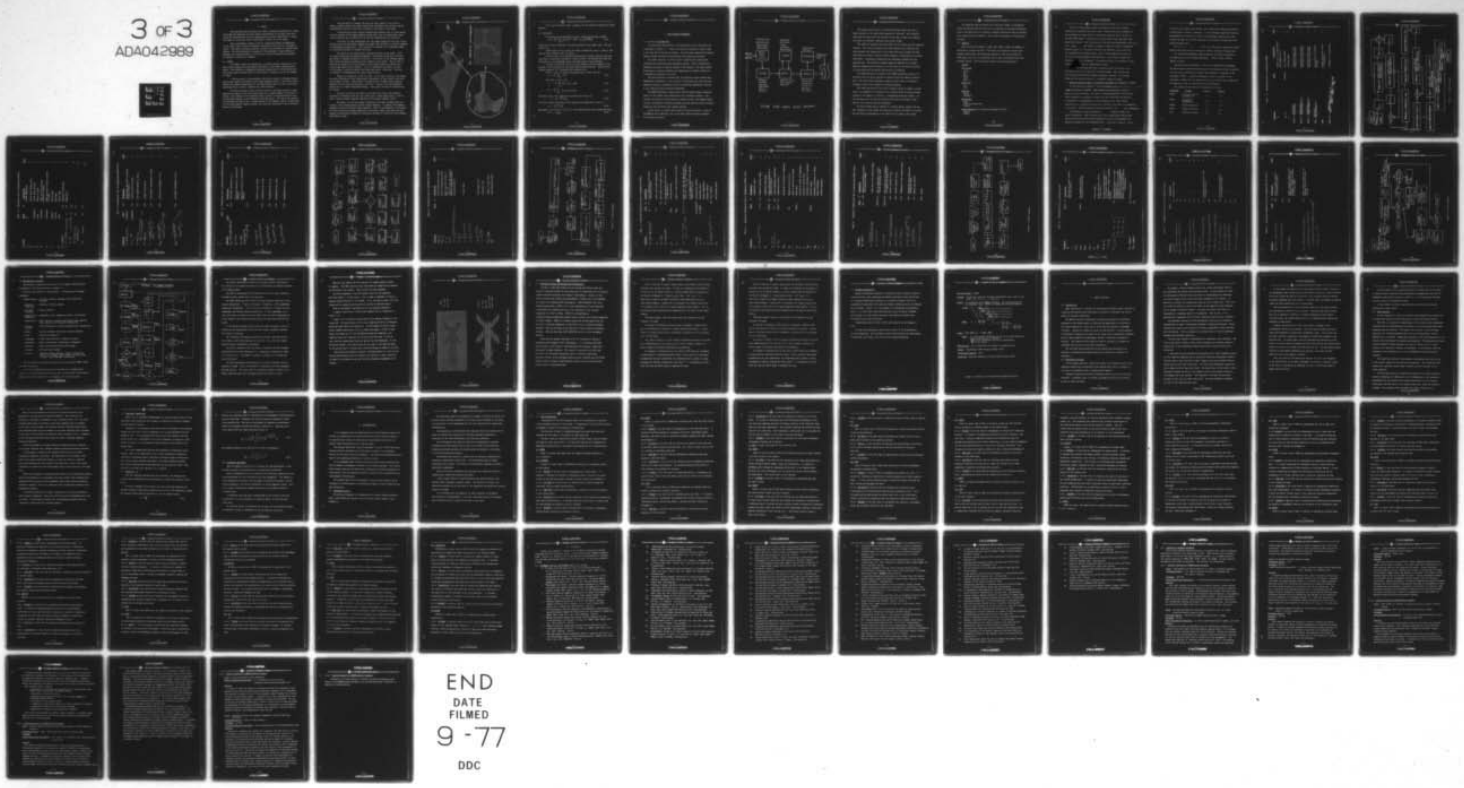

END
DATE FILMED
9-77
DDC

6. SENSOR

The subroutine SENS transforms the spatial intensity distribution of target and background signatures with the spatial transmittance of the sensor and integrates the residues which are then compared with the sensor sensitivity to obtain the signal to noise ratio and/or transformed to derive the error signal.

Input requirements consist of the two dimensional spatial transmittance of the sensor field of view or modulation transform for the case of a radiometric sensor. The spatial pattern and optical resolution are required for reticled type sensors. The noise equivalent irradiance at the wavelength of peak response is necessary for computing signal to noise ratios, while the demodulation mechanism is required to derive error signals.

6.1 METHOD

The method consists of generating a convolution matrix consisting of elements which possesses the same element resolution as the target signature mosaic matrix. Each element is assigned an amplitude proportional to the specified spatial point spread response function of the sensor, but whose sum over all elements is unity.

A reticle matrix is then generated which also consists of elements possessing the same angular resolution as the target signature matrix. The reticle matrix defines the angular transmittance of the instantaneous field of view of the sensor including optics, detector, aperture and reticle pattern.

The reticle matrix is then convolved with the convolution matrix by superimposing the center of the convolution matrix over a given element of the reticle matrix. Each element of the underlying reticle mosaic is then multiplied by each corresponding element of the overlying convolution matrix. The sum of the products thus obtained are entered into a sensor matrix at the element location corresponding to the reticle matrix element location over which the centerline of the convolution matrix was positioned.

This procedure is repeated for each and every element of the reticle matrix, thereby creating the sensor matrix which represents the convolved spatial transmittance function of the sensor referred to the plane of the target.

(Convolving the sensor spatial transmittance function with the point spread function instead of the target signature mosaic means only one convolution operation is required per run instead of one for each signature and LOS position.)

The matrix is then superimposed over the target signature mosaic and corresponding points are multiplied together and summed over the matrix to obtain a measure of instantaneous signal power. This procedure is repeated for a sufficient number of rotational positions to complete one cycle.

The center of the sensor matrix represents the LOS of the sensor. Thus, the sensor matrix may be laterally displaced to preselected positions on the target matrix to simulate variations in the LOS. In the case of the reticled sensor, this action facilitates deriving an error signal for the sensor. This is used to describe the nature of the error signal a given sensor design will provide on a given target under given conditions. Also, it determines null points or spots on the target to which the sensor would home under static conditions. This data is relevant to countermeasure and sensor design studies.

Figure 6.1 illustrates a case in point. In the upper portion of the figure, the spatial intensity of the target mosaic (represented in gray scale) for an aircraft target is shown. This aircraft is viewed from a 30 degree aspect angle as measured from the nose and possesses a -60° roll. The sun is in the foreground giving rise to a shadow along the fuselage. Solar glint can also be observed from the canopy.

The tail root section is shown in the lower left insert which exhibits gradations in intensity over the body section and a strong plume signal. This depicts a typical target signature contained in the target signature mosaic.

The insert, in the lower right, illustrates the result obtained from convolving a line scanning sensor with the target signature. It depicts the relative strength of the horizontally derived gradients. This is accomplished by convoluting the scan spot with the target signatures at successive points along each line and taking the differential between the successive positions to derive the line scanning differential output.

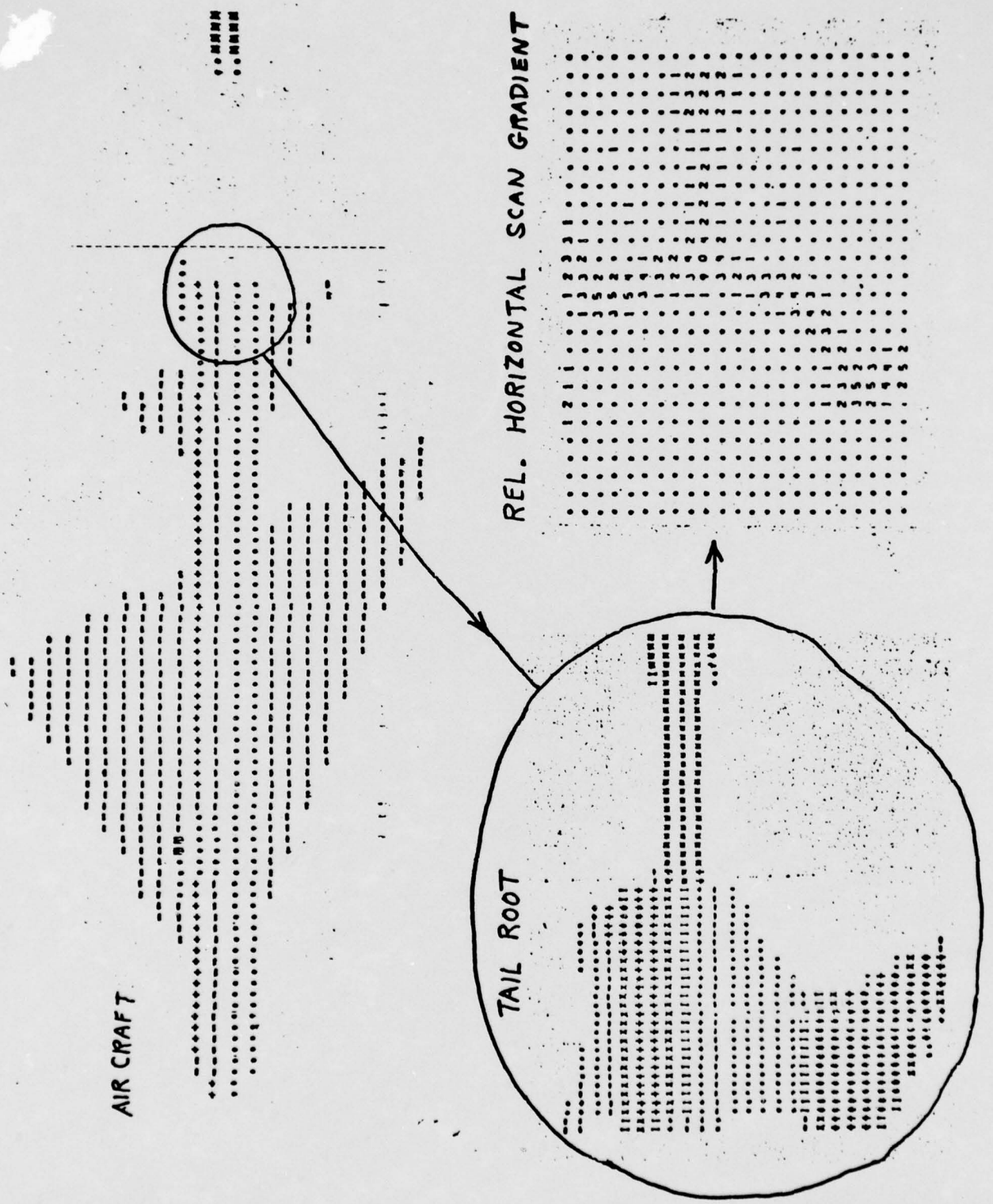

Figure 6.1 3-5u A/C Grey Scale Signature

More complex patterns than a scanning spot can easily be evaluated by these methods.

6.2 PROCEDURE

The deviations and magnitude of error comes from the basic formula:

$$S(t) = \frac{a_0}{2} + \sum_{n=1}^{\infty} \left\{ a_n \cos (2\pi nt)/T + b_n \sin (2\pi nt)/T \right\} \qquad (6\text{-}1)$$

This fourier series represents the signal produced by the sensor spin. The spin period is T.

Three terms of (6-1) supply the needed information; the D.C. term a_o, and the two first harmonic terms, a_1 and b_1.

Given a scene and a convolved reticle pattern (sensor matrix), the spin axis will be positioned according to input LOS data. The reticle will then scan the scene in a pre-programmed cycle, producing data at N scan positions.

The data obtained at each of the scan positions is the integral of the product of the scene and the convolved reticle (sensor matrix). These are the discrete samples, S(i) associated with formula (6-1).

The D.C. term is simply the average value of S(t), that is:

$$a_o = \frac{1}{T} \sum_{i=1}^{N} S(i). \qquad (6\text{-}2)$$

The terms a_1 and b_1 are:

$$a_1 = \frac{2}{T} \sum_{i=1}^{N} S(i) \cos (2\pi i/N) \qquad (6\text{-}3)$$

$$b_1 = \frac{2}{T} \sum_{i=1}^{N} S(i) \sin (2\pi i/N). \qquad (6\text{-}4)$$

The phase angle, which indicates the direction of error, is

$$\Phi = \tan^{-1} (b_1/a_1). \qquad (6\text{-}5)$$

The first harmonic amplitude, which indicates the magnitude of error is

$$A_1 = \sqrt{a_1^2 + b_1^2} \qquad (6\text{-}6)$$

The signal to noise ratio is the D.C. term divided by the noise equivalent power:

$$S/N = a_o/_{NEP} \qquad (6\text{-}7)$$

7. HIDE COMPUTER-PROGRAMMING

7.1 Overview of Program-Flow

The functional relationships of the subroutines of the HIDE Model are illustrated in Figure 7.2. "HIDE", the executive routine, is used to read in the data and initialize the program. The input data comprises the mission profile defined in terms of meteorological and operating conditions.

The PLUME subroutine is called first to establish the turbine exit conditions and consequent plume dispersion pattern. This is necessary to determine the extent of exhaust heating of the fuselage. The plume spatial distribution of partial pressures and temperatures of exhaust products in 3 dimensions are stored in an array.

The BODY subroutine is called next, and performs a minor surface self-determination computation. This consists of subdividing the tail boom into separate surfaces in accordance with the intersecting temperature contours of the plume which were previously determined.

The TEMPS subroutine is then called, and the thermal balance equations solved for the steady state temperatures of all external surfaces. This includes the effects of solar heating, internal sources, aero heating and/or cooling, environmental radiation exchange and plume heating as well as mutual conduction and convection with coupled surfaces.

If the option for dynamic heat balance has been exercised, a clock is started and the differential form of the heat balance equations iterated for transient solutions.

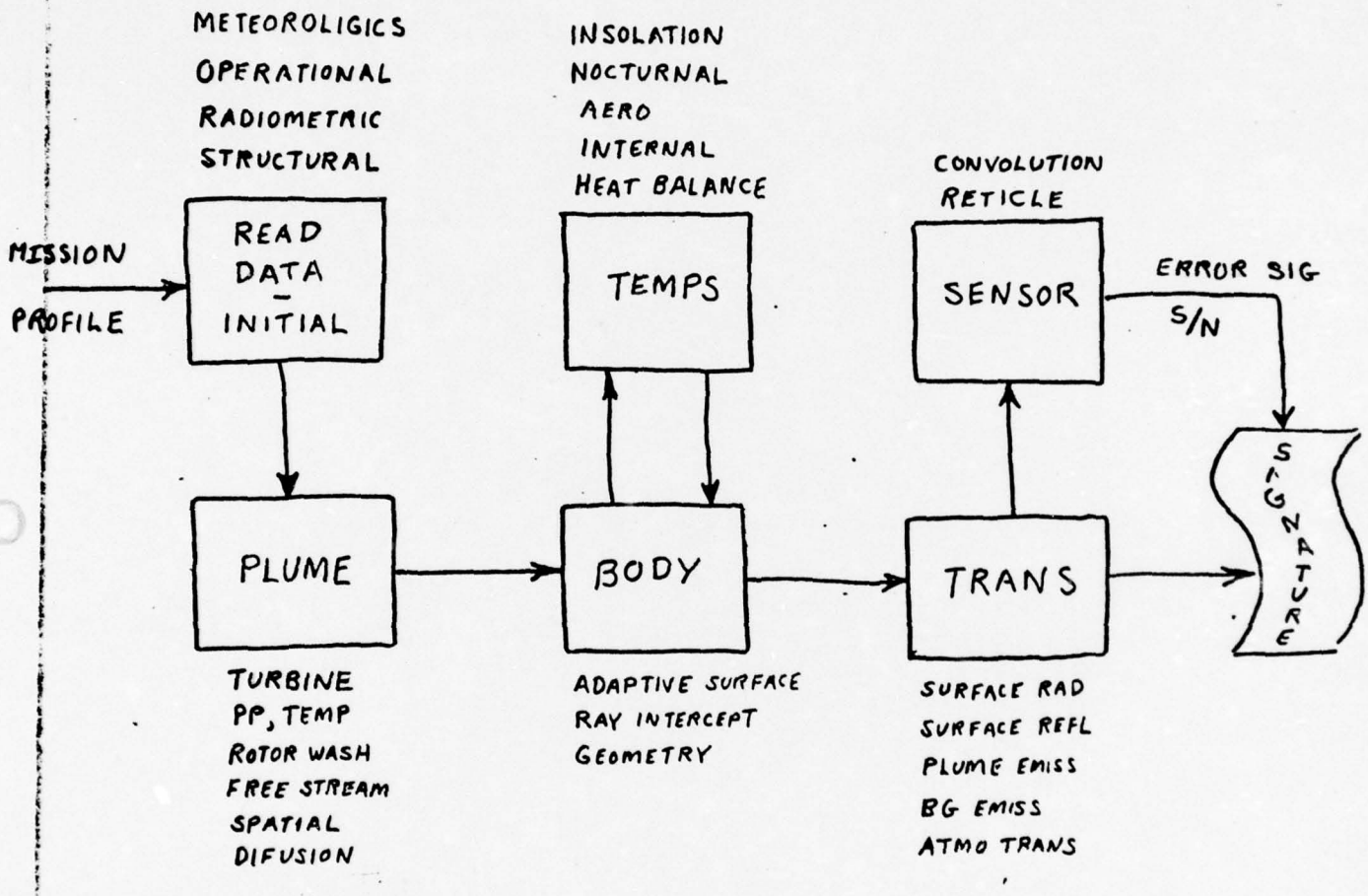

FIG. 7-1 HIDE MODEL BLOCK DIAGRAM

The program flow returns to the BODY subroutine, where the line of sight intercept of the body surface geometry is obtained. This operation identifies the major and minor surfaces in the line of sight, and computes the angles of incidence, reflection, and surface normal.

The radiative transfer subroutine TRANS is then called, and the signature obtained. This routine computes the surface emission and reflection, and plume emission and combinations of both where the plume eclipses the body. (Obscuration of plume or body by surface elements is established in the BODY subroutine). Atmospheric transmission and background radiance are also computed here. The resultant infrared signature weighted by the sensor spectral response may be printed out at this point in the form of a matrix of values depicting the spatial distribution of intensity.

The signature data is utilized in the SENSOR subroutine, where it is convolved with the spatial pattern of sensor reticle and detector field of view. This facilitates obtaining a signal to noise ratio for detection evaluation and/or error signals for tracking analysis.

The output may be put in the form of tabular values of signal to noise ratios (or probability of detection) for iterated values of target azimuth, elevation, and range so to provide a 3 dimensional detection profile. Or, the data may be put on tape and plotted later with the CALCOMP or other digital curve plotting interface equipmebt.

The error signals may be handled in a similar manner, except that two more dimensions in the arrays are required to reflect the effect of vertical and horizontal displacements of the sensor line of sight on the target.

The signatures may be printed out in pictorial format, or optionally stored on tape and read out later on to a kinescope via an analog conversion where a polaroid print of the spatial intensity distribution may be obtained with a gray scale for intensity. This output is analogous to thermo-vision pictures.

7.2 Approach

Each of the five submodels, PLUME, BODY, TEMPS, TRANS, and SENSOR, is developed as a module of HIDE. HIDE itself is an executive routine that handles input/output, the calling and transfer to and from subroutines. HIDE directs the flow of a particular set of runs in accordance with user selected options. The user should be given the following options:

Targets

Helicopters

- AH-56
- UH-1
- AH-1
- CH-47
- CH-54
- OH-6

Fixed Wing

- OV-1
- U-21

Missiles

- REDEYE
- Charparal

Bakcgrounds

- Earth
- Clear and Cloudy Sky
- Diurnal

Countermeasures (not actually implemented in HIDE)

- Jamming
- Flares

The above cited options should be available to the user by merely selecting and inputting the proper codes. These options and information on how to prepare the input decks for particular scenarios should be part of the HIDE Users Manual. Every effort should be made to make user-input data preparation nominal. Each HIDE module should have documented-default parameters, this means that nominal, average, or expected values of parameters should be preset in the various submodels and scenarios options and that all documentation including comment cards in the program should alert the user of the current parameter assigned value. The sources of these data should also be fully documented. Documentation should be considered a major requisite in a program as comprehensive as HIDE.

Special routines that may be required should be supplied in the HIDE deck as part of the auxiliary routines package. Such routines are the continued fractions and Gaussian integration routines. All program coding in HIDE should be done in a "standard" Fortran IV subset.

7.3 Computer Oriented Summary of Equations Programmed and Submodels Flowchart

In this section, we present a few illustrative examples of the tabular equation-summaries and their flowcharts. These equations are derived or presented in more detail in earlier sections. The tabular listings presented in this section merely summarize for purposes of reader and user visibility the equations or constants to be programmed, a brief explanation, the units, and an indication as to whether the equation or constant is an input, an assignment, or an output. These listings are grouped according to the major subprograms.

Corresponding to each subprogram, a computer program flow chart is presented. These flowcharts plus the corresponding summary sheet should form the day-to-day working material for both the programmers and engineers responsible for implementing HIDE. Particular attention should

be given to the common error sources; units, geometries used, and explanations or definitions of terms or equations. If the programmer implements numerical approximations or solutions to some of the presented equations, he should indicate the same on his update versions of the equation listings and flowcharts presented here.

The flowcharts primarily indicated logic flow and not necessarily actual machine operations (such as clearing out arrays, declaring storage, etc.).

For illustrative purposes, tabular equation listings and flowcharts are presented for the following subprograms: CONFRA, ATMOSP, SENSOR, TURBIN, and BODY.

One should use the flowchart to follow the computational sequencing. The tables should provide the definitions of the equations, terms, constants, and units and an indication as whether the expression is computed in the subprogram (I/O/C). I means the expression value is an input to the subprogram; O means that the expression value is an output, and C means that the expression value is computed within the subprogram.

The tables and flow charts are presented as follows:

Subprogram	Purpose	Table #	Figure #
CONFRA	Continued fraction interpolation	7.1	7.2
ATMOSP	Atmospheric transmission	7.2	7.3
SENSOR	Reticle simulation	7.3	7.4
TURBIN	Engine Simulation	7.4	7.5
BODY	Ray/Body Intercept	7.5	7.6

Table 7.1 Expressions Used in Implementing CONFRA

Equations	UNITS	EXPLANATION	I/O/C
N		Number of X_i, Y_i data points; here assume to be 5	I
X_i, Y_i	Arbitrary	Set of data points	I
I	"	Counting index	C
$RH\phi1(I) = \frac{X(I)-X(I+1)}{Y(I)-Y(I+1)}$	"	Auxiliary vector of 1st reciprical differences	I
$RH\phi2(I) = \frac{X(I)-X(I+2)}{RH\phi1(I)-RH\phi1(I+2)}$	"	Auxiliary vector of 2nd recriprical differences	C
$RH\phi3(I) = \frac{X(I)-X(I+3)}{RH\phi2(I)-RH\phi2(I+3)}$	"	Auxiliary vector of 3rd recriprical differences	C
$RH\phi4 = \frac{X(1)-X(5)}{RH\phi3(I)-RH\phi3(2)}$	"	4th reciprical difference constant	C
$XN\phi W$	"	Present value that routine is interplating	C
$YN\phi W = X(1) + \frac{XN\phi W-X(1)}{RH\phi1(1) + \frac{XN\phi W-X(2)}{RH\phi2(1) + \frac{XN\phi W-X(3)}{RH\phi3(1) + \frac{XN\phi W-X(4)}{RH\phi4}}}}$		resultant of interpolation	

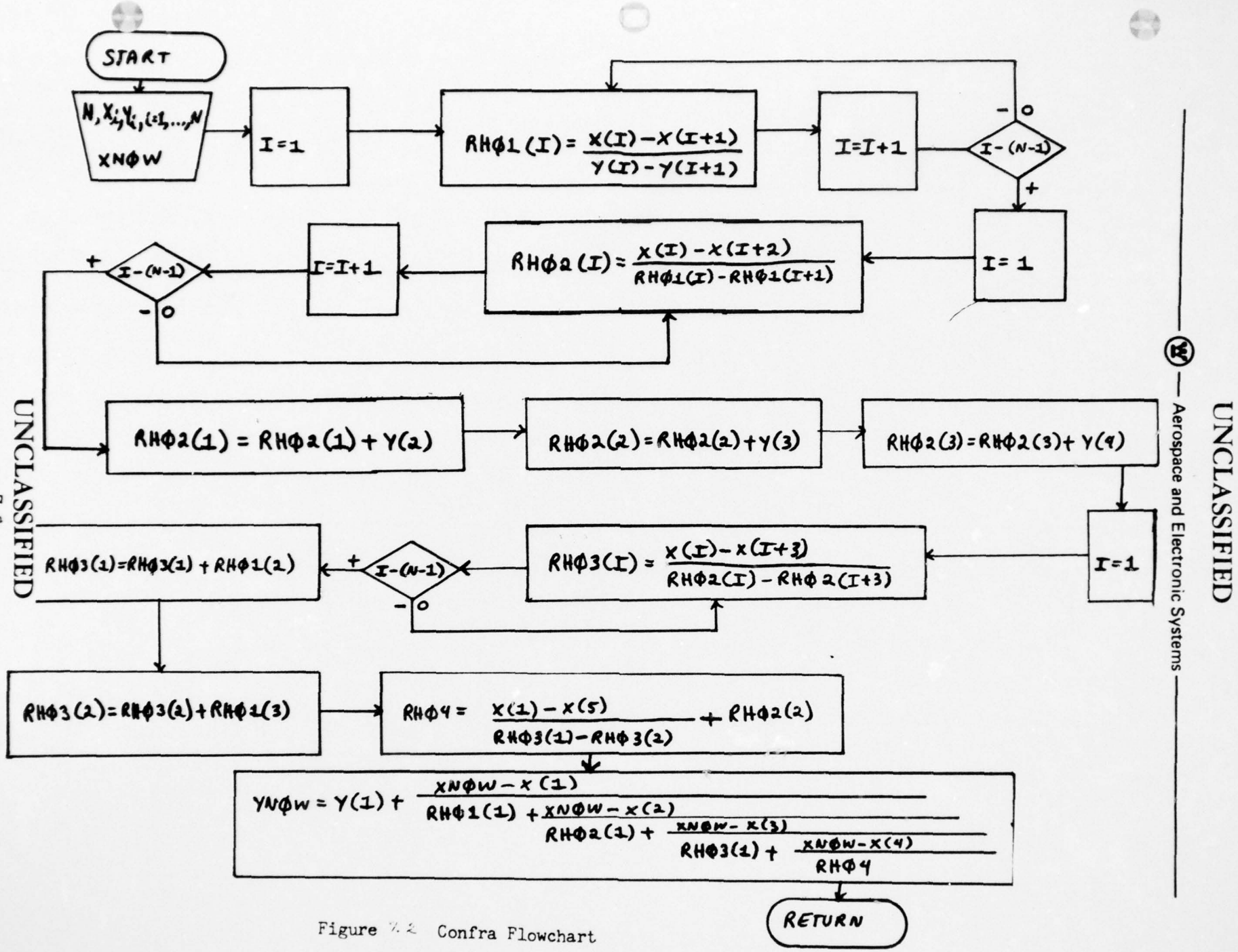

Figure 7.2 Confra Flowchart

Table 7.2 Expressions Used in Implementing ATMOSP

Equations	UNITS	#	EXPLANATION	I/O/C
T_o	^oK		Ground Temperature	I
M_o			Ground level mixing ratio	I
P_o	atmospheres		Ground level pressure	I
R_e	miles		Radius of earth	I
h_i	kilometers		Lower altitude of either observer or target	I
h_2	kilometers		Upper altitude of either observer or target	I
Z	degrees		Zenith angle	I
	microns		Wavelength	I
VR	miles		Visual range	I
$K = 2.152/(VR)$		(1)	extinction coefficient	C
$T = T_o - (72/11)H, 0 \leq H \leq 11km$	^oK	(2)	Temperature	C
$= T_o - 72$, $11 < H \leq 25km$	^oK	(3)	"	C
$T_o - 72 + (72/23)(H-25)$, $25 < H \leq 48$ KM	^oK	(4)	"	C
T_o, $H > 48$ KM	^oK	(5)	"	C

Table 7.2 Expressions Used in Implementing ATMOSP (Cont.)

Equations	Units	#	Explanation	I/O/C
H = either h_1 or h_2	kilometers		height above the earth; auxiliary program variable	I
$P = P_o^{-H/8}$	atmospheres	(6)	pressure above the earth	C
$R = -(R_e+h_1)\cos z + \sqrt{(R_e+h_1)^2\cos^2 z + (R_e+h_2)^2 - (R_e+h_1)^2}$	miles	(7)	path length between h_1 and h_2	C
$SF = R/\lvert h_2-h_1\rvert$		(8)	airmass scale factor	C
$W_{H_2O} = \frac{818 M_0 P_0^2 (1-e^{-0.747H})}{T_0^{3/2}}$		(9)	precipitable centimeters of water	C
$W_{CO_2} = 32\left[(P_0)^2\left(\frac{300}{T}\right)^{3/2}\left\{4.4 - (7.6e^{-3.14H} - 3.2e^{-4.71H^{1.057}})\right\}\right]$		(10)	equivalent centimeters of CO_2	C
$W_{N_2O} = 0.28\left[(P_0)^2\left(\frac{300}{T}\right)^{3/2}\left\{4.4 - (7.6e^{-3.14H} - 3.2e^{-4.71H^{1.057}})\right\}\right]$		(11)	equivalent centimeters of N_2O	C

Table 7.2 Expressions Used in Implementing ATMOSP(Continued)

Equations	Units	#	Explanation	I/O/C
$W_{O_3} = W_P(1+\exp[(H-Y_P)/4.63])^{-1}$		(12)	equivalent centimeters of O_3	C
$W_P = 0.218$			empirically derived O_3 distribution constant	I
$Y_P = 23.25$			empirically derived O_3 distribution constant	I
$\gamma_s = EXP(-SF \cdot K/A (e^{-Ah_1} - e^{-Ah_2}))$		(14)		C
$A = (inputted)$			inverse of scale height	C
$\gamma_{H_2O} = e^{-a_{H_2O}(SF \cdot W_{H_2O})^{b_{H_2O}}}$		(15)	transmission due to H_2O	C
$\gamma_{CO_2} = e^{-a_{CO_2}(SF \cdot CO_2)^{b_{CO_2}}}$		(16)	transmission due to CO_2	C
$\gamma_{N_2O} = e^{-a_{N_2O}(SF \cdot N_2O)^{b_{N_2O}}}$		(17)	transmission doe to N_2O	C
$\gamma_{O_3} = e^{-a_{O_3}(SF \cdot O_3)^{b_{O_3}}}$		(18)	transmission due to O_3	C

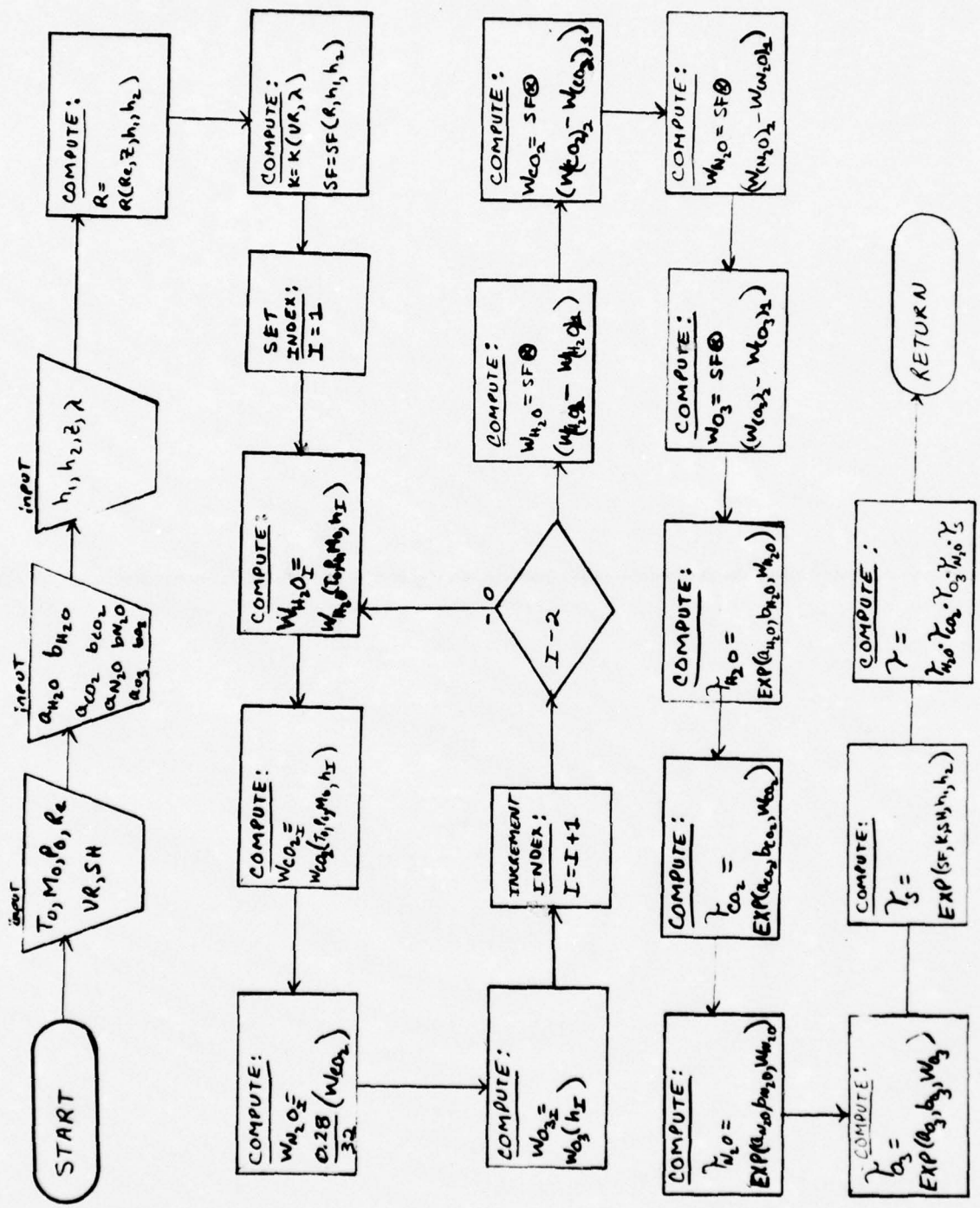

Figure 7.3 ATMOS Flowchart

Table 7.3 Expressions Used in Implementing SENSOR

Equations	Units	#	Explanation	I/O/C
$P(X_i, Y_i)$			Point spread function matrix	I
$R(X_i, Y_i)$			Reticle transmission matrix	I
$I_1 \quad J_1$			Number rows and columns in $P(X_i, Y_i)$	I
I_2, J_2			Number of rows and columns in reticle transmission matrix	I
$C(X_i, Y_i) = \sum_{I,J} P(X_K - X_i'; Y_i - Y_j') R(X_i', Y_j') \Delta X_i' \Delta Y_j'$			Convolution Matrix	C
$A_o = \sum_{K=1}^{n} N_K$				
$A_1 = \sum_{K=1}^{n} N_K \cos 2\pi/K/n$			Fourier Sums	
$B_1 = \sum_{K=1}^{n} N_K \sin 2\pi K/n$				
$\Phi = Tan^{-1}(B_1/A_1)$			Phase angle error	
$E = \sqrt{B_1^2 + A_1^2}$			Amplitude error	
$S/N = A_o/NEP$			Signal to noise ratio	
NEP			Noise-equivalent power	

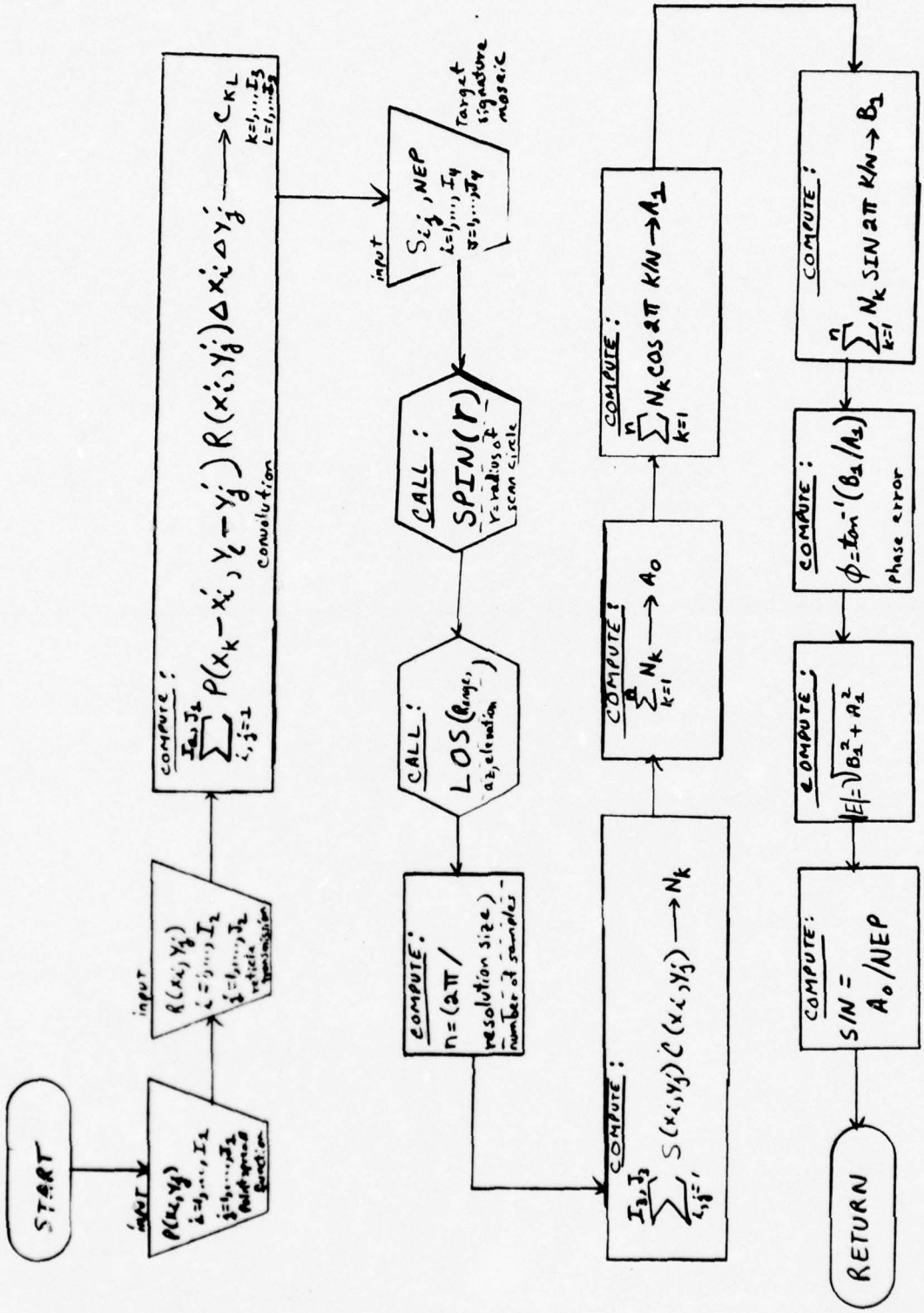

Figure 7.4 SENSOR FLOWCHART

Table 7.4 Analytical Expressions Used in Implementing TURBIN

Equations	Units	#	Explanation	I/O/C
$T_2 = T_o(1+ (K_2-1)/2)\ M_o^2)$	^oR	(1)	Total temperature of the ramair leaving the diffuser	C
T_o	^oR		static free stream temperature	I
$M_o = V_o/A_o$		(2)	Mach number of aircraft velocity	I
$K_2 = C_P/(C_P-R/MJ)$		(3)	Average specific heat ratio of air at temperature T_2	C
V_o	(fps)		Aircraft velocity	I
A_o	(fps)		Speed of sound (function of altitude)	C
$C_p = 0.239 \quad T \leq 800\ ^\circ R$ $0.230 + 0.1T/900 \quad T > 800^\circ R$	BTU/LB-°R	(4)	Linear curve fits for specific heat, $\bar{C}_P(T_x, T_y) = (\bar{C}_{P_x} + \bar{C}_{P_y})/2$ average value of the average specific heat between temperatures T_x, T_y	C
$R = 1544$	ft-lb/mole-^oR		Universal gas constant	
$J = 778$	ft-lb/BTU		Conversion factor	
t_o			Ambient Temperature	I
P_o			Ambient Pressure	I
$P_2 = P_o(1+((1+\frac{K_2-1}{2} M_o^2)^{\frac{K_2}{K_2-1}}-1) E_{rr})$		(5)	Total Pressure	C
E_{rr}			Ram Recovery Factor	I

UNCLASSIFIED

Table 7.4 Analytical Expressions Used in Implementing TURBIN (Cont.)

Equations	Units	#	Explanation	I/O/C
V_c			Compression factor	I
$\Delta h_c' = \bar{C}_{p_{23}'} T_2 \left(r_c^{(K_{23}'-1)/K_{23}'} - 1\right)$	BTU/LB	(6)	Adiabatic enthalpy change	C
N_C			Compression Efficiency	I
	BTU/LB	(7)	Actual enthalpy change due to compression losses	C
$\Delta h_c = \Delta h_c' / N_C$				
$T_3 = \Delta h_c / \bar{C}_{p_{23}} + T_2$	^oR	(8)	Actual compression temperature	C
$P_3 = P_2 r_c$	Lb/Ft^2	(9)	Compression Pressure	C
N_{MC}			Mechanical efficiency of compressor	I
W_A	Lbs		Weight of a unit of air	I
f			Ratio of fuel and air weights	I
L_S	BTU/Lb		Shaft work	I
X			Fraction air bleed off compressor	I
[illegible]			Hydrogen to carbon ratio	I
N_{MC}			Mechanical efficiency of compressor	I
L_λ	BTU/Lb		Parasite losses	I
N_{Mt}			Mechanical efficiency of turbine	I
η_η			Nozzle efficiency	I
η_t			Turbine efficiency	I

Table 7.4 Analytical Expressions Used in Implementing TURBIN (Cont.)

Equations	Units	#	Explanation	I/O/C
$W_g = W_A(1+f)$	Lbs	(10)	Weight of the mixture leaving the combustion chamber	I
$f' = \frac{\bar{C}_{p43}(T_4-T_3)}{0.5\,t_L + 15648 + 1312\,\alpha - \bar{C}_{p4}T_4}$			ideal fuel to air ratio by weight	
$h_f = 0.5\,t_L - 287$	BTU/Lb	(11)	Heat of vaporization of fuel (liquid hydrocarbon fueld)	
$L_c = \Delta h_c / N_{Mc}$	BTU/Lb	(12)	Work required by the compressor to compress one pound of air	C
$PP(CO_2) = \frac{1}{(4.764 + 1.1911\,\alpha)\,f_o/f' + 0.250\,\alpha}$		(13)	Partial Pressure of CO_2	C
$PP(H_2O) = PP(CO_2)\,\alpha/2$		(14)	Partial pressure of H_2O	C
$T_5 = T_4 - L_t/(N_{Mt}\,\bar{C}_{p45})$		(15)	Temperature of gas leaving turbine	C
$T_6 = T_5\left\{1 - \eta_N \frac{\bar{C}_{56}'}{\bar{C}_{56}}\left[1 - \left(\frac{P_o}{P_5}\right)^{(K_{56}'-1)/K_{56}'}\right]\right\}$		(16)	Temperature of the exhaust gas leaving the nozzle	C
$V_j = \sqrt{2g\,\bar{C}_{56}(T_5-T_6)\,J}$		(17)	Exhaust gas velocity	C
$F_j = \dot{W}_A\left[(1-x)(1+f)V_j - V_o\right]/g$		(18)	Thrust	C

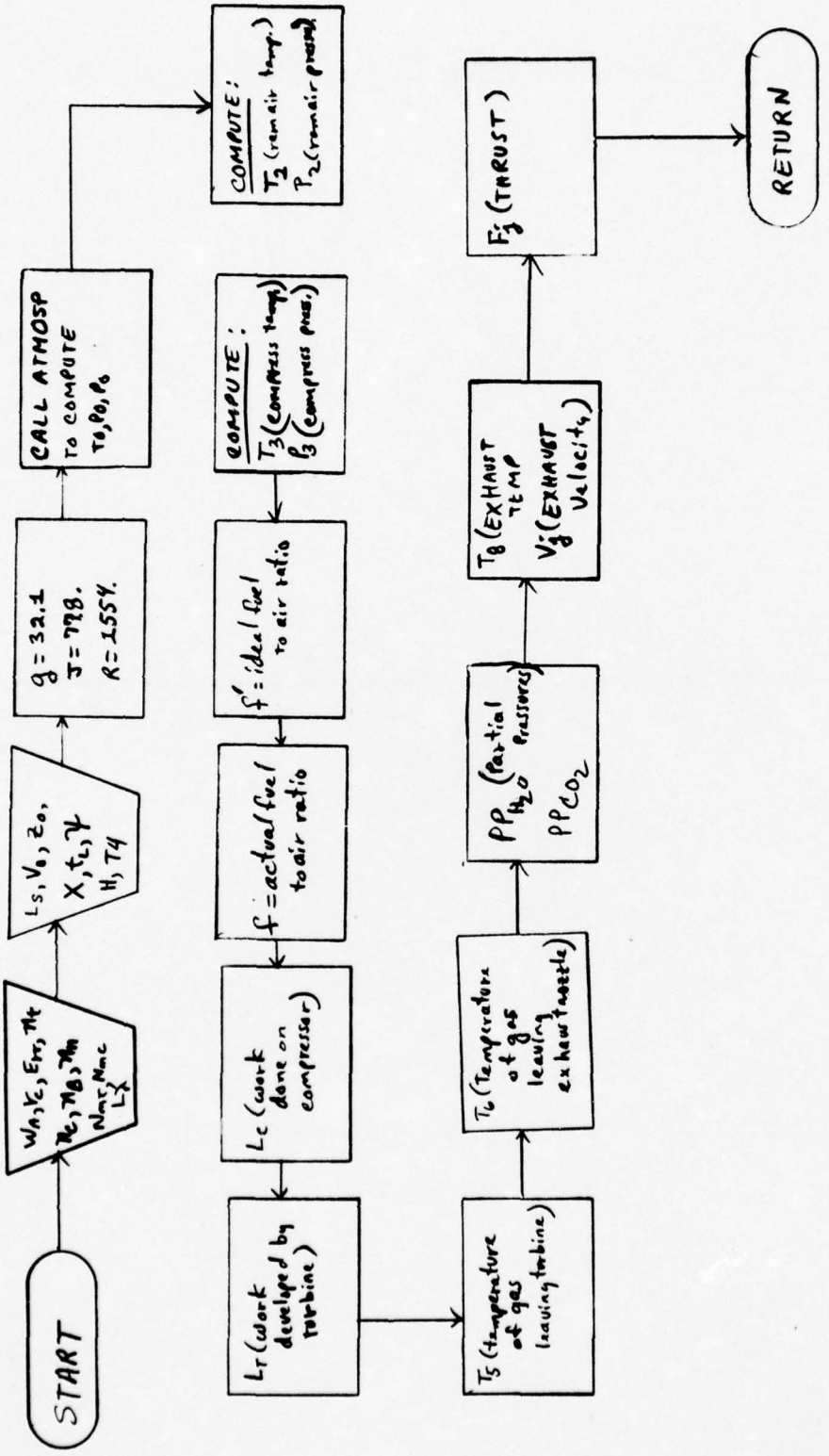

Figure 7.5 TURBIN Flowchart

Table 7.5 Expressions Used in Implementing BODY

Equations	Units	#	Explanation	I/O/C
SR			Code used to indicate surface rank (major/minor)	I
γ				
β max				
γ max	Degrees		Size parameters defined according to surface type	I
β min				
γ min				
SN			Surface number	I
STYPE			Surface type (cone, sphere, cylinder, etc.)	I
R_X, R_Y, R_Z			Position of observer(sensor) in (X_e, Y_e)(earth referenced)	I
r_x, r_y, r_z			coordinates to surface coordinate system)	
$[T_{i,x_e,y_e,z_e}] = \begin{bmatrix} \lambda_{xi} & \mu_{xi} & \nu_{xi} \\ \lambda_{yi} & \mu_{yi} & \nu_{yi} \\ \lambda_{zi} & \mu_{zi} & \nu_{zi} \end{bmatrix}$		(1)	Transformation matrix for transforming from the ( ) coordinates to the i-th surface coordinates; with the appropriate changes, this transformation matrix is used for other program transformation.	C
$\lambda_{xi} = \cos\phi\cos\psi$		(2)	direction cosines	C
$\lambda_{yi} = -\sin\phi\cos\psi$		(3)	"	C

Table 7.5 Expressions Used in Implementing BODY (Cont.)

Equations	Units	#	Explanation	I/O/C
$\lambda_{zi} = \sin\psi$		(4)	direction cosines	C
$\mu_{xi} = \sin\phi\cos\omega - \cos\phi\sin\psi\sin\omega$		(5)	"	C
$\mu_{yi} = \cos\phi\cos\omega + \sin\phi\sin\psi\sin\omega$		(6)	"	C
$\mu_{zi} = \cos\psi\sin\omega$		(7)	"	C
$\nu_{xi} = -\sin\phi\sin\omega - \cos\phi\sin\psi\cos\omega$		(8)	"	C
$\nu_{yi} = -\cos\phi\sin\omega + \sin\psi\sin\phi\cos\omega$		(9)	"	C
$\nu_{zi} = \cos\psi\cos\omega$		(10)	"	C
$E \equiv R_{xj} - R_{xi} + \lambda_{xj}x_j + \mu_{xj}y_j + \nu_{xj}z_j$		(11)	Auxiliary scalars used in the intercept solution	C
$F \equiv R_{yj} - R_{yi} + \lambda_{yj}x_j + \mu_{yj}y_j + \nu_{yj}z_j$		(12)	"	
$G \equiv R_{zj} - R_{zi} + \lambda_{zj}x_j + \mu_{zj}y_j + \nu_{zj}z_j$		(13)	"	
$R_1 = \lambda_{xi}E + \lambda_{yi}F + \lambda_{zi}G$		(14)	Scalar constants needed in the intercept solution	C
$R_2 = \mu_{xi}E + \mu_{yi}F + \mu_{zi}G$		(15)	"	
$R_3 = \nu_{xi}E + \nu_{yi}F + \nu_{zi}G$		(16)	"	
$C_1 = \lambda_{xi}r_x + \lambda_{yi}r_y + \lambda_{zi}r_z$		(17)	"	

Table 7.5 Analytical Expressions Used in Implementing BODY (Cont.)

Equations	Units	#	Explanation	E/O/C
$C_2 = \mu_{x_i} r_x + \mu_{y_i} r_y + \mu_{z_i} r_z$		(18)	Scalar constants needed in the intercept solution	
$C_3 = \nu_{x_i} r_x + \nu_{y_i} r_y + \nu_{z_i} r_z$		(19)	"	
$\delta = (\alpha - R_3)/C_3$		(20)	Scalar constants needed in the intercept solution for flat surfaces defined in section 3.0 of this report	C
$\delta = -(2R_1C_1 + 2R_2C_2 - 2cR_3C_3 - bC_3) \pm \{(2R_1C_1 + 2R_2C_2 - 2cR_3C_3 - bC_3)^2 - 4(C_1^2 + C_2^2 - cC_3^2)[R_1^2 + R_2^2 - a - (b + cR_3)R_3]\}^{1/2} \div 2(C_1^2 + C_2^2 - cC_3^2)$		(21)	Scalar constant needed for the intercept solution of conic surfaces	C

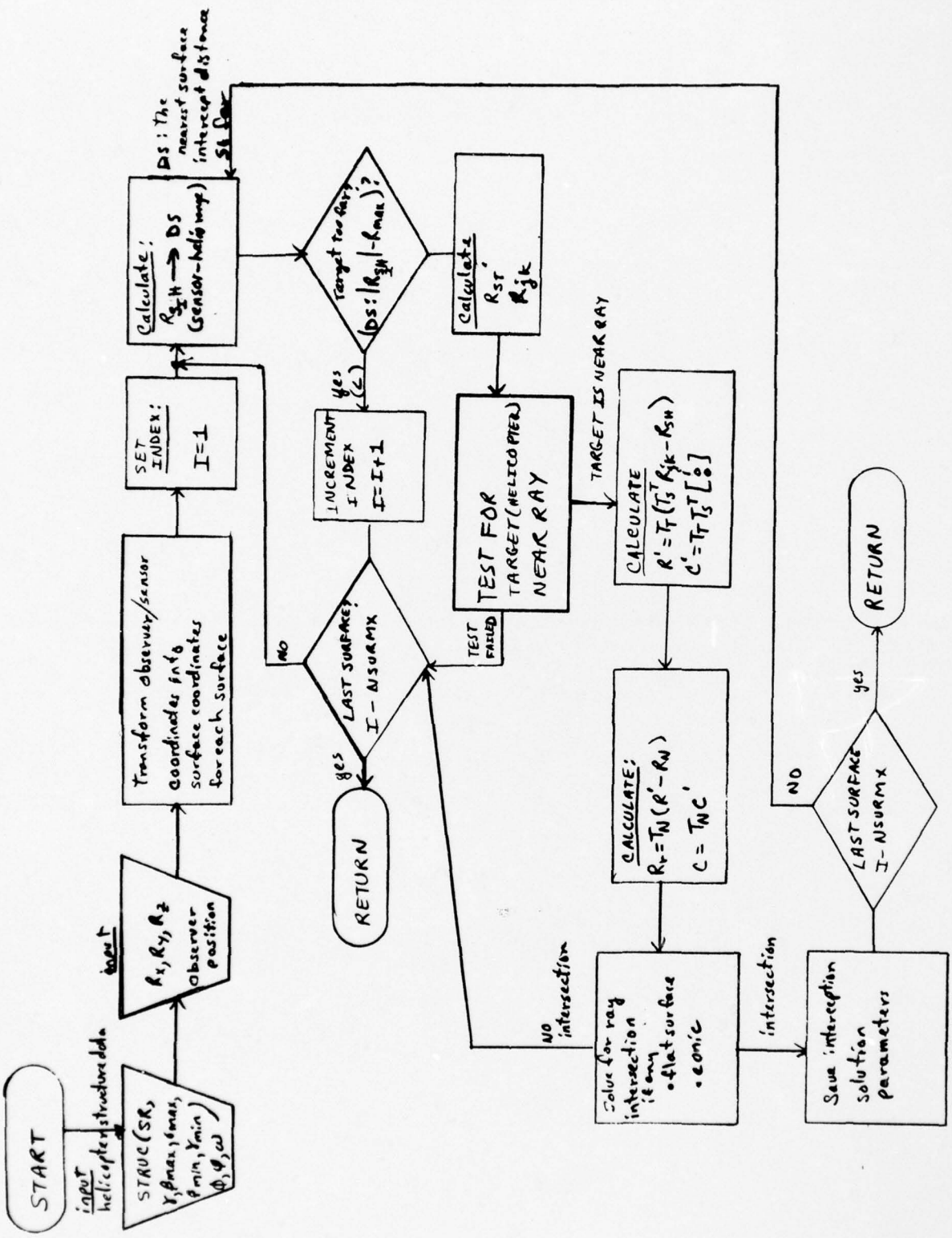

Figure 7.6 BODY Flowchart

7.4 Hide Executive Sequence

The sequence of operations carried out in the computer model HIDE are illustrated in the flow chart shown in Figure 7.7.

The first step consists of reading data. It comprises the following categories.

- o Meteorologics - Air temp; humidity; pressure; wind velocity and direction
- o Operation Conditions - Altitude, velocity, payload
- o A/C Specifications - Torque, attitude
- o Engine Specifications - Compression ratio, temperature limits, efficiencies
- o Surface Data - Major and minor surfaces; reflectivity type; specific heat; conductivity; thickness; absorptivity
- o Internal Sources - Power dissiptation; surface conductivity and convectivity
- o Sensor - Spectral response; sensitivity; spatial response
- o Solar - Azimuth and elevation
- o Topography - Height above sea level; proximity to target
- o Background - Types; distribution; coefficients; reflectance
- o Observer - Range, azimuth and elevation from target
- o Position - LOS positions on target
- o Options - Transient thermal response; signal to noise ratio and/or error signals; output formats on cards, tape or paper; input from tape or data cards

The next series of operations consists of initializing the TRANS, PLUME and BODY subroutines.

The TRANS initiialization consists of solving the LOS geometry and computing the amount of absorber H_2O, CO_2, N_2O, O_3 and scatter in the various paths as well as the temperature at selected points along each path.

FIG. 7.7 "HIDE" FLOWCHART

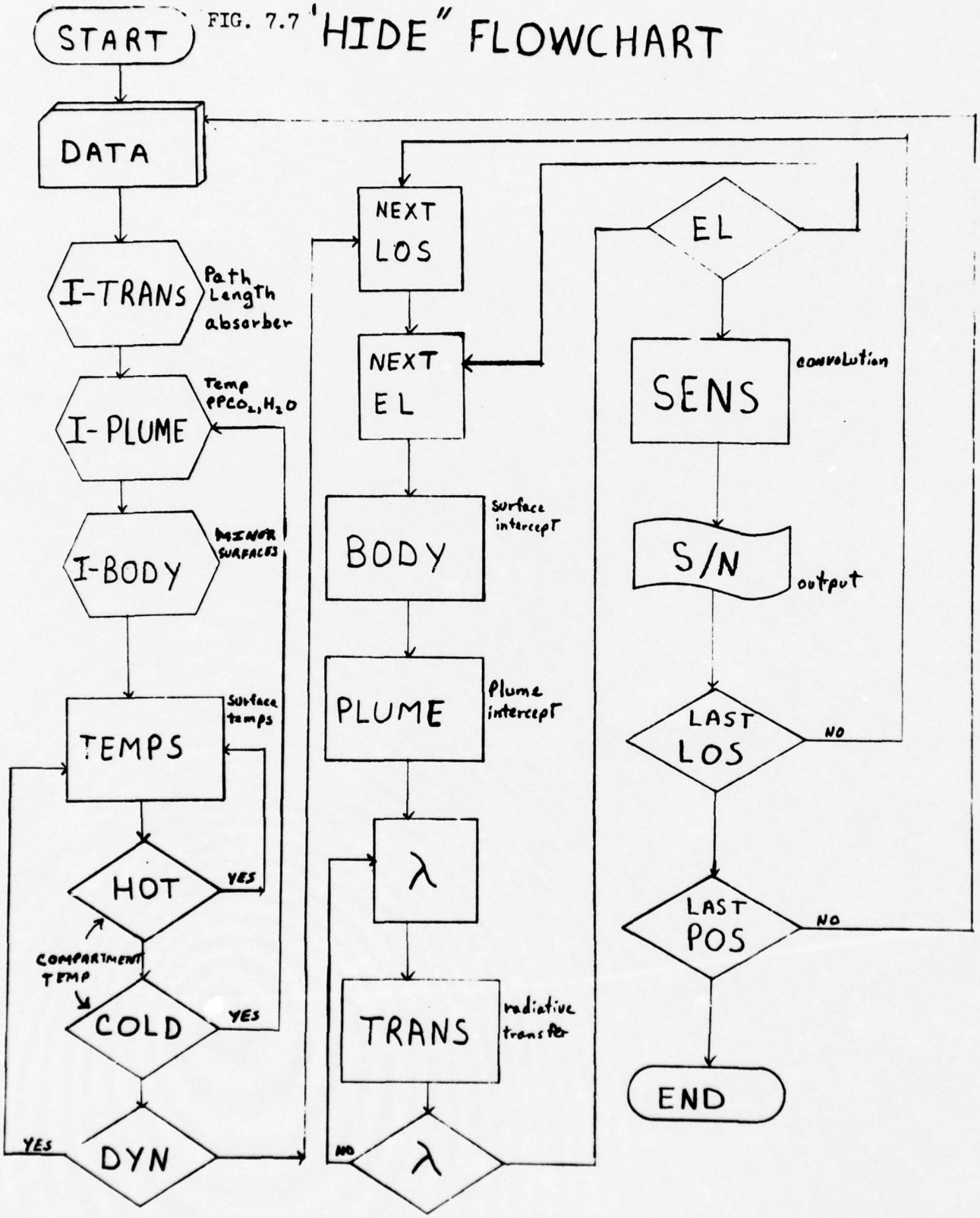

The PLUME initialization consists of defining the exit conditions of the turbine and the spatial distribution of temperatures and partial pressures of the exhaust gases.

The BODY is initialized by self-determination of the minor surfaces as dictated by their contact with hot plume gases.

The TEMPS subroutine then solves the thermal balance equations for the surface temperatures. A test is then made to determine 'is the compartment temperature inhabitable.' If it is too hot, ambient air is vented into the compartment and the heat balance redetermined. If the compartment is too cold, the heater is turned on and the PLUME, BODY and TEMPS resequenced due to the change in the turbine operation because of compressor bleed for the heater.

If the option for dynamic heat balance has been exercised, a clock is started and the differential form of the heat balance equations iterated for transient solutions.

This completes the program initialization and the first LOS position data (range, azimuth and elevation) is selected. Also, the first target signature mosaic coordinates are assigned.

The BODY is entered to find the surface intercepted and the attendant characteristics for that intercept (i.e., temperature, reflectivity, angle of incidence, etc.). The PLUME is checked to determine if the plume has been intercepted.

The first wavelength is selected and the radiative transfer solution obtained in TRANS. A test is then made to determine if the last wavelength has been reached. If it has, then this radiometric value is stored in the target signature mosaic and the program moves onto the next element.

When the last element has been reached, the target signature mosaic is complete. The SENS subroutine then transforms the signature and computes the S/N and/or error signals. These results are then outputted.

The flow progresses in the above manner until all LOS positions have been handled. At this point, a test is made to determine if there is another mission condition to be treated. If so, new data is read in for the change and the program reinitialized and recycled as described above.

When no new mission requirements exist, the program terminates.

A typical output from a similar type computer run is illustrated in Figure 7.8.

Figure 7.8 is a printout in gray scale of the spatial intensity of the listed AAM. The upper figure is for a case using active TV at .85 microns, while the lower case is for passive IR. In both cases, the AAM is viewed from 12 degrees nose aspect with a 45 degree roll angle. In the TV case shown, the bright sun lit cloud background caused the signature to be negative except for a specular sun reflection off the nose. In the IR case, the aero heated body stands out against the sky background. In this particular example, the viewing angle was set equal to the specular angle of sun giving rise to a strong solar reflection along the length of the body.

These particular signature examples, including Figure 6.1, point up the various manifestations that the signature can exhibit and thus, testify to the need for including the many and detailed phenomena encompassed by the program.

GREY SCALE CODE

0 1 2 3 4 5 6 7 8 9

. - + I X 王 丰 田 ⋈

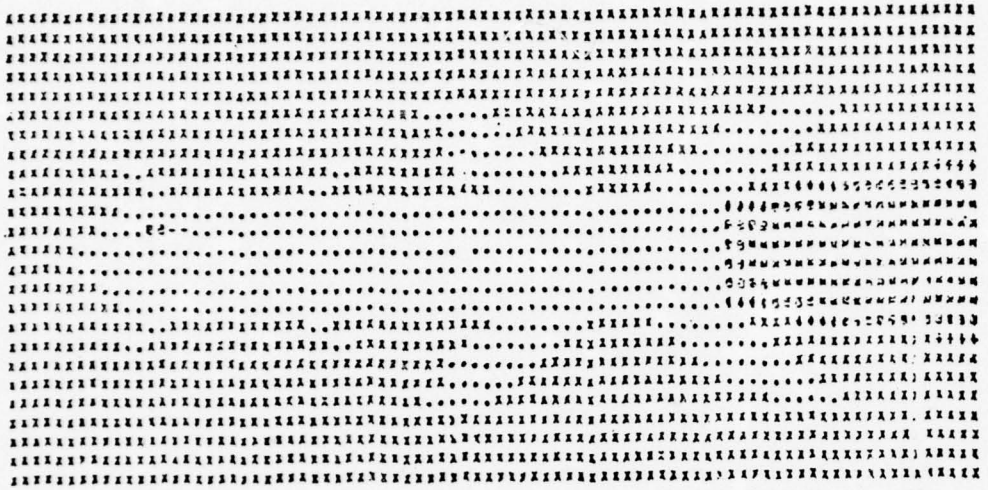

.85μ

TV DAY

CLD BG

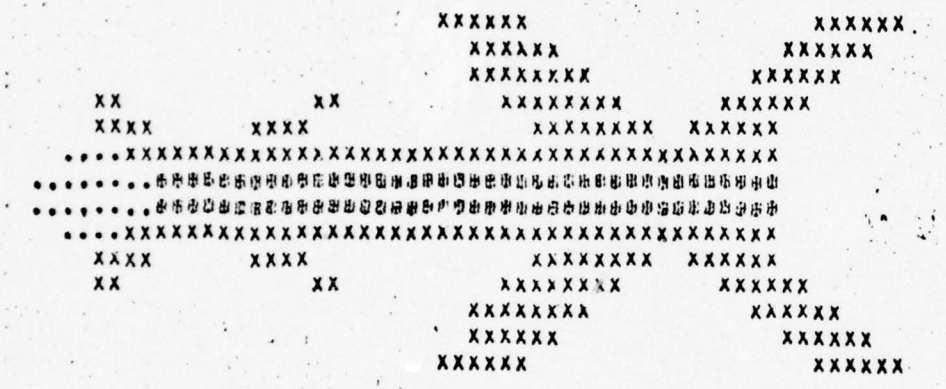

3-5μ

IR DAY

SKY BG

SOLAR GLINT

AERO HEAT

FIG. 7.8 SAMPLE AAM SIGNATURES

7.5 Estimated Storage and Running Time Requirements

In order to make some estimate of the storage and running times that should be required by HIDE, we have drawn upon our experiences with two similar computer programs developed and running at Westinghouse. Namely, we have used the storage and running time requirements of MOSAIC and FLEET SIGNATURE as a basis for estimating HIDE requirements. FLEET SIGNATURE (the actual program encoded name is FLEET 2) is a very comprehensive program developed for the Navy that predicts and aids in the evaluation of the infrared signatures of a fleet of ships. MOSAIC is a comprehensive, currently-running program that predicts electro-optical and infrared signatures of aerial targets. MOSAIC is currently being used by Westinghouse and the Air Force to evaluate signatures of particular class of advanced strategic weaponry. HIDE can use many of the same aerial target signature evaluation routines. HIDE can draw upon FLEET SIGNATURE heavily for the atmospheric effects.

Combining the computer teachings of the two programs one obtains a reasonably good estimate of HIDE requirements. It is expected that HIDE should require on the order of forty-thousand words (decimal, UNIVAC-1108 equivalent) storage locations. This number is expected to be sufficient for HIDE, its five major subroutines, and all auxiliary subroutines. Auxiliary routines do not encompass special purpose routines such as CALCOMP graphic output routines or tape-handling routines because currently these routines are not required by HIDE.

HIDE is expected to require running times on the order of 60-90 central processor unit seconds per image. An image is a depiction of the amount of energy seen by the sensor presented in matrix format where the elements of the matrix correspond to a "shade-of-grey level". See Figure 7.8 . This time is based on an image grid/matrix whose dimensions are on the order 60x60 elements. Running time is expected to be roughly proportional to the square of the size of the target signature element matrix. This is true because body intersection determination has to be made for each target element.

HIDE main program, input and output data, are included in the 40K estimate of storage.

No special I/O handling routines should be required. Magnetic tapes may be used merely for purposes of storing selected data samples. Graphic output to calcomp plotters can be considered, but should not be an integral part of HIDE output.

Any special routines or other program considerations should be weighted by an understanding of the potential use of HIDE, storage, running time, ease of usage, and machine independence considerations.

All changes or modifications at any level of HIDE should be documented to some extent on "document-as-you-go" basis. Such a policy of continuing documentation may seem unwarranted, but experience with a number of large, comprehensive computer programs has shown that through documentation is well worth the time and effort spent to generate the same.

HIDE is expected to require running times on the order of 60-90 central processor unit seconds per image. An image is a depiction of the amount of energy seen by the sensor presented in matrix format where the elements of the matrix correspond to a "shade-of-grey level". See Figure 7.8 . This time is based on an image grid/matrix whose dimensions are on the order 60x60 elements. Running time is expected to be roughly proportional to the square of the size of the target signature element matrix. This is true because body intersection determination has to be made for each target element.

HIDE main program, input and output data, are included in the 40K estimate of storage.

No special I/O handling routines should be required. Magnetic tapes may be used merely for purposes of storing selected data samples. Graphic output to calcomp plotters can be considered, but should not be an integral part of HIDE output.

Any special routines or other program considerations should be weighted by an understanding of the potential use of HIDE, storage, running time, ease of usage, and machine independence considerations.

All changes or modifications at any level of HIDE should be documented to some extent on "document-as-you-go" basis. Such a policy of continuing documentation may seem unwarranted, but experience with a number of large, comprehensive computer programs has shown that through documentation is well worth the time and effort spent to generate the same.

7.6 Program Documentation

Beyond the detailed analytical or theoretical basis writeups covered in earlier sections, each subprogram and special auxiliary routine should have 1) a computer mechanization writeup, 2) a detailed flowchart, and 3) an abbreviated documentation that supplies summary information about the program and its useage. Figure 7.9 is an example of an abbreviated documentation sheet. At a later date, these same materials should be edited, expanded and included in a Users Manual along with some numerical examples that should show how to use the routine.

Arrangements should be made to keep users updated on any changes to HIDE.

An input data description sheet should be part of the documentation for each subprogram. This information sheet should present the relationships between data card formats, the units, and the program nmemonics.

Subroutine Name: CONFRA

Purpose: To perform a continued fraction interpolation over a set of five points $(X_1, Y_1).....(X_5, Y_5)$

Method: An independent value XNØW is inputted. The routine solves for the dependent value Y(XNØW) by forming the continued fraction

$$Y(XN\emptyset W) = Y_1 + \cfrac{XN\emptyset W - X_2}{P_1 + \cfrac{XN\emptyset W - X_2}{P_2 - Y_1 + \cfrac{XN\emptyset W - X_3}{P_3 - P_1 + \cfrac{XN\emptyset W - X_4}{P_4 - P_2}}}}$$

where: $P_2 = \dfrac{X_2 - X_2}{Y_2 - Y_1}$, $P_2 - Y_1 = \dfrac{X_3 - X_2}{\dfrac{X_3 - X_1}{Y_3 - Y_1} - \dfrac{X_2 - X_1}{Y_2 - Y_1}}$

Usage: CALL CØNFRA (X, Y, XNØW, YNØW)

where: X, Y are vectors containing the set of five data points over which interpolation is performed.
XNØW is the undependent value to be interpolated
YNØW is the result

Restrictions: The X values must be arranged in ascending order

Length: Approximately 2008 storage location (1108)

Subroutines required: None

Reference: Numerical Analysis by Francis Schied (Schaum, 1968)

Figure 7.9 Example of An Abbreviated Documentation Sheet

8. MODEL VALIDATION

8.1 Introduction

Model validation is a process for eliminating irrevalent inputs, empirically correcting deficiencies and establishing the degree of confidence that can be placed on the model predictions.

The method consists of performing a sensitivity analysis by conducting exercises on the computer model to establish the magnitudes of deviations in the output signature for variations in input data and internally programmed functions. Insensitive program functions are then deleted. An error analysis is performed to determine the spread in the output due to measurement tolerances which is then compared with measurement results to establish the degree of validity. This degree and the spread are used in conjunction to assess the confidence one can place in the model predictions.

The following sections describe the philosophy and methodology to be employed in validating the computer model and in defining a criterion for validation.

8.2 Sensitivity Analysis

In the context used here, sensitivity refers to the change induced in the signature composition as predicted by the computer model due to a change in the value of a parameter used in computing the signature.

Signature composition includes intermediate effects as well as the final signature. Parameters refer to internal programmed functions and constants as well as input variables.

For example, relative humidity affects the turbine performance which in turn determines the exhaust plume characteristics. It also affects the value of environmental radiation which contributes to establishing the temperature of a given surface as well as the reflected component off the surface. In addition, it affects the transmission along the line of sight path. Thus it is not sufficient merely to look at the effect on the composite output signature due to changes in relative humidity. One must also look at the effect on intermediate or component parts of the composite. This is necessary to identify which components are of critical importance and which are irrelevant.

The procedure consists of first postulating a diverse set of scenarios representing the means in anticipated extremes of operating conditions. These represent base cases which provide the reference signatures for which variances will be obtained. This is necessary as the sensitivity of various parameters changes with operating conditions.

The next step consists of identifying all independent input variables. The flow of each input variable is then traced throughout the computer program to identify all of the intermediate effects which they influence directly and indirectly.

A base case is then selected and the program run to obtain reference values for the composite signature and all previously identified intermediate effects. The base case is then rerun with a small change in one input variable with all others held at their base case values. The final and intermediate outputs are then compared with the base case values. The sensitivity at each output is then obtained by taking the ratio of the change in each of the various outputs to the changein the input variable. This sequence is followed for each input variable in turn until all have been cycled. The same procedure is repeated for each of the remaining base cases.

In this manner the sensitivity of the composite final output to values of the independent input variables may be ascertained and trivial inputs identified. The trivial inputs may then be either built in as constant values or deleted altogether depending upon their nature. In either event, the number of required inputs and their sensitivity will be established.

Next the sensitivity of the intermediate effects to the input variables are scrutinized to identify trivial effects. These may then also be either built in as constants or deleted all together depending on their nature. In either event, the program composition will be simplified and running time shortened to some degree.

Finally, the sensitivity of the final output to changes in the intermediate effects may be assessed. This may require rerunning the base cases and independently varying each intermediate effect , as was done with the input variables, depending on the degree of interaction obtained in the previous runs. In either event, this will establish the sensitivity of the output to various physical phenomena which have been modeled and identify those which are critical to accuracy and those which are not. This may permit simplification of some modeled phenomena while pointing up the need for more sophistication in the modeling of others.

Thus, one result of the sensitivity analysis will be a self diagnosis of the applicability of the model development resulting in corrective action in the form of simplifying and expanding the model in identified areas of excesses and deficiencies.

A second result will be to have identified the sensitivity of the output to various analytic functions depicting physical phenomena which will aid in determining where and by how much to make empirical corrections in the model to yield a best fit to measured results.

A third result is to have established the sensitivity of the output predictions to input values.

8.3 Error Analysis

An error analysis is required to determine the expectation with which one can expect the predicted output signatures to agree with measured values.

The first step consists of identifying all of the model input independent variables and then establishing the tolerance on the accuracy with which these parameters may be specified. For example, the tolerance on the instrument accuracies are used where measured data such as air temperature, relative humidity etc, is required. Engine specifications, paint specifications, etc. are used to derive tolerances for program data parameters. The exactness with which a modeled geometric shape represents the real air frame, such as a right cylinder for a section of fuselage, is estimated. In this manner, judicious estimates of the tolerances of all of the independent variable values are obtained.

The second step consists of developing a correlation table with the aid of the results obtained in the sensitivity exercises. The correlation table defines the covariance between input variables in their influence on the output signature.

The third step consists of obtaining the values of the input variables (relative humidity, air temperature, etc.) corresponding to the radiometric measurement data set against which computer predictions will be compared. These values are then input to the computer model and a predicted signature obtained. This signature then represents the "mean" predicted value.

Next, the input variables are altered by an amount predicted on the magnitude of the previously determined tolerances. The polarity of the alteration is adjusted in accordance to the correlation chart. (i.e. all input variables which cause an increase in the output signature with an increase in the value of the variable, are increased by their tolerance value and all input variables which cause an increase in the output signature with a decrease in the value of the variable are reduced by their tolerance value.) A computer run is then made using these input values to obtain a "maximum" signature prediction deviation.

The above procedure is repeated using the opposite polarity tolerances on all input variables and a "minimum" signature prediction deviation obtained.

In this manner, a spread in the signature prediction for the given measurement conditions is obtained. The implication of this spread is that even if the computer model were perfect, it could not predict a signature any more accurately then the accuracy of the input data. Hence, this spread represents the prediction error attributable solely to the accuracy of the input data.

These error analyses in conjunction with results of the sensitivity analysis point up deficiencies in the exactness with which certain input parameters are specified and thus point up those parameters which should be more accurately measured or modeled. This is an important result in proposing validation type measurement programs.

If the error spread is too large, validation with the given radiometric data set may be ambiguous. Hence, this data set would be disregarded and a new one tried. If the spread is narrow, the corresponding radiometric data set represents a viable case for validating against.

8.4 Empirical Corrections

After a set of radiometric measurements has been selected by virtue of the smallness of the prediction error spread, the radiometric values are compared with the predicted values.

In general, if the measured value falls within the spread of the predicted values, the model prediction is considered to be in good agreement with the measured value. If the measured value falls outside the spread of the predicted values, it is considered to be in poor agreement in proportion to the amount with which it lies outside the spread relative to the extent of the spread itself.

All of the compared data sets are then analyzed for sensitivity correlations. That is the sensitivity of the various intermediate effects are considered to determine where an emperical modification might be made which will bring the most measured data points within their respective spreads. The impirical modification is then performed and the data sets rerun. This process is continued until the best fit is obtained.

8.5 Validation

After all impirical modifications have been made, the resultant predictions may be compared with the measurements to assess the validity of the model.

Validity is related to the accuracy with which the model predicts the measured signature, hence may be expressed as a ratio of the difference, between the measured value M and the prediction P, and the measured value.

$$V = \frac{M-P}{M} \qquad (8\text{-}1)$$

However, the predicted value is influenced by the measurement errors associated with the input data. Therefore, the validity should be weighted for these error possibilities. This may be approximated by assuming the measurement errors to be normally distributed yielding a deviation σ depicted by the error spread about the "mean" prediction value, Po.

$$V_P = \frac{1}{\sigma}\sqrt{\frac{2}{\pi}} \int_0^{\infty} \left[\frac{M-P}{M}\right] e^{-\frac{1}{2}\left(\frac{P-P_0}{\sigma}\right)^2} dP \qquad (8\text{-}2)$$

The average validity of all sets, $\bar{V}_P$ could then be expressed as

$$\bar{V}_P = \sqrt{\frac{1}{N}\sum_{S=1}^{N}\left[V_P(S)\right]^2} \qquad (8\text{-}3)$$

8.6 Prediction Confidence

Once the degree of validation of the model has been ascertained, it may be used to assess the confidence level of operational predictions.

This is accomplished by first predicting the operational signature and the spread associated with the tolerance on the input parameters. This spread is then increased in accordance with the degree of validation achieved. The new spread represents a probability distribution of actual signature levels. This may be used as defining the probable deviation in the signature from the predicted value.

A confidence level may then be established in the context of what the probability is that the signature (or detection range) is less than some given value.

In a similar manner, the deviation may be used in the vulnerability model to establish a degree of confidence in the vulnerability prediction.

9. RECOMMENDATIONS

It is recommended that the methodology that has been developed under this contract for synthesizing the flight and mission profile infrared signatures of specified Army aircraft as described in the preceeding sections now be applied toward construction of the computer model.

The computer model which would be programmed is called "HIDE" (Helicopter Infrared Detection Estimate) and is described in detail in the preceding section of this report covering programming. Its concept and implementation are based on the methodology described in earlier sections.

It is recommended that initially only one aircraft type be addressed and that the model be programmed in Fortran IV on in-house computers. The initial effort should establish the feasibility of modeling the infrared signatures of Army aircraft, with the fidelity required to properly assess vulnerability and countermeasure effectiveness.

The program repitoire can be expanded to include other aircraft and be translated to AVSCOM computers, including users manuals, after feasibility has been established.

9.1 Recommended Action

The action recommended is to synthesize a helicopter infrared signature model, called HIDE, and program it on an in-house digital computer using FORTRAN IV.

The HIDE model should be programmed and debugged to predict the flight and mission profile infrared signatures of one Army aircraft selected on the basis of availability of best measurement data for both suppressed and unsuppressed configurations.

Upon completion, an error-sensitivity analysis should be conducted on the model to establish the sensitivity of infrared signatures predicted to variations in the input environmental and operating conditions.

The environmental and operating conditions corresponding to measured radiometric data sets should then be input to the model and the resultant signatures predicted covering a tolerance spread as dictated by the results of the error-sensitivity analysis.

The measured data should be compared with the predicted signatures and analyzed to assess model deficiencies. Such deficiencies may be readily identified and corrected. Bias errors, if sufficiently consistent, should be empirically compensated.

After all obvious refinements have been made, the comparison should be repeated and a prediction accuracy formulated.

A final report should be issued describing the refined version of the computer model including a program listing. The results of the error and sensitivity analyses as well as those of the comparisons and prediction accuracy should be included.

It is estimated that the magnitude of effort required to accomplish this objective is approximately a 3 man year level which could be compressed most efficiently into a 9 month period with a 4 man level.

9.2 Task Descriptions

A description of the HIDE signature model to be constructed is contained in the preceding sections of this report. A description of how the effort should be expended to attain this objective is defined here.

The procedure consists of establishing major and minor tasks and then defining the work items to be carried out under each task.

The major tasks are identified by capitol letters, minor tasks by numbers and items by lower case letters. All tasks and items are also designated by appropriate abbreviations to facilitate time schedule and cost identification.

A - PLUME

Plume is a major task named after the computer program subroutine it is to construct.

A-1 - TURBINE

Turbine is a minor task of PLUME which constructs the turboshaft portion of the program.

A-1 a) PROGRAM is the work item for programming the turbine model. It consists of defining the analytics, identifying inputs, functions, and units as well as writing the program, punching the deck, running and debugging it.

A-1 b) A/C SPECS is the work item for obtaining the required program and input data from the engine specifications.

A-1 c) SENS ANAL is work item for performing a sensitivity and error analysis on the turbine model.

A-1 d) VALIDATION is the work item for comparing turbine performance predictions with engine specifications. It includes modifying coefficients to achieve best fit and assessing the quality of the fit obtained.

A-1 e) DOCUMENT is the work item for documenting the analytics, programming, specifications, analysis and validation results.

A-2 ROTOR

Rotor is a minor task of PLUME which constructs the rotor down wash portion of the program.

A-2 a) PROGRAM is the work item for programming the rotor down wash model. It consists of defining analytics, including circulation, identifying inputs, functions, and units as well as writing the program, punching the deck, running and debugging it.

A-2 b) A/C SPECS is the work item for obtaining the required rotor data from the aircraft specifications including pitch, tilt, thrust, torque, size and rpm as a function of operating conditions.

A-2 c) SENS ANAL is the work item for performing a sensitivity and error analysis on the rotor model.

A-2 d) VALIDATION is the work item for comparing rotor performance predictions with the air frame specifications. It includes modifying coefficients for best agreement and assessing the variance.

A-2 e) DOCUMENT is the work item for documenting analytics, programming, and specifications used in the rotor model along with the results of the analyses and validations.

A-3 FLOW

Flow is the minor task of PLUME which constructs the exhaust plume flow field by combining all velocity components.

A-3 a) PROGRAM is the work item for programming the flow field. It includes defining analytics, coordinates, displacement and velocity vectors, as well as identifying inputs, writing the program, punching the deck, running and debugging it.

A-3 b) SENS ANAL is the work item for performing a sensitivity and error analysis on the flow model.

A-3 c) VALIDATION is the work item for checking the viability of the flow model. It consists of obtaining data from thermocouple measurements on the tail boom and comparing them with the spatial position of the predicted plume contour at the same temperature. This requires inputting the turbine and rotor with the test conditions. Where reasonable, coefficients will be adjusted for best fit and an estimate of the overall accuracy postulated.

A-3 d) DOCUMENT is the work item for documenting the flow field development, programming, analysis and validation.

B - BODY A major task named for the subroutine BODY.

B-1 MAJOR

Major is the minor task of BODY which defines the major air frame surfaces to be used as data in the program.

B-1 a) A/C SPECS is the work item for reducing the air frame specifications to obtain the major surface shapes, sizes and orientations. It consists of securing layout drawings and designing surface grid to the drawing scale. The grids are then superimposed over the layouts and major surfaces defined and dimensioned. The surface data is then compiled.

B-1 b) DOCUMENT is the work items for documenting all specifications used and their sources.

B-2 MINOR

Minor is a minor task of BODY which defines the minor surface boundaries and characteristics within the major surfaces.

B-2 a) A/C SPECS is the work item for reducing the air frame specifications to obtain minor surface dimensions from thermal and radiometric considerations. A technical manual is secured and minor surfaces defined by emissivity differences (windows and paint types) and thermal effects (compartment interface, insulation, material differences, solar heating, etc.). The surface grids are used to obtain size factors.

B-2 b) DOCUMENT is the work item for compiling all minor surface data for machine use.

B-3 REFL

REFL is a minor task of BODY which defines the reflectivity characteristics of the surface materials.

B-3 a) A/C SPECS is the work item for procuring the surface finishes such as paint specifications on the specified aircraft.

B-3 b) DATA AQ is the work item for obtaining the bidirectional reflectivity on the surface finishes defined above from the University of Michigan's data bank.

B-3 c) DOCUMENT is the work item for compiling the reflectivity data and minor surface assignments.

B-4 GEOM

Geom is the minor task in BODY which constructs the surface assemblage and geometric intercept model.

B-4 a) PROGRAM is the work item for programming the geometrical model. It consists of defining the analytics for intercept geometry and target signature mosaic. It also includes defining inputs, writing the program, punching the deck, running and debugging the model.

B-4 b) VALIDATION is the work item for checking out the physical model construction and isolating surface dimension and orientation errors. This is accomplished by making high resolution print outs of the surface model (digital pictures) for comparison with the actual air frame configuration.

B-4 c) DOCUMENT is the work item for documenting the analytics, programming inputs and validation results of the geom model.

B-5 ADAPT

ADAPT is a minor task of BODY to construct a model for self defining surface boundaries of surfaces heated by the exhaust plume.

B-5 a) PROGRAM is the work item for programming the surface self definition criteria. It consists of defining the analytics for plume intercept of the tail boom, selecting a temperature gradient and defining the logic for determining automatically the surface temperature, size and location parameters for the boom heated surfaces as a function of operating conditions. Also included is writing the program, punching the deck, running and debugging it.

B-5 b) SENS ANAL is the work item for performing a sensitivity and error analysis on the ADAPT model.

B-5 c) VALIDATION is the work item for obtaining measurement data and operating conditions from "2nd Source" report and running model to make comparisons, emperical corrections and validation.

B-5 d) DOCUMENT is the work item for documenting the self-adaptive analytics, logic, programming and results of the analyses and validations.

C - TEMPS

TEMPS is a major task named after the computer program subroutine it is to construct.

C-1 DATA

DATA is a minor task in TEMPS for specifying the thermal characteristics of the minor surfaces.

C-1 a) A/C SPECS is the work item for deriving the thermal attributes of each surface and internal heat sources from air frame specifications. It entails compiling a list of internal sources and the heat dissipation rates or temperatures obtained from the technical manuals, including electrical

equipment, auxiliary heaters, oil coolers, mechanical power transfer coupling losses, etc. The conductive and convective heat transfer coefficients for each identified source to each coupled surface is defnned. Also the conductivity and specific heat of each minor surface as well as the total emissivity and solar absorptivity of its exterior is to be established.

C-1 b) DOCUMENT is the work item for documenting all specifications used and their reference sources.

C-2 BALANCE

BALANCE is a minor task in TEMPS for programming the thermal model.

C-2 a) PROGRAM is a work item for programming the thermal model. It consists of defining the analytics for thermal balance, internal transfer, mutual conduction, aero-heating, solar heating, environmental radiation exchange and compartment temperatures. Also included is identifying input parameters, writing the program, punching the deck, running and debugging the program.

C-2 b) SENS ANAL is the work item for performing a sensitivity and error analysis on the thermal model.

C-2 c) VALIDATION is the work item for comparing the prediction accuracy of the surface temperatures. It consists of deriving thermocouple measurement data and comparing them with model predictions using the measurement operating conditions. Coefficients will be empirically adjusted for best fit where reasonable and a measure of prediction accuracy postulated.

C-2 d) DOCUMENT is the work item for documenting the analytics, programming, analysis and validation work on the thermal model.

D. TRANS

TRANS is a major task named after the computer program subroutine which it is to construct.

D-1 COEFS

COEFS is a minor task in TRANS for deriving atmospheric transmission coefficients.

D-1 a) DATA is the work item for collecting and reducing transmission measurements to data format.

D-1 b) PROGRAM is the work item for programming a curve fit routine to transmission data to derive the atmospheric coefficients required for .1 micron spectral resolution. It includes writing the program, punching the deck, running and debugging it.

D-1 c) SENS ANAL is the work item for performing a sensitivity and error analysis on the derived coefficients in the transmission function to be used in the HIDE model.

D-1 d) VALIDATION is the work item for securing measurement data, meteoroligcs and running the transmission function with the derived coefficients and comparing the results with the measured values of transmittance.

D-1 e) DOCUMENT is the work item for recording all of the source data used, the analytics for the curve fits, the program and the results of the analyses and validation exercises.

D-2 DIST

DIST is a minor task in TRANS for programming the atmospheric distributions.

D-2 a) PROGRAM is the work item for programming the atmospheric distributions. It consists of defining the analytics for the variation with altitude of temperature, water vapor, carbon dioxide, nitrous oxide, ozone, aerosols, and pressure; identifying input requirements; writing the program; punching the deck; running and debugging it.

D-3 GEOM

GEOM is a minor task in TRANS for programming the line of sight path through the atmosphere.

D-3 a) PROGRAM is the work item for programming the line of sight path and determining the quantity of absorber in the path. It includes defining the line of sight geometry, interfacing it with the distributions and obtaining the equivalent sea level absorber quantities, as well as programming them, punching cards, running and debugging it.

D-4 ATTEN

ATTEN is a minor task in TRANS for programming the atmospheric attenuation model.

D-4 a) PROGRAM is the work item for programming the atmospheric attenuation model. It includes tabulating the wavelength absorption coefficients and defining the transmissivity of each absorbing or scattering species. It also includes integrating the geometry and distribution functions as well as programming all of these, punching cards, running and debugging the deck.

D-4 b) SENS ANAL is the work item for performing a sensitivity and error analysis on the transmission model.

D-4 c) VALIDATION is the work item for comparing the transmission predictions with field measurements. It consists of running selected measurement conditions of Yates and Taylor, Street, and/or GD and comparing predicted transmissions with the measured data to estimate a prediction accuracy.

D-4 d) DOCUMENT is the work item for tabulating the coefficients and documenting the analytics, programming, analysis and validation of the transmission model.

D-5 EMISS

EMISS is a minor task in TRANS to program the atmospheric emission model.

D-5 a) PROGRAM is the work item for programming the atmospheric emission model. It consists of defining the algorithm for computing emission, interfacing with the attenuation model, writing the program, punching, running and debugging the deck.

D-5 b) SENS ANAL is the work item for performing a sensitivity and error analysis on the EMISS model.

D-5 c) VALIDATION is the work item for comparing the EMISS model predictions with measurements by Moller, GD or other suitable sources.

D-5 d) DOCUMENT is the work item for recording the analytics, programming, and results of the analyses and validation runs.

D-6 SOLAR

Solar is the minor task in TRANS to program the direct and scattered solar radiation.

D-6 a) PROGRAM is the work item for constructing the program to predict direct and difuse solar radiation. It consists of defining the solar constant and scattering function, relating them to the line of sight transmission, programming, punching, running and debugging the deck.

D-6 b) SENS ANAL is the work item for conducting a sensitivity and error analysis on the SOLAR model.

D-6 c) VALIDATION is the work item for comparing direct and difuse solar predictions with measurements and imperically correcting model for best fit.

D-6 d) DOCUMENT is the work item for documenting the analytic formulation, programming construction, analyses and validation results.

D-7 REFL

REFL is a minor task in TRANS for determining the reflected radiation off a surface into the line of sight.

D-7 a) PROGRAM is a work item for programming the reflection model. It consists of defining the analytics for the reflection model to include the direction of reflection, radiance computation from that direction, directional reflectance function for the surface of incidence, and integration over a hemisphere as well as identifying inputs, writing the program, punching, running and debugging it.

D-7 b) DATA AQ is a work item for obtaining background reflectance data from the University of Michigan's Data Compilation file.

D-7 c) SENS ANAL is the work item for conducting a sensitivity and error analysis on the REFL model.

D-7 d) VALIDATION is the work item for comparing the accuracy of the REFL model predictions with measured data from the University of Michigan.

D-7 e) DOCUMENT is the work item for documenting the analytics, programming, data inputs, analysis and validation results.

D-8 EXHAUST

EXHAUST is a minor task in TRANS for programming the exhaust plume emission.

D-8 a) PROGRAM is a work item for programming the exhaust plume emission model. It consists of defining imperical curve fits to the absorption coefficients for water vapor and carbon dioxide as a function of temperature, integrating with the plume flow model, defining radiometric computations, writing the program, punching, running and debugging the deck.

D-8 b) DATA AQ is a work item for securing and tabulating the absorptivity data.

D-8 c) VALIDATION is a work item for comparing plume predictions with measured data to the extent feasible to obtain an estimate of the model's viability.

D-8 d) DOCUMENT is the work item for reporting the original data used to derive absorption coefficients, the curve fit routines used, the analytics and programming for the plume radiance and the results of validation runs.

D-9 RAD

RAD is a minor task in TRANS for programming the combination of all radiative transfer mechanisms to obtain an effective apparent radiance.

D-9 a) PROGRAM is the work item for constructing the program to combine radiative transfer components. It consists of defining the sequence of radiometric computations and defining the analytics to combine them, as well as identifying inputs, writing the programs, punching, running, and debugging the deck.

D-9 b) SENS ANAL is the work item for conducting a sensitivity and error analysis on the composite radiative transfer model.

D-9 c) VALIDATION is the work item for securing operational measured data and comparing them against predictions to ascertain accuracy.

D-9 d) DOCUMENT is the work item for reporting the programming details for integrating the radiative transfer model components and the results of the sensitivity and validation exercises.

E - SENS

SENS is a major task named after the computer subroutine it will construct.

E-1 CONV

CONV is a minor task in SENS for programming the routine of convolving the point spread function of the sensor optics with the sensor reticle.

E-1 a) PROGRAM is the work item for constructing the convolution program. It consists of defining input requirements, convolution matrix construction rational, as well as programming, punching, running and debugging the deck.

E-1 b) DATA AQ is the work item for securing the point speed function for the sensor type to be used.

E-1 c) DOCUMENT is the work item for documenting the analytics and programming used to perform the convolution operation and the point spread function incorporated as data in the program.

E-2 RETICLE

RETICLE is a minor task in SENS for programming the generation of the reticle matrix.

E-2 a) PROGRAM is a work item for constructing the reticle matrix and convolving it with the point spread function. It consists of defining the algorythm for representing the spatial transmittance of the convolved reticle pattern and analytics for overlaying with the target matrix to derive detection and error signals. It includes identifying input requirements, programming, punching, running and debugging the deck.

E-2 b) DATA AQ is a work item for obtaining and defining the reticle spatial transmittance function for the sensor type used.

E-2 c) VALIDATION is the work item for reporting the reticle specification, convolution algorythym analytics, programming and results of the sensitivity analysis and validation.

E-3 CM

CM is a minor task in SENS for programming the simulation of countermeasures.

E-3 a) PROGRAM is the work item for defining the analytics representing both decoys and modulators and translating into program language. It includes defining input requirements programming, punching, running and debugging the deck.

E-3 b) SENS ANAL is the work item for conducting a sensitivity and error analysis on the CM model.

E-3 c) DOCUMENT is the work item for recording the conceptual approach, program implementation and results of the sensitivity analysis.

F - HIDE

HIDE is a major task named after the program whose executive routine it will construct and on which it will perform sensitivity analyses and validation exercises.

F-1 EXEC

EXEC is a minor task in HIDE for constructing the executive routine and performing a sensitivity analysis on the overall program.

F-1 a) PROGRAM is a work item for constructing the executive routine for the overall computer program. It consists of defining the interface between subroutines, the content of common data the initialization steps and running sequence. In addition, it will contain the definition of input and output formats and provide options for inputing and outputing data. It also includes writing the program, punching cards, running and debugging the deck.

F-1 b) SENS ANAL is a work item for performing a sensitivity analysis on the composite computer model. It consists of varying input parameters about some mean value and assessing their effect on the output signature. The ratio of the output to input variance comprises a measure of sensitivity of the signature to a given input parameter.

F-1 c) DOCUMENT is the work item for documenting the executive routine developed and the results of the sensitivity analysis.

F-2 VALIDATION

VALIDATION is a minor task in HIDE to perform a comparison analysis with measured data to assess the prediction accuracy of the composite model.

F-2 a) PROGRAM is a work item for revising the computer program to output data in the form suitable for comparison with measured data. It includes writing programs for reading in data tapes, performing error analyses and statistical averaging of comparative results.

F-2 b) DATA AQ is a work item for selecting a measurement set for comparison and extracting the program input data from the measurement operating conditions. It includes securing data tapes from MEWTA and GD, and also obtaining operating conditions and meteorlogic data which may not be recorded on the tapes.

F-2 c) VALIDATION is the work item for running the comparisons and reducing the results to establish the prediction accuracy within the credibility of the sensitivity to the tolerance of the input parameters. It includes establishing a measure of validity for the model based on the validation criterior defined in this report.

F-2 d) DOCUMENT is the work item for writing up the procedures used and results obtained for the validation exercise.

F-3 REPORT

REPORT is a minor task in HIDE for documenting the composite model construction.

F-3 a) DOCUMENT is the work item for writing, editing and printing the final report for the composite model construction. It will include complete program listings, operating description, results of comparisons where performed, assessment of model viability and future recommendations.

10. REFERENCES

Section 10.1 presents a listing of the documents received and reviewed (primarily from DDC) during this phase of the Army aircraft infrared signature study. Section 10.2 presents a set of Westinghouse-edited abstracts on documents that have been particularly pertinent to the development of particular submodels of HIDE.

10.1 DOCUMENTS RECEIVED AND REVIEWED UNDER THIS CONTRACT

1. "A Study of the Secondary IR Sources on the UH-1H Helicopter"; by T.C.Duncan and J.W.Shirie; General Dynamics EDD, Pomona, Cal.; 14 May 1971, TM-6-332-60.28-3 (Secret)
2. "Preliminary Test Report, Infrared Signature Evaluation of a UH-1H Helicopter With and without Bell Shield" by L. Gastineau; General Dynamics EDD, Pomona, Cal.; 15 Dec. 1971, TM-6-125-PH-342 (Secret)
3. "Preliminary Test Report, Infrared Signature Evaluation of a UH-1H Helicopter with Garrett Suppressor", by L. Gastineau and F.A. Jepson; General Dynamics EDD, Pomona, Cal.; 7 Jan. 72, TM6-125-PH-345 (Secret)
4. "Test Plan, Infrared Signature Evaluation of a CH-47-C Helicopter", by G.W. Ashley, N.D. Barton and D.W. Blay; General Dynamics EDD, Pomona, Cal.; 28 July 1971; TM6-125PH-330 (Unclassified)
5. "Infrared Signature Evaluation of a CH-47C Helicopter", Volume 1, Summary of Results by G.W. Ashley, et.al., General Dynamics EDD, Pomona, Cal.; January 1972; TM6-125PH-341 (Secret)
6. "CH-47 Helicopter Infrared Suppression Device-Radiation Characteristics and Effectiveness Against IR Seeking Missiles", by Leonard H. Holden, Jr.; MEWTA, White Sands, N.M.; Nov. 1970, ECOM-5342 (Secret)
7. "Redeye Acquisition Ranges and Infrared Spectral Signature for the AH-1G Helicopter", by Leonard H. Holden, Jr.; MEWTA, White Sands, N.M.; Apr. 1971, ECOM-5375 (Secret)
8. "Redeye Acquisition Ranges and Infrared Spectral Signature for the OH-58 Helicopter", by Leonard H. Holden, Jr.; MEWTA, White Sands, N.M.; Apr. 1971, ECOM-5382 (Secret)
9. "OH-6 Helicopter Infrared Suppression Devices - Radiation Characteristics and Effectiveness Against Infrared Seeking Missiles", MEWTA, White Sands, N.M.; Sept. 1971, ECOM-5389 (Secret)

10. "IRCM Hardware and Tests Chronology", by Richard Poletsky, AMCPM-IRCM, 11 February 1971 (Unclassified)

11. "A Geometrical Model for the Synthesis of Interval Covers", by R.S. Michalski, Dept. Comp. Science, Univ. Ill, 24 June 71, Report No. 461, (Unclassified)

12. "Grass: Remote Facilities Guide", by R. Haskin, J. Nickolls, and M. Michel, Dept. Comp. Science, Univ. Ill, July 1971, Report No. 466 (Unclassified)

13. "PAGAN, A Three Dimensional Pattern Generator", by Richard Lane Partridge, Dep. Comp. Science, Univ. Ill, August 1971, Report No. 464 (Unclassified)

14. "Infrared Spectral Radiant Intensities of Various Helicopters", George F. Linsteadt, NOTS, China Lake, Cal., 8 Jan. 1962, NAVWEPS Report 7874 (Confidential)

15. "Operator's Manual Army Model AH-1G-Helicopter", HDQ Dept. Army, April 1969, TM 55-1520-221-10 (Unclassified)

16. "Army Model AH-1G Helicopter", Operator's Manual Change No. 10, HDQ Dept. Army, Aug. 1970, TM-55-1520-221-10 C10 (Unclassified)

17. "Recommended Changes to TM 55-1520-210-10" Draft (Unclassified)

18. Aircraft Engine, T63-A-5A Interim Report (U), December 1966 TIR 18.3.1.2 AD805966 (Unclassified)

19. Spectral Transmissivity of the Earth's Atmosphere in the 250 to 500 Wave Number Interval. Part I. Meteorological Data Processing (U), Sept. 1964, Report Number ERDA-186 AD 448 070 (Unclassified)

20. Identification of Exhaust Species from the Combustion of LM and LMH Fuels. Third Quarterly Report (U), July 1967, Report No. DRI #2408, AD 818106 (Unclassified)

21. Aircraft Engine, T55-L-13 Interim Report (U), July 1967, Report Number TIR 18.3.1.4, AD 819378 (Unclassified)

22. Aircraft Engine, T53-L-13 Interim Report (U), July 1967, Report Number TIR 18.3.1.1, AD819382 (Unclassified)

23. Thermodynamic Properties of Rocket Combustion Products Third Quarterly Technical Report, 15 April - 15 July 1968 (U), August 1968, Report Number U-4432, AD 838785 (Unclassified)

24. Search Control No. 079204 A Report Bibliography on Emission/Absorption Coefficients (U), March 1972, WEC Document No 86-53220 (Secret)

25. Search Control No. 079203 A Report Bibliography on Exhaust Plumes (U), March 1972, WEC Document No. 86-53218 (Secret)

26. Search Control No. 079202, A Report Bibliography on Helicopter Engine Performance (U), March 1972, WEC Document No. 86-53219 (Secret)

27. A DDC Bibliography on Helicopter Engine and Rotors (U), Volume III of III Volumes, Report Number DDC-TAS-68-59, WEC Document No. 86-53221, AD-395-500 (Secret)

28. AVCO/Lycoming Division Turbine Engine Model Specification Number 104:28 for the T53-L-11,-11A,-11B engines (U), January 1966 (Unclassified)

29. AVCO/Lycoming Division Turbine Engine Model Specification Number 104:33 for the T53-L-13,-13A,-13B Engines (U), September 1969 (Unclassified)

30. AVCO/Lycoming Division Turbine Engine Model Specification Number 104.35 for the T52-L-15 Engine, September 1969 (Unclassified)

31. AVCO/Lycoming Division Turbine Engine Model Specification Number 104.39 for the T53-L-701 Engine, February 1969 (Unclassified)

32. AVCO/Lycoming Division Turbine Engine Model Specification Number 124.31 for the T55-L-7C, September 1968 (Unclassified)

33. AVCO/Lycoming Division Turbine Engine Model Specification Number 124.38 for the T55-L-11A, August 1971 (Unclassified)

34. Pratt & Whitney Aircraft Engine Model Specification Number A-2456 for the T73-P-7000 Engine; April 1970 (Unclassified)

35. Operator's Manual Army Model UH-1D/H Helicopters TM55-1520-210-10, 25 August 1971, (Unclassified)

36. Operator's Manual Army Model UH-1C/M Helicopter TM55-1520-220-10, November 1968

37. Organizational Maintenance Manual TM55-1520-218-20 Army Model UH-1A Helicopter, February 1969 (Unclassified)

38. Organizational Maintenance Manual Army Model UH-1D/H Helicopters TM 55-1520-210-30, 10 September 1971

39. Operator's Manual Army Model C H-47B and CH-47C Helicopters TM55-1520-227-10, 10 December 1971

40. "Model Specification E1123-C Engine, Aircraft, Turboshaft: T64-GE-16" 10 March 1971, General Electric Company, (Unclassified)

41. Preliminary Model Specification E1181 Engine, Aircraft, Turboshaft T64-GE-16" 10 March 1971, General Electric Company (Unclassified)

42. The Measurement of the Exhaust Composition of Selected Helicopter Armament, June 1967, Army Aeromedical Research Unit, AD 655844 (Unclassified)

43. Continuous Deployment of Decoys, First Interim Report, 1 Jan through 31 March 196i, Oct. 1968, University of Michigan, WEC Document Number 86-53541, AD393298 (Secret)

44. Continuous Deployment of Decoys, Third Interim Technical Report 1 July through 30 September 1968, October 1968, University of Michigan, WEC Document Number 86-53490 AD393300(Secret)

45. A Simplified Mathematical Description of the Redeye Model 60A Electro-Optical Seeker, August 1968 Ballistic Research Labs, Aberdeen Proving Ground, AD392,681, (Confidential)

46. Exploratory Research Program for Turbo-Propulsion Exhaust Systems Volume I Analytical Capabilities Final Report, 1 July 1965 to 1 July 1968, United Aircraft Corp., Pratt Whitney AC Division, September 1968, AD502706 (Confidential)

47. A Study of Radiation Characteristics and its Suppression From the Plume of a Jet Aircraft During Afterburner Operation, December 1967, Wright Patterson AFB, AD386762 (Secret - Group 3)

48. Infrared Fuze Triggering Model (U), May 1971, Naval Weapons Center AD515 501 (SECRET)

49. Preliminary Study of Anti-Aircraft Rocket Radiation Characteristic January 1967, University of Michigan, AD378382 (Secret)

50. Vulnerability of Tactical U.S. Jet Aircraft to Redeye-Type Missiles, July 1962, Ballistic Research Labs AD332522 (Secret)

51. UH-1 Compound Research Helicopter Flight Test Program Interim Report No. 19, Army Aviation Material Labs., AD 477,913 (Unclassified)

52. Spectral Radiances & Emissivities of Rocket Exhaust Plumes, Volume I December 1961, North American Rockwell-Rocketdyne, AD382-992 (Confidential)

53. Aircraft Protection by Infrared Decoy 3-D Trajectory Analysis, February 1969, General American Research, AD 508 723 (Secret)

54. High Performance Aircraft Defense Techniques Volume I Systems Analysis February 1966 Hughes Aircraft Company, AD37173 (Secret)

55. A Study of Target Signatures for Jet Aircraft (U) Characteristics of Infrared Radiation from Jet Engines, Hughes Aircraft Company, AD517178 (Secret)

56. Operator's Manual Army Model UH-1A Helicopter TM-55-1520-218-10 February 1969.

57. Organizational Maintenance Manual Army Model AH-1G Helicopter TM55-1520-221-20, 10 September 1971.

58. Optical Properties of the Atmosphere (AFCRL-71-0269) May 1971 (Unclassified)

59. Target Detection Through Visual Recognition: A Quantitative Model (RAND-RM6158/1-PR) February 1970 (Unclassified)

60. Chrysler Improved Numerical Differencing Analyzer for 3rd Generation Computers, TN-AP-67,287, October 20, 1967

61. The Relative Importance of Contrast and Motion in Visual Target Detection (RAND-R-688-PR), March 1971 (Unclassified)

62. An Experimental Investigation of the Effect of Target Motion on Visual Detection, (RAND-R614-PR), February 1971 (Unclassified)

63. Thermal Analyzer Computer Program for the Solution of General Heat Transfer Problems (LR-18920,Lockheed) February 1967 (Unclassified)

64. Engineering Flight Test of An IR Suppression Kit Installation on the OV-1B Aircraft (USAASTA #67-23), July 1969 (Unclassified)

65. T44-L-11 Engine Support for CH-47C Aircraft U.S. Army Test Programs Progress Report #2, (AVCO/Lycoming Division) June 1969

66. Investigation of Ablative Material as a Means of Infrared Suppression (AVCO/Lycoming Division Report #1519.7.18) August 1971

67. Review of Thermal Radiation from Liquid and Solid Propellant Rocket Exhaust, (NASA TMS-53579) February 1967 (Unclassified)

68. An Investigation of Gas Turbine Combustors with High Inlet Air Temperatures, (TM-70-3; Purdue University) February 1970

69. Infrared Plume Target (HIC-ER-1525) February 1968 (Unclassified)

70. An Investigation of Gas Turbine Combustors with High Inlet Air-Temperature, Analytical Developments, (Purdue University TM-70-2) February 1970

71. Final Engineering Report T64-GE12/-16 Engine Development Program, General Electric, August 1968 (Unclassified)

72. A Bibliography on Helicopter Engines and Rotors. Volume II of III Volumes, TAS-68-58, November 1968 (Unclassified)

73. Study of Infrared Plume Effects, General Electric AFAPL-TR-70-32, May 1970 (Unclassified)

74. Experimental IR Suppression Kit for CH-47A Helicopter, USAAVLABS-TR-65-50, November 1962, (Unclassified)

75. Design of Infrared Suppression Devices for UH-1B, UH-1D, and CH-47A Helicopters, TRECOM-TR-64-32, August 1964 (Secret)

76. Powerplant Studies for Shaft-Driven Helicopter, USAAVLABS TR65-49 July 1965 (Unclassified)

77. Redeye Countermeasures for Low Performance Aircraft, HW67-6594 December 1967 (Secret)

78. Infrared Radiance Due to Molecular Emission in the Atmosphere, SAMSO-TR-70-35, September 1969 (Secret)

79. Infrared Radiation from Rocket Exhaust Plumes in Space, University of Michigan Report #3211-1-F, October 1970 (Confidential)

10.2 ABSTRACTS OF SELECTED DOCUMENTS

This section presents selected abstracts of documents that contain information particularly relevent to the development of HIDE. These abstracts are presented as they relate to one of the five major submodels of HIDE, i.e., documents abstracts are related primarily to PLUME, BØDY, TEMPS, TRANS, and SENSØR. In some instances, Westinghouse has edited the abstracts. All abstracts are unclassified.

10.2.1 Selected Abstracts of PLUME-related Documents

Title: Investigation of Ablative Material as a Means of Infrared Suppression
Government Monitor: U.S. Army Air Mobility Research & Development Lab. Fort Eustis, Virginia.
AD-Number: 888 568L
Author/Originating Agency/Date: J. Powell/AVCO-Lycoming Division/August 1971
Abstract:

This report contains the results of an analytical study to select ablative material and low-emittance-type coatings for use in the reduction of infrared emission from a T53-L-13 engine. Thermo-gravimetric analysis and burner tests formed the basis for selection of the candidate ablative material, cycloaliphatic epoxy for use in the design of a test exhaust tailpipe. Various base metals, both natural and anodized, were considered, and gold plating was selected for the low-emittance coating and because of its optical properties. Test hardware was fabricated and dynamic tests were conducted at White Sands, New Mexico.

Title: An Analytical Model for Predicting the Radiation From Jet Plumes In the Mid-Infrared Spectral Region
Government Monitor: Army Missile Command Redstone Arsenal, Alabama
AD-Number: 871 980
Author/Originating Agency/Date: H. Tracy Jackson/Army Missile Command; April 1970
Abstract:

The report describes an analytical model for predicting the emission of radiation from a jet plume in the mid-infrared spectral region. It is assumed that the dominant radiation arises for the CO2 molecule. Results are therefore reported for the 4.3-micrometer band of gaseous carbon dioxide which is assumed to cover the spectral region 2050 to 2400/CM (4.17-4.88 micrometers). The temperature range that is considered varies from 300 to 3100K. The objective of the reported program was to develop a computerized program for predicting

radiant energy emissions which could be readily integrated into a flow field calculation. A description is given of both the radiation model and the flow field model. The described program provides both the spectral and spatial intensity distributions of the emitted radiation.

Title: The Grumman Jet Engine Radiance Program
Government Monitor: IDEP
AD-Number: 845-572
Author/Originating Agency/Date: E. Stokes Fishburne/Grumman Aircraft Engineering Corp., Bethpage, N.Y./November 1968

Abstract:

A computer program has been deviced that, given the engine conditions and plume flow field, predicts the infrared signature of a jet engine. Designated the Grumman Jet Engine Radiance Program, it is based on a program originally developed by NASA for the theoretical computation of base plate heating on the Saturn launch missile due to radiation from the hot exhaust gas. The basic program has been substantially modified to include radiation from engine hot parts, atmospheric absorption, and a more detailed plume structure. Information obtained from this program has been employed for the prediction of the IR signature of the Grumman-proposed VFX. Other uses involve the evaluation of various IR suppression systems, determination of the lock-on range of missiles, and evaluation of the overall IR signature of jet aircraft.

Title: Exploratory Research Program for Turbopropulsion Exhaust Systems Volume I, Analytic Capabilities
Government Monitor: AFAPL
AD-Number: 502 706

Abstract:

This report presented the findings of a series of analytical studies related to, among other things, infrared signatures of turbopropulsion exhaust systems. A series of computer programs were developed covering simulation of (1) internal flow fields and performance of multiple flow convergent and convergent-divergent nozzles, (2) external body pressure distributions for subsonic, transonic, and supersonic flows, and (3) the simulation of combined internal-external nozzle flow fields and performance.

Title: A Study of Target Signatures For Jet Aircraft, Characteristics of Infrared Radiation from Jet Engines

Government Monitor: IDA/HQ, ARPA

AD-Number: 517 178

Abstract:

The state-of-the-art in jet aircraft target signatures arising from the engine and its plume is reviewed. The report opens with a discussion of the most important factor in the signature, the engine. Several analytical models currently in use are compared, and results of calculations for different altitudes, flight speeds, and engines are presented. The Hughes Aircraft Company Computer model is described in detail. Various measurement programs are discussed, and the experimental results compared with HAC Analytical predictions. Spatial distribution of radiation (important for missile terminal guidance) and source spectral distributions (important for background and flare discriminations and atmospheric attenuation calculations) are examined. Both analytical predictions and experimental evidences of hot spots are presented. The report concludes with a number of recommendations for improvements in analytical models and future measurement programs.

10.2.2 Selected Abstracts of BODY-related Documents

Title: Users Manual for "RAVFAC" A Radiation View Factor Digital Computer Program

Government Monitor: NASA - Marshall Space Flight Center, Alabama

AD-Number:

Author/Originating Agency/Date: J.K. Lovia, et.al./Lockheed Missiles & Space Company/November 1969

Abstract:

A technique for calculating diffuse radiation view factors was developed using contour integrals. This technique along with the finite difference (double summation) was incorporated into a Radiation View Factor Digital Computer Program (RAVFAC).

Two techniques for calculating radiation view factors were included in RAVFAC because the contour integral offers greater accuracy and the finite difference offers faster run times. A combination of the two provides accurate results and keeps the run time within reason.

A technique was also developed and incorporated into RAVFAC to account for the effects of shading by other surfaces. The calculation of shading effects is lengthy and requires a significant amount of computer time. A computer routine was developed that reduces the run time by eliminating surfaces that cannot cause shading on the areas for which the view factors are being calculated.

This technical report contains:

- Documentation of techniques and equations used to calculate the view factors and to account for the shading effects.
- A description of how RAVFAC works
- A detailed input guide and definition of all input parameters, including a sample problem
- A description of the program output
- A comparison of the contour integral and finite difference techniques
- A comparison of RAVFAC with other similar programs
- Suggestions for expanding the capabilities of RAVFAC.

This report fully documents the RAVFAC computer program. It contains information for those who want to know how the program works, what equations were used and how to use the program.

10.2.3 Selected Abstracts of TEMPS-related Documents

Title: Chrysler Improved Numerical Differencing Analyzer for Third Generation Computers

Government Monitor: NASA - Manned Spacecraft Center, Houston, Texas

AD-Number:

Author/Originating Agency/Date: D.R. Lewis, et.al./Chrysler Corp, Space Division/ October 1967

Abstract:

The computer programs described herein, Chrysler Improved Numerical Differencing Analyzer for 3rd Generation computers (CINDA-3G), was developed by the Thermodynamics Section of the Aerospace Physics Branch of Chrysler Corp. Space Division at the National Aeronautic and Space Administration's Michoud Assembly Facility. Programming and systems integration for the Univac-1108 computer was performed by the COSD Computation Services Group at the NASA Central Computer Facility, Slidell, Louisana. A major portion of this work was done under contract NAS9-7043 from the Manned Spacecraft Center, Houston, Texas.

This program appears virtually identical to its predecessor (CINDA, COSD-TN-AP-66-15) but has been almost completely rewritten in order to take advantage of the improved systems software and machine speeds of the 3rd generation computers. The entire programming approach has changed. Whereas CINDA was virtually a self contained program having its own Update, Monitor and Compiler; the CINDA-3G foundation consists of a preprocessor (written in Fortran) which accepts the same user input data and converts it into advanced Fortran language subroutines and block data input which is then passed onto the system Fortran compiler. While this requires a double pass on data where previously only one was required, the increased speed and improved software of the 3rd generation machines more than compensates. Transient thermal analysis solutions realize the increased machine speeds and in addition, perform fewer operations which further reduces solution times.

The CINDA-3G program options offer the user a variety of methods for solution of thermal analog models presented to it in a network format. The network representation of the thermal problem is unique in that it has a one-to-one corespondence to both the physical model and the mathematical model. This analogy enables engineers to quickly construct mathematical models of complex thermophysical problems and prepare them for program input. In addition, the program contains numerical subroutines for handling interrelated complex phenomena such as sublimation, diffuse radiation within enclosures, simultaneous 1-D incompressible fluid flow including valving and transport delay effects, etc. The optional combination of these capabilities in conjunction with model size allowable (> 4000 nodes for a linear 3-D system on 65K core) makes CINDA-3G an extremely potent analytical tool for thermal systems analysis in the hands of an engineer analyst.

10.2.4 Selected Abstracts of TRANS-related Documents

Title: Optical Properties of the Atmosphere

Author/Originating Agency/Date: R.A. McClatchey, et.al./Air Force Cambridge Research Laboratories/May 1971

Abstract:

A series of tables and charts is presented from which the atmospheric transmittance between any two points in the terrestrial atmosphere can be determined. This material is based on a set of five atmospheric models ranging from tropical to arctic and two aerosol models. A selected set of laser frequencies has been defined for which monochromatic transmittance values have been given. For low resolution transmittance prediction, a series of charts has been drawn providing the capability for predicting transmittance at a resolutinn of 20 wave-numbers. Separate sections are included on scattered solar radiation, infrared emission, refractive effects, and attenuation by cloud and fog.

Title: Band-Model Methods for Computing Atmospheric Slant/Path Molecular Absorption

Government Monitor: Office of Naval Research

AD-Number: 815 481

Author/Originating Agency/Date: David Anding/University of Michigan/February 1967

Abstract:

The general transmissivity equation for computing slant-path molecular absorption spectra is developed and two methods for evaluating this equation, the direct integration and that which assumes a model of the band structure, are discussed. Five band models are discussed and twelve methods for computing molecular absorption based on these band models are presented. Spectra computed by band-model methods are compared with spectra calculated by direct integration of the general transmissivity equation and with open-air field measurements of absorption spectra. Conclusions concerning the capability of band-model methods for predicting slant-path absorption spectra are stated and recommendations for future research are outlined. A summary of open-air field measurements of absorption spectra and laboratory measurements of absorption spectra for homoteneous paths is presented and a computer program for computing the equivalent sea-level path, the Curtis-Godson equivalent pressure, and the absorber concentration for atmospheric slant paths for any model atmosphere is given.

10.2.5 Selected Abstract of SENSØR-related Documents

Currently, it is very difficult to provide any useful information about either of the SENSØR-related documents in an unclassified manner, therefore, no abstracts are presented here.